NASA TECHNICAL MEMORANDUM

NASA TM X-73990

NASA TM X-73990

(NASA-TM-X-73990) TWO-DIMENSIONAL AERODYNAMIC CHARACTERISTICS OF SEVERAL ROTORCRAFT AIRFOILS AT MACH NUMBERS FROM 0.35 TO 0.90 (NASA) 179 p HC A04/MF A01 CSCL 01A G3/02

N77-14999

Unclas 59022

TWO-DIMENSIONAL AERODYNAMIC CHARACTERISTICS OF SEVERAL ROTORCRAFT AIRFOILS AT MACH NUMBERS FROM 0.35 TO 0.90

By Kevin W. Noonan and Gene J. Bingham
Langley Directorate
U.S. Army Air Mobility R&D Lab.

This informal documentation medium is used to provide accelerated or special release of technical information to selected users. The contents may not meet NASA formal editing and publication standards, may be revised, or may be incorporated in another publication.

NASA
National Aeronautics and Space Administration
Langley Research Center
Hampton, Virginia 23665

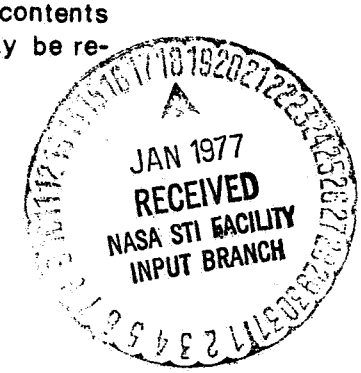

1. Report No.	2. Government Accession No.	3. Recipient's Catalog No.
NASA TM X-73990		

4. Title and Subtitle	5. Report Date
Two-Dimensional Aerodynamic Characteristics of Several Rotorcraft Airfoils at Mach Numbers From 0.35 to 0.90 (U)	January 1977
	6. Performing Organization Code

7. Author(s)	8. Performing Organization Report No.
Kevin W. Noonan and Gene J. Bingham	
	10. Work Unit No. 505-06-33-07
9. Performing Organization Name and Address	11. Contract or Grant No.
NASA-Langley Research Center Hampton, Virginia 23665	
	13. Type of Report and Period Covered
12. Sponsoring Agency Name and Address	NASA Technical Memorandum
National Aeronautics and Space Administration Washington, D. C. 20546	14. Sponsoring Agency Code

15. Supplementary Notes

Kevin W. Noonan and Gene J. Bingham, Langley Directorate, U.S. Army Air Mobility R&D Laboratory

16. Abstract

An investigation has been conducted in the Langley 6- by 28-inch transonic tunnel and the 6- by 19-inch transonic tunnel to determine the two-dimensional aerodynamic characteristics of several rotorcraft airfoils at Mach numbers from 0.35 to 0.90. The airfoils differed in thickness, thickness distribution, and chamber. The FX69-H-098, the BHC-540, and the NACA 0012 airfoils were investigated in the 6- by 28-inch tunnel at Reynolds numbers (based on chord) from about 4.7×10^6 to 9.3×10^6 at the lowest and highest test Mach numbers respectively and the FX69-H-098, the NLR-1, the BHC-540, and the NACA 23012 airfoils were investigated in the 6- by 19-inch tunnel at Reynolds numbers from about 0.9×10^6 to 2.2×10^6 at the lowest and highest test Mach numbers respectively.

17. Key Words (Suggested by Author(s))	18. Distribution Statement
Aerodynamics Airfoils	Unclassified - Unlimited

19. Security Classif. (of this report)	20. Security Classif. (of this page)	21. No. of Pages	22. Price*
Unclassified	Unclassified	179	$7.50

* For sale by the National Technical Information Service, Springfield, Virginia 22161

TWO-DIMENSIONAL AERODYNAMIC CHARACTERISTICS OF SEVERAL ROTORCRAFT AIRFOILS AT MACH NUMBERS FROM 0.35 TO 0.90

Kevin W. Noonan and Gene J. Bingham*
Langley Research Center

SUMMARY

An investigation has been conducted in the Langley 6-by 28-inch transonic tunnel and the 6-by 19-inch transonic tunnel to determine the two-dimensional aerodynamic characteristics of several rotorcraft airfoils at Mach numbers from 0.35 to 0.90. The airfoils differed in thickness, thickness distribution, and camber. The FX69-H-098, the BHC-540, and the NACA 0012 airfoils were investigated in the 6-by 28-inch tunnel at Reynolds numbers (based on chord) from about 4.7×10^6 to 9.3×10^6 at the lowest and highest test Mach numbers respectively and the FX69-H-098, the NLR-1, the BHC-540, and the NACA 23012 airfoils were investigated in the 6-by 19-inch tunnel at Reynolds numbers from about 0.9×10^6 to 2.2×10^6 at the lowest and highest test Mach numbers respectively. The airfoils were tested at geometric angles of attack from about -2.0° to 14.0° at 2.0° increments. All models except the NACA 23012 were tested with natural transition as well as with artificial roughness applied to the surface to fix the location of the boundary-layer transition.

The results of this investigation indicate that the FX69-H-098 airfoil was superior to both the BHC-540 and the NACA 0012 airfoils with respect to maximum normal-force coefficients at Mach numbers from 0.40 to 0.55 (corresponding Reynolds numbers of about

*Langley Directorate, U.S. Army Air Mobility R&D Laboratory

Preceding page blank

5×10^6 and 7×10^6), with respect to maximum normal-force-to-drag ratios at Mach numbers from 0.40 to 0.65 ($R \approx 5 \times 10^6$ and 8×10^6), and with respect to drag divergence Mach number at zero normal force coefficient ($R \approx 9 \times 10^6$). The trends of these three parameters of the FX69-H-098 airfoil relative to those of the BHC-540 airfoil were qualitatively the same as the trends determined at Reynolds numbers from about 1.0 to 2.0×10^6. At Reynolds numbers up to about 2.0×10^6, the FX69-H-098 airfoil was superior to the NLR-1 airfoil with respect to maximum normal-force coefficients ($M = 0.40$ to 0.55) and with respect to maximum normal-force-to-drag ratios ($M = 0.40$ to 0.65), but had a drag divergence Mach number at zero normal-force coefficient about 0.06 lower than the NLR-1 airfoil. Also at these low Reynolds numbers, the maximum normal-force-to-drag ratios at Mach numbers higher than 0.44 and the drag divergence Mach number at zero normal-force coefficient of the FX69-H-098 airfoil exceeded those of the NACA 23012 airfoil but the maximum normal-force coefficients of the FX69-H-098 airfoil were less than those for this five-digit-series airfoil at all Mach numbers up to 0.52.

INTRODUCTION

During a single revolution in forward flight, an airfoil section of a conventional helicopter rotor can experience lift coefficients from negative values to maximum lift and free stream Mach numbers from low subsonic to transonic (ref. 1). Therefore, the rotor performance depends on the efficiency of the airfoil section over

this Mach number and lift coefficient range as well as on the compromises in the number of blades, the blade planform, and the blade twist distribution. The aerodynamic characteristics of an airfoil section depend on the thickness-to-chord ratio, the thickness distribution, and the camber in addition to the Mach number and Reynolds number experienced on a particular application. The Reynolds number for a current gunship helicopter rotor in hover increases linearly from near-zero at the blade root to about 10×10^6 at the blade tip ($M \approx 0.67$). The Reynolds numbers at the blade tip for the same rotor at 175 knots forward flight speed range from about 14×10^6 at the 90° azimuth position ($M \approx 0.90$) to about 6×10^6 at the 270° azimuth position ($M \approx 0.44$).

The present investigation was undertaken to determine the two-dimensional aerodynamic characteristics of several rotorcraft airfoils which differed in thickness, thickness distribution, and camber. These airfoils are of special interest because they are either currently used on helicopter rotors or were specifically designed for rotorcraft application. The investigation was initiated in the 6- by 19-inch transonic tunnel because of the availability of the tunnel and the models. Although the Reynolds number capability of this facility (0.9×10^6 and 2.2×10^6 at $M = 0.35$ and 0.90 respectively) was recognized to be lower than full scale requirements by about a factor of 6, these test results would provide qualitative data to determine which airfoils to test at Reynolds numbers near full scale in the 6-by 28-inch transonic tunnel when that new facility became operational. The airfoils investigated

in the 6- by 19-inch tunnel were the FX69-H-098, the NLR-1, the BHC-540, and the NACA 23012 and those investigated in the 6- by 28-inch tunnel were the FX69-H-098, the BHC-540, and the NACA 0012.

The normal-force, pitching-moment, and drag data as well as the chordwise pressure distributions are presented for Mach numbers from about 0.35 to 0.90. The Reynolds numbers range from about 4.7×10^6 to 9.8×10^6 for the 6-by 28-inch tunnel data and from about 0.9×10^6 to 2.2×10^6 for the 6-by 19-inch tunnel data at the lowest and highest test Mach numbers respectively. Data which indicates the effect of artificial roughness applied to the airfoil surface are also presented.

SYMBOLS

The units used for the physical quantities of this paper are given both in the International System of Units (SI) and in the U.S. Customary Units. The measurements and calculations were made in the U.S. Customary Units.

c airfoil chord

c_d section profile-drag coefficient, $\sum_{\text{wake}} c'_d \left(\frac{\Delta h}{c}\right)$

c'_d point drag coefficient

$$2\left(\frac{p}{p_\infty}\right)^{6/7}\left[\frac{\left(\frac{p_t}{p}\right)^{2/7}-1}{\left(\frac{p_{t_\infty}}{p_\infty}\right)^{2/7}-1}\right]^{1/2}\left\{\left(\frac{p_t}{p_{t_\infty}}\right)^{1/7}-\left[\frac{\left(\frac{p_t}{p_\infty}\right)^{2/7}-1}{\left(\frac{p_{t_\infty}}{p_\infty}\right)^{2/7}-1}\right]^{1/2}\right\}$$

REPRODUCIBILITY OF THE ORIGINAL PAGE IS POOR

c_m section pitching-moment coefficient about the quarter chord, $c_m = \sum_{U.S.} C_p(0.25 - x/c)\left(\frac{\Delta x}{c}\right) + \sum_{L.S.} C_p(0.25 - x/c)\left(\frac{\Delta x}{c}\right)$

c_n section normal-force coefficient, $\sum_{U.S.} C_p\left(\frac{\Delta x}{c}\right) + \sum_{L.S.} C_p\left(\frac{\Delta x}{c}\right)$

C_p static pressure coefficient, $\frac{p_l - p_\infty}{q_\infty}$

h height of the wake survey probe tubes from a given reference plane

M Mach number

M_{dd} Mach number for drag divergence

p static pressure N/m^2 (psi)

q dynamic pressure, $1/2\ \rho v^2$, N/m^2 (psi)

R Reynolds number based on airfoil chord and free stream conditions

t airfoil thickness, cm (in.)

v velocity, m/sec (ft/sec)

x airfoil abcissa, cm (in.)

z airfoil ordinate, cm (in.)

z_c ordinate of airfoil mean line, cm (in.)

α angle of attack, angle between airfoil chord line and airstream direction, deg.

α_c angle of attack corrected for lift interference effects

ρ density, kg/m^3 ($slugs/ft^3$)

Subscripts:

l	local
t	total
∞	freestream

APPARATUS AND METHODS

Airfoils

The airfoil profiles, thickness distributions, and mean lines are presented in figures 1 and 2 and the design coordinates are presented in tables I through V. Airfoils which had been applied to some rotorcraft in the past and for which there was some data from other facilities were included in the present investigation in order to provide a baseline for comparison with the other rotorcraft airfoils. The baseline airfoil selected for the 6- by 19-inch tunnel investigation was the NACA 23012 primarily because of the model availability. The baseline airfoil selected for the 6- by 28-inch tunnel investigation was the NACA 0012 because of both model availability and the use of this airfoil on helicopter rotors in the past. A description of the NACA four-digit and five-digit-series airfoils is given in reference 3.

The BHC-540 airfoil is currently being used on the AH-1G helicopter and was included as a "present-day" baseline rotorcraft airfoil. The symmetrical BHC-540 (10.16 cm chord) was derived from the NACA 0012 in the following manner: the NACA 0012 ordinates were used from the leading edge to 0.513 x/c (based on a 7.90 cm chord) on both surfaces and then straight lines tangent to the upper and lower surface ordinates at that station were drawn to ordinates of 0.001 z/c and -0.001 z/c respectively at an x/c of 1.0 (based on a 10.16 cm chord). The resultant airfoil has a maximum thickness of 9.3 percent chord which is located at the 25 percent chord station.

The FX69-H-098 airfoil and the NLR-1 airfoil represent two approaches to rotorcraft airfoil design. The FX69-H-098 airfoil was designed by Wortmann whose design approach is discussed in detail in reference 3. The FX69-H-098 airfoil is cambered and has a maximum thickness of 9.8 percent which is located at 30 percent chord. The NLR-1 airfoil was designed by the method described in reference 4 (therein also referred to as NLR 7223-62) with the design objective to develop an airfoil which had a higher drag divergence Mach number at near zero lift coefficient than the FX69-H-098 but had both a maximum lift coefficient at M = 0.50 and a lift-to-drag ratio at conditions appropriate to hover similar to that of the FX69-H-098. An additional requirement of this airfoil was that the pitching-moment coefficient should not exceed $|0.02|$ at Mach numbers and lift coefficients appropriate to hover. The NLR-1 airfoil is cambered and has a maximum thickness of 8.6 percent which is located at the 40 percent chord station.

The airfoil models were machined from stainless steel and have chords of 10.16 cm (4.0 in.) and spans of 15.24 cm (6.0 in.) except for the NACA 0012 model which has a chord of 15.24 cm. In general, the models have 22 upper surface orifices (tables VI to X) located in one row 1.91 cm (0.75 in.) to the right of centerspan and 22 lower surface orifices located in one row 1.91 cm to the left of centerspan. The 0.343 mm (0.0135 in.) diameter orifices were drilled perpendicular to the local surface contour. The orifice locations for the BHC-540 and the FX69-H-098 airfoils are presented only once although there are two models of each airfoil since the design orifice locations are identical for the two models of the same configuration.

Wind Tunnels

The 6- by 28-inch transonic tunnel is a blowdown wind tunnel with a 0.125-open-slotted floor and ceiling and is generally operated at stagnation pressures from about 207 kN/m^2 (30 psia) to 620 kN/m^2 (90 psia) and at Mach numbers from 0.35 to 0.90 for airfoil testing (ref. 5). At 620 kN/m^2 stagnation pressure, the maximum Reynolds number, based on a 15.24 cm chord, varies from about 7.4×10^6 at a Mach number of 0.35 to about 14.4×10^6 at a Mach number of 0.90. Mach number is controlled by hydraulically actuated choker doors located downstream of the test section. The airfoil model spans the 15.24 cm width of the tunnel and is rigidly attached to two circular endplates which are driven by a hydraulic actuator to position the airfoil at the desired angle of attack (fig. 3). A test run usually consists of an angle of attack sweep at a constant Mach number and Reynolds number.

The 6- by 19-inch transonic tunnel is also a blowdown wind tunnel with a 0.125-open-slotted floor and ceiling. This tunnel can also be operated at Mach numbers from about 0.35 to 0.90 for airfoil testing but it does not have independent control of Mach number and stagnation pressure (ref. 6). The Reynolds numbers, based on a 10.16 cm chord, range from about 0.9×10^6 to 2.2×10^6 at Mach numbers of 0.35 and 0.90 respectively. The airfoil model is rigidly supported by circular endplates which are manually rotated to vary the angle of attack. A test run usually consists of a Mach number sweep at a constant angle of attack and a decreasing Reynolds number.

Apparatus

Wake survey probe.- A traversing wake survey probe is cantilevered from one tunnel sidewall to measure the profile drag of the airfoils. The probe sweeprate, which was selected as a result of an experimental determination

of acceptable lag-time in the pressure measurements, was about 2.54 cm/sec (1.0 in/sec).

The probe used in the 6- by 28-inch tunnel (fig. 3) was located 2.75 chords (based on 10.16 cm chord model) downstream of the airfoil trailing edge and has a maximum travel of about ±27.9 cm (±11.0 in.) from the tunnel centerline. This survey probe has six total pressure tubes which are made of 1.53 mm O. D x 1.02 mm I. D. (0.060 in. x 0.040 in.) stainless steel tubing with spacing laterally as shown in figure 4. The lower tube located on the tunnel centerline, the two tubes to the left of centerline (looking upstream), and the tube 0.953 cm to the right of centerline were used to acquire the data (figs. 3 and 4).

The probe used in the 6- by 19-inch tunnel was similar to the one used in the 6- by 28-inch tunnel except for having three rather than six total pressure tubes: one located on the tunnel centerline, one 0.76 cm to the left of centerline, and one 0.64 cm to the right of centerline. The tubes were made of 1.27 mm O. D. x 1.02 mm I. D. (0.050 in. x 0.040 in.) stainless steel tubing. The probe was located 1.77 chords (based on 10.16 cm chord model) downstream of the airfoil trailing edge and has a maximum stroke travel of ±10.16 cm from the tunnel centerline.

Instrumentation.- All measurements made during the 6- by 28-inch tunnel test program were obtained with the use of a high speed, computer-controlled digital data acquisition system and were recorded by a high-speed tape recording unit (ref. 5). Each of the two basic tunnel pressures from which all free stream conditions were determined, all airfoil surface pressures, and all wake pressures were measured with high-precision capacitive potentiometer-type pressure transducers. The electrical outputs from each of these

transducers were connected to individual autoranging signal conditioners which have seven available ranges. The output signals from the four signal conditioners measuring the wake pressures were filtered with 20 Hz low-pass filters before input to the data acquisition system; the range of frequencies to be passed were experimentally determined. The geometric angle of attack was determined from the output of a digital shaft encoder attached to a pinion engaging a rack on one model support endplate.

All measurements made during the 6- by 19-inch tunnel investigation were obtained with a "hard-wired" digital data acquisition system (ref. 6) and were recorded on a magnetic tape unit. Transducers with fixed ranges were used to measure the two basic tunnel pressures, all airfoil surface pressures, and wake pressures. The output signals from the three transducers used to measure the wake pressures were filtered with 20 Hz low-pass filters before input to the data acquisition system as a result of an experimental determination of acceptable signal rise-time. Geometric angle of attack was determined prior to each run with the use of an inclinometer.

Tests and Methods

The 6- by 28-inch tunnel tests were made at a constant stagnation pressure at Mach numbers from 0.35 to 0.90 which resulted in Reynolds numbers of about 4.7×10^6 and 9.3×10^6 at the lowest and highest test Mach numbers respectively. Geometric angles of attack ranged from about -4.0° to 14.0° at 2.0° increments at the lower test Mach numbers; this range was decreased at the higher test Mach numbers. Each airfoil was tested with both a smooth surface and with a narrow strip of No. 220 carborundum grit applied to the upper and lower surfaces to assure boundary layer transition. The grit size was determined by the method of reference 7. The 1.2 mm (0.047 in.) wide grit strip

was centered at the 0.088 chord station on the two 10.16 cm chord models but was centered at the 0.10 chord station on the 15.24 cm chord model. A grit coverage density of 5 to 10 percent was used on all models. A small number of oil flow photographs were taken at a Mach number of 0.35 on two airfoils to evaluate the two-dimensionality of the flow at high angles of attack. A mixture of motor oil and lampblack was placed on the upper surface of the model in a pattern of dots prior to making each run. Each oil-flow run was terminated about 5 seconds after the tunnel flow was stabilized at the desired Mach number and angle of attack; the model was then removed from the test section and photographed as quickly as possible.

The 6- by 19-inch tunnel tests were also made for a range of Mach numbers generally from 0.35 to 0.90. As previously noted, the stagnation pressure varied with Mach number so that the Reynolds numbers ranged from about 2.2×10^6 to 0.9×10^6 at the highest and lowest test Mach numbers respectively. Geometric angles of attack were varied from about -2.0° to 14.0° at 2.0° increments. The range of Mach numbers investigated were decreased with increased angle of attack. At selected angles of attack, test conditions were repeated with a strip of No. 220 carborundum grit applied to the upper and lower surfaces of all the models except the NACA 23012 airfoil. The trailing edge of the 1.2 mm wide grit strip was located at the 0.10 chord station for all the airfoils and the grit coverage density was about 5 to 10 percent. Oil flow photographs were taken of one airfoil at high angles of attack to evaluate the two-dimensionality of the flow. The oil-flow technique was the same as that used in the 6- by 28-inch tunnel.

Section normal-force and pitching-moment coefficients were calculated from the airfoil surface pressures by a trapezoidal integration of the

pressure coefficients and each of these coefficients represent the average of 5 measurements obtained in a 1 second interval. A form of the equation described in reference 8 was used to calculate the point drag coefficients from the measured wake pressures and a trapezoidal integration of the point drag coefficients was used to calculate the drag coefficient. The static pressures used in the wake drag calculation were measured with tunnel sidewall orifices located at the same longitudinal tunnel station as the tips of the tubes on the two wake survey probes. All of the drag coefficients presented in this report represent the mean of the measurements made with 4 total pressure tubes on the wake survey probe in one sweep through a wake in the case of the 6- by 28-inch tunnel data and the mean of the three measurements made in one sweep through a wake in the case of the 6- by 19-inch tunnel data. The corrections for lift interference (ref. 9) which have been applied to the angles of attack for some of the data are given by the following equations:

$$\alpha_c = \alpha + \Delta\alpha$$

where $\Delta\alpha$ (deg) $= -c_n$ (c) (0.2744) 6- by 19-inch tunnel

$\Delta\alpha$ (deg) $= -c_n$ (c) (0.1876) 6- by 28-inch tunnel

and where c is in centimeters

PRESENTATION OF RESULTS

The results of this investigation have been reduced to coefficient form and are presented as follows:

REPRODUCIBILITY OF TH
ORIGINAL PAGE IS POOR

Results	Airfoil	Wind Tunnel	Figure
c_n against α_c, c_m and c_d against c_n	FX69-H-098 BHC-540 NACA 0012	6-by 28-inch TT	8 9 10
c_n against α_c, c_m and c_d against c_n c_n, c_m, and c_d against M	FX69-H-098 NLR-1 BHC-540 NACA 23012	6-by 19-inch TT	11, 12 13, 14 15, 16 17, 18
$c_{n_{max}}$ against M	FX69-H-098 BHC-540 NACA 0012	6-by 28-inch TT	19
	FX69-H-098 NLR-1 BHC-540 NACA 23012	6-by 19-inch TT	20
$(c_n/c_d)_{max}$ against M	FX69-H-098 BHC-540 NACA 0012	6-by 28-inch TT	21
	FX69-H-098 NLR-1 BHC-540 NACA 23012	6-by 19-inch TT	22
c_n against M_{dd}	FX69-H-098 BHC-540 NACA 0012	6-by 28-inch TT	23
	FX69-H-098 NLR-1 BHC-540 NACA 23012	6-by 19-inch TT	24

DISCUSSION

Two-dimensionality of flow.- At the outset of the testing in the 6- by 28-inch tunnel, it was recognized that the ability to maintain two-dimensional flow on the airfoils at all test conditions was an unresolved question. Therefore, surface oil flow investigations were made on two airfoils to examine the two-dimensionality of the flow with the models at high angles of attack. This technique was successful only at the lowest test Mach number (0.35) because the oil was scrubbed off before the tunnel flow was stabilized at Mach numbers above 0.35. The surface oil flow patterns obtained on both the FX69-H-098 and the BHC-540 airfoils at 12^{0} geometric angle of attack ($\alpha_c \approx 9.9^{0}$) indicated reversed flow at the airfoil-end plate juncture from the airfoil trailing edge to about 0.15 x/c and 0.05 x/c respectively and attached flow in the center-span region. This region of reversed flow would be expected to grow with increasing angle of attack and thus have a significant influence on the pressure distributions at angles of attack which correspond to $c_{n_{max}}$ for both the FX69-H-098 and the BHC-540. For this reason, the separation of the tunnel sidewall boundary layer is believed to have limited $c_{n_{max}}$ at M = 0.35 for both airfoils. A comparison of the chordwise pressure distributions measured on the FX69-H-098 airfoil at Mach numbers from 0.40 to 0.50 and at a geometric angle of attack of about 12^{0} with those measured at M = 0.35 indicates a similar pressure rise near the leading edge on the upper surface (figs. 5(a) and 5(b)). This similarity suggests that a premature separation of the tunnel sidewall boundary-layer occurred at these Mach numbers also. The

BHC-540 and the NACA 0012 airfoil pressure distributions display the same trends (figs. 6(a) and 6(b), and 7(a) and 7(b)). Therefore the maximum normal-force coefficients measured in the 6- by 28-inch tunnel on these airfoils should be considered to be conservative values and qualitatively correct. Although it is not possible to precisely determine the loss in maximum normal-force coefficients of these airfoils, a comparison of the NACA 0012 data measured in this investigation with unpublished data from two other facilities can be useful in determining the magnitude of these losses. Data measured in the Langley low turbulence pressure tunnel and the United Technology's eight foot tunnel at a Mach number of about 0.36 are higher by about 0.15. The differences between the data of this report and the United Technology data decrease with increasing Mach number so that at a Mach number of about 0.55 the data reported herein is about 0.1 lower.

A surface oil flow investigation was also conducted with the FX69-H-098 airfoil in the 6- by 19-inch tunnel and this study together with the measured pressure distributions suggest that the maximum normal-force coefficients measured in this tunnel were also limited by a separation of the tunnel sidewall boundary layer.

Airfoil requirements.- The specific requirements for a rotorcraft airfoil will vary with different rotorcraft manufacturers design philosophies and the type of rotorcraft on which the airfoil is to be applied. However, the requirements of most rotorcraft manufacturers should be within the broad criteria stated here: (1) a maximum lift

coefficient as high as possible at Mach numbers from 0.40 to 0.60 for maneuverability, (2) a lift-to-drag ratio as high as possible at Mach numbers from 0.40 to 0.65 and at lift coefficients from 0.5 to 0.7 for hover efficiency, (3) a drag divergence Mach number at near zero lift coefficient as high as possible for minimum drag on the advancing blade in forward flight, and (4) a pitching-moment coefficient near zero at each of the three previous requirements. Lift coefficients are not presented in this report because the values depend on the angle of attack which must be corrected for interference effects; normal-force coefficients are presented instead. A complete set of pressure distributions for each of the airfoils is presented in the appendix.

Normal-force.- The maximum normal-force coefficients of the FX69-H-098, the BHC-540, and the NACA 0012 airfoils at Reynolds numbers near full scale have been determined from the normal-force data presented in figures 8 to 10 and are plotted as a function of Mach number in figure 19. The $c_{n_{max}}$ values at Mach numbers greater than about 0.60 were not measured because they are outside the range of interest for rotorcraft application. The maximum normal-force coefficients of the FX69-H-098 airfoil vary from about 1.15 to 1.10 for Mach numbers from 0.35 to 0.54 at corresponding Reynolds numbers ranging from about 5.4×10^6 to 7.0×10^6 and these values exceed those of both the BHC-540 and the NACA 0012 airfoils over this Mach number range. The $c_{n_{max}}$ values for the BHC-540 are nearly identical to those of the NACA 0012 and they decrease from about 1.10 to 0.90 with increases in Mach number from 0.35 to 0.55. Examination of the pressure distributions of these three airfoils presented in figures A1 to A3

indicates that the FX69-H-098 airfoil delays the development of supercritical flow and its associated recompression to higher angles of attack than both the BHC-540 and the NACA 0012 airfoils for Mach numbers up to 0.55. Thus, the thickening of the turbulent boundary layer due to the pressure rise of the shock and its eventual separation is delayed to higher normal force coefficients on the FX69-H-098 airfoil. For example, the pressure distributions at a Mach number of about 0.40 indicate that the FX69-H-098 airfoil does not develop supercritical flow until a corrected angle of attack of 12.4^{o} ($c_n = 1.10$) whereas the BHC-540 and the NACA 0012 airfoils develop supercritical flow at $\alpha_c = 6.9^{o}$ ($c_n = 0.84$) and $\alpha_c = 7.6^{o}$ ($c_n = 0.88$) respectively and the FX69-H-098 airfoil first experiences a separation of the boundary layer at $\alpha_c = 12.4^{o}$ but the BHC-540 and the NACA 0012 airfoils first experience separation at $\alpha_c = 10.3^{o}$ and $\alpha_c = 11.5^{o}$ respectively. The higher maximum normal-force coefficients of the FX69-H-098 airfoil are also due in part to the camber. The pressure distributions indicate that the FX69-H-098 airfoil is more heavily loaded on the upper surface particularly in the region from 0.075 x/c to 0.40 x/c than both the symmetrical sections for nearly the same Mach numbers and angle of attack thus providing additional normal force. The reversal in the $c_{n_{max}}$ trend of the FX69-H-098 airfoil with increasing Mach number is also believed to be due to the supercritical flow development although there is a Reynolds number variation with Mach number. The pressure distributions of the FX69-H-098 airfoil indicate that the pressure recovery on the upper surface near the leading edge at an angle of attack near $c_{n_{max}}$

($\alpha_c \approx 12.4$) becomes more severe with increasing Mach number above 0.35 up to M = 0.44 as a result of decreasing pressures in the supersonic field. This steeper pressure recovery results in increasing pressures (less negative C_p) from near the leading edge to about 0.40 x/c which decrease $c_{n_{max}}$ at Mach numbers of 0.40 and 0.44. However, the pressure distributions at Mach numbers of 0.50 and 0.54 indicate lower pressures particularly in the regions from about 0.025 x/c to 0.10 x/c and 0.05 x/c to 0.20 x/c respectively than were indicated at lower Mach numbers for corrected angles of attack of about 6.3^0 and higher. These lower pressures which probably are the result of a more favorable reflection pattern within the supersonic field (as Wortmann intended) provide an increase in $c_{n_{max}}$ over that obtained at a Mach number of 0.44. For Mach numbers from about 0.35 to 0.55, the pressure distributions of both the BHC-540 and the NACA 0012 airfoils at angles of attack near $c_{n_{max}}$ indicate the same phenomenon is occurring as that just described for the FX69-H-098 airfoil at Mach numbers up to 0.44 so that the $c_{n_{max}}$ values decrease with increasing Mach number. For this same range of Mach numbers, these three airfoils experience a gradual stall and the pressure distributions indicate a trailing edge type of separation is occurring.

The addition of artificial roughness to fix the location of boundary layer transition had an inconsistent effect on the variation of maximum normal-force coefficients with Mach number of the three airfoils (fig. 19). The $c_{n_{max}}$ values of the FX69-H-098 airfoil were reduced only for Mach numbers greater than about 0.43 whereas those of the BHC-540 were not measurably

reduced at any Mach number and those of the NACA 0012 were reduced at all Mach numbers.

The maximum normal-force coefficients of the FX69-H-098, the NLR-1, the BHC-540, and the NACA 23012 airfoils at Reynolds numbers less than 2.0×10^6 were determined from the normal-force data presented in figures 11, 13, 15, and 17 and are plotted as a function of Mach number in figure 20. At Mach numbers from about 0.39 to 0.55 (corresponding Reynolds numbers of 1.0 to 1.4×10^6), the maximum normal-force coefficients of the FX69-H-098 airfoil exceed those of both the BHC-540 and the NLR-1 airfoils over this entire range but exceed those of the NACA 23012 airfoil only at Mach numbers higher than about 0.52. The $c_{n_{max}}$ values of the FX69-H-098 airfoil range from about 0.97 to 1.07 for Mach numbers from 0.39 to 0.55. The differences in the $c_{n_{max}}$ values measured on the FX69-H-098 and the BHC-540 airfoils in the two test facilities are predominantly a Reynolds number effect. The trend of the maximum normal-force coefficient of the FX69-H-098 airfoil to be higher than that of the BHC-540 airfoil for all Mach numbers presented at these low Reynolds numbers is consistent with the trend of these two airfoils indicated by the near full scale Reynolds number data.

The pressure distributions presented in figures A4 through A7 suggest that the FX69-H-098 airfoil delays the development of supercritical flow to higher angles of attack than the other three airfoils for Mach numbers at least up to about 0.55. However, the development of supercritical flow on the NACA 23012 airfoil at lower angles of attack compared to that of the FX69-H-098 airfoil is not detrimental until the Mach number is increased above about 0.50 unlike the case of the NLR-1 and the BHC-540 airfoils.

A comparison of the pressure distributions of the FX69-H-098 and the NACA 23012 airfoils at a Mach number of about 0.50 indicates that supercritical flow first develops on the NACA 23012 at an $\alpha_c = 5.6^o$ versus $\alpha_c = 7.3^o$ on the FX69-H-098 but separation is first seen at about the same corrected angle of attack (11.4^o for FX69-H-098 vs 11.2^o for the NACA 23012). Apparently the NACA 23012 airfoil has a favorable reflection pattern within the supersonic field which permits the chordwise expansion of this low pressure region compared to that of the FX69-H-098 airfoil at the same α_c without giving rise to a separation of the boundary layer for angles of attack from $\alpha_c = 5.6^o$ to at least 8.9^o. As a result, the NACA 23012 airfoil is more heavily loaded than the FX69-H-098 airfoil over the first 20 percent chord for the same α_c thus providing a higher $c_{n_{max}}$ at this Mach number. The NACA 23012 airfoil experiences the same phenomenon at a Mach number of about 0.46, the lowest Mach number at which $c_{n_{max}}$ was measured on this airfoil. At a Mach number of about 0.55, the reflection pattern on the NACA 23012 airfoil delays an extensive separation of the boundary layer to an α_c between 7.3^o and 9.3^o but the reflection pattern on the FX69-H-098 airfoil permits the chordwise expansion of its supercritical flow region attained at $M \approx 0.50$ without a significant separation of the boundary layer up to an α_c between 9.0^o and 11.4^o. For these reasons, there is a reversal in the $c_{n_{max}}$ trend of these two airfoils at Mach numbers higher than about 0.50. The pressure distributions of the NLR-1 airfoil at a Mach number of about 0.50 first indicate the presence of supercritical flow at an $\alpha_c = 5.6^o$. The development of the supersonic flow field on this airfoil with increasing α_c is accompanied by a more

severe recompression which results in an extensive separation of the boundary layer at an α_c about 2^0 lower than that on the FX69-H-098 airfoil at a $M \approx 0.50$. The pressure distributions of the NLR-1 airfoil at a Mach number of about 0.55 indicate that the difference in α_c at which extensive separation occurs compared to the FX69-H-098 airfoil is about the same as that occurring at $M \approx 0.50$ so that the NLR-1 airfoil also has a lower $c_{n_{max}}$ than the FX69-H-098 airfoil at this Mach number as a result.

At low Reynolds numbers, the normal-force curves of the FX69-H-098 airfoil at Mach numbers up to about 0.69 display a slope change which was not indicated by the near full-scale Reynolds number data (figs. 8 and 11). A comparison of the BHC-540 airfoil normal-force curves at low and near full-scale Reynolds number does not indicate slope changes like those of the FX69-H-098 airfoil. However, the low Reynolds number data of the other two cambered sections (figs. 13 and 15) and data reported on other airfoils at Reynolds numbers from 1.0 to 2.0×10^6 (ref. 10) do indicate slope changes of nearly the same magnitude as those of the FX69-H-098 airfoil. The differences may be entirely a Reynolds number effect.

Pitching moment.- The pitching-moment coefficient at zero normal force (the moment about the aerodynamic center) of the FX69-H-098 airfoil ranges from about -0.015 to -0.02 at subcritical Mach numbers due to the camber (fig. 8(b)). At supercritical Mach numbers i.e., above about 0.64 based on the pressure coefficients of figure A1, the corresponding pitching-moment coefficient increases to as much as -0.045 which is twice the desirable level of $|0.02|$ noted by some (ref. 3). At all Mach numbers except 0.84, the pitching-moment coefficient approaches zero with increasing

positive normal-force coefficients to indicate the forward movement of the center of pressure. The slope of the c_m vs c_n curves remain near constant to a c_n of about 1.0 for Mach numbers up to about 0.59. This favorable result was not obtained with the BHC-540 and the NACA 0012 airfoils because these symmetrical sections have lower maximum normal-force coefficients at corresponding Mach numbers (figs. 9(a,b), and 10(a,b)). At all conditions presented in figures 9(b) and 10(b) the pitching-moment coefficients at zero normal-force of the BHC-540 and the NACA 0012 airfoils are zero which is characteristic of symmetrical airfoils. The trend of the pitching-moment coefficients of these two airfoils to remain near zero with increasing normal-force coefficients until (1) near the onset of boundary-layer separation (ref. 2), (2) the alteration of the pressure distribution by substantial supercritical flow or (3) a combination of both itens (1) and (2) is also believed to be characteristic of symmetrical airfoils. These influences cause changes or even reversals in the slope of the c_m vs c_n curves such as those occurring at the maximum normal-force coefficients of these two airfoils.

A comparison of the pitching-moment coefficients of the FX69-H-098 and the BHC-540 airfoils at Reynolds numbers less than 2.0×10^6 indicates the same qualitative results as that of the near full-scale Reynolds number data (figs. 11(b), and 15(b)). The pitching-moment coefficients of the NLR-1 airfoil are generally equal to or less negative than those of the FX69-H-098 airfoil at corresponding Mach numbers and normal-force coefficients (fig. 13). However, the superior maximum normal-force coefficient capability of the FX69-H-098 airfoil at Mach numbers from

about 0.39 to 0.60 delays increases in pitching-moment to higher normal-force coefficients. The pitching-moment coefficients of the NACA 23012 airfoil at zero normal-force coefficient and low Reynolds number vary from about -0.015 to -0.02 for Mach numbers up to about 0.80. At higher Mach numbers, the pressure distributions at near zero normal-force and thus the pitching-moment coefficients change significantly with increasing Mach number (fig. A7). At all normal-force coefficients up to near stall or to the development of supercritical flow the pitching-moment coefficients are within the $|0.02|$ level.

Drag.- The minimum drag of the FX69-H-098, the BHC-540, and the NACA 0012 airfoils at Reynolds numbers near full scale is about 0.0065 for Mach numbers less than the critical Mach number ($\sim$ 0.75 to 0.80) although the maximum thickness of these airfoils varies from 0.093 t/c to 0.12 t/c (figs. 8(c), 9(c), and 10(c)). This result is attributed to the fact that the minimum profile drag at subcritical Mach numbers is predominantly skin friction-drag which would be nearly the same for airfoils of about the same thickness ratios as suggested in reference 11. The addition of roughness increased the minimum drag of the FX69-H-098 and the BHC-540 by about 0.0005 to 0.0010 at most Mach numbers but increased that of the NACA 0012 by about 0.0005 or less at all Mach numbers. The minimum drag of the FX69-H-098, the NLR-1, the BHC-540 and the NACA 23012 airfoils at Reynolds numbers less than 2.0×10^6 is about 0.0060 to 0.0065 at subcritical Mach numbers (figs. 11(c), 13(c), 15(c), and 17(c)). The insensitivity of the minimum drag of the FX69-H-098 and the BHC-540 airfoils to the Reynolds number differences

in the two test facilities is believed to be characteristic of airfoils having thickness ratios less than about 12 percent and maximum cambers less than about 2 percent. For example, the minimum drag data of the NACA 0012 airfoil in reference 12 indicates a drag reduction of only about 0.0005 for an increase in Reynolds number from 1.0×10^6 to 9.0×10^6.

The maximum normal-force-to-drag ratios at Reynolds numbers near full scale were determined from the drag data presented in figures 8(c), 9(c), and 10(c) and these are plotted as a function of Mach number in figure 21. The maximum normal-force-to-drag ratios of the FX69-H-098 airfoil exceed those of the BHC-540 and the NACA 0012 airfoils at all Mach numbers from 0.35 to 0.80. At Mach numbers appropriate to hover (M = 0.40 to 0.65), the $(c_n/c_d)_{max}$ values of the FX69-H-098 airfoil range from a high of 120 at M = 0.50 to a low of 66 at M = 0.65. Also for the hover Mach number conditions, the maximum normal-force-to-drag ratios of the BHC-540 range from a high of 102 down to 64 and those of the NACA 0012 range from 95 to 56. The $(c_n/c_d)_{max}$ values of the FX69-H-098 airfoil are higher than those of the other two airfoils due to both the aforementioned delayed supercritical flow development and the camber which allows this airfoil to attain higher normal-force coefficients than the symmetrical sections while still maintaining low drag coefficients. The $(c_n/c_d)_{max}$ values of the FX69-H-098 and the BHC-540 airfoils were reduced more by the addition of roughness than those of the NACA 0012 airfoil over most of the Mach number range (fig. 21). The values of the FX69-H-098 airfoil at Mach numbers up to about 0.60 were generally more sensitive to the roughness than those at higher Mach numbers. Unfortunately,

the pressure distributions of the FX69-H-098 airfoil at precisely the angles of attack corresponding to $(c_n/c_d)_{max}$ are not available. However, the pressure distributions of the smooth FX69-H-098 model suggest that a favorable pressure gradient on the upper surface extends aft of the chordwise location of the grit strip at Mach numbers of 0.64 and higher which could diminish the disturbance in the boundary layer caused by the grit strip.

The maximum normal-force-to-drag ratios at Reynolds numbers less than 2.0×10^6 were determined from the drag data presented in figures 11(c), 13(c), 15(c), and 17(c) and are plotted as a function of Mach number in figure 22. At these low Reynolds numbers, the maximum normal-force-to-drag ratios of the FX69-H-098 airfoil exceed those of the BHC-540 airfoil over the entire Mach number range from 0.35 to 0.80 and those of the NLR-1 airfoil at all Mach numbers up to about 0.71 which is primarily the reason the NLR-1 airfoil was not investigated in the 6- by 28-inch tunnel. The $(c_n/c_d)_{max}$ values of the FX69-H-098 airfoil also exceed those of the NACA 23012 airfoil for Mach numbers higher than about 0.44. The trend of the $(c_n/c_d)_{max}$ value of the FX69-H-098 airfoil to be higher than that of the BHC-540 airfoil at all Mach numbers presented at Reynolds numbers less than 2.0×10^6 is consistent with the trend of these two airfoils determined from the near full scale Reynolds number data but the values of both airfoils are lower due to the Reynolds number influence on both c_n and c_d.

The trends of the $(c_n/c_d)_{max}$ curves of the other two airfoils relative to that of the FX69-H-098 airfoil can be explained by the section data

presented in figures 11, 13, and 17 and the pressure distributions presented in figures A4, A5, and A7 although there is not always an exact correlation in Mach number between data on these airfoils and in addition, the data at precisely the angles of attack corresponding to $(c_n/c_d)_{max}$ generally are not available. Figures 17(a) and 17(c) along with figures 11(a) and 11(c) indicate that the corrected angles of attack corresponding to $(c_n/c_d)_{max}$ for the NACA 23012 airfoil and the FX69-H-098 airfoil are about 7.8^o and 7.6^o respectively for Mach numbers up to about 0.44. The pressure distributions of the NACA 23012 airfoil suggest that its flow field is entirely subcritical at $(c_n/c_d)_{max}$ up to a Mach number between 0.40 and 0.45 and the pressure distributions of the FX69-H-098 airfoil suggest that $(c_n/c_d)_{max}$ for this airfoil occurs at subcritical flow conditions up to a Mach number between 0.44 and 0.50 so that the drag coefficients at $(c_n/c_d)_{max}$ for these two airfoils should be similar up to these same Mach numbers. A comparison of the pressure distributions of the NACA 23012 airfoil at a Mach number of about 0.40 with those of the FX69-H-098 airfoil at a Mach number of about 0.38 indicates that the NACA 23012 airfoil would be more heavily loaded from about the leading edge to 0.40 x/c at α_c for $(c_n/c_d)_{max}$ thus providing more normal force. Therefore, the higher $(c_n/c_d)_{max}$ for the NACA 23012 airfoil at Mach numbers less than 0.44 is the result of both the delayed supercritical flow development and the camber. The section characteristics at a Mach number of about 0.50 indicate that the $(c_n/c_d)_{max}$ values of the NACA 23012 and the FX69-H-098 airfoils are occurring at an α_c of about 6.5^o and 7.4^o respectively. The pressure distributions at this Mach number indicate that the NACA 23012 airfoil has lower minimum

REPRODUCIBILITY OF THE
ORIGINAL PAGE IS POOR

pressures in the supersonic field and its supersonic field extends further aft than that of the FX69-H-098 airfoil at the same α_c (for example $\alpha_c = 7.3^o$). These differences result in a higher wave drag on the NACA 23012 airfoil compared to the FX69-H-098 airfoil. On the NACA 23012 airfoil, the wave drag resulting from the supersonic flow field apparently predominates over the increased normal-force that the supersonic flow field also provides so that the $(c_n/c_d)_{max}$ value of this airfoil is lower than that of the FX69-H-098 airfoil. This phenomenon on the NACA 23012 airfoil begins to become important at a Mach number near 0.44 resulting in the reversal of the $(c_n/c_d)_{max}$ curves of this airfoil and that of the FX69-H-098 airfoil. The section characteristics of the NLR-1 airfoil indicate that the $(c_n/c_d)_{max}$ values for this airfoil occur at lower corrected angles of attack than those of the FX69-H-098 airfoil for Mach numbers up to about 0.65 and the pressure distributions presented in figure A5 suggest that the $(c_n/c_d)_{max}$ values of the NLR-1 airfoil occur at subcritical flow conditions up to a Mach number between 0.42 and 0.50. A comparison of the pressure distributions of the NLR-1 airfoil at a Mach number of about 0.37 ($(c_n/c_d)_{max}$ @ $\alpha_c \approx 5.2^o$) with those of the FX69-H-098 airfoil at a Mach number of about 0.38 indicates that for about the same α_c the NLR-1 airfoil is more heavily loaded over about the first 10 percent chord thus providing more normal-force but the adverse pressure gradient on the upper surface near the leading edge is also steeper on the NLR-1 which gives rise to additional drag. This higher drag apparently predominates over the additional normal force so that the $(c_n/c_d)_{max}$ value of the NLR-1 is lower than that of the

FX69-H-098 airfoil. At a Mach number of about 0.66, a comparison of the pressure distribution of the NLR-1 at $\alpha_c = 2.6^o$ $((c_n/c_d)_{max}$ @ $\alpha_c \approx 2.5^o)$ with that of the FX69-H-098 at $\alpha_c = 2.5^o$ $((c_n/c_d)_{max}$ @ $\alpha_c \approx 2.6^o)$ suggests that the additional loading on the NLR-1 airfoil over the first 13 percent chord is balanced by additional loading on the FX69-H-098 airfoil from 13 to 30 percent chord so that the normal-force would be nearly equal. The lower $(c_n/c_d)_{max}$ value of the NLR-1 airfoil at this Mach number apparently is the result of a higher wave drag associated with the differences in the supersonic flow fields on these two airfoils. The reversal of the curves of these two airfoils at Mach numbers higher than about 0.71 is attributed to a reduction in the growth of the wave drag with increasing Mach on the NLR-1 airfoil compared to that on the FX69-H-098 airfoil. The pressure distributions at a corrected angle of attack of about 1.0^o at Mach numbers of about 0.69 $((c_n/c_d)_{max}$ @ $\alpha_c \approx 2.0)$ and 0.74 $((c_n/c_d)_{max}$ @ $\alpha_c \approx 1.6)$ on the NLR-1 airfoil and at nearly the same Mach numbers on the FX69-H-098 airfoil $((c_n/c_d)_{max}$ @ $\alpha_c \approx 1.4$ and 0.9 respectively) suggest this conclusion. The supersonic field on both of the airfoils expands in the chordwise direction with the increase from the lower to the higher of these two Mach numbers but the recompression terminating the supersonic zone on the NLR-1 airfoil appears to become less severe at the higher Mach number (consistent with design objectives) while that on the FX69-H-098 airfoil appears to become more severe suggesting a larger wave drag increase on the FX69-H-098 airfoil.

The drag data in figures 8 to 10 were cross plotted as a function of Mach number at constant geometric angles of attack so that the drag

divergence Mach numbers could be determined. The drag divergence Mach number as used in this report is defined as the Mach number at which the slope $\frac{d(c_d)}{dM} = 0.1$. The drag divergence Mach numbers and the corresponding normal-force coefficients for the FX69-H-098, the BHC-540, and the NACA 0012 airfoils are presented in figure 23. The FX69-H-098 airfoil has a higher normal-force coefficient for a given drag divergence Mach number than either the BHC-540 or the NACA 0012 airfoils except for Mach numbers between about 0.70 to 0.76 where the normal-force coefficients of the FX69-H-098 and the NACA 0012 airfoils are essentially equal. The drag divergence Mach number at zero normal-force coefficient of the FX69-H-098 airfoil is about 0.81 and that for both the BHC-540 and the NACA 0012 airfoils is about 0.80.

The pressure distributions presented in figures A1, A2, and A3 can be useful in explaining these trends although the data at precisely the angles of attack for drag divergence are generally not available. For a drag divergence Mach number of 0.54, the section characteristics of the FX69-H-098 and the BHC-540 airfoils indicate that the corresponding value of α_c is about 6.6^o and 6.0^o respectively. For a given free stream Mach number, the drag divergence usually results from sonic flow moving aft of the airfoil crest (chordwise location at which the airfoil surface is tangent to the free stream) due to increases in angle of attack as noted in reference 1. At this Mach number, the pressure distribution of the FX69-H-098 airfoil at $\alpha_c = 6.3^o$ indicates supercritical flow extends to about 0.15 x/c (crest $\approx$ 0.15 x/c at $\alpha_c = 6.6^o$) and the pressure distribution of the BHC-540 airfoil at M = 0.55 and $\alpha_c = 6.6^o$ indicates

supercritical flow extends to about 0.12 x/c (crest $\approx$ 0.115 @ $\alpha_c = 6.0^o$) suggesting that the cause of drag divergence for both of these airfoils is the usual one just mentioned. A comparison of these same two pressure distributions indicates that the FX69-H-098 airfoil is more heavily loaded from about 0.10 x/c to 0.90 x/c thus providing more normal force. Therefore the FX69-H-098 airfoil has a higher normal-force coefficient at this drag divergence Mach number because of its delayed supercritical flow development and its more rearward crest ($-2^o \leq \alpha_c \leq 14^o$) which together allow this airfoil to attain a higher angle of attack than that of the BHC-540 airfoil at the drag rise condition. For a drag divergence Mach number of about 0.70, the section characteristics indicate a corresponding α_c of about 1.6^o for the FX69-H-098 airfoil and about 2.4^o for the BHC-540 airfoil. The pressure distribution of the FX69-H-098 airfoil at $\alpha_c = 1.3^o$ at M = 0.69 indicates supercritical flow extending to about 0.26 x/c (crest $\approx$ 0.23 x/c @ α_c = 1.6) and the pressure distribution of the BHC-540 airfoil at $\alpha_c = 3.1^o$ at M = 0.70 also (crest $\approx$ 0.17 x/c @ α_c = 2.4) indicates supercritical flow to about 0.26 x/c suggesting that the cause of drag divergence is still the extension of sonic flow behind the crests of the airfoils. These pressure distributions also suggest that the FX69-H-098 airfoil first develops supercritical flow at a lower angle of attack than that of the BHC-540 airfoil. Therefore, the normal-force coefficients of these two airfoils at this drag divergence Mach number are nearly equal because now the BHC-540 airfoil delays the movement of sonic flow aft of its crest to a higher angle of attack than does the FX69-H-098 airfoil and the supercritical flow region on the BHC-540

airfoil develops a pressure distribution similar to that at a lower angle of attack on the FX69-H-098 airfoil. For a drag divergence Mach number of 0.59, the section characteristics of the NACA 0012 and the FX69-H-098 airfoils indicate that the corresponding values of α_c are about 5.0^o (crest $\approx$ 0.16 x/c) and 4.6^o (crest $\approx$ 0.18 x/c) respectively. The pressure distributions at this Mach number suggest that both airfoils first develop supercritical flow at about the same α_c ($\sim$ 3.0) and that both airfoils encounter drag divergence as a result of supercritical flow moving aft of the crests. Thus the FX69-H-098 airfoil has a higher normal-force coefficient at this drag divergence Mach number due to its camber which produces a greater loading from about 0.10 to 0.90 x/c for corrected angles of attack between about 3.0^o and 6.0^o. The section characteristics indicate that the corrected angles of attack for a drag divergence Mach number of 0.69 are about 2.6^o for the NACA 0012 airfoil (crest $\approx$ 0.22 x/c) and about 1.6^o for the FX69-H-098 airfoil (crest $\approx$ 0.23 x/c). The pressure distributions at this Mach number suggest that the NACA 0012 and the FX69-H-098 airfoils first develop supercritical flow at an α_c close to 1.5^o and -0.3^o respectively and that both airfoils experience drag divergence for the same reason as at M = 0.59. Thus for a drag divergence Mach number of 0.69, the normal-force coefficient of the NACA 0012 airfoil is equal to that of the FX69-H-098 airfoil due to the delayed supercritical flow development of the NACA 0012 airfoil and its more rearward crest location (for angles of attack less than 4.0^o) which together permit this airfoil to attain a higher angle of attack than the FX69-H-098 airfoil at the drag rise condition. For these three airfoils, the

addition of roughness reduced the drag divergence Mach numbers at zero normal-force coefficient less than about 0.01 from the smooth surface values but generally increased the drag divergence Mach numbers at all other normal force coefficients by about 0.01. These differences due to roughness are believed to be within the accuracy of the measurements.

The drag divergence characteristics at Reynolds numbers less than 2.0×10^6 were determined from the data presented in figures 12, 14, 16 and 18 and are shown in figure 24. At these low Reynolds numbers, the FX69-H-098 airfoil has a higher normal-force coefficient for a given drag divergence Mach number than both the NACA 23012 and the BHC-540 airfoils for the entire range of Mach numbers presented and than the NLR-1 airfoil at Mach numbers up to about 0.64. The NLR-1 airfoil has a significantly higher normal-force coefficient than the other airfoils at drag divergence Mach numbers in excess of about 0.75 due to the shockless design goal at near zero normal-force. At zero normal-force coefficient, the drag divergence Mach number of the NLR-1 airfoil is about 0.86 and that of the FX69-H-098 airfoil is about 0.80 so that one of the design objectives of the NLR-1 airfoil was fulfilled. A comparison of the drag divergence characteristics of the FX69-H-098 and the BHC-540 airfoils measured in the two test facilities indicates that the trend of the FX69-H-098 airfoil to have a higher c_n than the BHC-540 airfoil at each of the drag divergence Mach numbers presented at low Reynolds number is consistent with trends shown by the near full scale Reynolds number data and that Reynolds number has very little effect on the values of c_n at a given drag divergence Mach number for both airfoils.

The pressure distributions presented in figures A4, A5, and A7 are useful in explaining the trends of the FX69-H-098, the NLR-1, and the NACA 23012 airfoils although the data at precisely the angles of attack for drag divergence are generally not available. For a drag divergence Mach number of 0.55, the section characteristics suggest a corresponging α_c of about 6.8^o (crest $\approx$ 0.15 x/c) for the FX69-H-098 airfoil and about 5.3^o (crest $\approx$ 0.13 x/c) for the NLR-1 airfoil. The pressure distribution of the FX69-H-098 airfoil at a Mach number of about 0.56 and an $\alpha_c = 7.1^o$ indicates that supercritical flow extends to about 0.18 x/c suggesting that drag divergence results from sonic flow moving aft of the crest but the pressure distribution of the NLR-1 airfoil at a Mach number of about 0.55 and an $\alpha_c = 5.6^o$ indicates that supercritical flow extends only to about 0.12 x/c which is upstream of the crest. This same pressure distribution of the NLR-1 airfoil indicates a steep pressure recovery terminating the supersonic field which suggests that drag divergence may be the result of wave drag. Therefore the FX69-H-098 airfoil has a higher normal-force coefficient at this drag divergence Mach number because it delays the sonic flow moving aft of the crest to a higher corrected angle of attack than the one required to develop significant wave drag on the NLR-1 airfoil. The section characteristics suggest that the corrected angles of attack for a drag divergence Mach number of 0.75 are about 0.2^o (crest = 0.27 x/c) and 1.4^o (crest = 0.28 x/c) for the FX69-H-098 and the NLR-1 airfoils respectively. A comparison of the pressure distribution of the FX69-H-098 airfoil at an $\alpha_c = -0.4$ at M = 0.74 with that of the NLR-1 airfoil at an $\alpha_c = -0.3$ at M = 0.77 suggests that the FX69-H-098 airfoil develops supercritical flow at a

lower corrected angle of attack. This same pressure distribution of the FX69-H-098 airfoil indicates that supercritical flow is present to about 0.31 x/c suggesting that the cause of drag divergence is the same as at M = 0.55 and the pressure distribution of the NLR-1 airfoil at an $\alpha_c = 1.2^o$ suggests that drag divergence is the result of wave drag similar to the lower Mach number case. For a drag divergence Mach number of 0.75, the NLR-1 airfoil now has a higher normal-force coefficient than the FX69-H-098 airfoil because the development of a supersonic field with a wave drag sufficient to cause drag divergence on the NLR-1 airfoil occurs at a corrected angle of attack about 1.2^o higher than the one at which sonic flow passes the crest on the FX69-H-098 airfoil. Section characteristics of the NACA 23012 airfoil indicate that the corrected angle of attack for a drag divergence Mach number of 0.55 is about 4.6^o (crest = 0.15 x/c). The pressure distribution for this airfoil at a Mach number of 0.54 at an $\alpha_c = 4.1^o$ indicates that supercritical flow is present at 0.15 x/c suggesting that the cause of drag divergence is the usual one. The normal-force coefficient of the FX69-H-098 airfoil is higher than that of this airfoil at a drag divergence Mach number of 0.55 because the FX69-H-098 airfoil delays the movement of sonic flow aft of its crest to an α_c about 2.2^o higher than that of the NACA 23012 airfoil. For a drag divergence Mach number of 0.75, the section characteristics of the NACA 23012 airfoil indicate that the corresponding α_c is about -0.8 (crest $\approx$ 0.25 x/c). The pressure distribution of this airfoil at a Mach number of 0.75 at an $\alpha_c = -0.4^o$ indicates that supercritical flow extends as far aft as about 0.37 x/c suggesting that the cause of drag divergence is the same as at M = 0.55. Thus the

normal-force coefficient of the FX69-H-098 airfoil at this drag divergence Mach number is higher than that for the NACA 23012 airfoil for the same reason it was higher at M = 0.55.

CONCLUSIONS

An investigation has been conducted in the Langley 6- by 28-inch transonic tunnel and the 6- by 19-inch transonic tunnel to determine the two-dimensional aerodynamic characteristics of several rotorcraft airfoils at Mach numbers from 0.35 to 0.90. The FX69-H-098, the BHC-540, and the NACA 0012 airfoils were tested in the 6- by 28-inch tunnel at Reynolds numbers (based on chord) from about 4.7×10^6 at M = 0.35 to about 9.3×10^6 at M = 0.90 and the FX69-H-098, the NLR-1, the BHC-540, and the NACA 23012 airfoils were tested in the 6- by 19-inch tunnel at Reynolds numbers from about 0.9×10^6 to 2.2×10^6 at the lowest and highest test Mach numbers respectively. Analysis of the test data has resulted in the following conclusions:

1. At Reynolds numbers near full scale, the FX69-H-098 airfoil was superior to both the BHC-540 and the NACA 0012 airfoils with respect to maximum normal-force coefficients at Mach numbers from about 0.40 to 0.55 (corresponding Reynolds numbers of about 5.0×10^6 and 7.0×10^6), to maximum normal-force-to-drag ratios at Mach numbers from about 0.40 to 0.65 ($R \approx 5.0 \times 10^6$ and 8.0×10^6), and to drag divergence Mach number at zero normal-force coefficient ($R \approx 9.0 \times 10^6$). For

the FX69-H-098 airfoil, the maximum normal-force coefficients were about 1.10 for Mach numbers from 0.40 to 0.54 and the maximum normal-force-to-drag ratios at Mach numbers from 0.40 to 0.65 ranged from a high of 120 at M = 0.50 to a low of 66 at M = 0.65. The drag divergence Mach number at zero normal-force coefficient of the FX69-H-098 airfoil was about 0.81. The trends of these three parameters of the FX69-H-098 airfoil relative to those of the BHC-540 airfoil were qualitatively the same as the trends determined by the data measured at Reynolds numbers of about 2.0×10^6 and lower.

2. At Reynolds numbers up to about 2.0×10^6, the FX69-H-098 airfoil was also superior to the NLR-1 airfoil with respect to maximum normal-force coefficients (M = 0.40 to 0.55) and to maximum normal-force-to-drag ratios (M = 0.40 to 0.65) but had a drag divergence Mach number at zero normal-force coefficient about 0.06 lower than the NLR-1 airfoil. For this same range of Reynolds numbers, the maximum normal-force-to-drag ratios at Mach numbers higher than 0.44 and the drag divergence Mach number at zero normal-force coefficient of the FX69-H-098 airfoil also exceeded those of the NACA 23012 airfoil but the maximum normal-force coefficients of the FX69-H-098 airfoil were less than those for

this five-digit-series airfoil at all Mach numbers up to 0.52. These trends in drag divergence Mach number and maximum normal-force-to-drag ratio should be qualitatively the same at higher Reynolds numbers.

3. The maximum normal-force coefficients of each of the airfoils at Mach numbers from 0.35 to 0.55 are believed to have been limited by a premature separation of the tunnel sidewall boundary layer in both test facilities. Therefore, the $c_{n_{max}}$ values presented in this report should be considered to be conservative values and qualitatively correct.

4. At Reynolds numbers near full scale, the pitching-moment coefficients about the aerodynamic center of the FX69-H-098 airfoil ranged from about -0.015 to -0.020 at subcritical Mach numbers ($M < 0.64$) and at supercritical Mach numbers they became more negative with increasing Mach number. The pitching-moment coefficients about the aerodynamic center of the BHC-540 and the NACA 0012 airfoils were about zero for all Mach numbers at near full scale Reynolds numbers. The trends of these pitching-moment coefficients of the FX69-H-098 and the BHC-540 airfoils are consistent with the trends determined by the data at Reynolds numbers of about 2.0×10^6 and less.

5. At Reynolds numbers up to about 2.0×10^6, the pitching-moment coefficients about the aerodynamic center of the FX69-H-098 airfoil were more negative at all Mach numbers than those of the NLR-1 and the NACA 23012 airfoils. These trends would be expected to be qualitatively the same at higher Reynolds numbers.

REFERENCES

1. Bingham, Gene J.: An Analytical Evaluation of Airfoil Sections for Helicopter Rotor Applications. NASA TN D-7796, 1975.
2. Abbott, Ira H.; von Doenhoff, Albert E.; and Stivers, Louis S., Jr.: Summary of Airfoil Data. NACA Rep. 824, 1945.
3. Wortmann, F. X.; and Drees, Jan M.: Design of Airfoils for Rotors. CAL/AVLABS Symposium Proceedings: Aerodynamics of Rotary Wing and V/STOL Aircraft, Vol. I - Rotor/Propeller Aerodynamics, Rotor Noise, June 18-20, 1969.
4. Kemp, Larry D.: An Analytical Study for the Design of Advanced Rotor Airfoils. NASA CR-112297, 1973.
5. Ladson, Charles L.: Description and Calibration of the Langley 6- By 28-Inch Transonic Tunnel. NASA TN D-8070, 1975.
6. Ladson, Charles L.: Description and Calibration of the Langley 6- By 19-Inch Transonic Tunnel. NASA TN D-7182, 1973.
7. Braslow, Albert L.; and Knox, Eugene C.: Simplified Method for Determination of Critical Height of Distributed Roughness Particles for Boundary-Layer Transition at Mach Numbers from 0 to 5. NACA TN-4363, 1958.
8. Baals, Donald D.; and Mourhess, Mary J.: Numerical Evaluation of the Wake-Survey Equations for Subsonic Flow Including the Effect of Energy Addition. NACA WRL-5, 1945.
9. Davis, Don D., Jr.; and Moore, Dewey: Analytical Study of Blockage-and-Lift-Interference Corrections for Slotted Tunnels Obtained by the Substitution of an Equivalent Homogeneous Boundary for the Discrete Slots. NACA RM L53E07b, 1953.

10. Graham, Donald J.; Nitzberg, Gerald E.; and Olson, Robert N.: A Systematic Investigation of Pressure Distributions at High Speeds Over Five Representative NACA Low-Drag and Conventional Airfoil Sections. NACA Report 832, 1945.

11. Schlichting, Hermann: (J. Kestin, transl.) Boundary Layer Theory. Sixth ed. McGraw-Hill Book Co., Inc., 1968.

12. Loftin, Laurence K., Jr.; and Smith, Hamilton A.: Aerodynamic Characteristics of 15 NACA Airfoils at Seven Reynolds Numbers From 0.7×10^6 to 9.0×10^6. NACA TN 1945, 1949.

TABLE I.- DESIGN COORDINATES FOR THE FX69-H-098 AIRFOIL

(Stations and ordinates given in percent airfoil chord)

Stations	Upper Surface	Stations	Lower Surface
0.00	0.00	0.00	0.00
.30	.79	.30	-.55
.60	1.14	.60	-.76
1.00	1.51	1.00	-.96
1.50	1.89	1.50	-1.15
2.50	2.51	2.50	-1.43
3.50	3.03	3.50	-1.65
4.50	3.49	4.50	-1.82
6.00	4.08	6.00	-2.03
7.50	4.58	7.50	-2.20
10.00	5.24	10.00	-2.44
12.50	5.73	12.50	-2.64
15.00	6.08	15.00	-2.80
17.50	6.33	17.50	-2.94
20.00	6.50	20.00	-3.05
25.00	6.67	25.00	-3.19
30.00	6.64	30.00	-3.25
35.00	6.52	35.00	-3.23
40.00	6.33	40.00	-3.18
45.00	6.10	45.00	-3.10
50.00	5.80	50.00	-2.99
55.00	5.45	55.00	-2.85
60.00	5.05	60.00	-2.69
65.00	4.59	65.00	-2.50
70.00	4.08	70.00	-2.28
75.00	3.53	75.00	-2.04
80.00	2.96	80.00	-1.78
85.00	2.33	85.00	-1.48
90.00	1.62	90.00	-1.15
95.00	.85	95.00	-.73
99.50	.17	99.50	-.20
100.00	.09	100.00	-.11

TABLE II.- DESIGN COORDINATES FOR THE BHC-540 AIRFOIL

[Stations and ordinates given in percent airfoil chord]

Stations	Upper surface	Stations	Lower surface
0.00	0.00	0.00	0.00
.20	.68	.20	-.68
.58	1.16	.58	-1.16
1.17	1.61	1.17	-1.61
1.95	2.03	1.95	-2.03
2.72	2.37	2.72	-2.37
3.89	2.78	3.89	-2.78
5.45	3.18	5.45	-3.18
7.00	3.51	7.00	-3.51
8.56	3.77	8.56	-3.77
10.11	3.98	10.11	-3.98
12.45	4.23	12.45	-4.23
14.78	4.42	14.78	-4.42
19.45	4.62	19.45	-4.62
27.22	4.63	27.22	-4.63
31.11	4.51	31.11	-4.51
35.00	4.34	35.00	-4.34
40.00	4.05	40.00	-4.05
45.00	3.72	45.00	-3.72
50.00	3.39	50.00	-3.39
55.00	3.06	55.00	-3.06
60.00	2.73	60.00	-2.73
65.00	2.40	65.00	-2.40
70.00	2.07	70.00	-2.07
75.00	1.75	75.00	-1.75
80.00	1.42	80.00	-1.42
85.00	1.09	85.00	-1.09
90.00	.76	90.00	-.76
95.00	.43	95.00	-.43
100.00	.10	100.00	-.10

TABLE III.- DESIGN COORDINATES FOR THE NACA 0012 AIRFOIL

[Stations and ordinates given in percent airfoil chord]

Stations	Upper surface	Stations	Lower surface
0.00	0.00	0.00	0.00
.25	.87	.25	-.87
.50	1.22	.50	-1.22
1.00	1.70	1.00	-1.70
1.50	2.06	1.50	-2.06
2.50	2.61	2.50	-2.61
3.50	3.04	3.50	-3.04
4.50	3.40	4.50	-3.40
6.00	3.84	6.00	-3.84
7.50	4.20	7.50	-4.20
10.00	4.68	10.00	-4.68
12.00	4.99	12.00	-4.99
15.00	5.35	15.00	-5.35
17.00	5.53	17.00	-5.53
20.00	5.74	20.00	-5.74
25.00	5.94	25.00	-5.94
30.00	6.00	30.00	-6.00
35.00	5.95	35.00	-5.95
40.00	5.80	40.00	-5.80
45.00	5.58	45.00	-5.58
50.00	5.29	50.00	-5.29
55.00	4.95	55.00	-4.95
60.00	4.56	60.00	-4.56
65.00	4.13	65.00	-4.13
70.00	3.66	70.00	-3.66
75.00	3.16	75.00	-3.16
80.00	2.62	80.00	-2.62
85.00	2.05	85.00	-2.05
90.00	1.45	90.00	-1.45
95.00	0.81	95.00	-0.81
99.00	0.27	99.00	-0.27
100.00	0.13	100.00	-0.13

REPRODUCIBILITY OF THE
ORIGINAL PAGE IS POOR

TABLE IV.- DESIGN COORDINATES FOR THE NLR-1 AIRFOIL

[Stations and ordinates given in percent airfoil chord]

Stations	Upper surface	Stations	Lower surface
0.00	0.00	0.00	0.00
.42	1.02	.27	-.52
.98	1.51	.45	-.64
1.75	2.01	.99	-.86
2.73	2.52	1.75	-1.07
3.96	3.02	2.77	-1.29
5.22	3.44	3.94	-1.48
5.97	3.65	5.28	-1.66
7.67	4.06	6.16	-1.76
8.98	4.31	7.73	-1.91
10.01	4.48	8.78	-2.01
12.63	4.73	10.66	-2.16
14.94	4.92	12.78	-2.31
18.73	5.15	15.04	-2.46
22.74	5.32	18.87	-2.66
27.19	5.44	22.83	-2.82
31.72	5.50	25.66	-2.91
41.23	5.48	31.70	-3.04
47.98	5.35	41.31	-3.12
54.75	5.13	48.13	-3.08
61.26	4.83	54.72	-2.96
67.76	4.44	61.49	-2.76
73.98	3.91	67.81	-2.51
79.87	3.05	74.11	-2.24
85.18	2.20	79.94	-1.95
90.96	1.26	85.30	-1.65
97.41	.35	90.90	-1.25
98.68	.16	97.35	-.35
100.00	.00	98.68	-.14
		100.00	.00

TABLE V.- DESIGN COORDINATES FOR THE NACA 23012 AIRFOIL

[Stations and ordinates given in percent airfoil chord]

Stations	Upper Surface	Stations	Lower Surface
0.00	0.00	0.00	0.00
.55	1.93	.50	-0.76
.76	2.19	.84	-1.03
.98	2.42	1.15	-1.21
1.44	2.84	1.45	-1.35
2.40	3.55	2.56	-1.75
3.40	4.15	3.60	-2.00
4.69	4.78	4.60	-2.19
6.26	5.40	6.05	-2.43
7.58	5.83	7.48	-2.62
10.78	6.59	10.06	-2.95
11.84	6.78	12.16	-3.19
15.00	7.18	15.00	-3.51
17.08	7.35	16.93	-3.70
20.13	7.50	19.87	-3.97
25.13	7.60	24.87	-4.28
30.13	7.55	29.87	-4.45
35.13	7.38	34.87	-4.51
40.13	7.13	39.87	-4.48
45.12	6.79	44.88	-4.37
50.12	6.40	49.88	-4.19
55.11	5.95	54.89	-3.96
60.10	5.45	59.90	-3.68
65.09	4.90	64.91	-3.36
70.08	4.33	69.92	-3.00
75.07	3.71	74.93	-2.61
80.06	3.06	79.94	-2.18
85.05	2.38	84.96	-1.72
90.03	1.67	89.97	-1.23
95.02	0.92	94.98	-0.70
98.01	0.45	97.99	-0.36
100.00	0.13	100.00	-0.13

TABLE VI.- STATIC PRESSURE ORIFICE LOCATIONS FOR THE FX69-H-098 AIRFOIL.

[Locations given in percent airfoil chord.]

Upper Surface	Lower Surface
Station	Station
1.15	1.29
2.42	2.45
4.90	4.97
7.50	7.48
9.97	10.00
15.00	15.00
20.04	20.01
25.03	25.03
30.03	30.05
35.09	35.04
40.11	40.05
45.08	45.07
50.04	50.04
55.06	55.07
60.04	60.07
65.03	65.05
70.05	70.05
75.07	75.05
80.03	80.08
85.09	85.08
90.07	90.07
95.05	95.10

TABLE VII.- STATIC PRESSURE ORIFICE LOCATIONS FOR THE BHC-540 AIRFOIL

[Locations given in percent airfoil chord]

Upper surface	Lower surface
Station	Station
1.23	1.18
2.45	2.45
4.90	4.91
7.47	7.40
9.96	9.94
15.00	15.02
20.00	19.98
25.01	25.01
30.02	29.96
35.03	35.03
40.01	40.10
45.03	45.02
50.03	50.02
55.01	55.02
60.00	60.01
65.01	65.02
70.01	70.02
75.03	75.02
80.03	80.02
85.04	85.03
90.03	90.02

TABLE VIII.- STATIC PRESSURE ORIFICE LOCATIONS FOR THE NACA 0012 AIRFOIL

[Locations given in percent airfoil chord]

Upper surface	Lower surface
Station	Station
0.00	0.00
1.22	1.20
2.55	2.48
4.93	4.97
7.56	7.53
10.14	10.04
15.01	15.08
19.95	20.03
24.93	25.00
29.94	29.99
34.97	34.97
39.94	39.95
44.95	44.97
49.94	49.92
54.94	54.90
59.91	59.89
64.87	64.88
69.92	69.87
74.89	74.90
79.90	79.87
84.90	84.82
89.85	89.83
	94.80
97.30	97.38

TABLE IX.- STATIC PRESSURE ORIFICE LOCATIONS FOR THE NLR-1 AIRFOIL

[Locations given in percent airfoil chord]

Upper surface	Lower surface
Station	Station
1.25	1.22
2.51	2.43
4.84	4.93
7.37	7.45
9.92	9.97
14.94	14.97
19.94	19.97
24.92	24.98
29.95	29.98
34.94	35.98
39.96	39.98
44.94	44.97
49.97	49.98
54.97	54.99
59.96	59.98
64.99	65.00
70.00	70.01
75.04	75.01
80.03	80.03
85.08	85.03
90.06	90.03
95.05	95.03

TABLE X.- STATIC PRESSURE ORIFICE LOCATIONS FOR THE NACA 23012 AIRFOIL

[Locations given in percent airfoil chord]

Upper surface	Lower surface
Station	Station
1.24	1.23
2.53	2.44
5.12	4.95
7.52	7.46
10.17	9.98
14.98	14.97
19.99	19.98
24.98	24.99
30.03	30.01
35.00	35.02
40.01	40.02
45.01	45.02
50.03	50.04
55.02	55.02
60.01	60.02
65.02	65.02
70.03	70.03
75.01	75.03
80.05	80.03
85.04	85.05
90.05	90.03
95.05	95.03

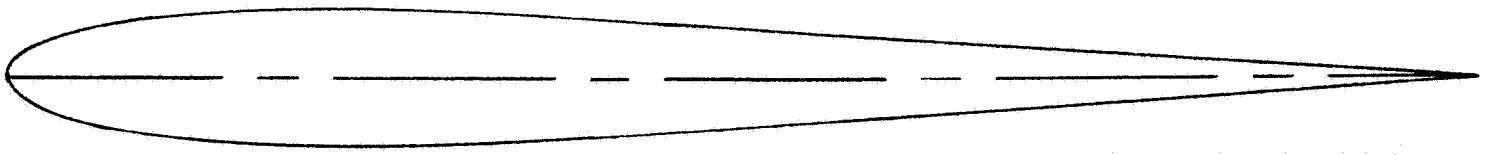

BHC – 540

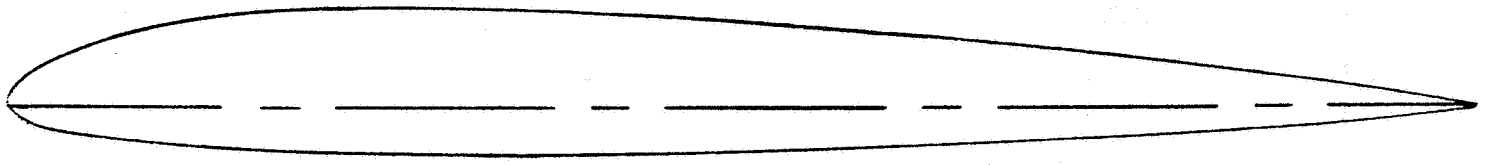

FX 69 – H-098

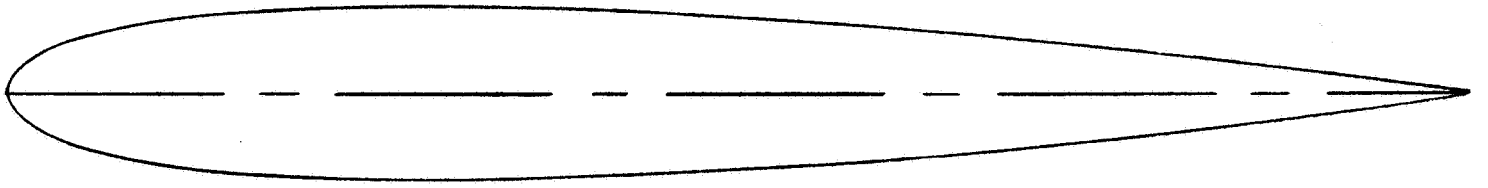

NACA 0012

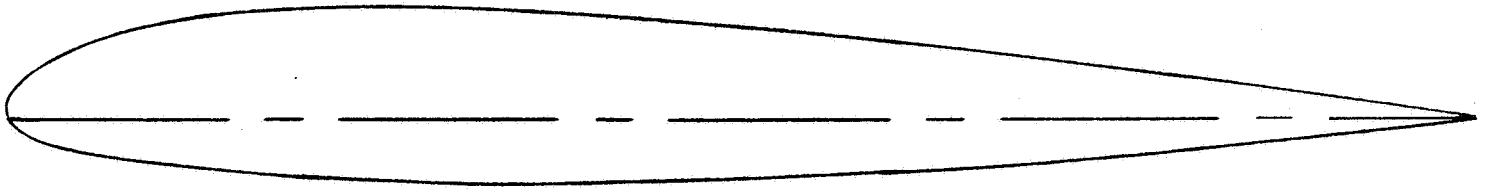

NACA 23012

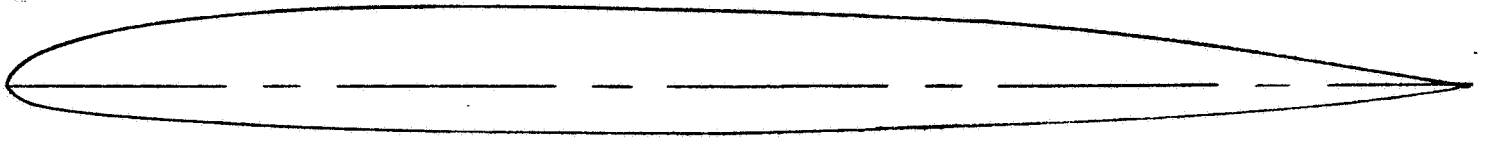

NLR – 1

Figure 1. - Airfoil profiles.

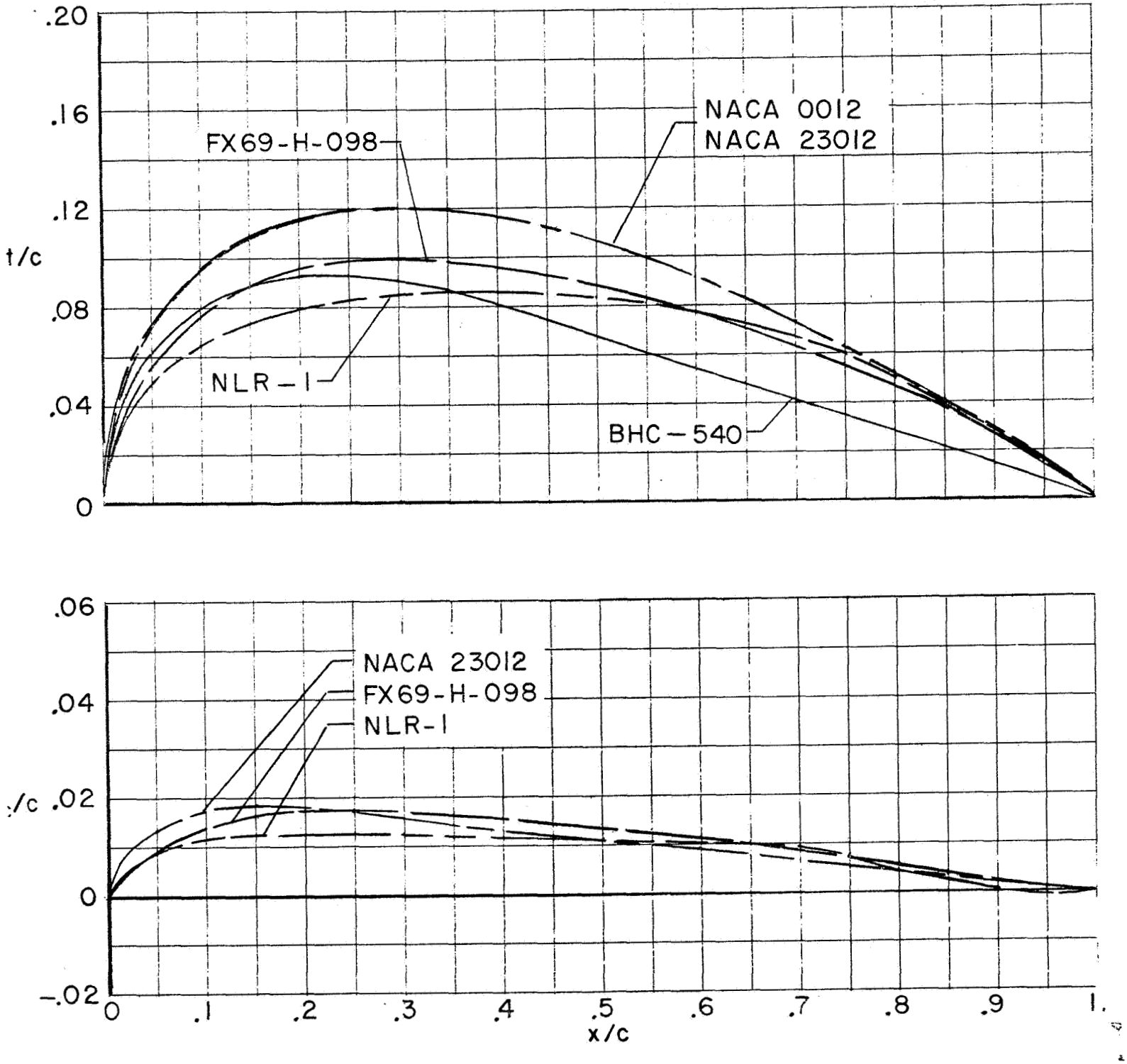

Figure 2. - Airfoil thickness distributions and mean lines.

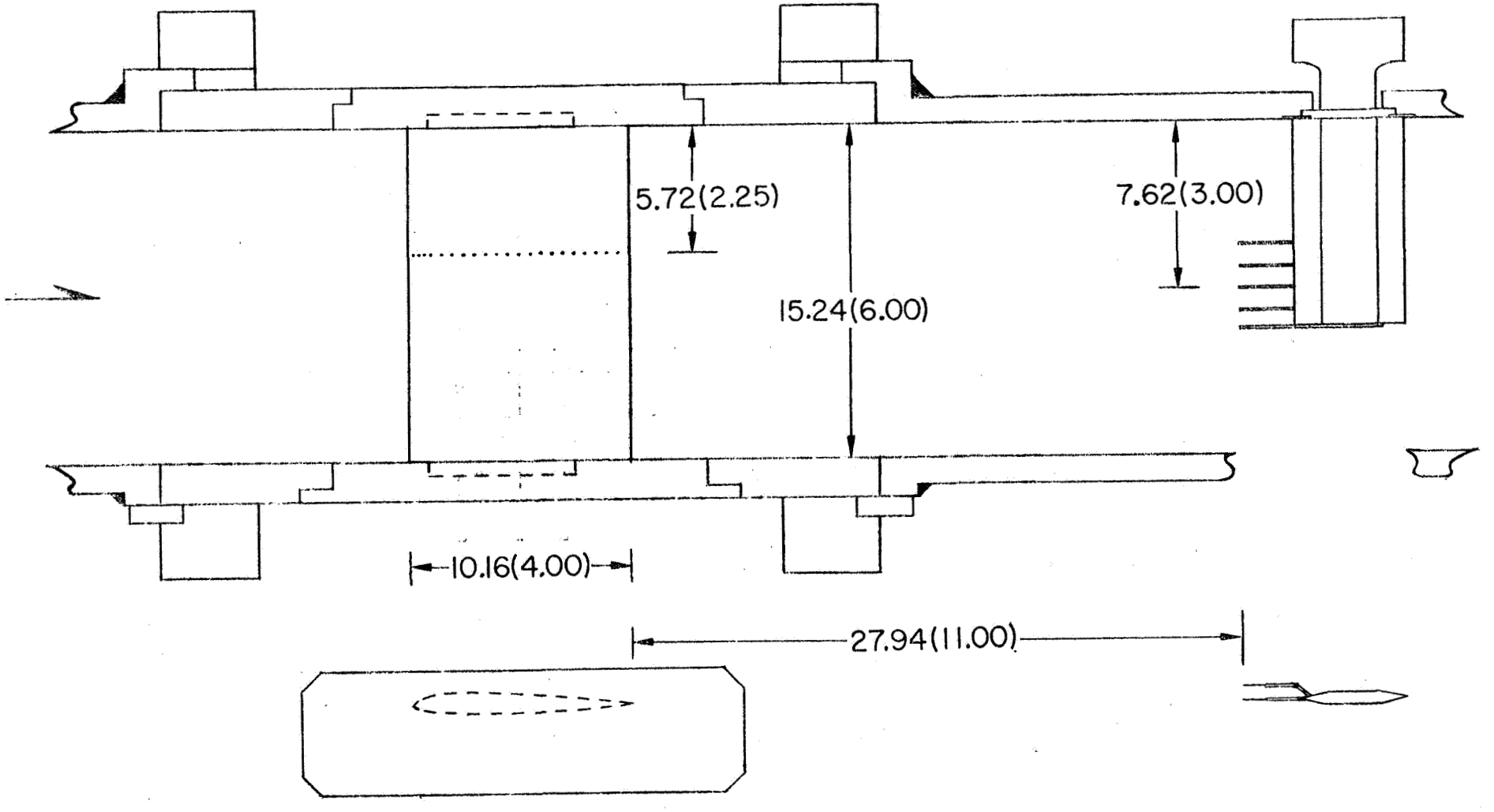

Figure 3. - Model and wake-survey probe installation in the Langley 6 x 28-inch transonic tunnel. All dimensions are in centimeters (inches).

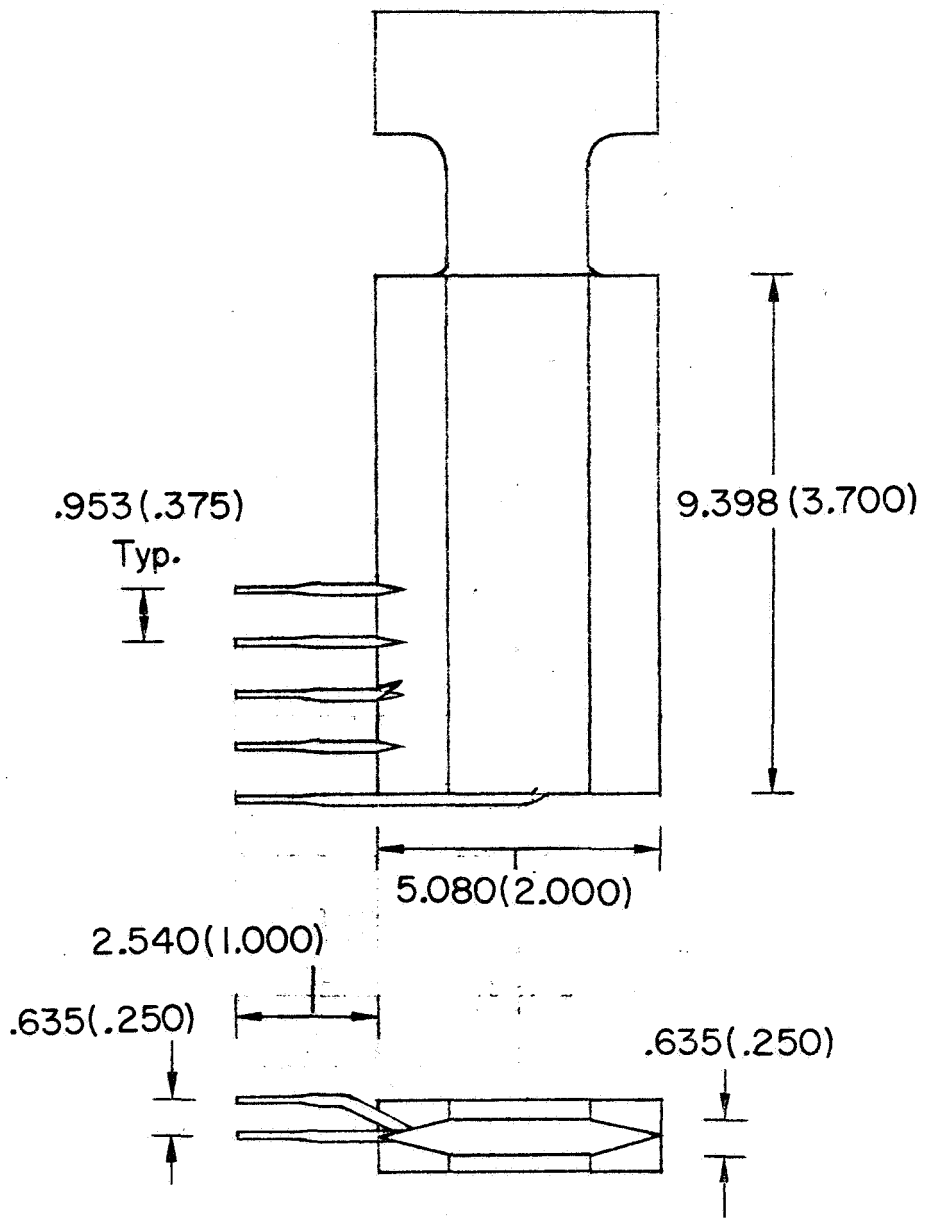

Figure 4. - Wake-survey probe used in the 6 x 28-inch transonic tunnel. All dimensions are in centimeters (inches).

REPRODUCIBILITY OF THE
ORIGINAL PAGE IS POOR

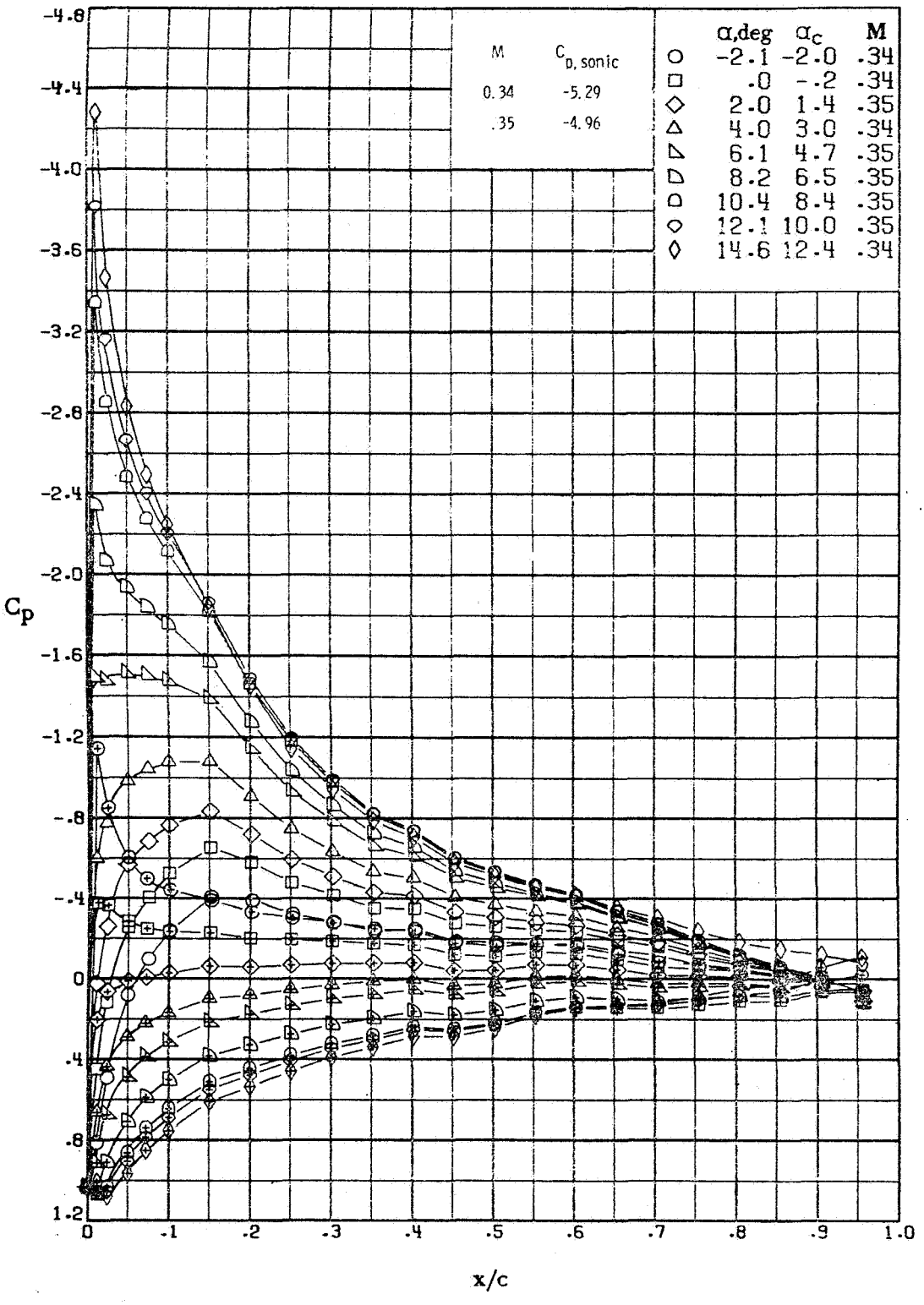

(a) $M \approx 0.35$; $R = 4.7 \times 10^6$.

Figure 5. - Selected pressure distributions of the FX69-H-098 airfoil measured in the Langley 6-x 28-inch transonic tunnel. Model smooth.

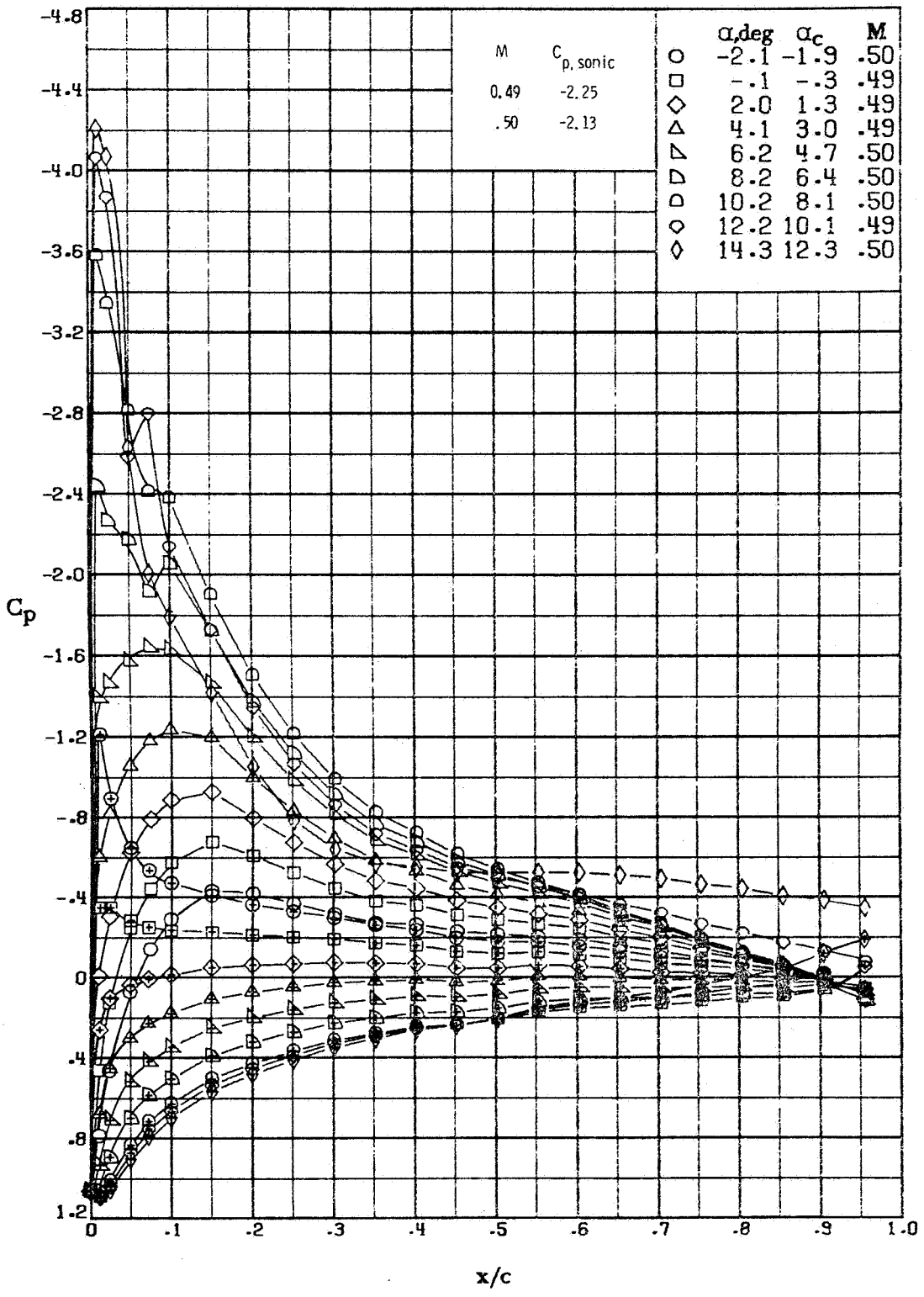

(b) $M \approx 0.50$; $R = 6.5 \times 10^6$.

Figure 5.- Concluded.

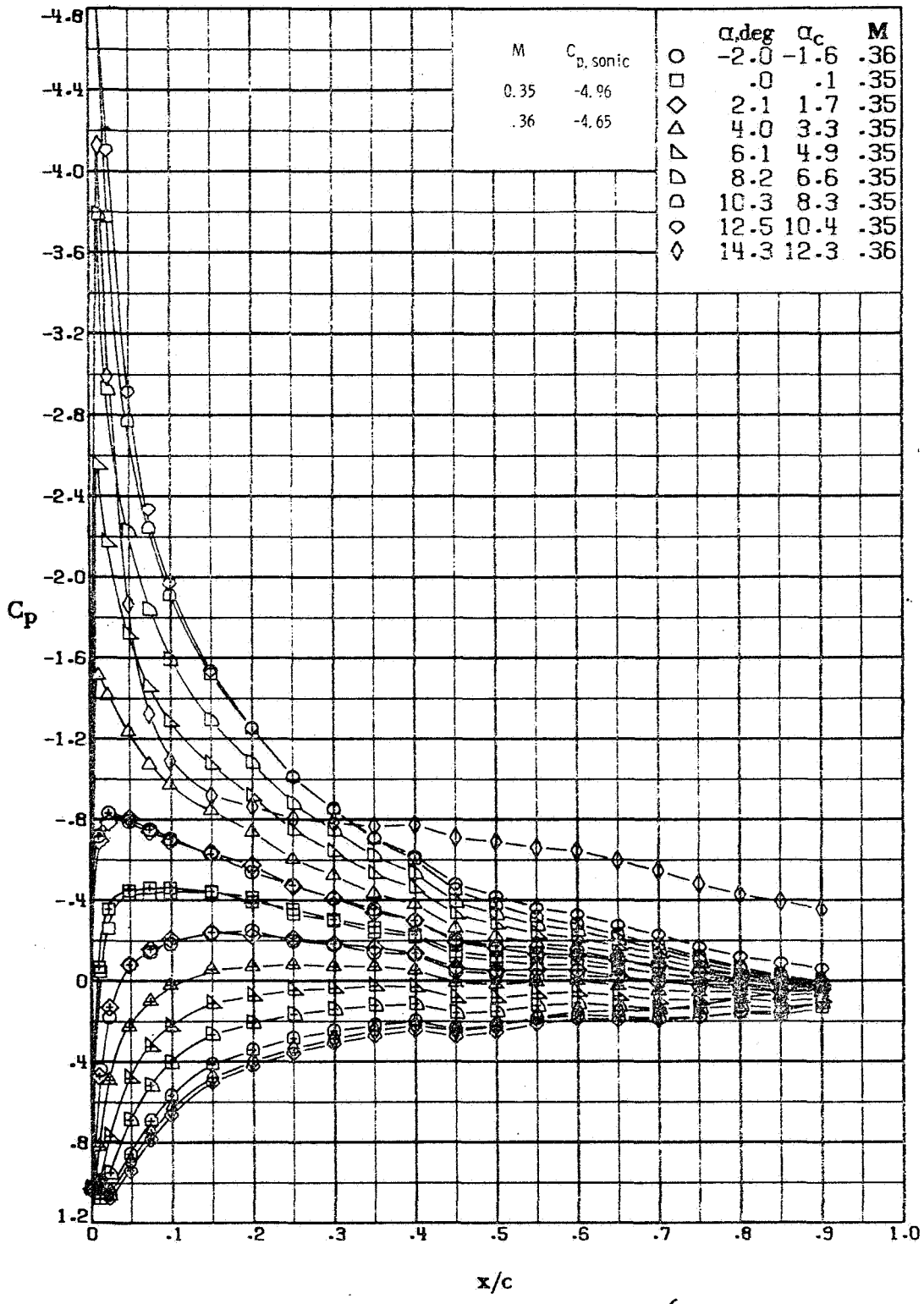

(a) $M \approx 0.35$; $R = 4.7 \times 10^6$.

Figure 6. - Selected pressure distributions of the BHC-540 airfoil measured in the Langley 6-x 28-inch transonic tunnel. Model smooth.

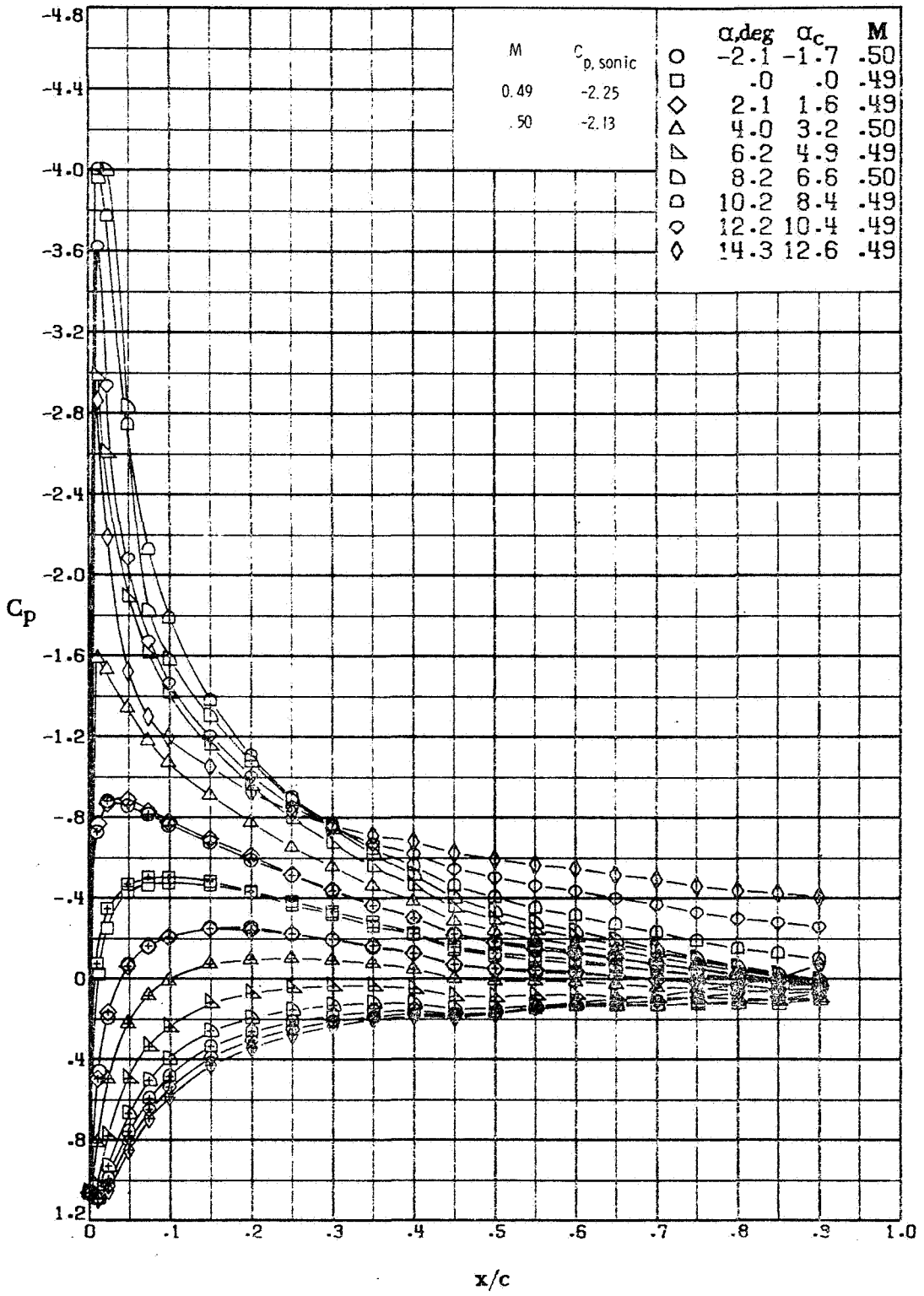

(b) $M \approx 0.49$; $R = 6.5 \times 10^6$.

Figure 6.- Concluded.

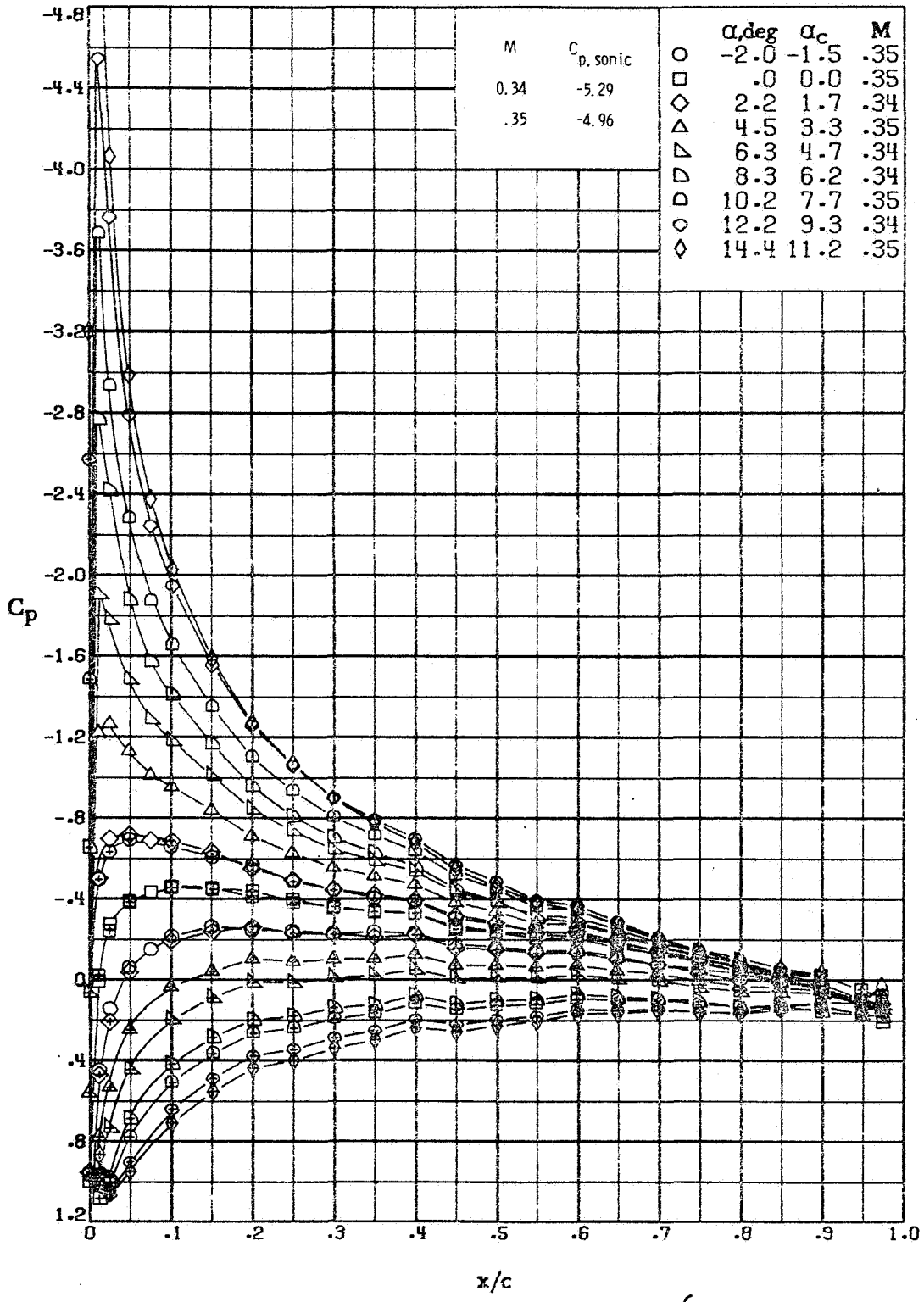

(a) $M \approx 0.35$; $R = 4.9 \times 10^6$.

Figure 7.- Selected pressure distributions of the NACA 0012 airfoil measured in the Langley 6-x 28-inch transonic tunnel. Model smooth.

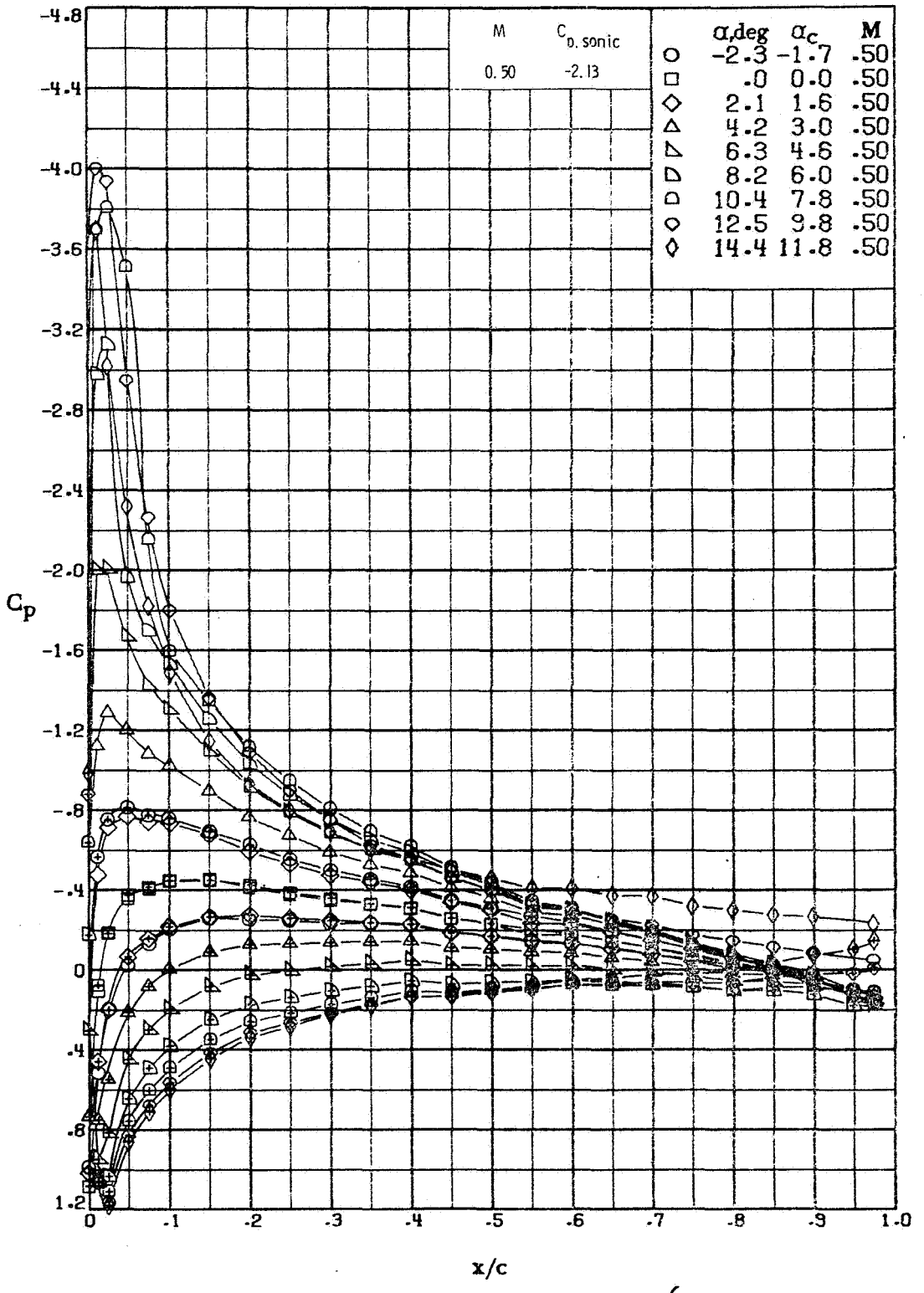

(b) $M \approx 0.50$; $R = 6.7 \times 10^6$.

Figure 7.- Concluded.

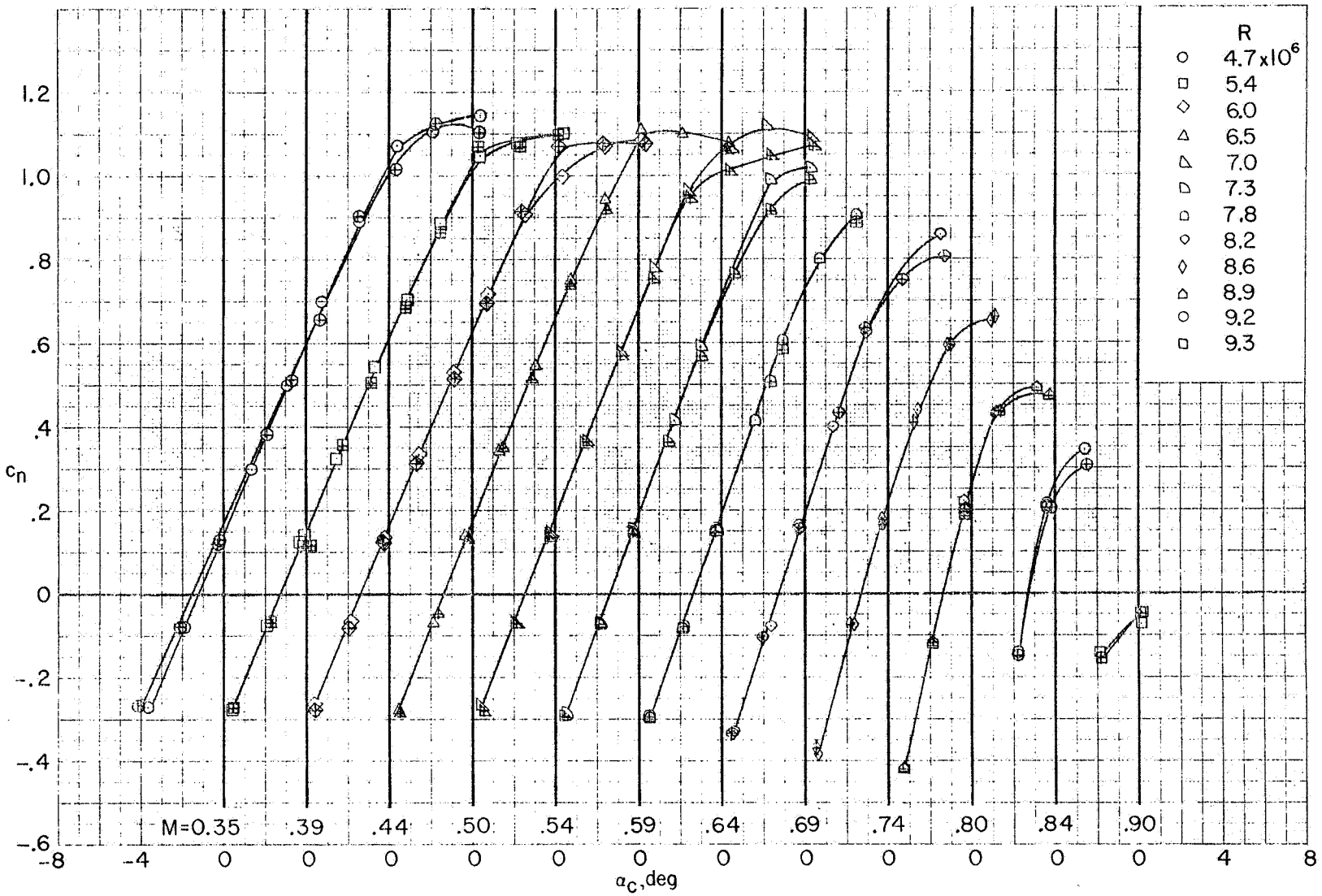

(a) Section normal-force coefficients.

Figure 8. - Aerodynamic characteristics of the FX69-H 098 airfoil measured in the Langley 6 x 28 inch transonic tunnel. Plain symbols indicate model smooth; centered symbols, transition fixed.

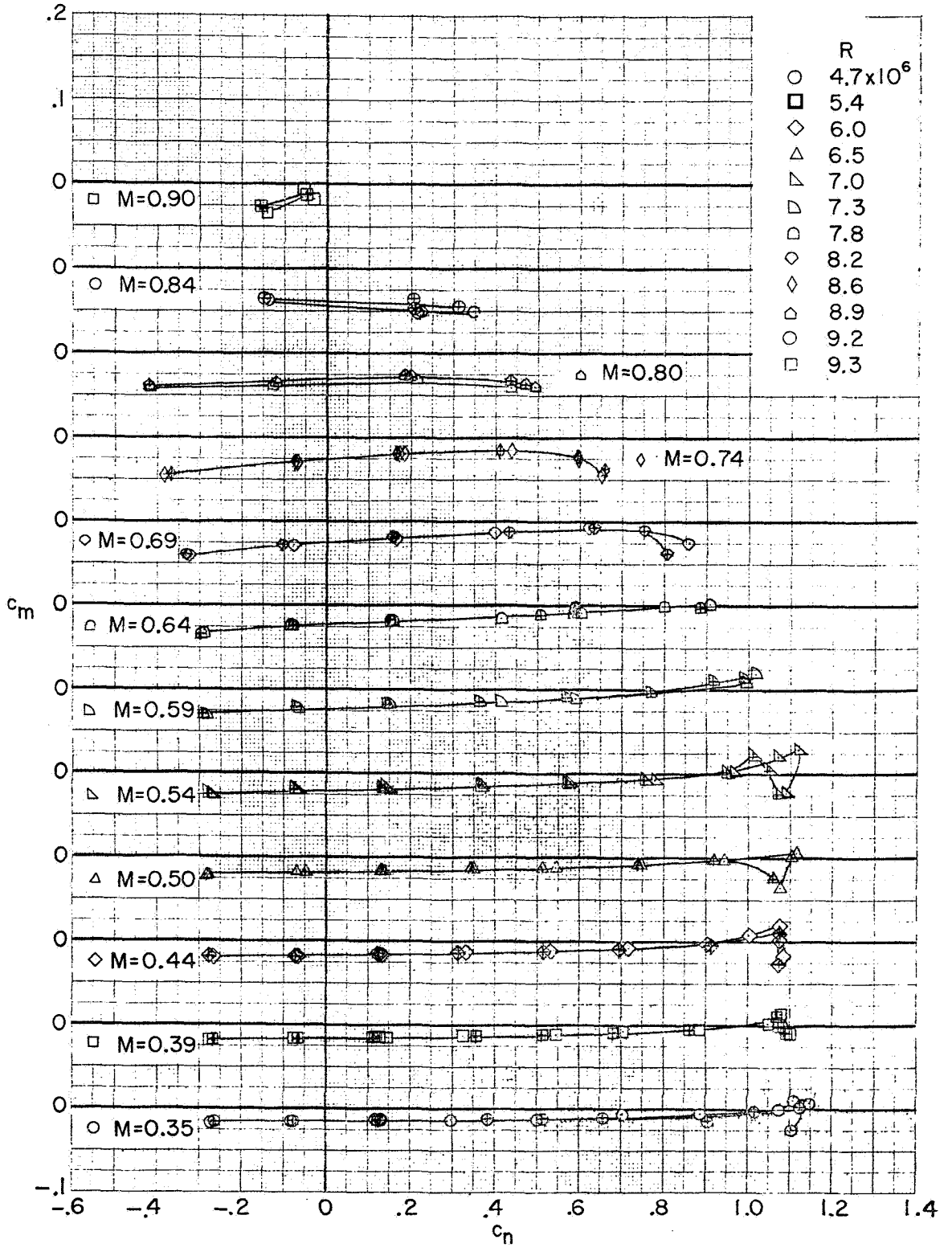

(b) Section pitching-moment coefficients.

Figure 8. - Continued.

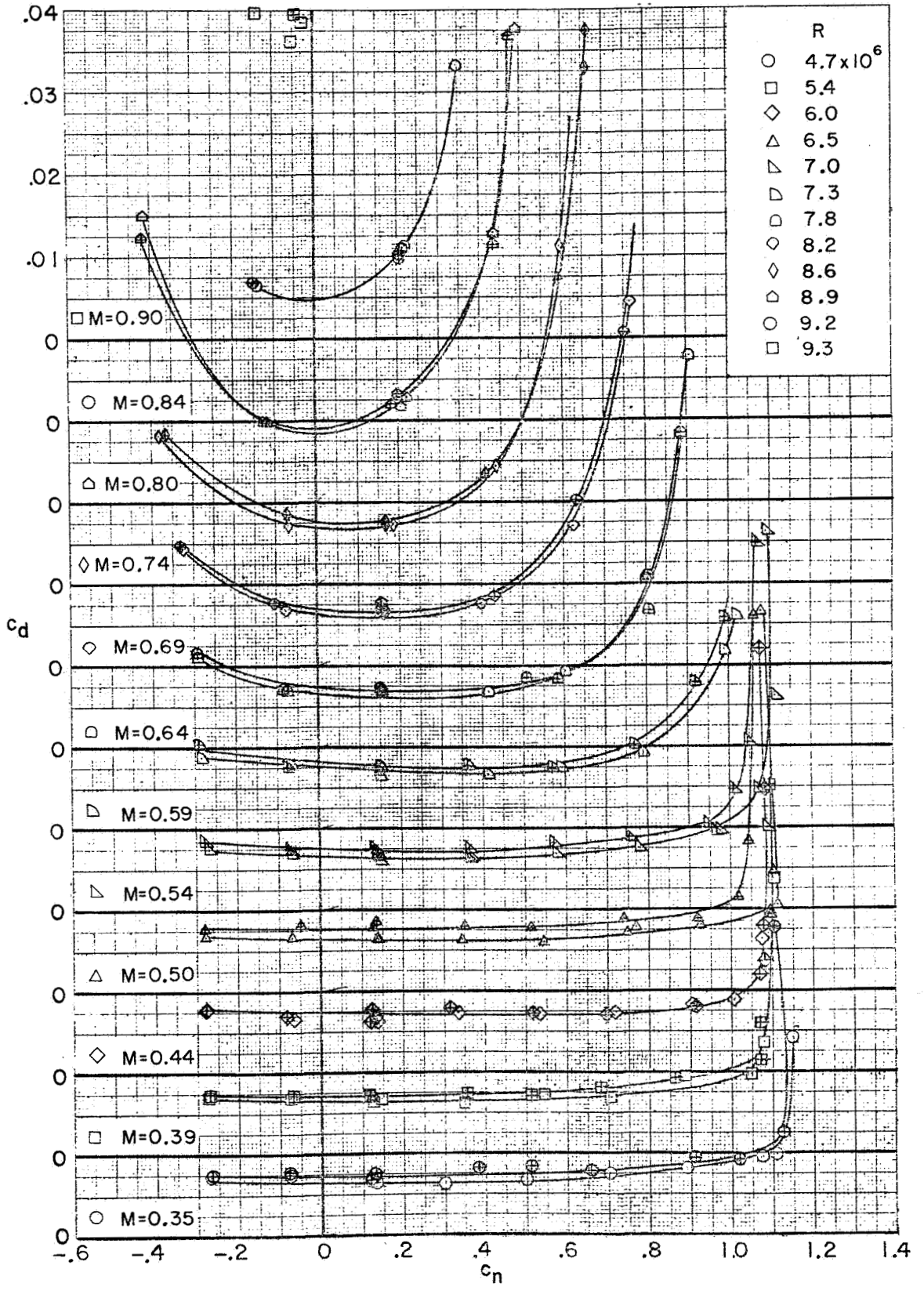

(c) Section drag coefficients.

Figure 8. - Concluded.

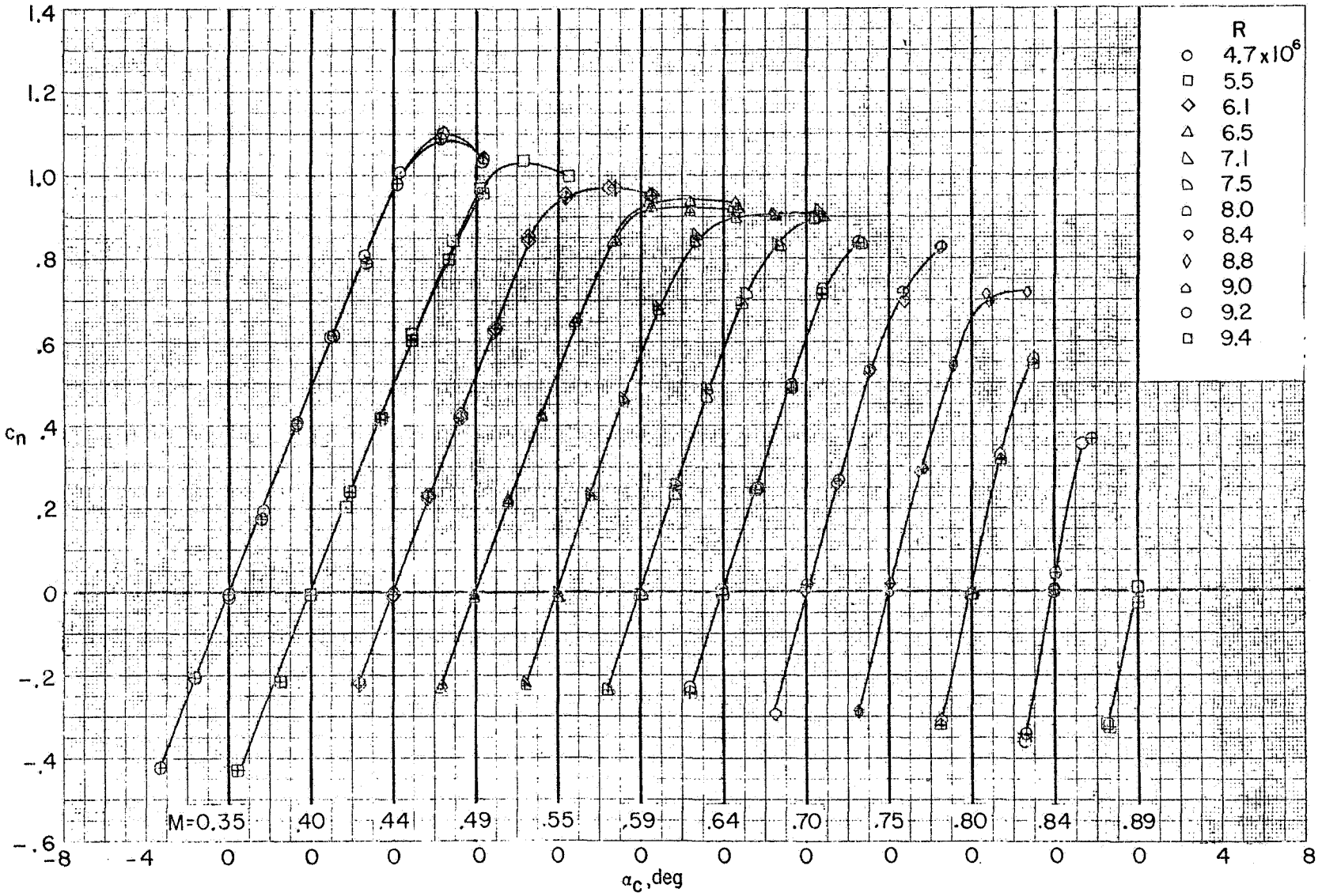

(a) Section normal-force coefficients.

Figure 9. - Aerodynamic characteristics of the BHC-540 airfoil measured in the Langley 6 x 28-inch transonic tunnel. Plain symbols indicate model smooth; centered symbols, transition fixed.

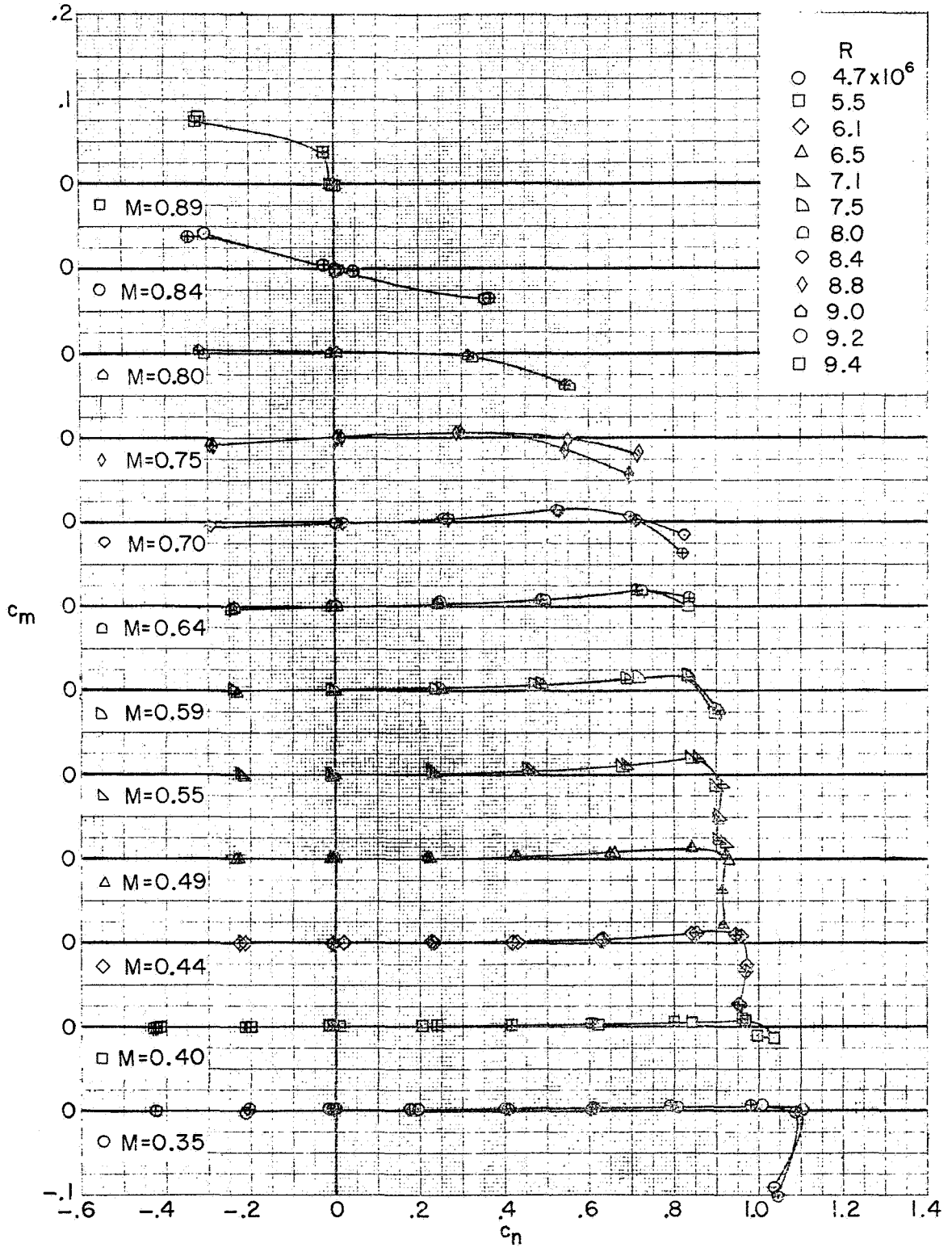

(b) Section pitching-moment coefficients.

Figure 9.- Continued.

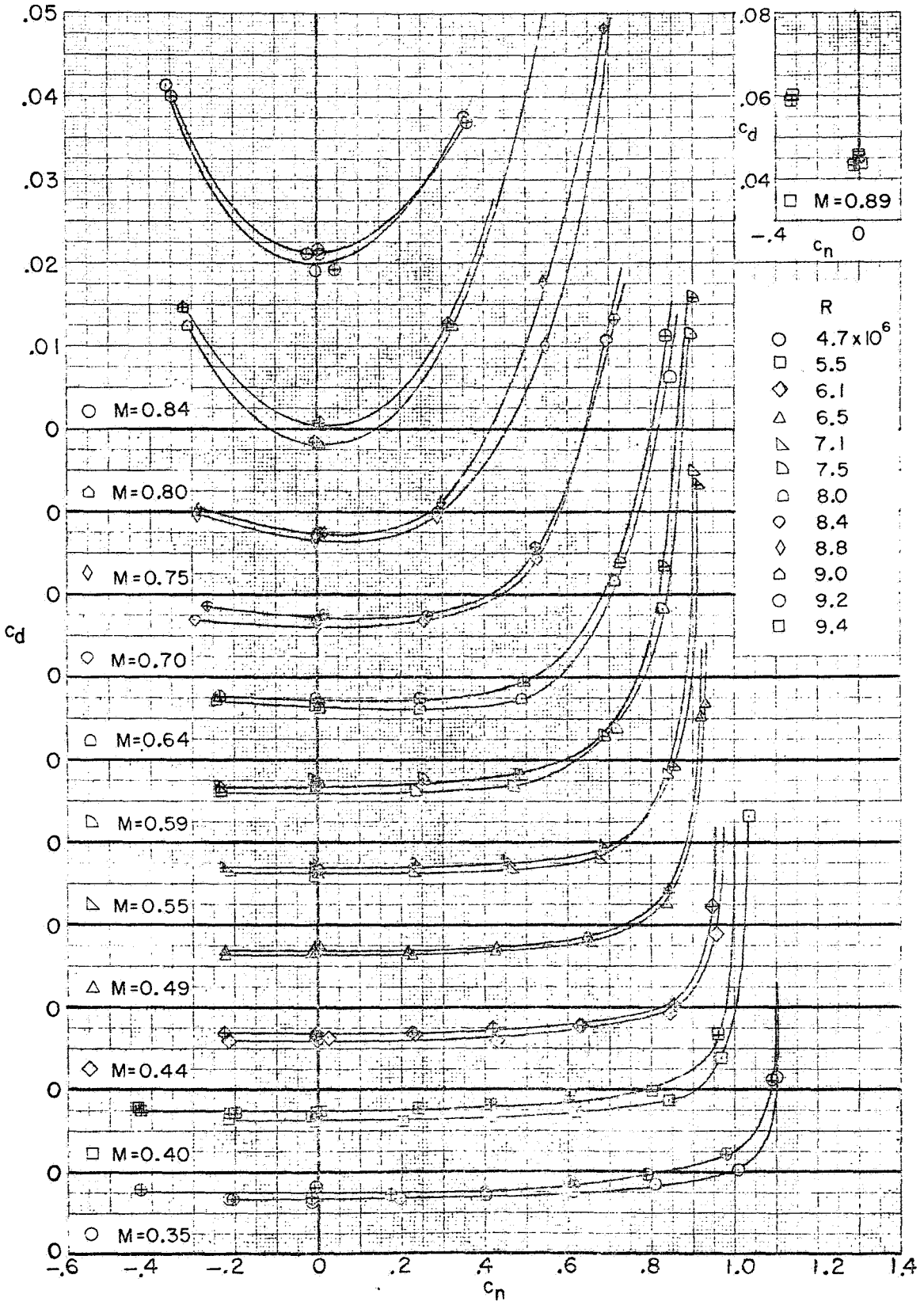

(c) Section drag coefficients.

Figure 9.- Concluded.

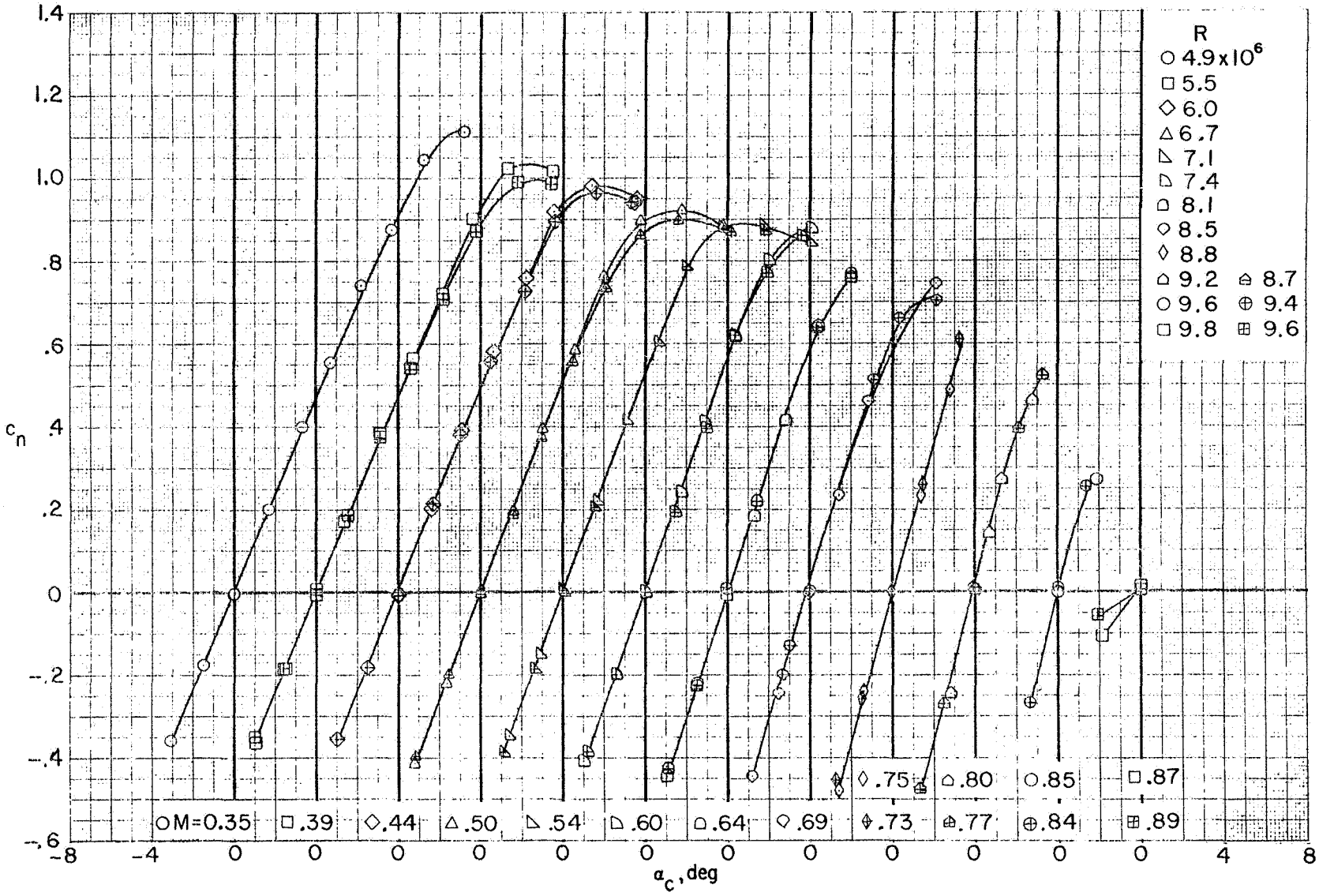

(a) Section normal-force coefficient.

Figure 10.- Aerodynamic characteristics of the NACA 0012 airfoil measured in the Langley 6 x 28-inch transonic tunnel. Plain symbols indicate model smooth; centered symbols transition fixed.

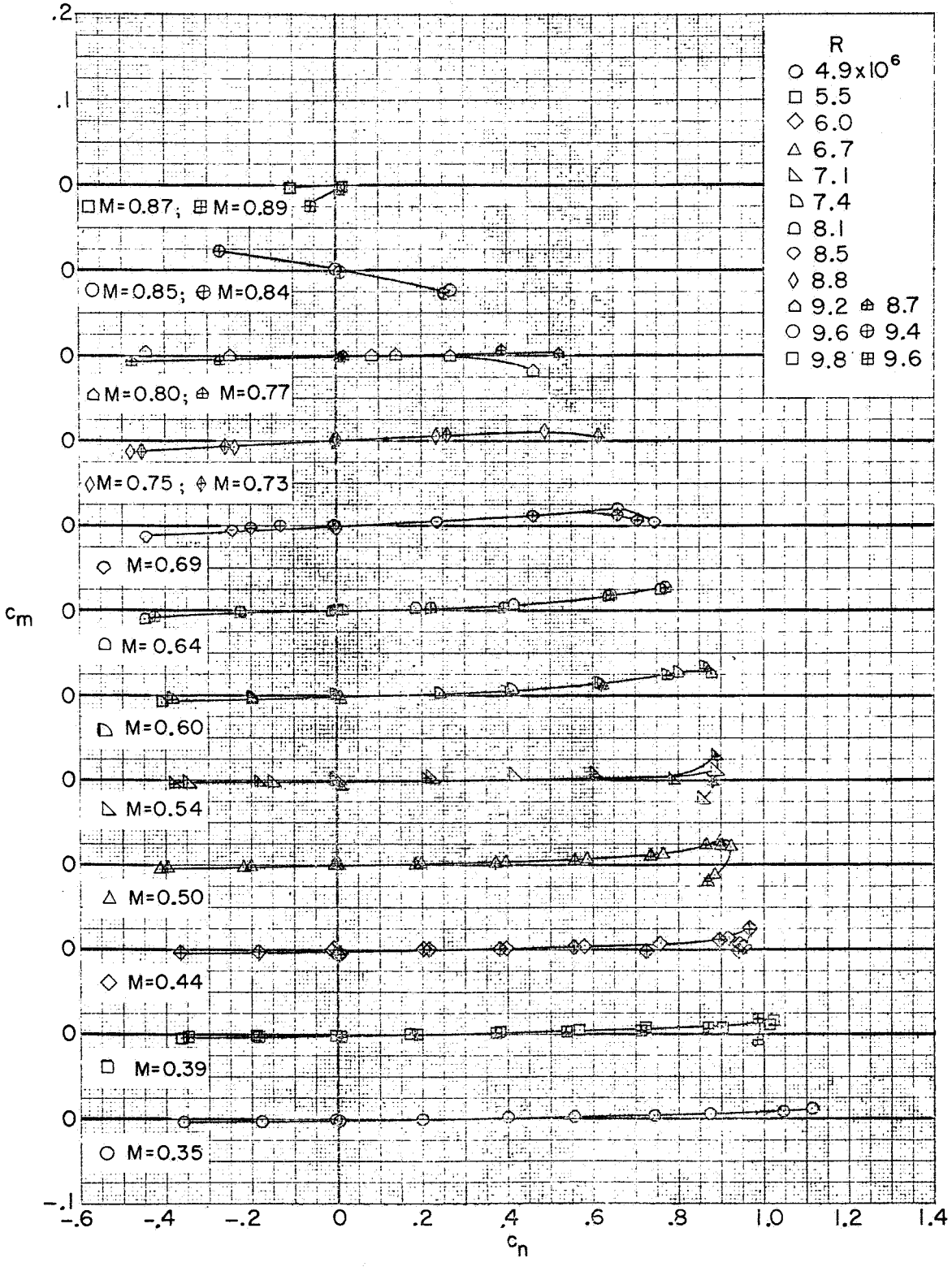

(b) Section pitching-moment coefficients.

Figure 10.- Continued.

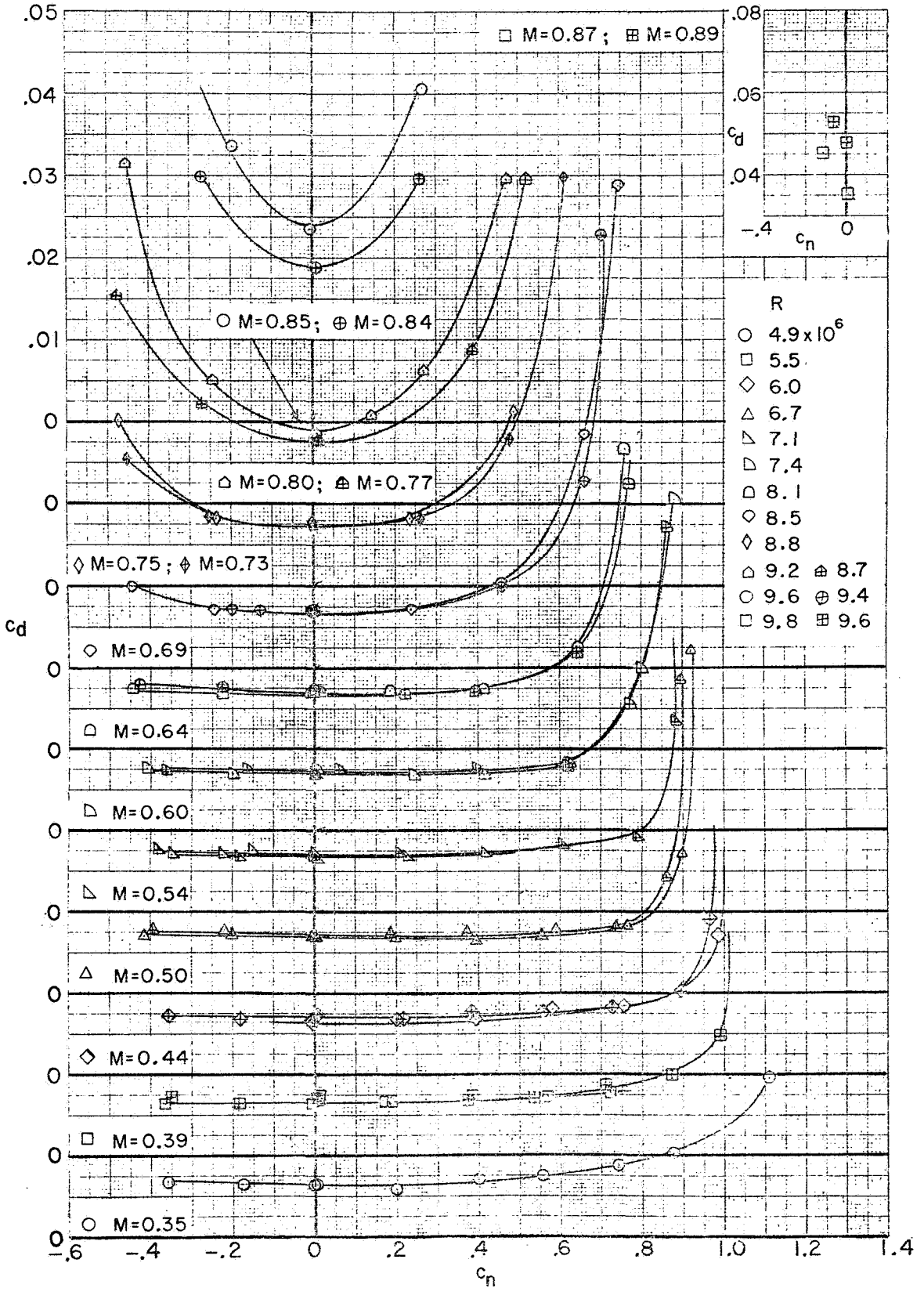

(c) Section drag coefficients.

Figure 10. - Concluded.

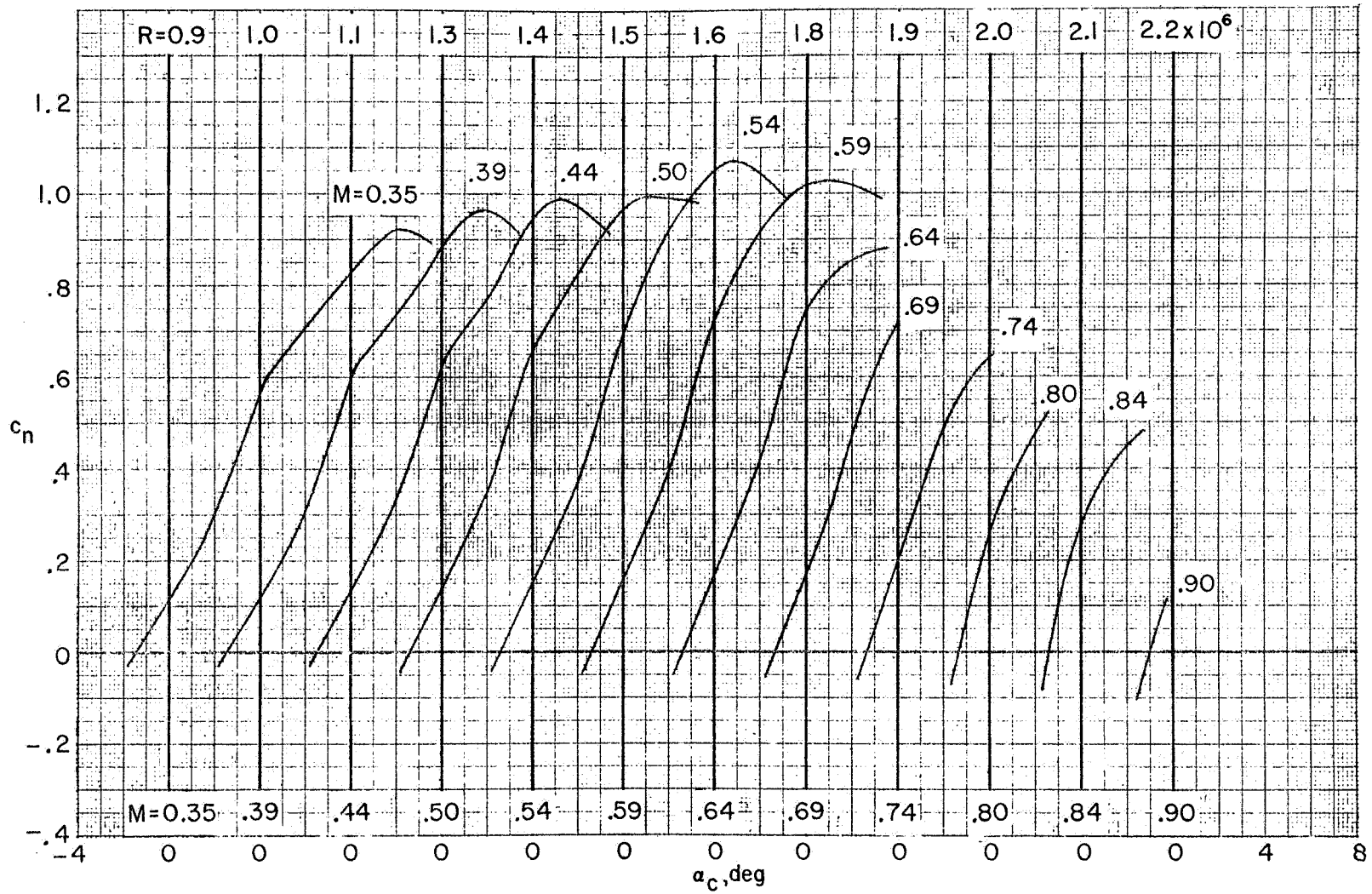

(a) Section normal-force coefficients.

Figure 11.- Aerodynamic characteristics of the FX69-H-098 airfoil measured in the Langley 6 x 19-inch transonic tunnel. Model smooth.

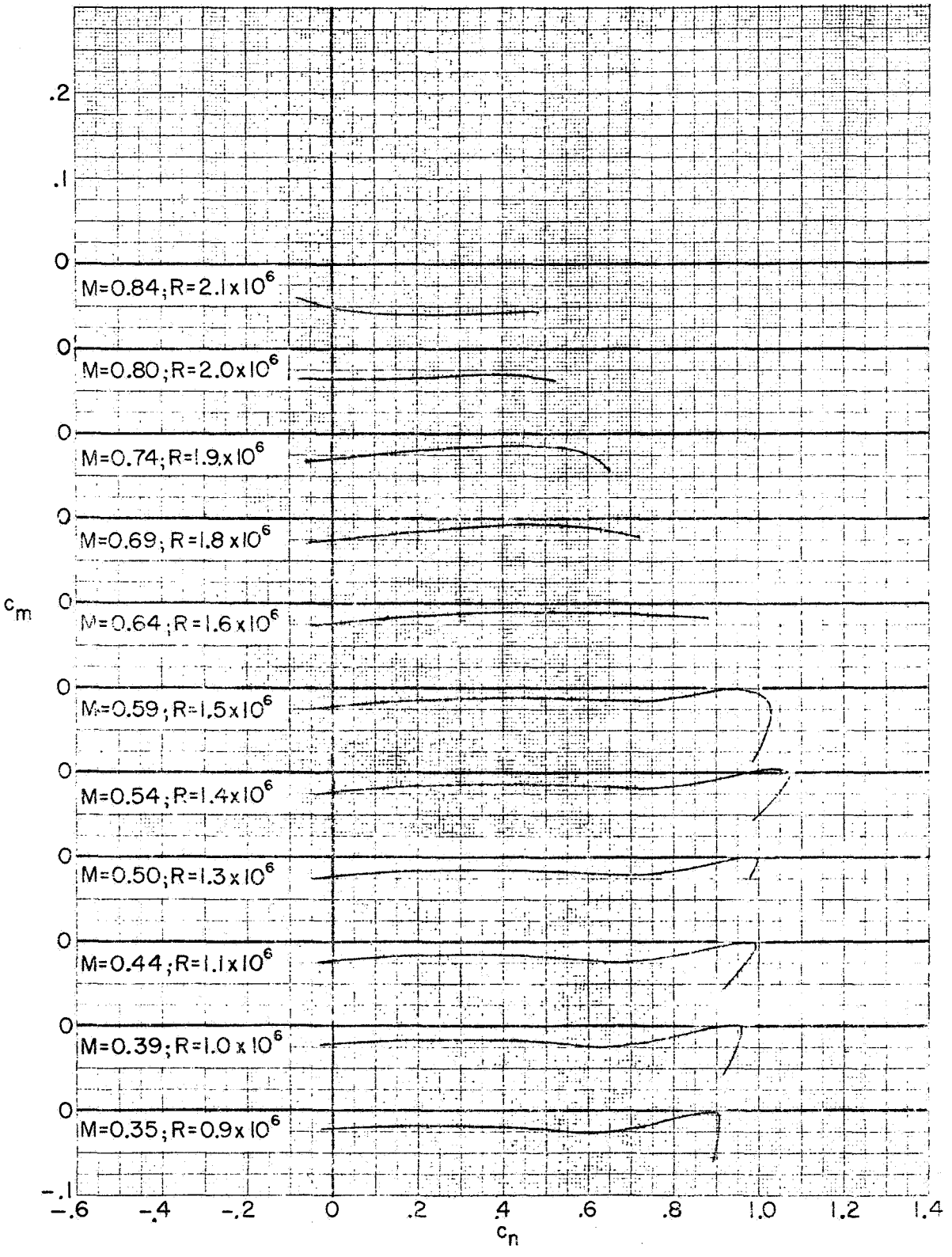

(b) Section pitching-moment coefficients.

Figure 11. - Continued.

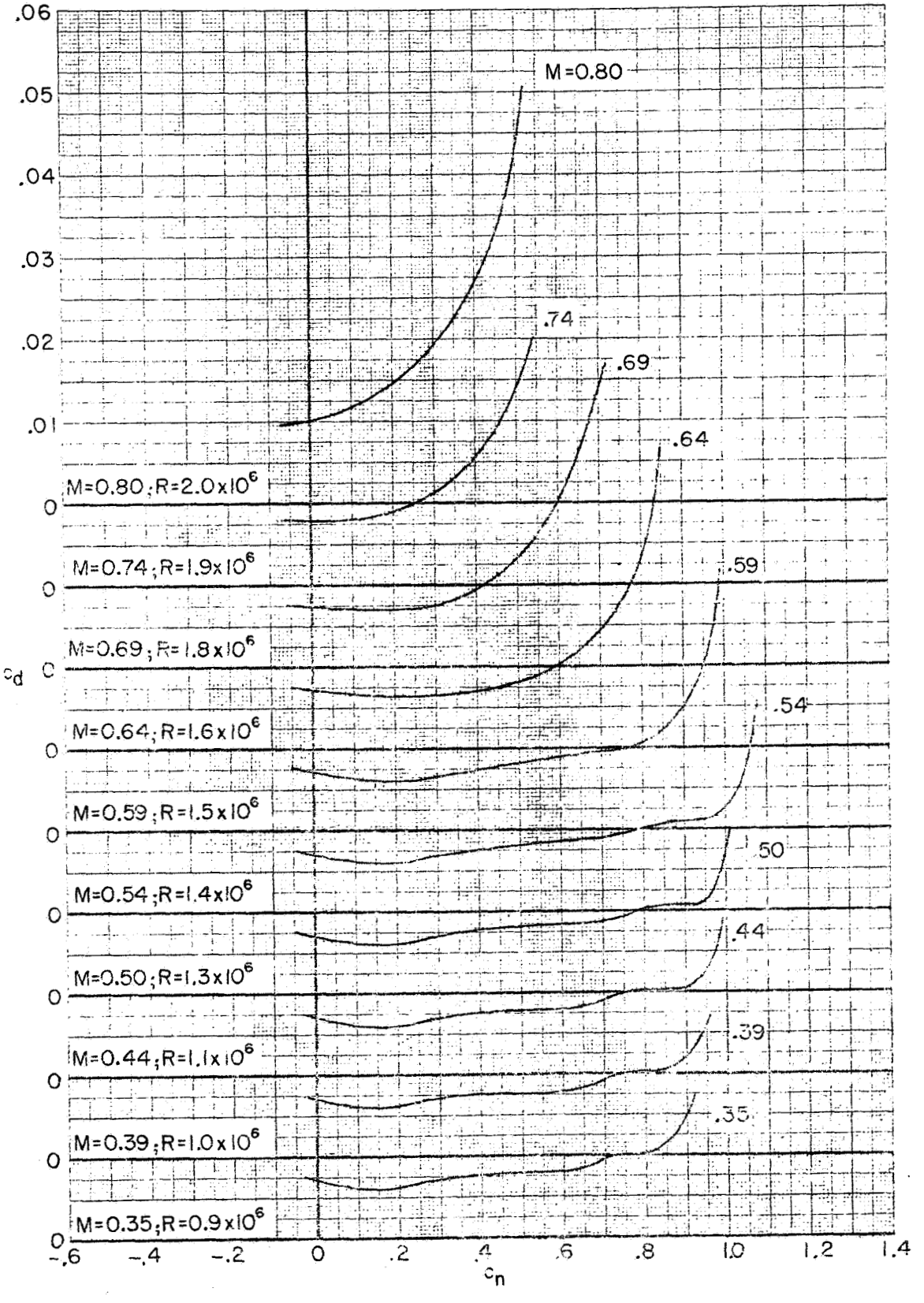

(c) Section drag coefficients.

Figure 11. - Concluded.

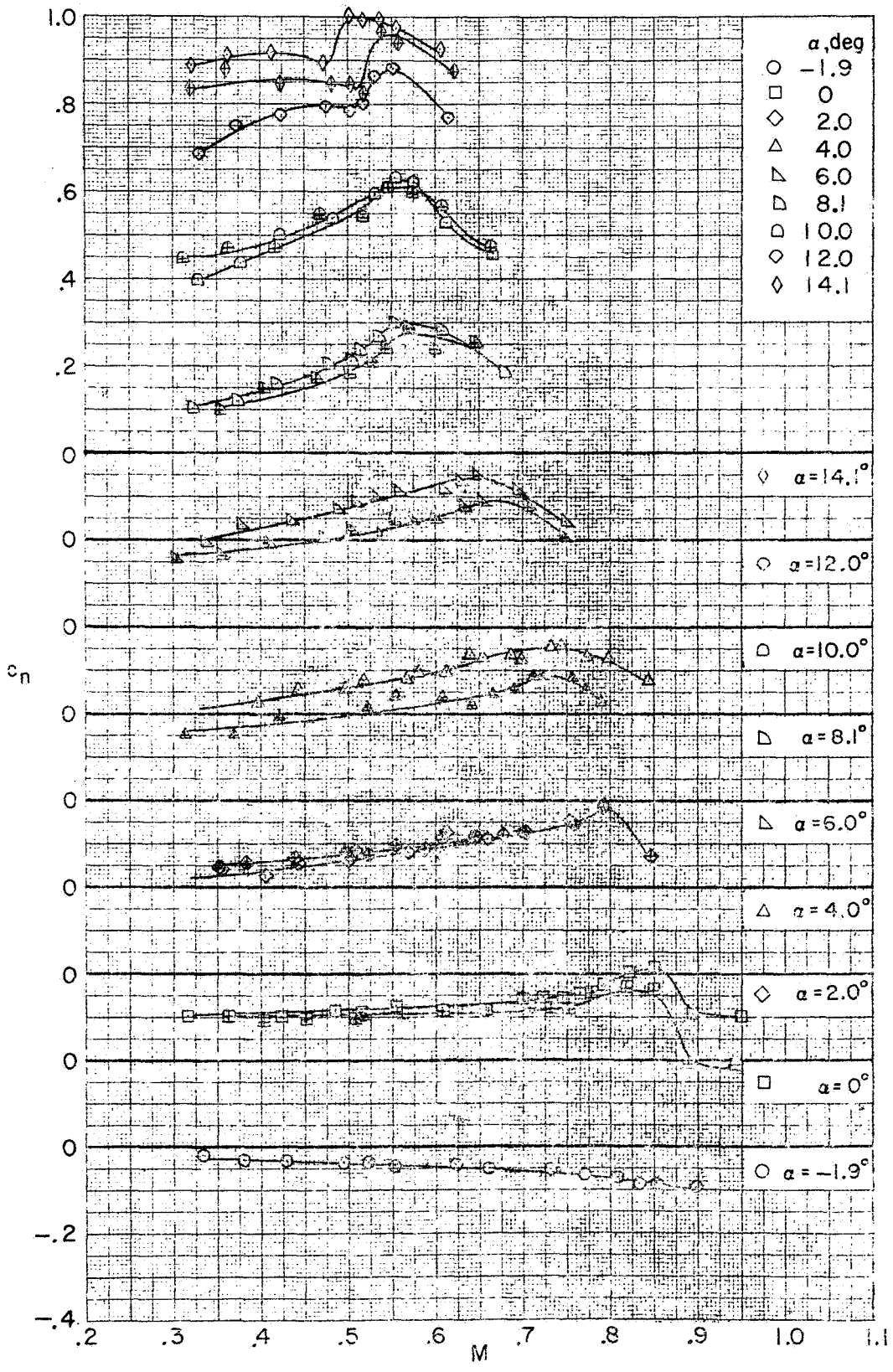

(a) Section normal-force coefficients.

Figure 12.- Aerodynamic characteristics against Mach number of the FX69-H-098 airfoil measured in the Langley 6 x 19-inch transonic tunnel. Plain symbols indicate model smooth; centered symbols indicate fixed tranition.

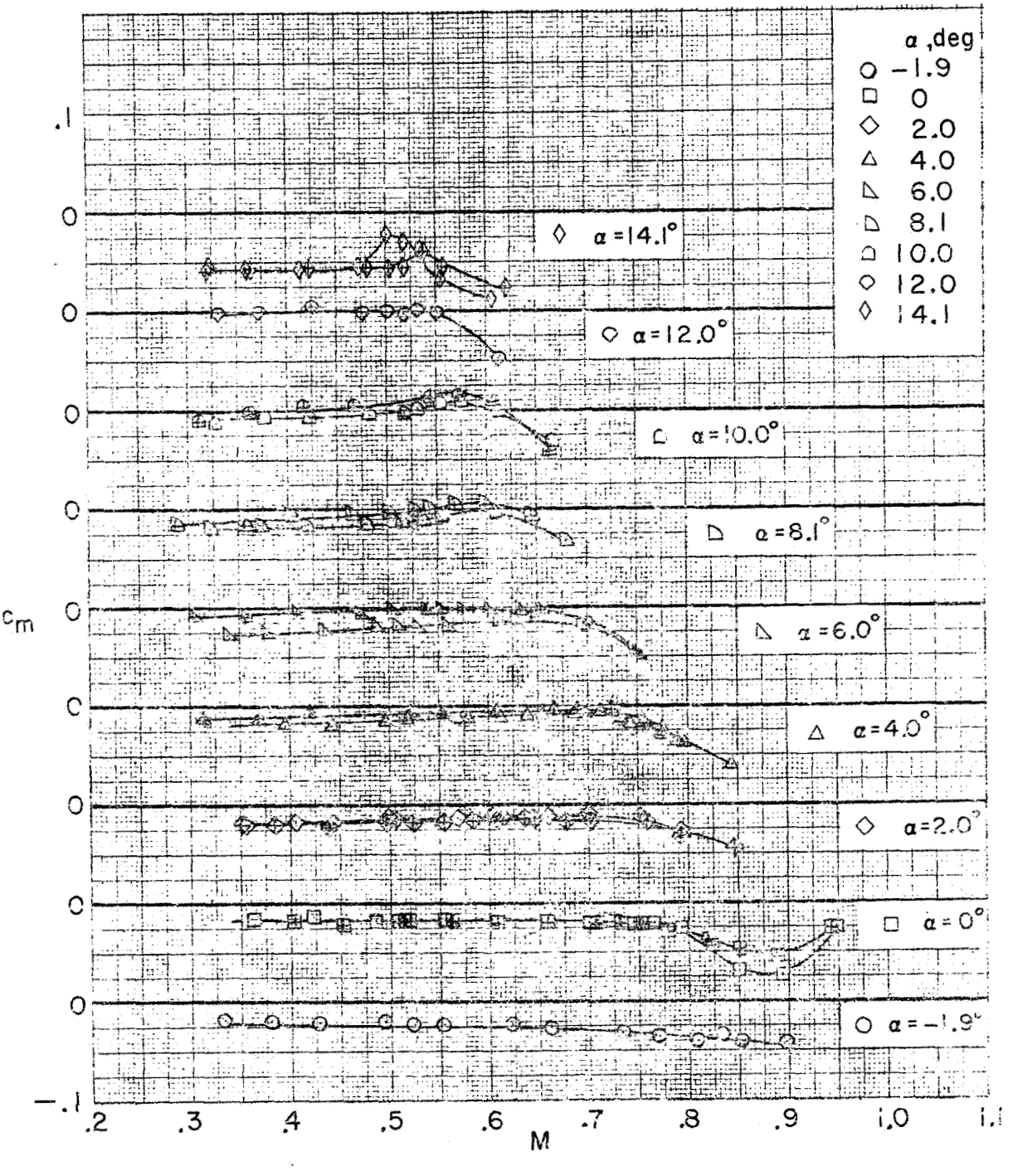

(b) Section pitching-moment coefficients.

Figure 12. - Continued.

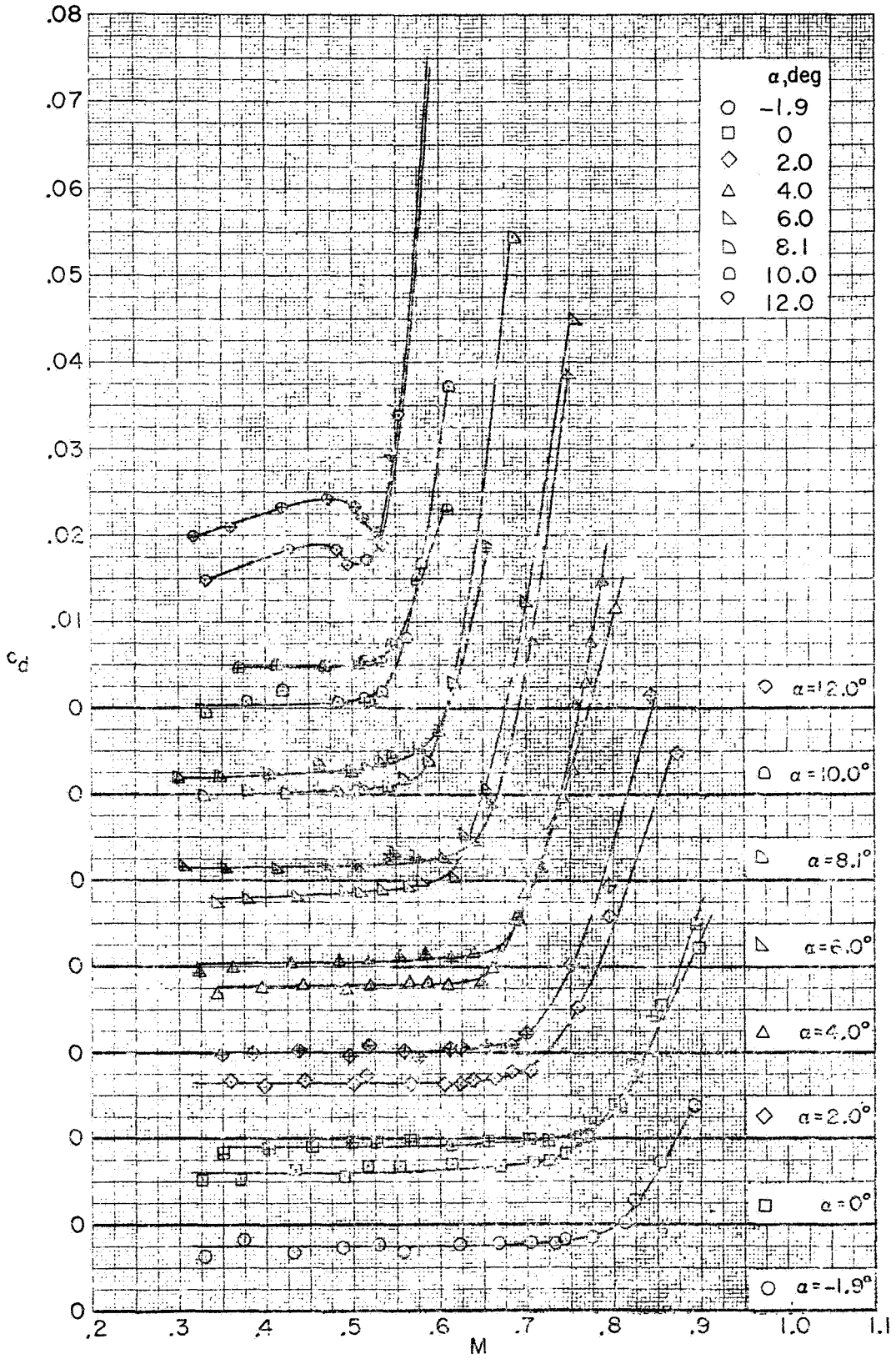

(c) Section drag coefficients.

Figure 12. - Concluded.

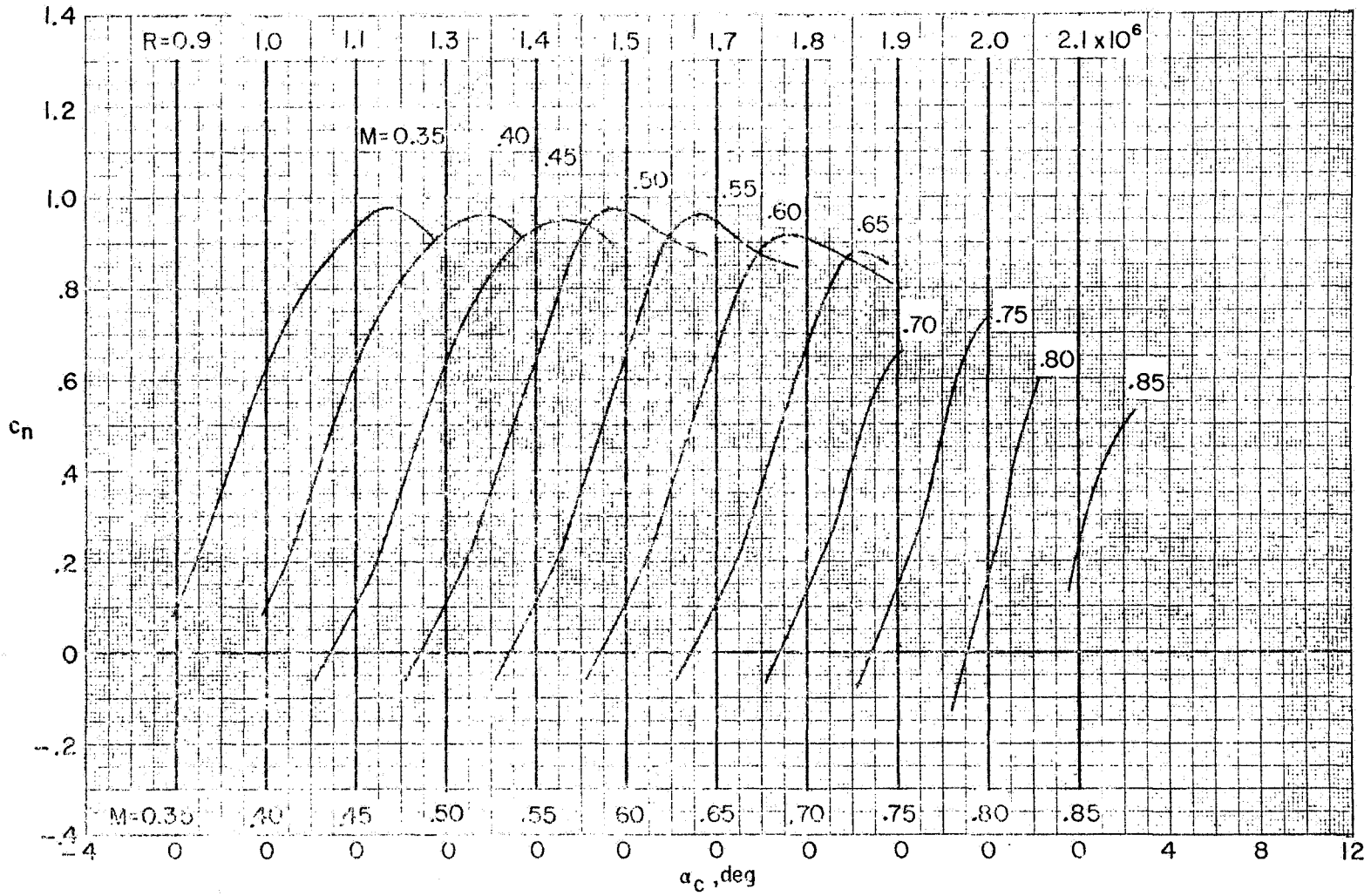

(a) Section normal force coefficients.

Figure 13.- Aerodynamic characteristics of the NLR-1 airfoil measured in the Langley 6 x 19-inch transonic tunnel. Model smooth.

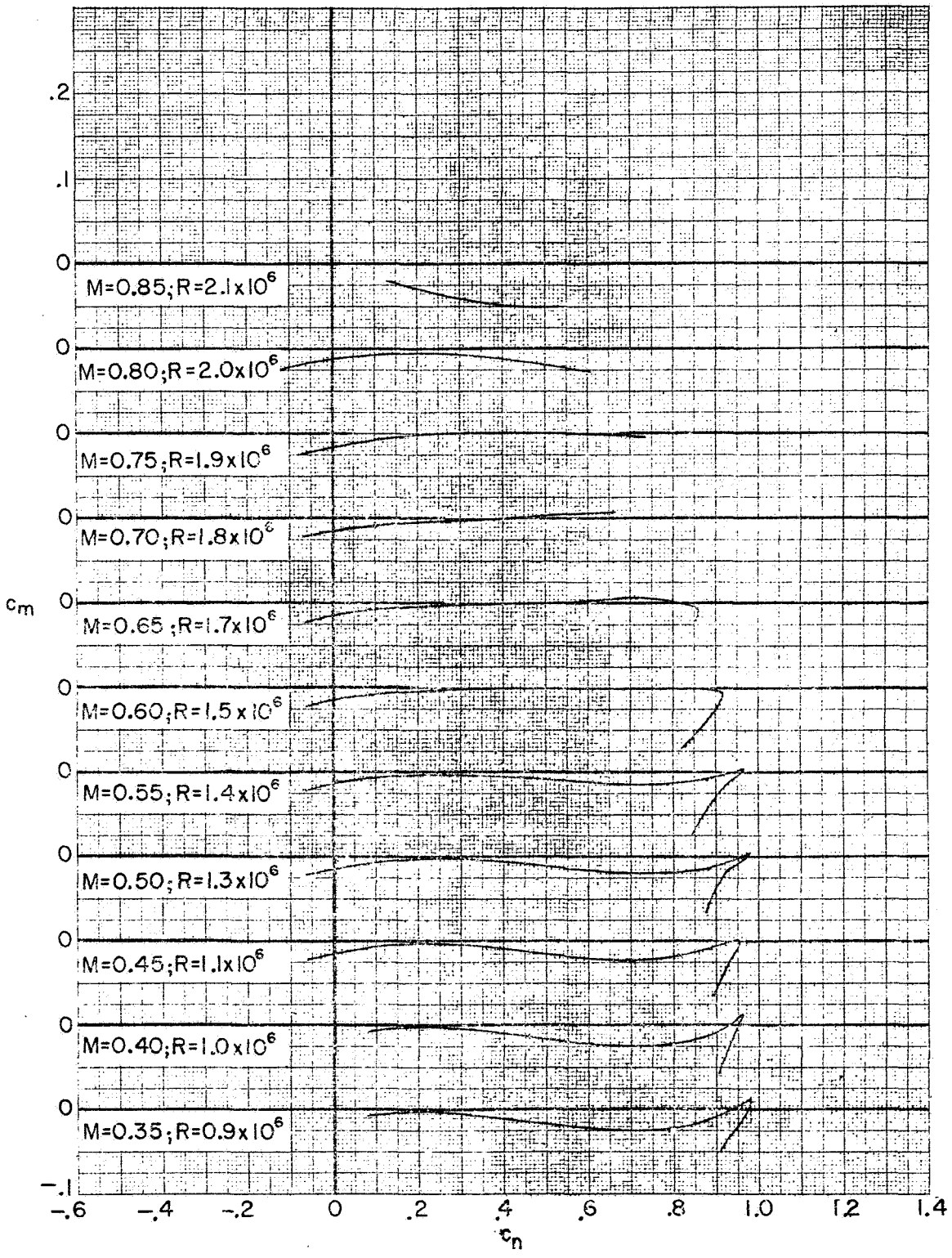

(b) Section pitching-moment coefficient.

Figure 13. - Continued.

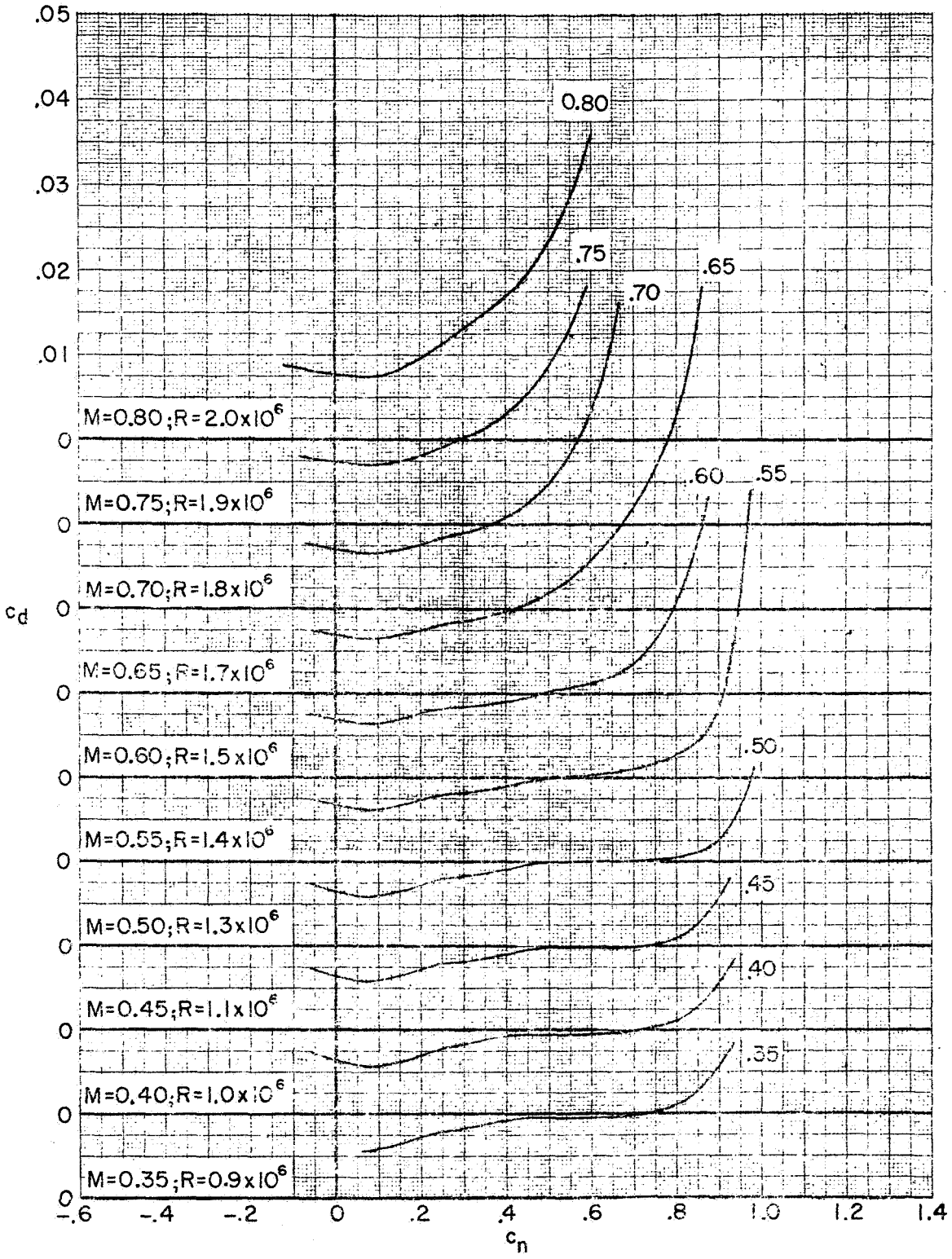

(c) Section drag coefficients.

Figure 13.- Concluded.

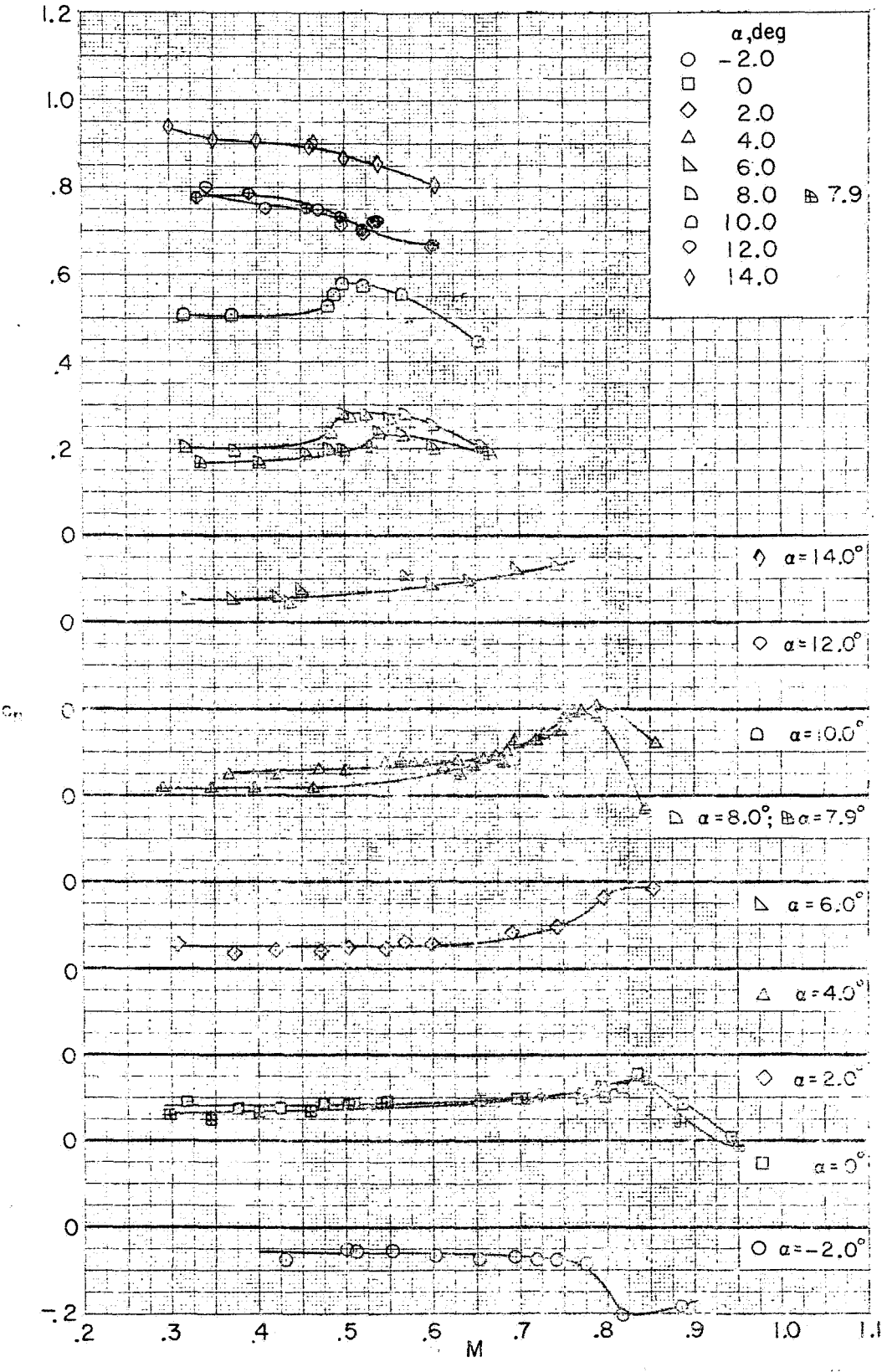

(a) Section normal-force coefficients.

Figure 14. - Aerodynamic characteristics against Mach number of the NLR-1 airfoil measured in the Langley 6 x 19-inch transonic tunnel. Plain symbols indicate model smooth; centered symbols indicate fixed transition.

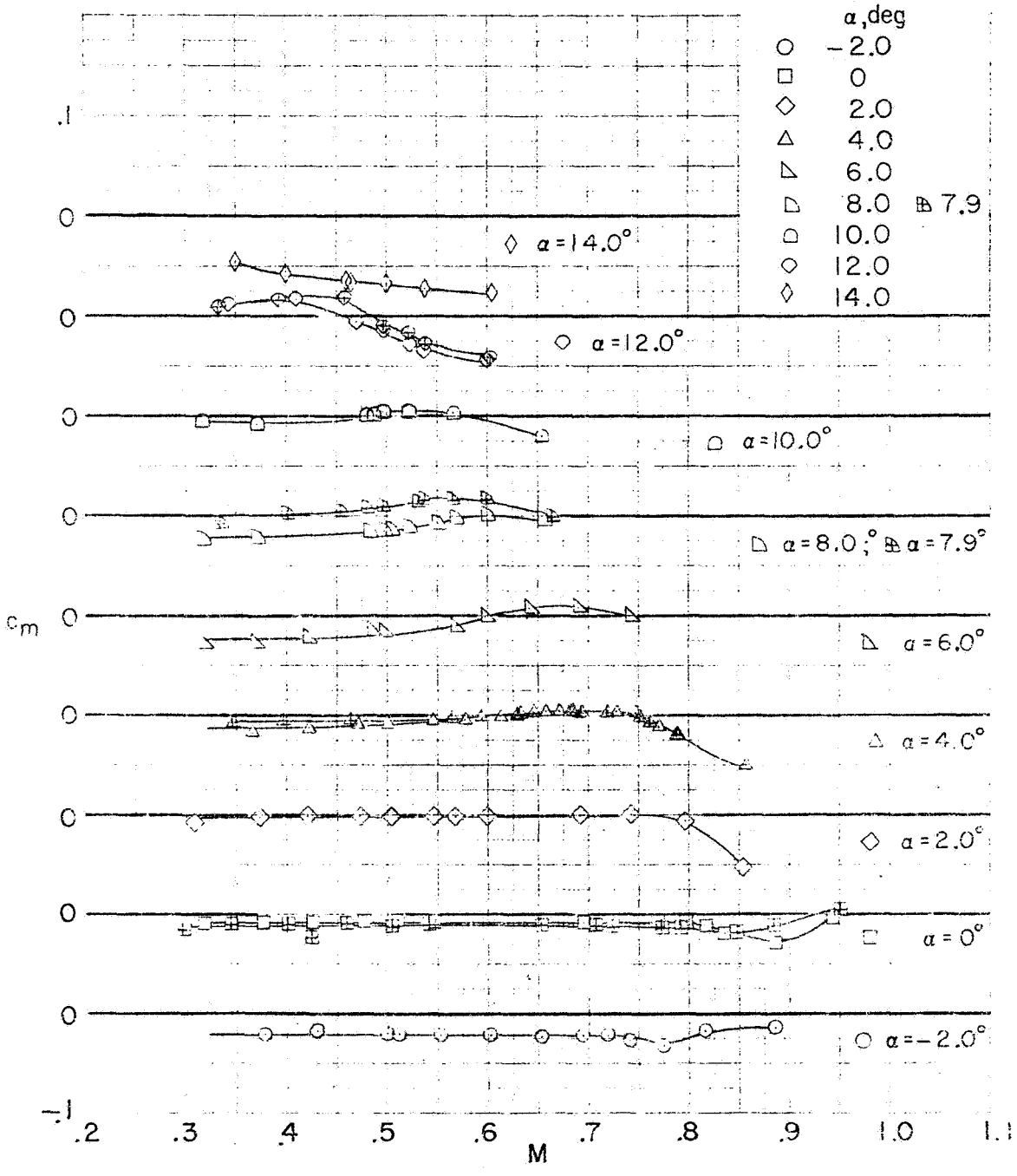

(b) Section pitching-moment coefficients.

Figure 14. - Continued.

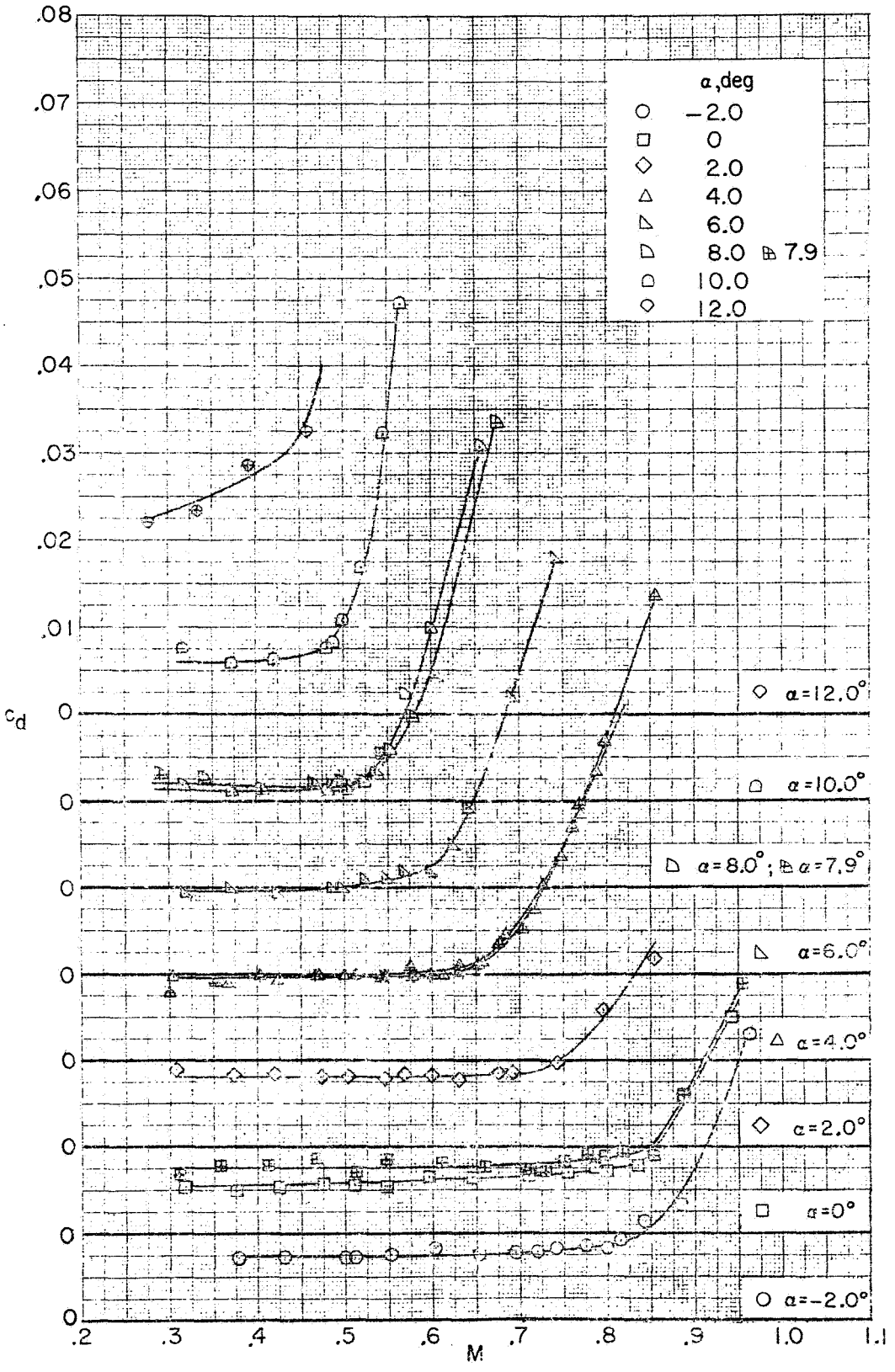

(c) Section drag coefficients.

Figure 14. - Concluded.

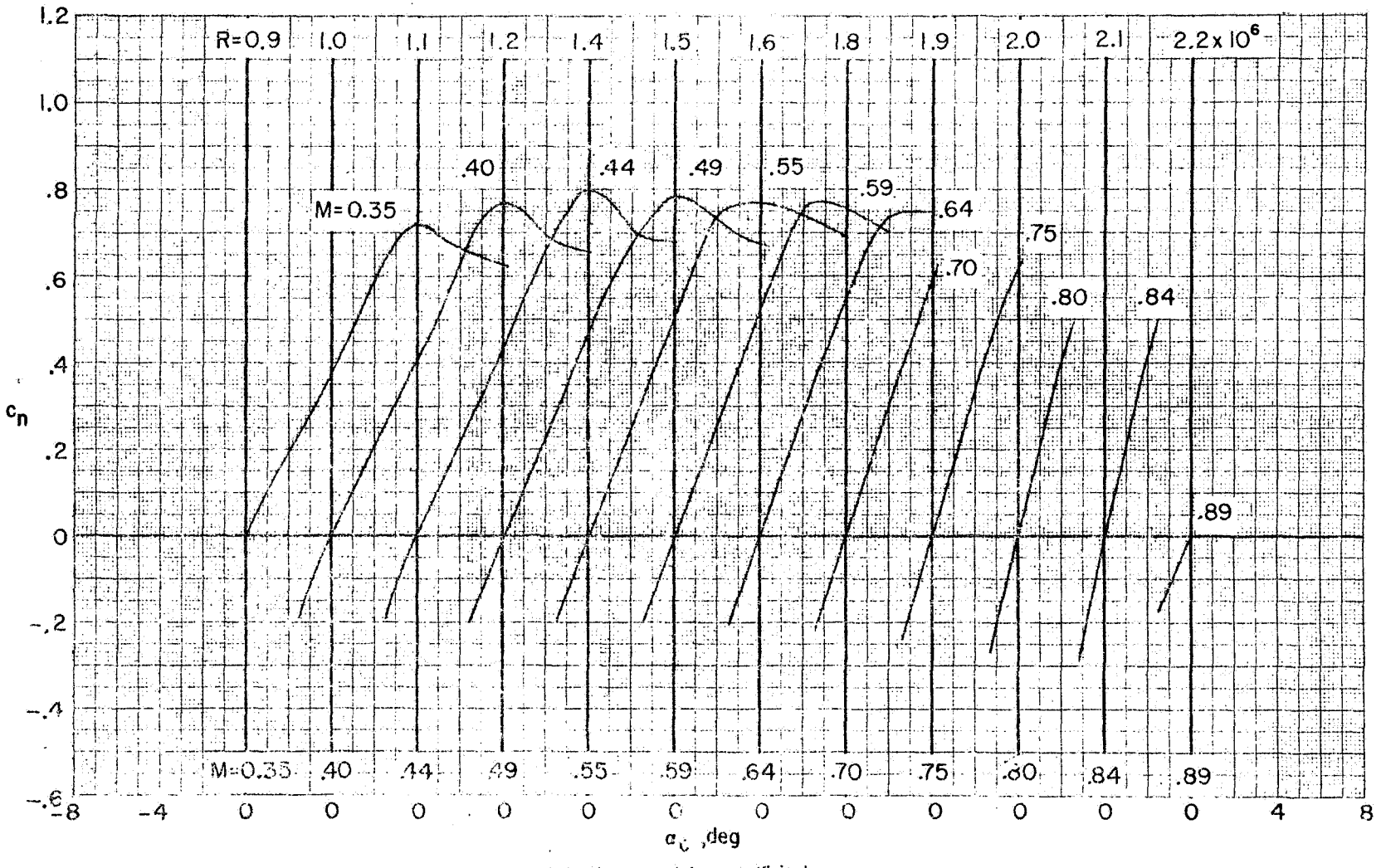

(a) Section normal-force coefficient

Figure 15. - Aerodynamic characteristics of the BHC-540 airfoil measured in the Langley 6×19-inch transonic tunnel. Model smooth.

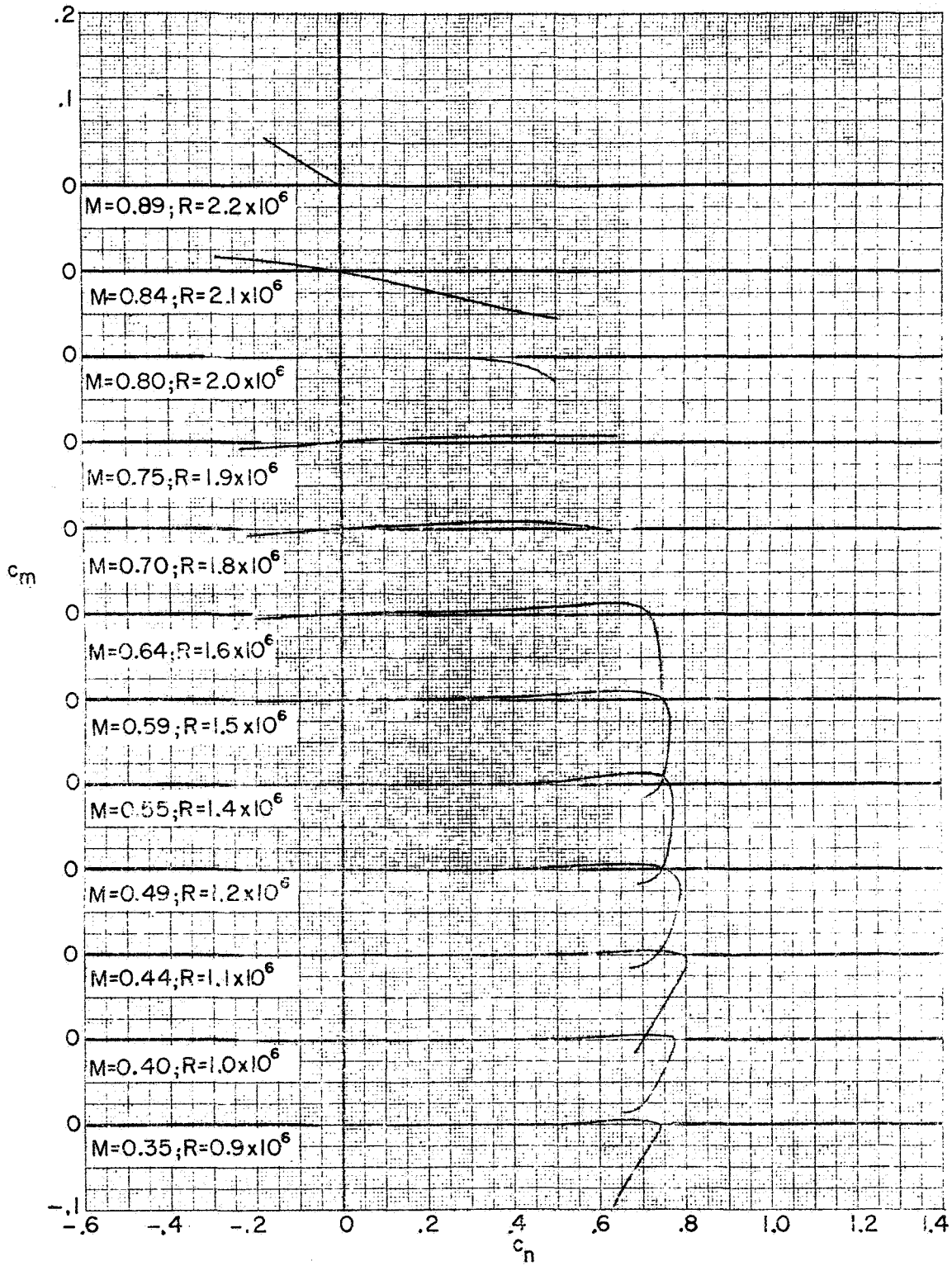

(b) Section pitching-moment coefficients.

Figure 15. - Continued.

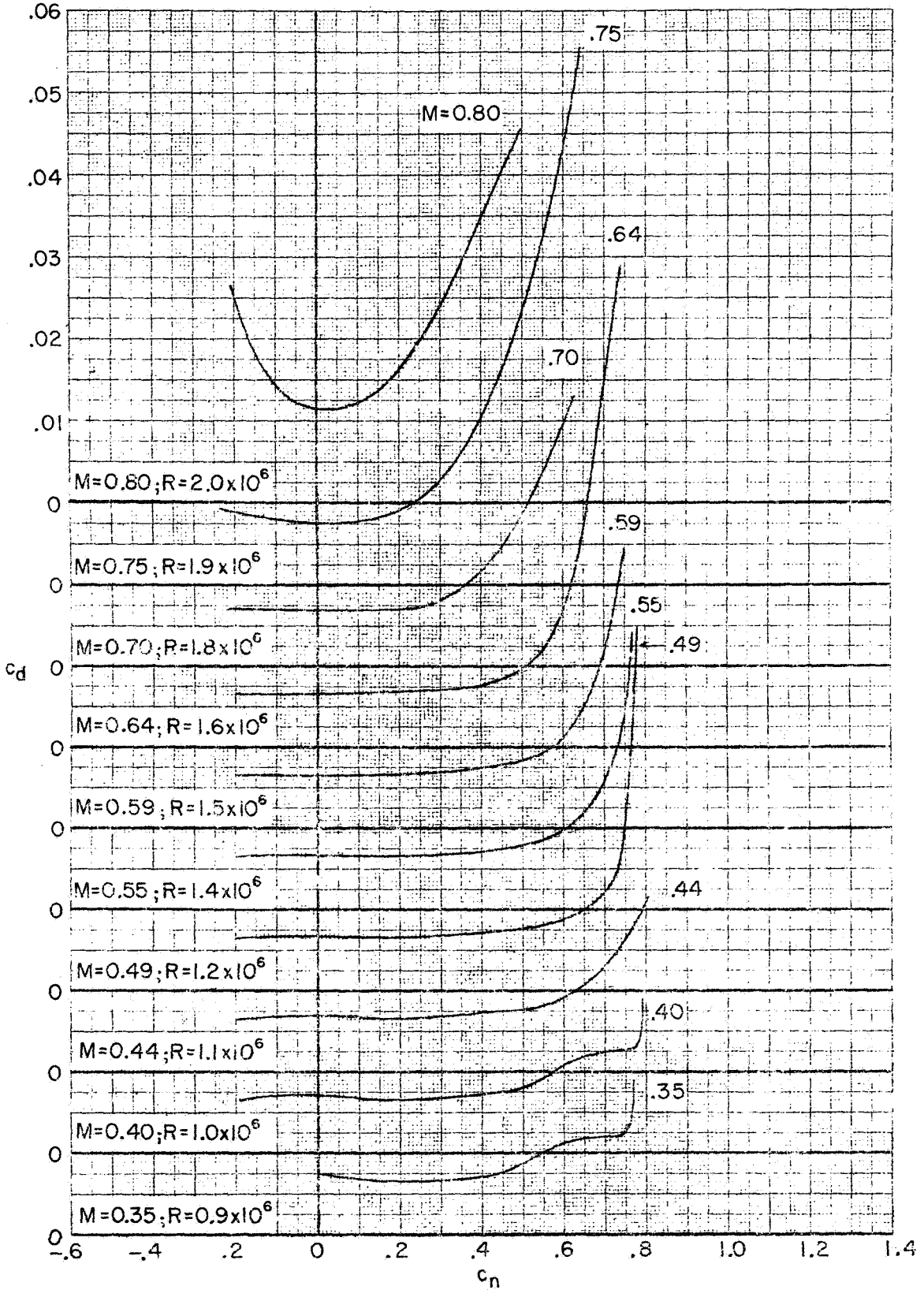

(c) Section drag coefficients.

Figure 15. - Concluded.

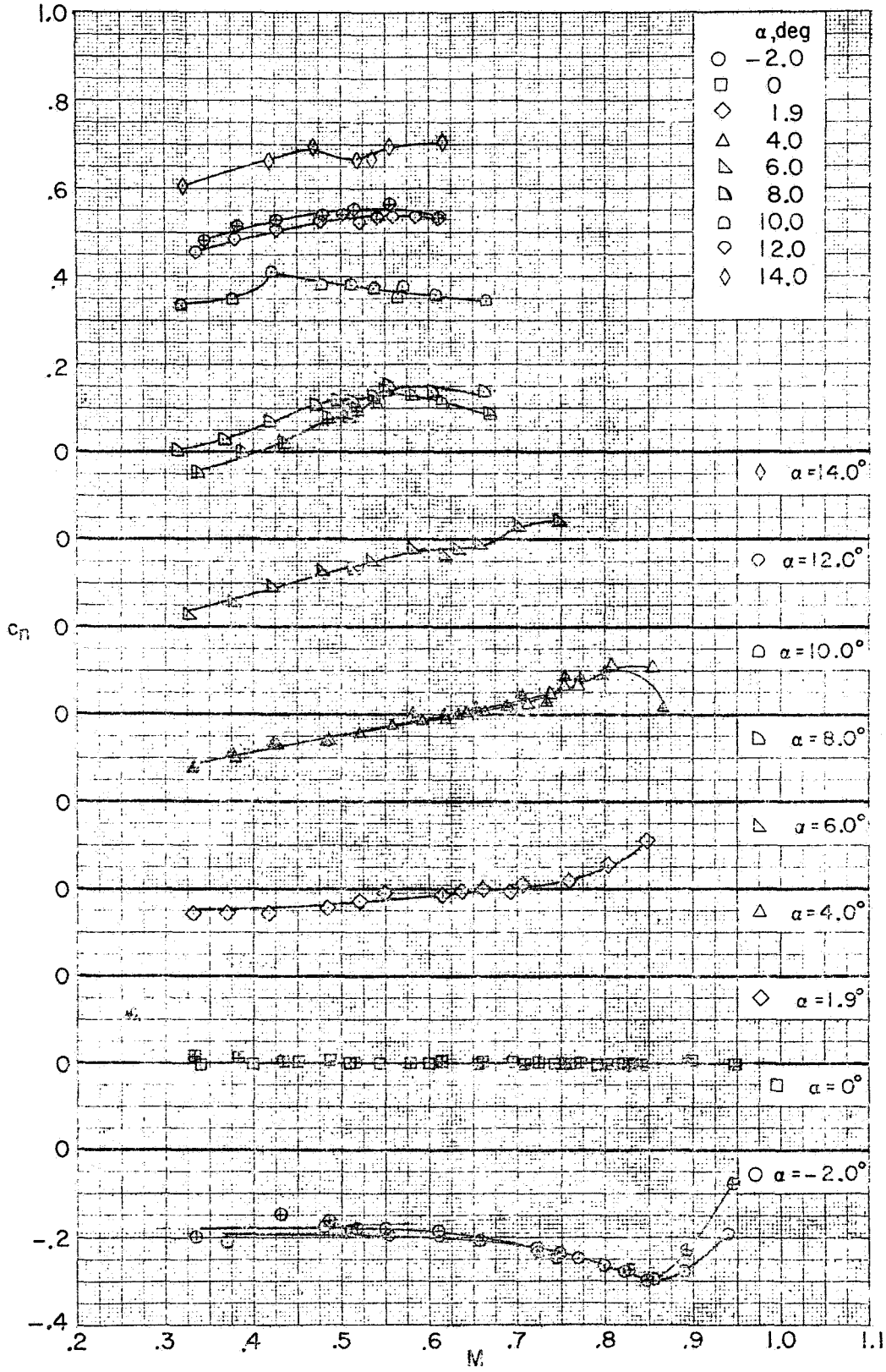

(a) Section normal-force coefficients.

Figure 16.- Aerodynamic characteristics against Mach number of the BHC-540 airfoil measured in the 6 x 19-inch transonic tunnel. Plain symbols indicate model smooth; centered symbols indicate fixed transition.

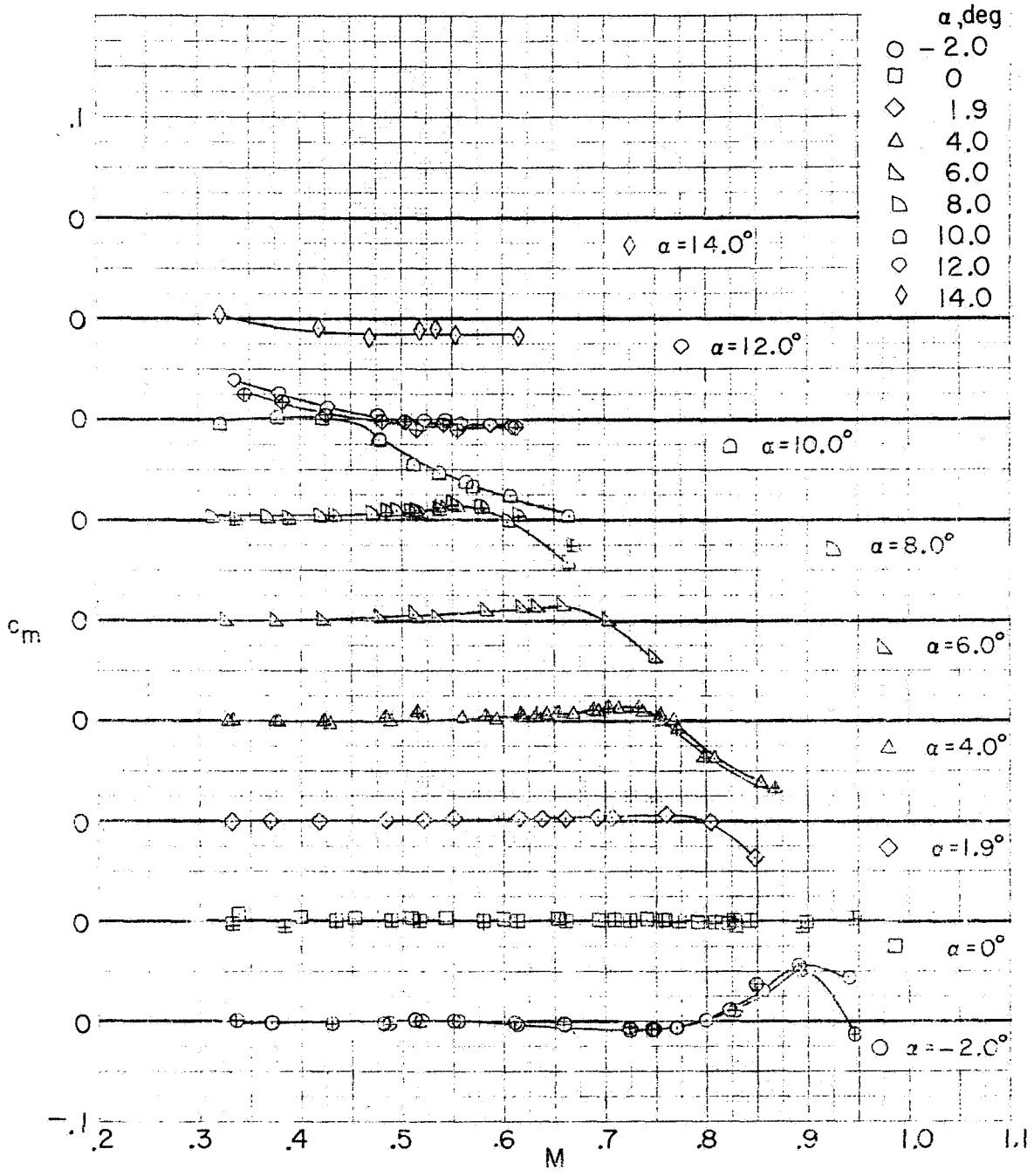

(b) Section pitching-moment coefficients.

Figure 16. - Continued.

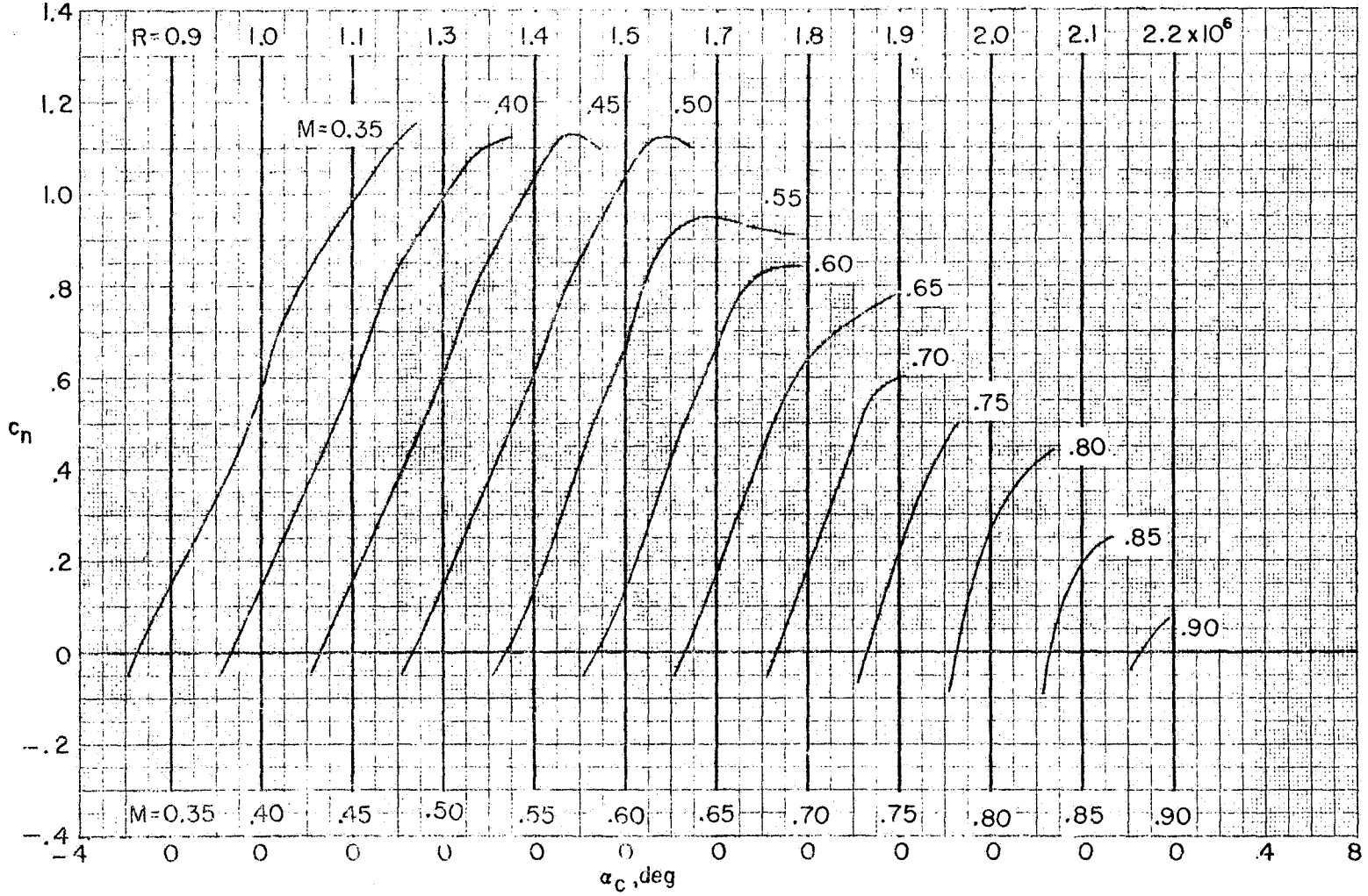

(a) Section normal-force coefficients.

Figure 17.- Aerodynamic characteristics of the NACA 23012 airfoil measured in the Langley 6×19-inch transonic tunnel. Model smooth.

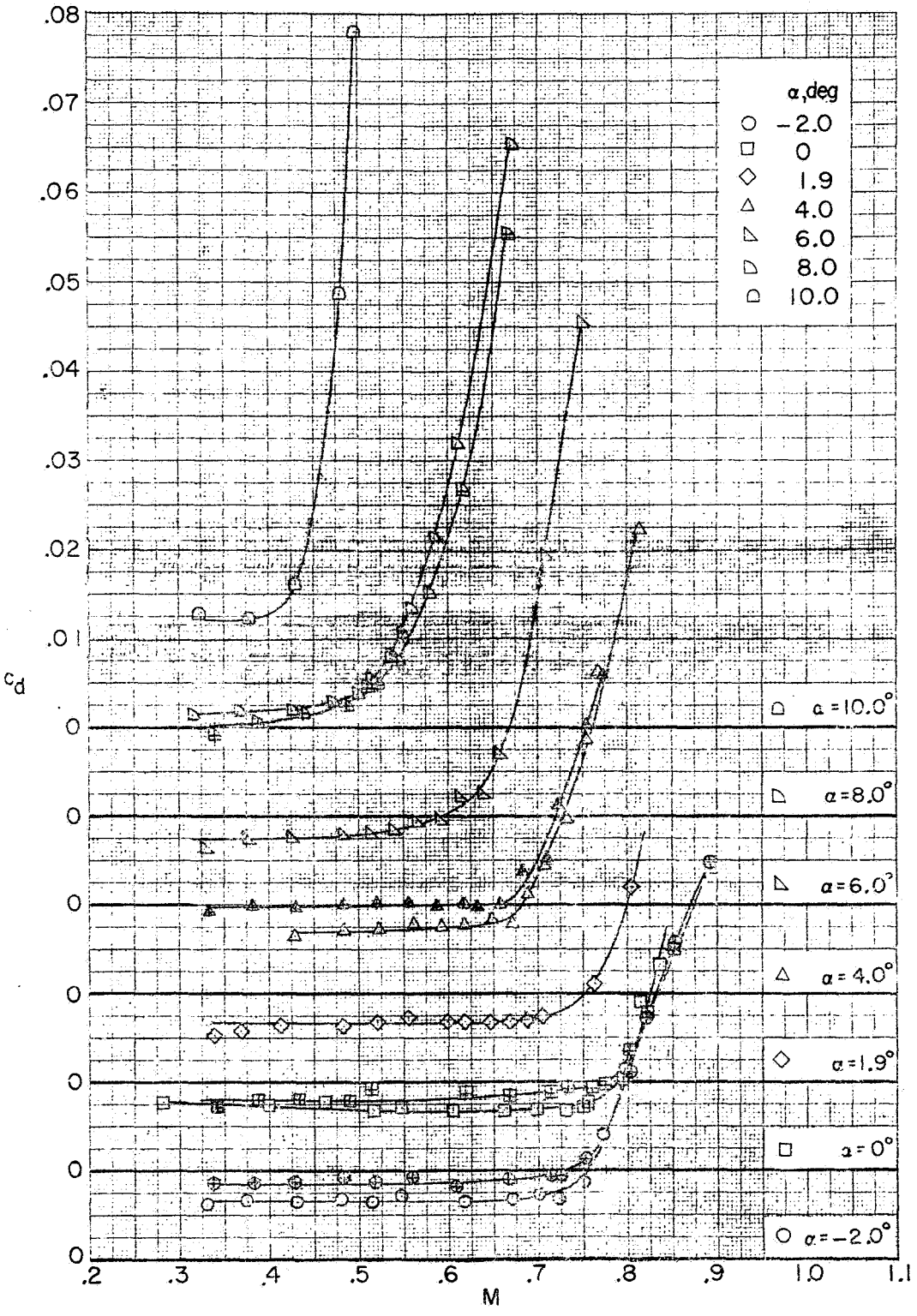

(c) Section drag coefficients.

Figure 16.- Concluded.

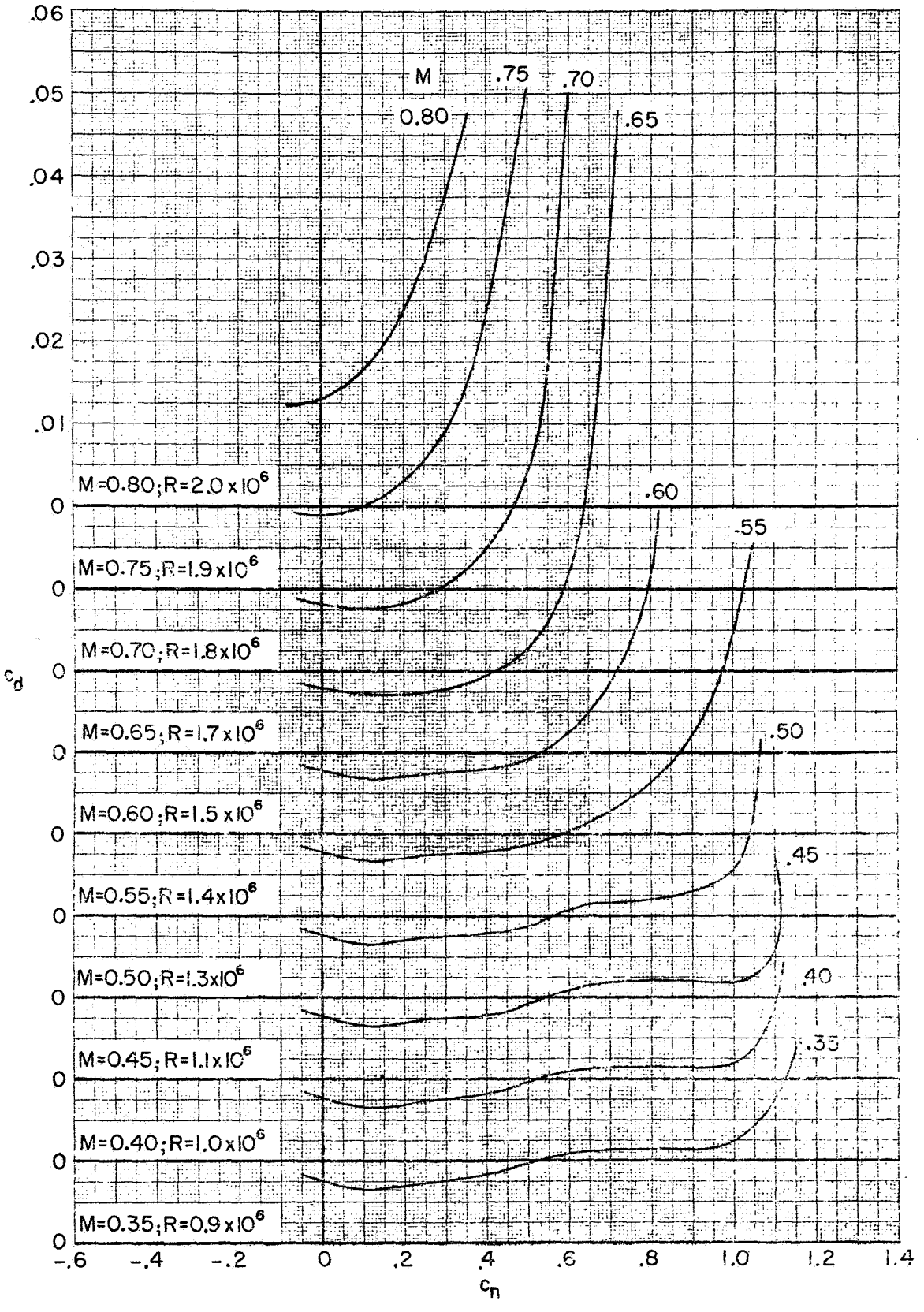

(c) Section drag coefficients.

Figure 17. - Concluded.

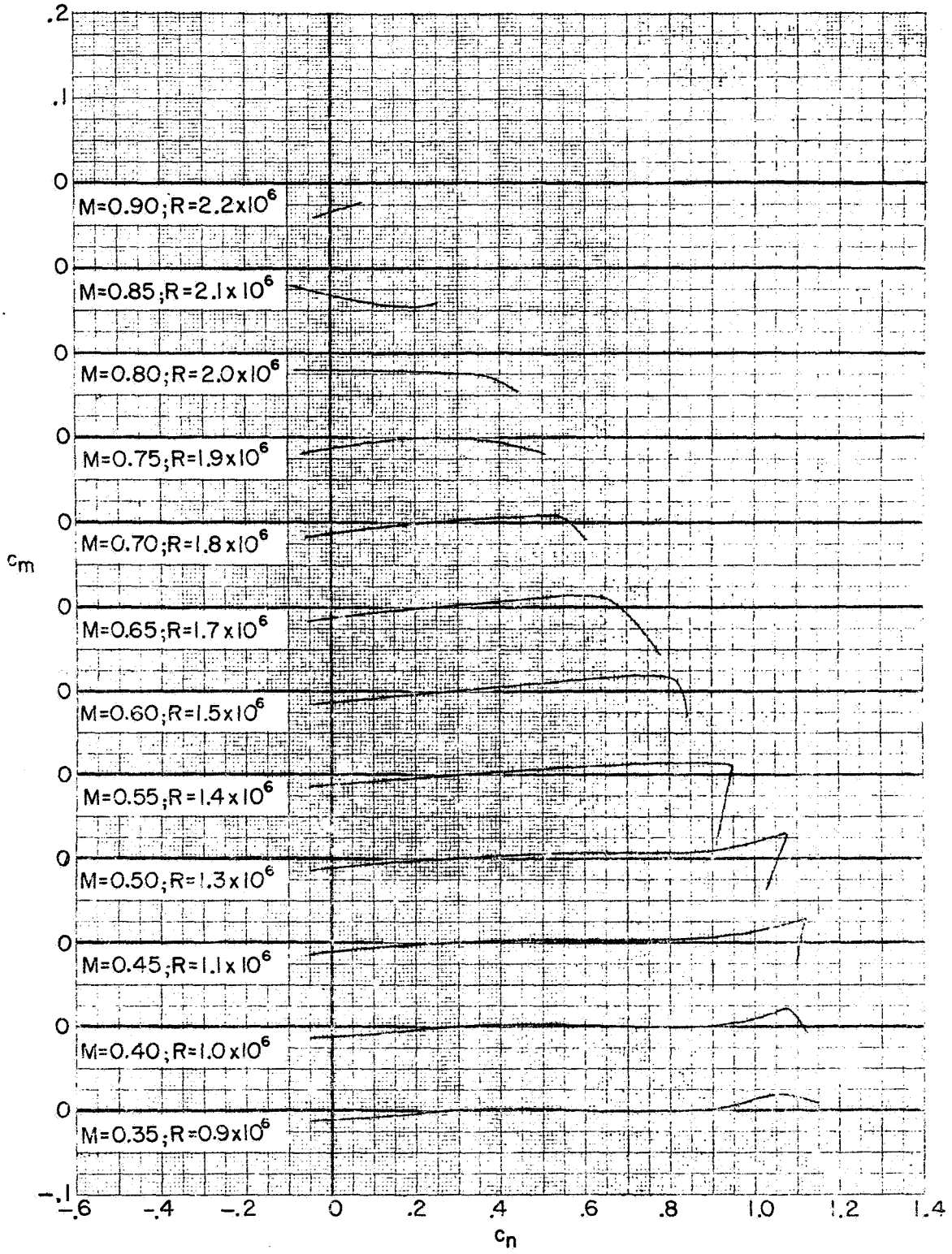

(b) Section pitching-moment coefficients.

Figure 17. - Continued.

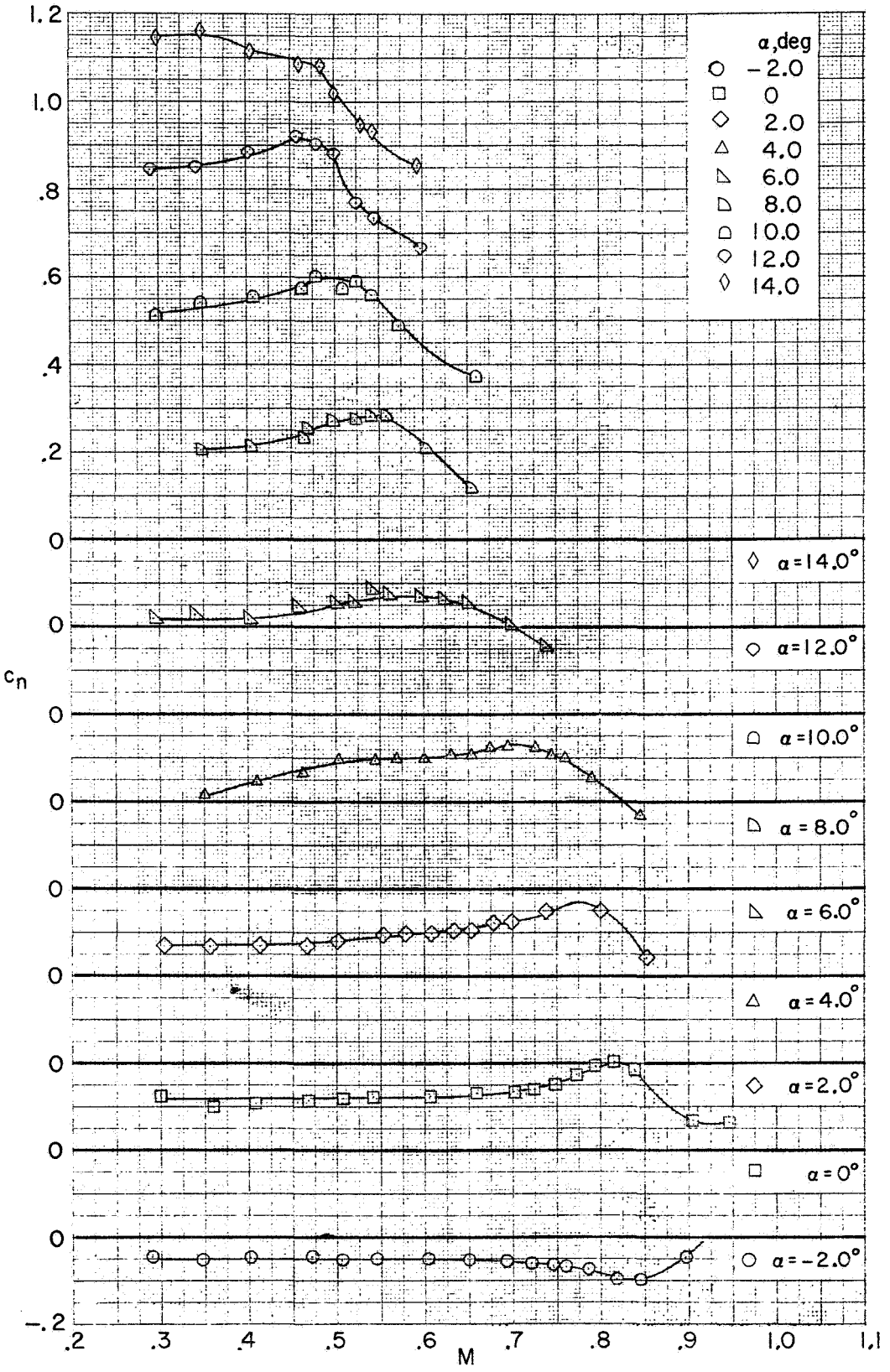

(a) Section normal-force coefficients.

Figure 18.- Aerodynamic characteristics against Mach number of the NACA 23012 airfoil measured in the 6 x 10-inch transonic tunnel. Model smooth.

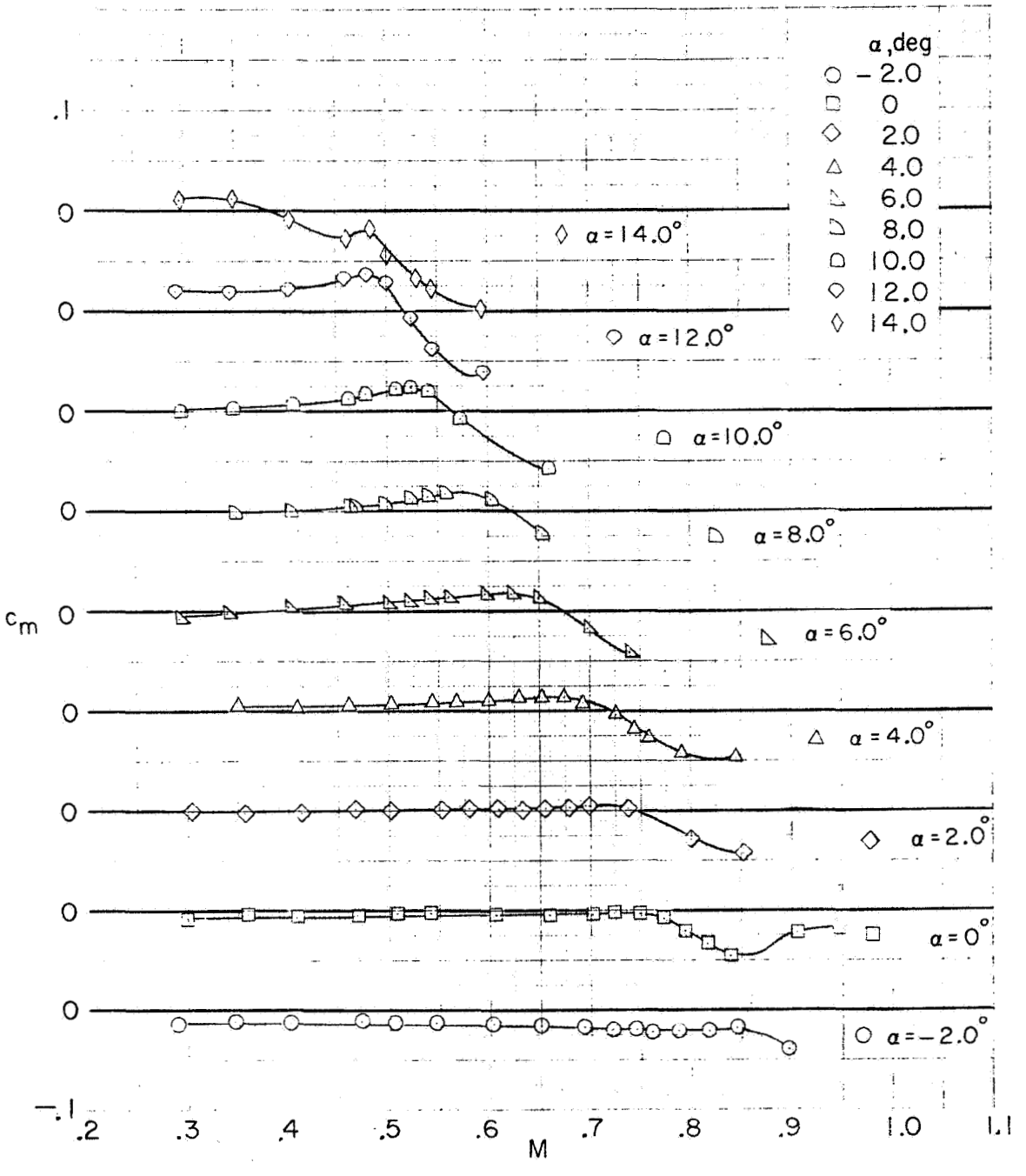

(b) Section pitching-moment coefficients.

Figure 18.- Continued.

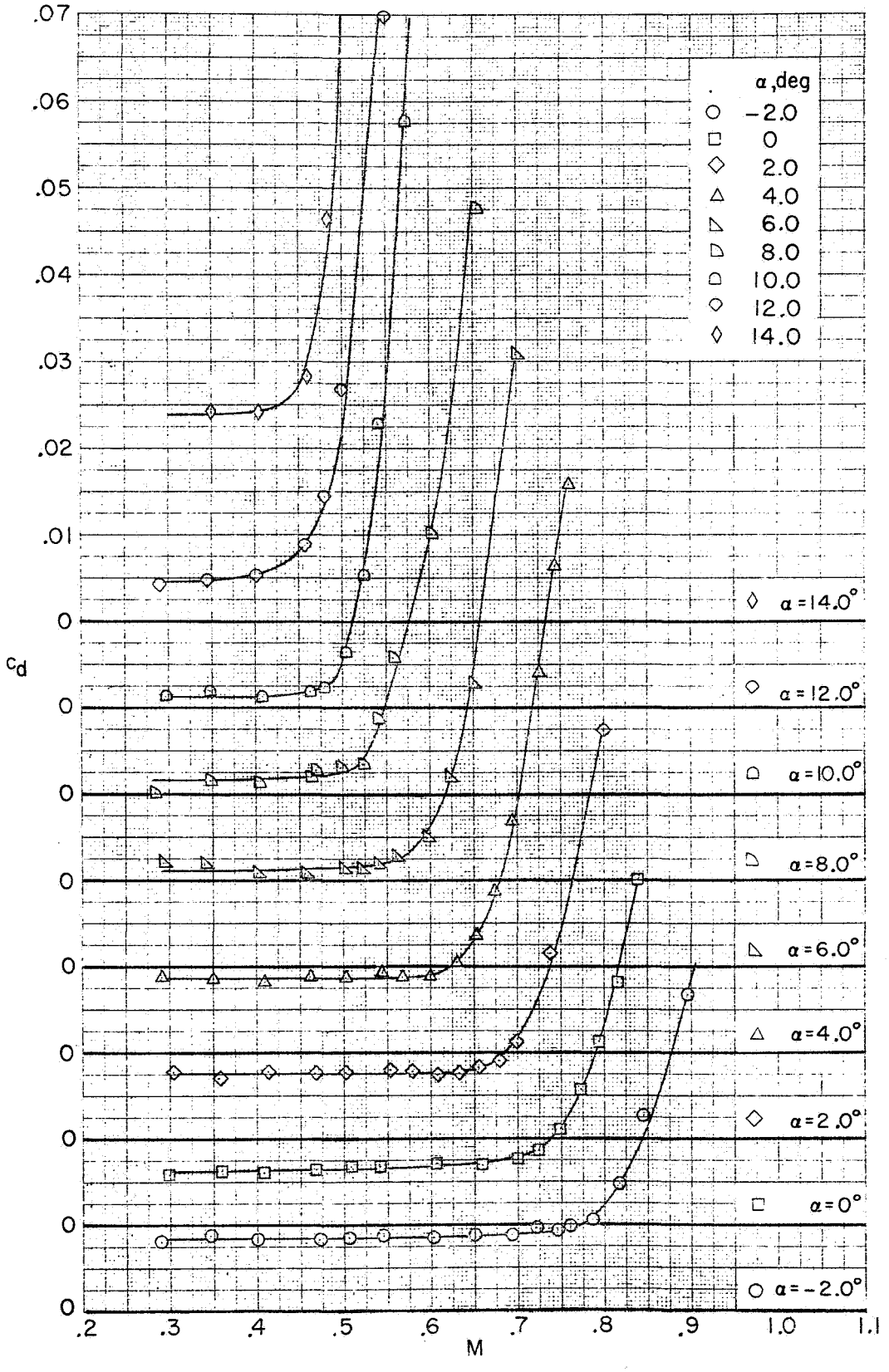

(c) Section drag coefficient.

Figure 18. - Concluded.

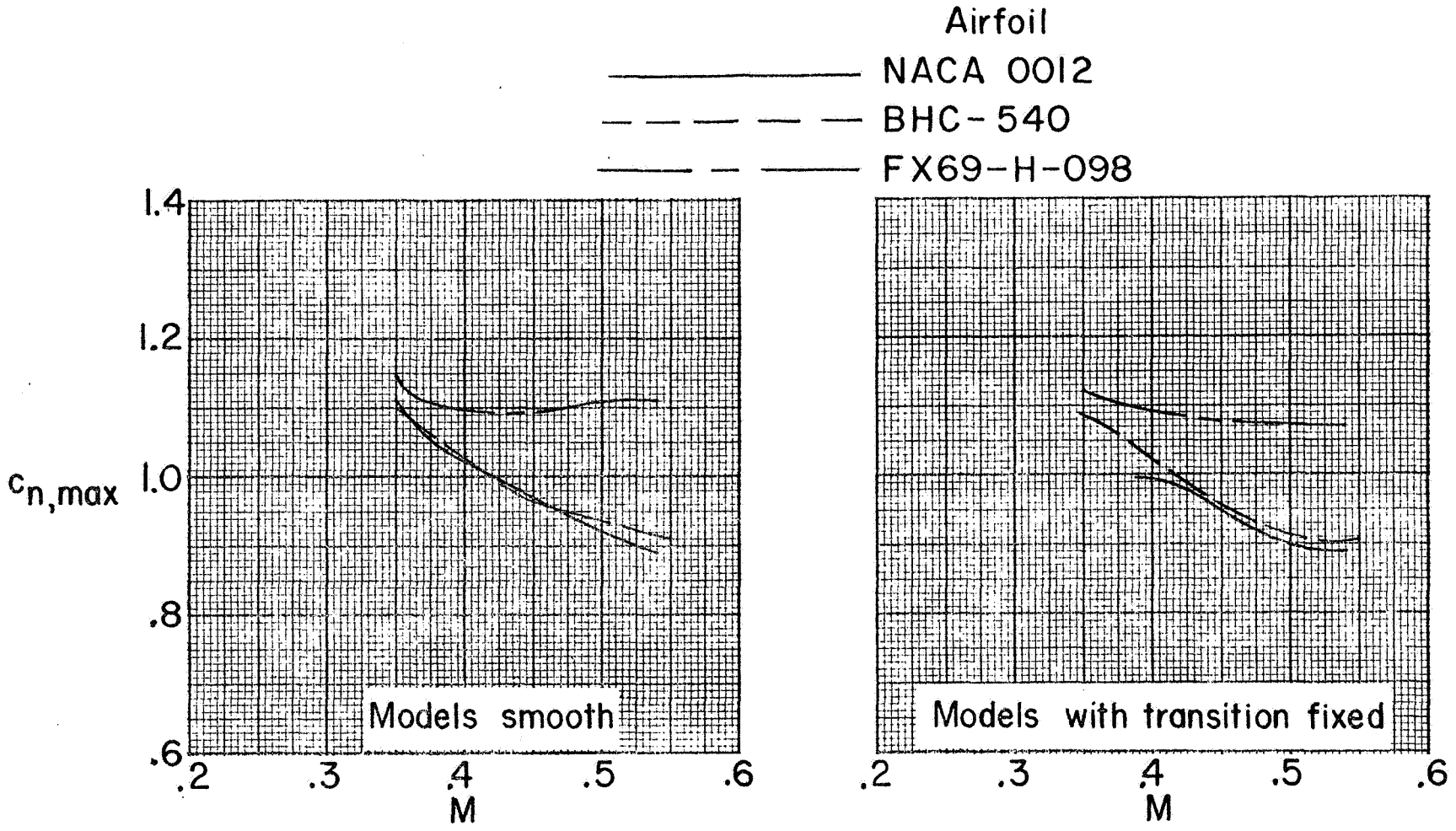

Figure 19. - Variation of maximum section normal-force coefficient with Mach number of the NACA 0012, the BHC-540, and the FX69-H-098 airfoils as measured in the Langley 6×28-inch transonic tunnel.

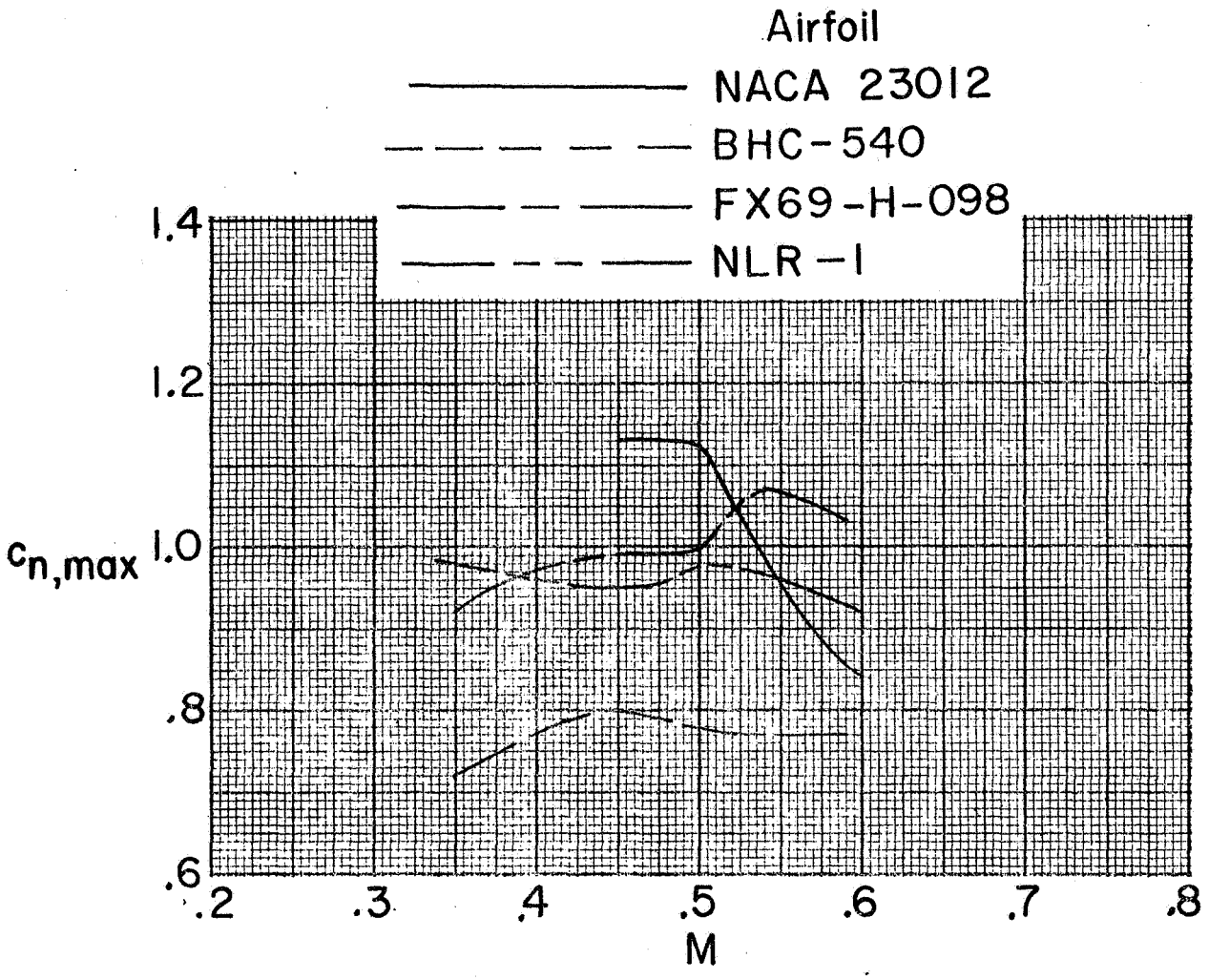

Figure 20. - Variation of maximum section normal-force coefficient with Mach number of the NACA 23012, the BHC-540, the FX69-H-098, and the NLR-1 airfoils as measured in the Langley 6×19-inch transonic tunnel. Models smooth.

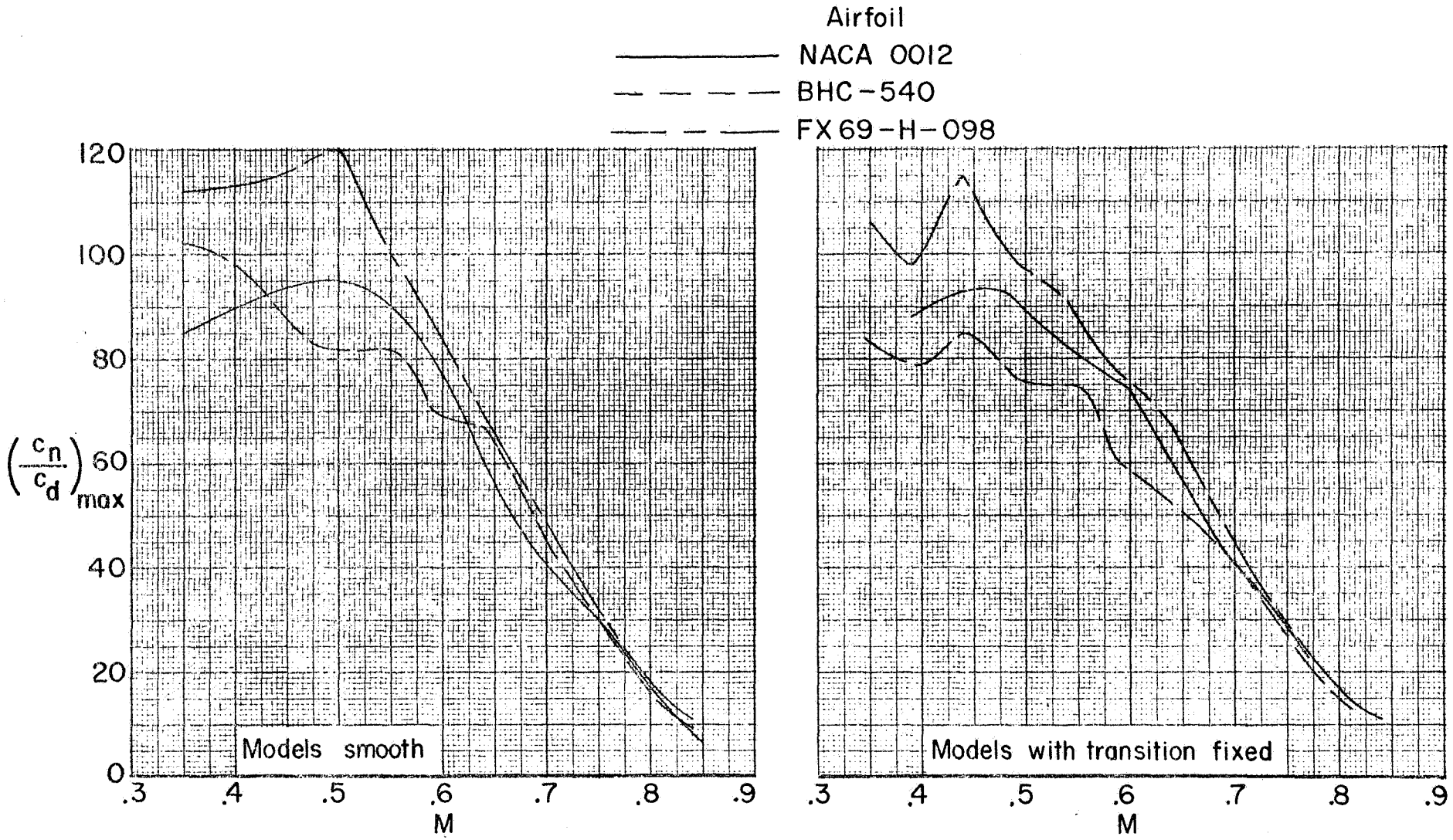

Figure 21. - Variation of maximum section normal-force-to-drag ratio with Mach number of the NACA 0012, the BHC-540, and the FX69-H-098 airfoils as measured in the Langley 6×28-inch transonic tunnel.

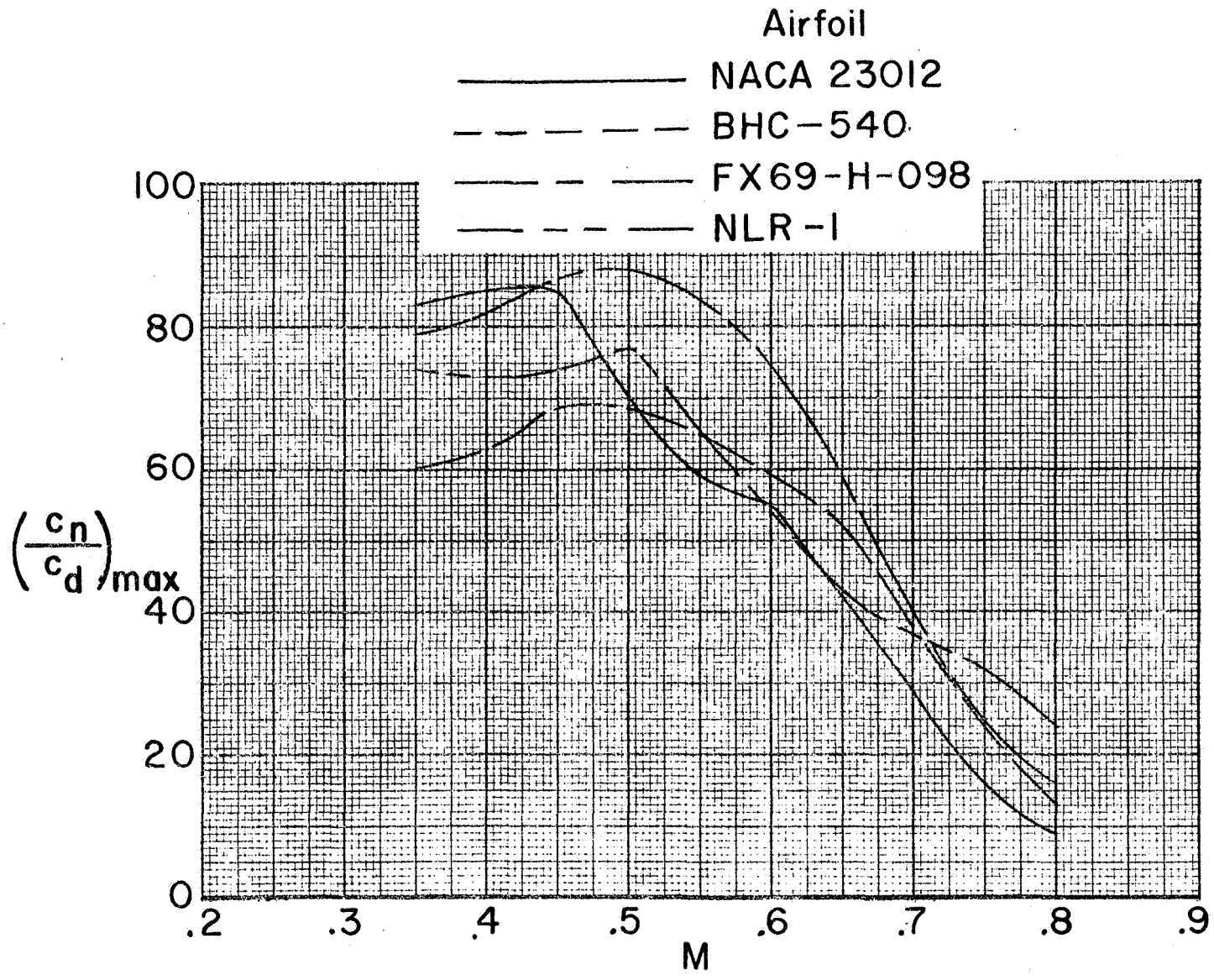

Figure 22. - Variation of maximum section normal-force-to-drag ratios with Mach number of the NACA 23012, the BHC-540, the FX69-H-098, and the NLR-1 airfoils as measured in the Langley 6×19-inch transonic tunnel. Models smooth.

REPRODUCIBILITY OF THE ORIGINAL PAGE IS POOR.

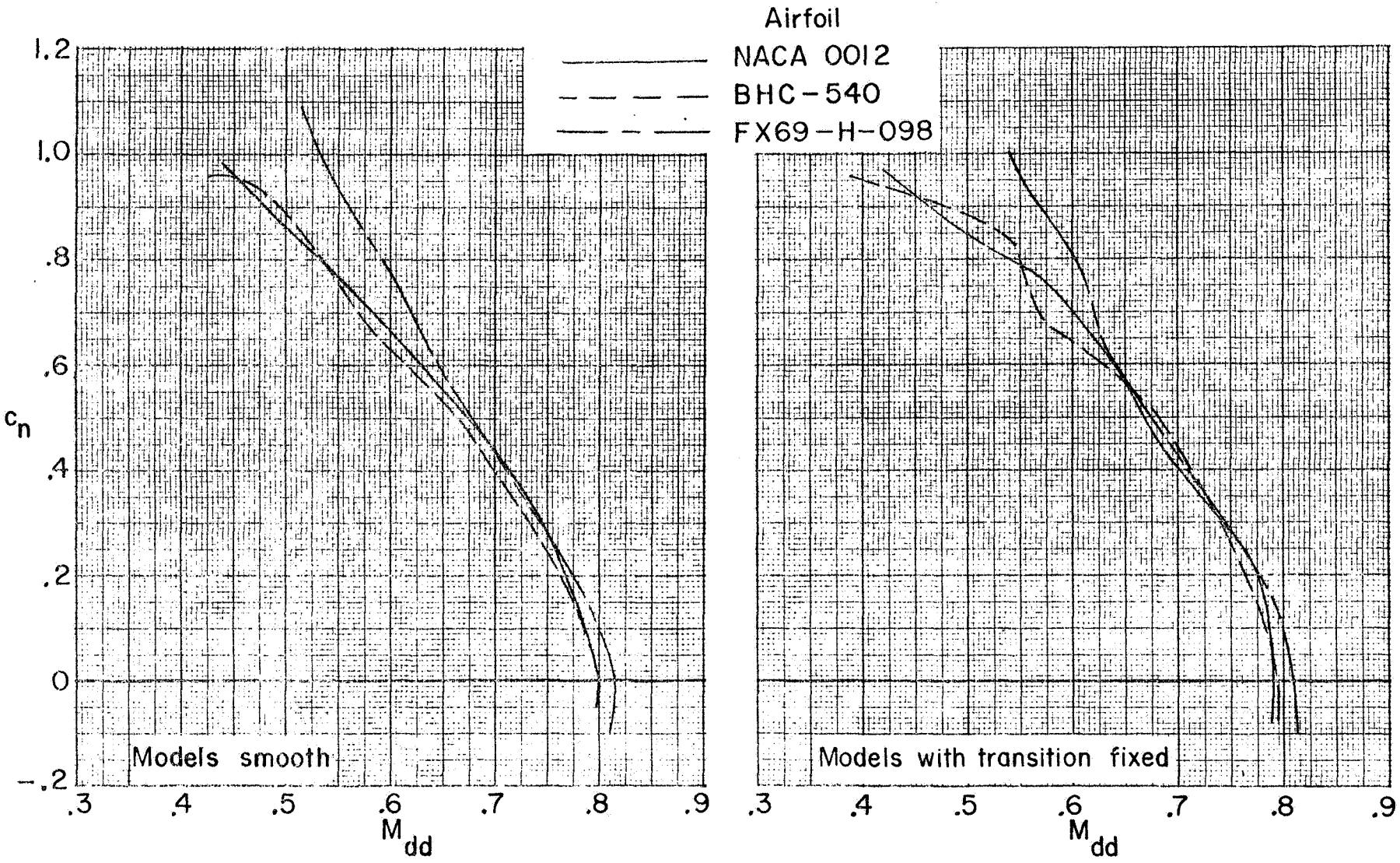

Figure 23.- Variation of section normal-force coefficient with drag divergence Mach number of the NACA 0012, the BHC-540, and the FX69-H-098 airfoils as measured in the Langley 6- by 28-inch transonic tunnel.

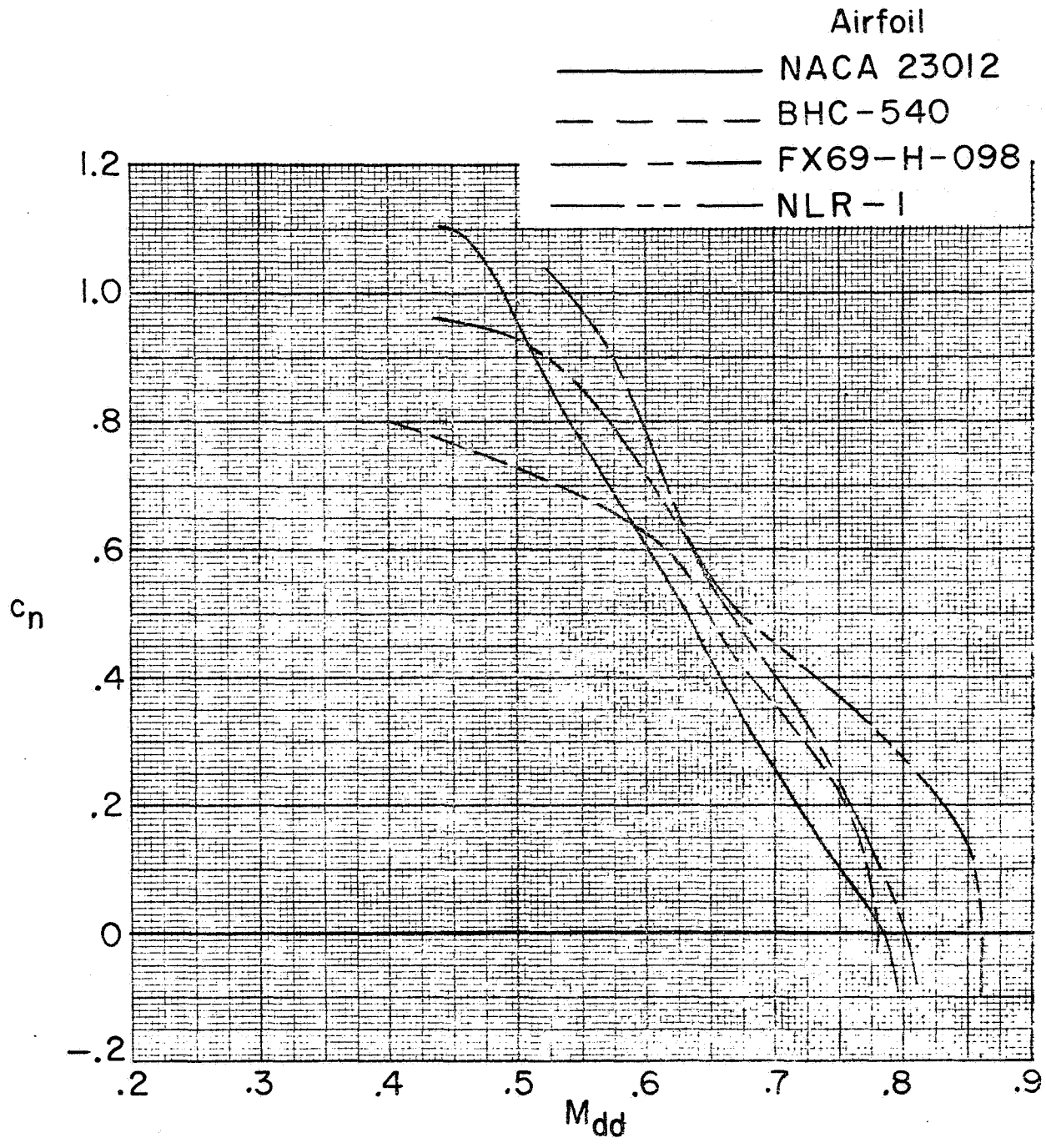

Figure 24. - Variation of section normal-force coefficient with drag divergence Mach number of the NACA 23012, the BHC-540, the FX69-H-098, and the NLR-1 airfoils as measured in the Langley 6×19-inch transonic tunnel. Models smooth.

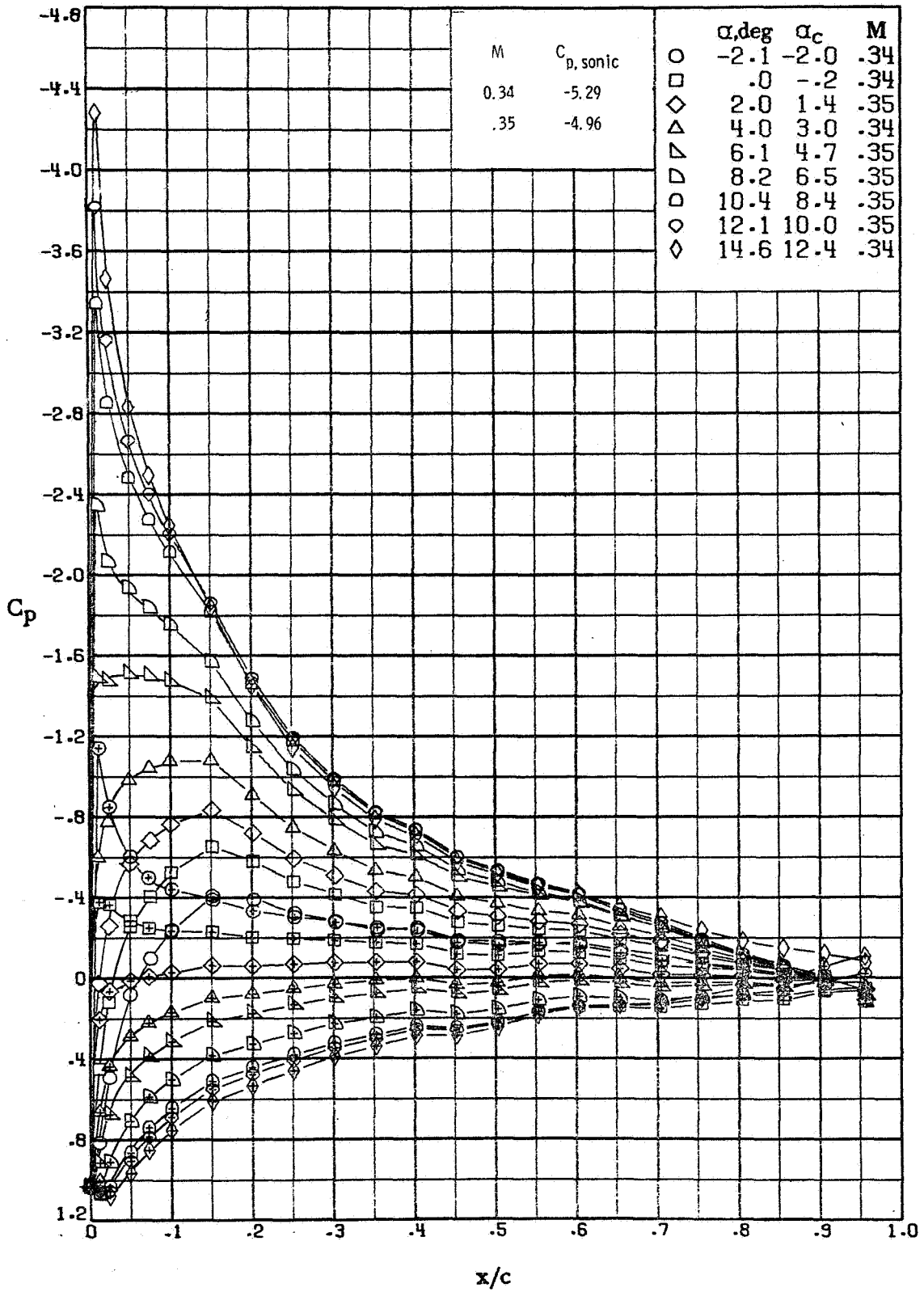

(a) $M \approx 0.35$; $R = 4.7 \times 10^6$.

Figure A1.--Effect of angle of attack on the chordwise pressure distribution of the FX69-H-098 airfoil measured in the Langley 6x28-inch transonic tunnel.

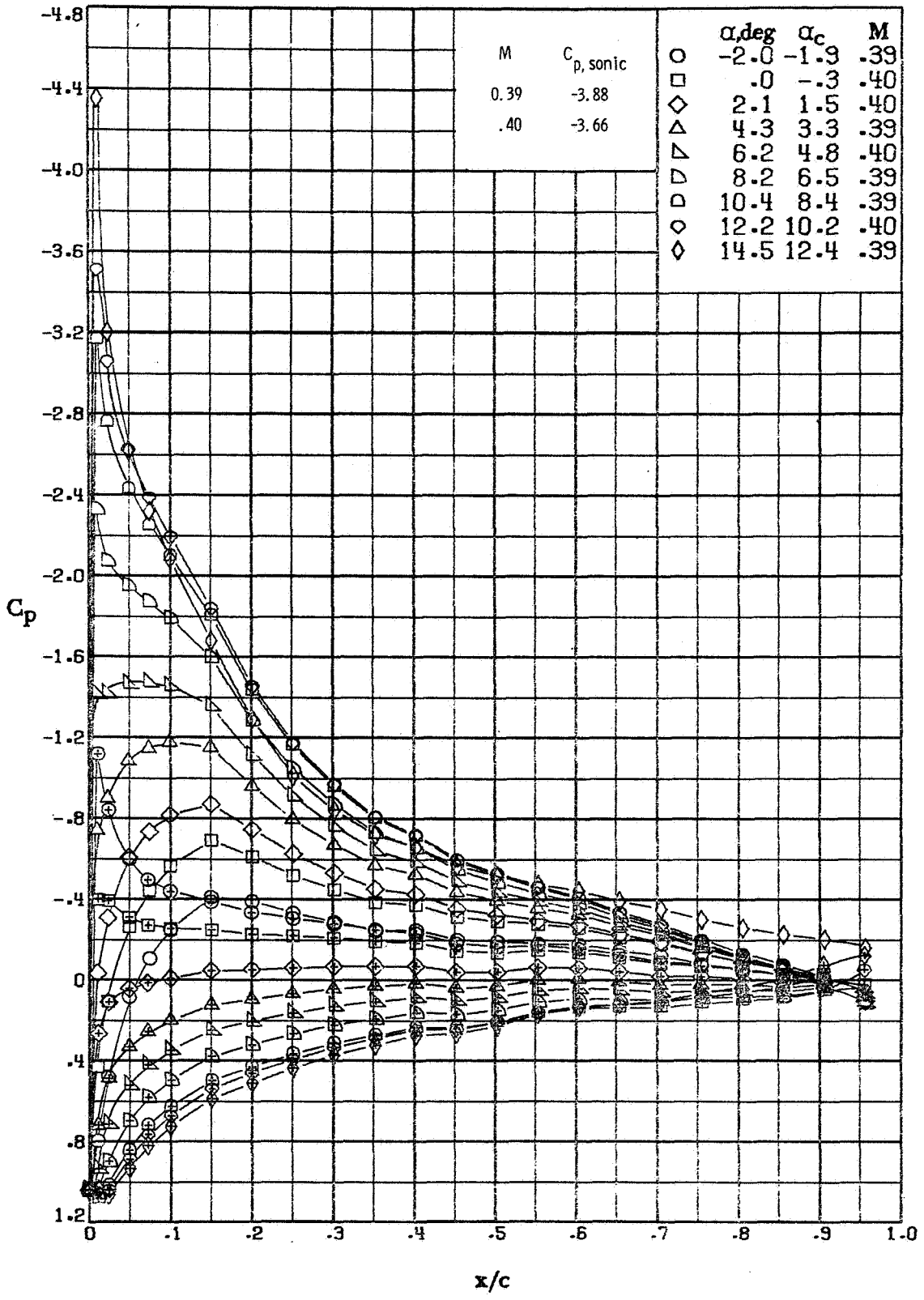

(b) $M \approx 0.40$; $R = 5.4 \times 10^6$.

Figure A1. - Continued.

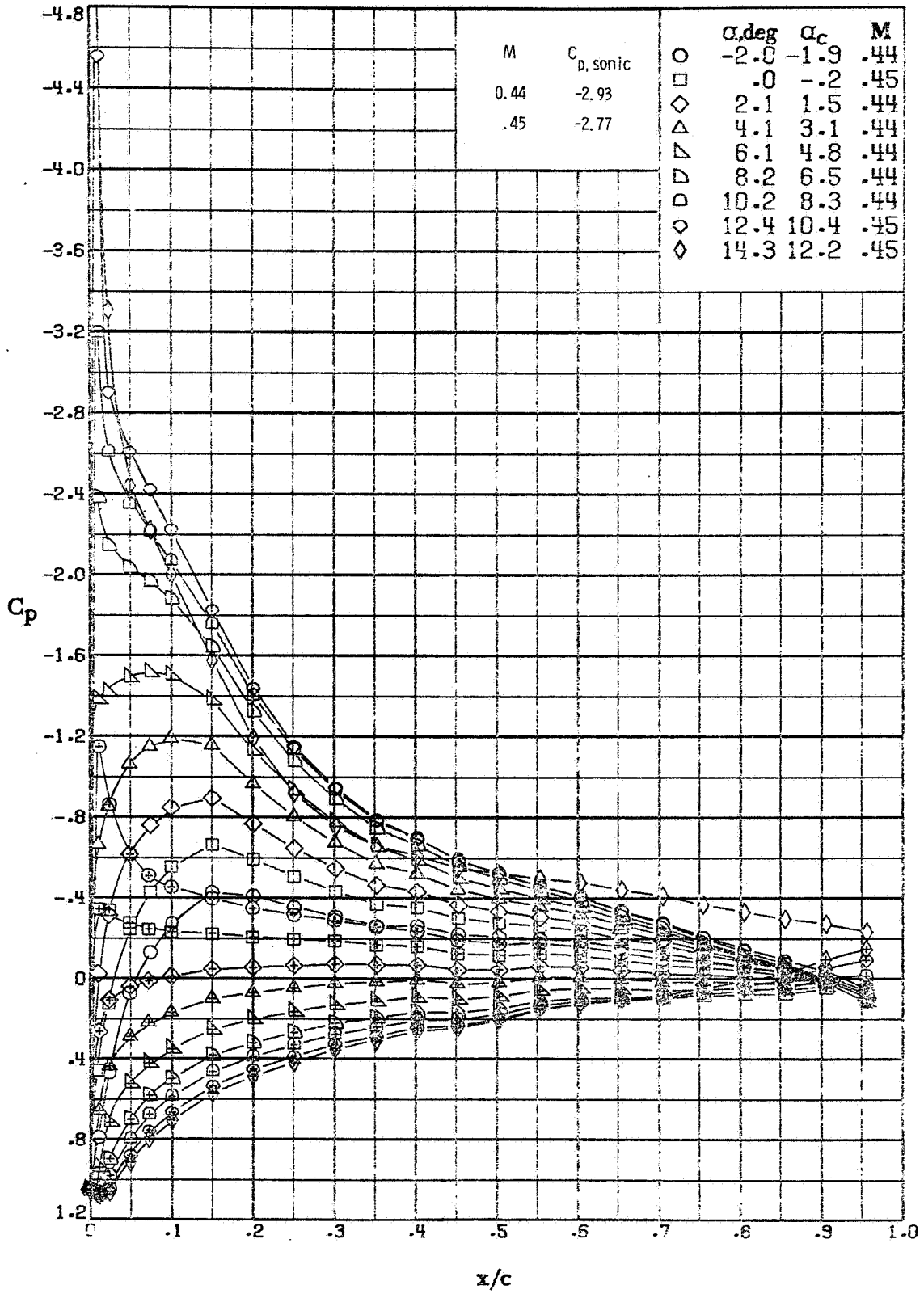

(c) $M \approx 0.44$; $R = 6.0 \times 10^6$.

Figure A1.- Continued.

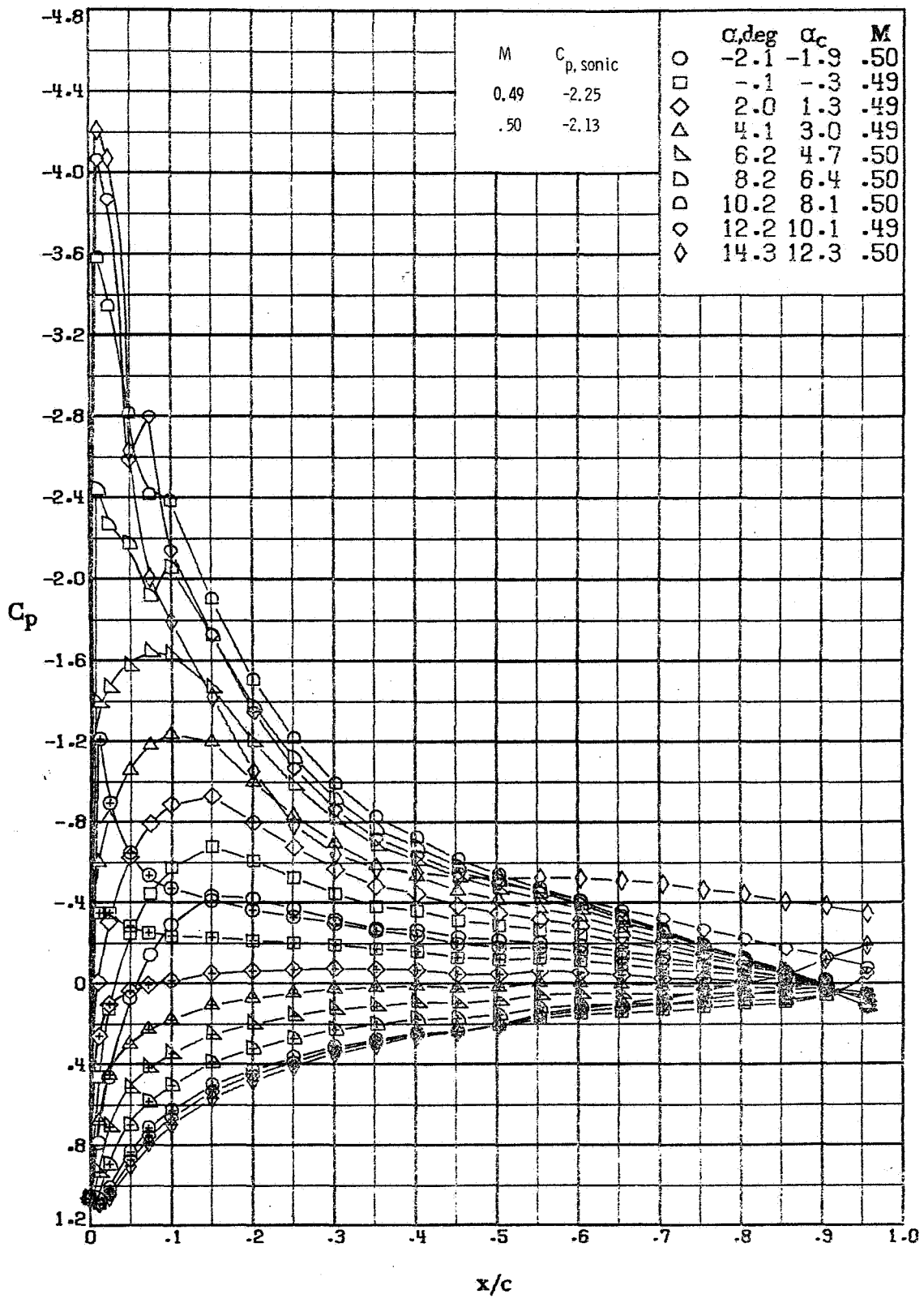

(d) $M \approx 0.50$; $R = 6.5 \times 10^6$.

Figure A1.- Continued.

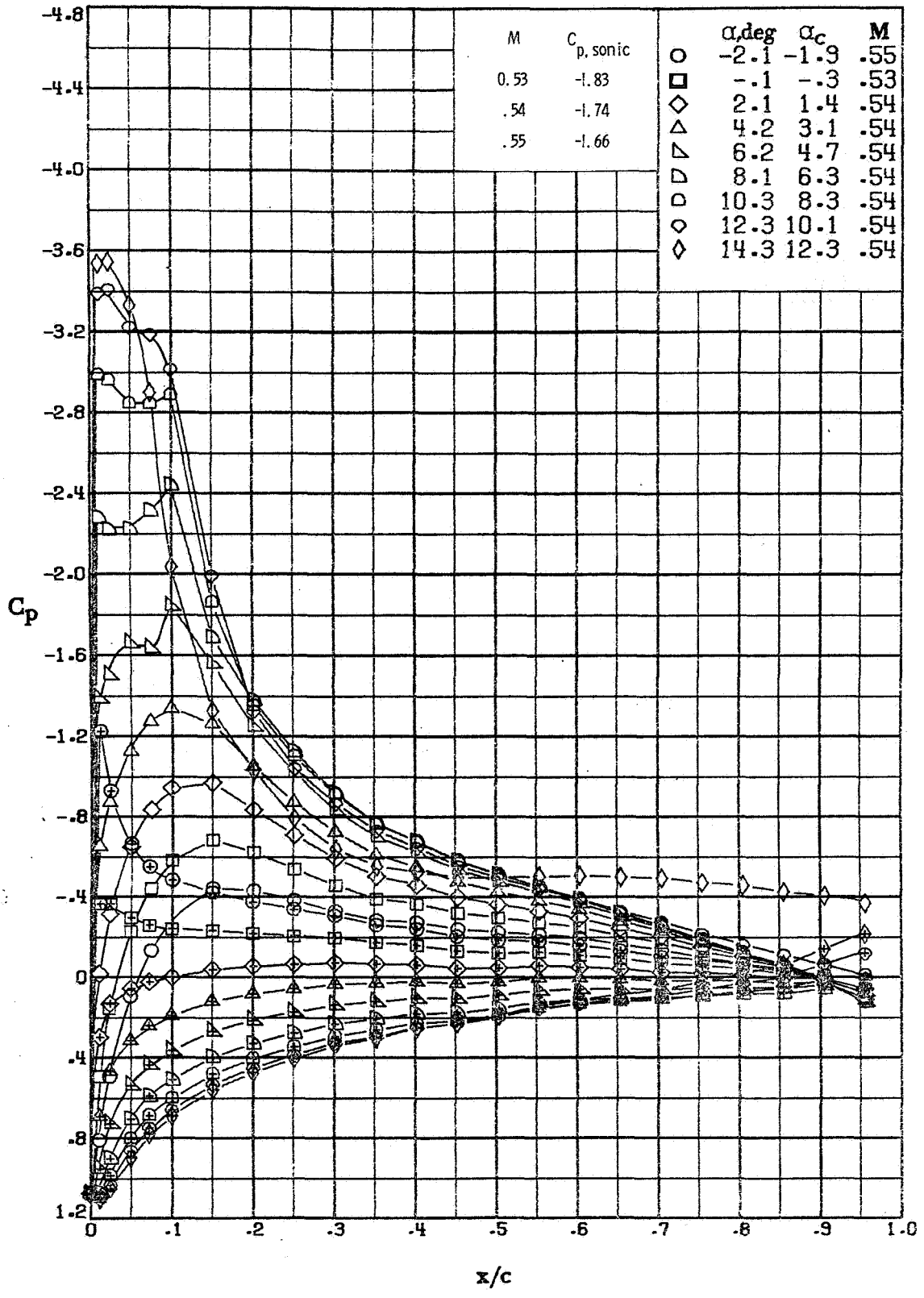

(e) $M \approx 0.54$; $R = 7.0 \times 10^6$.

Figure A1. - Continued.

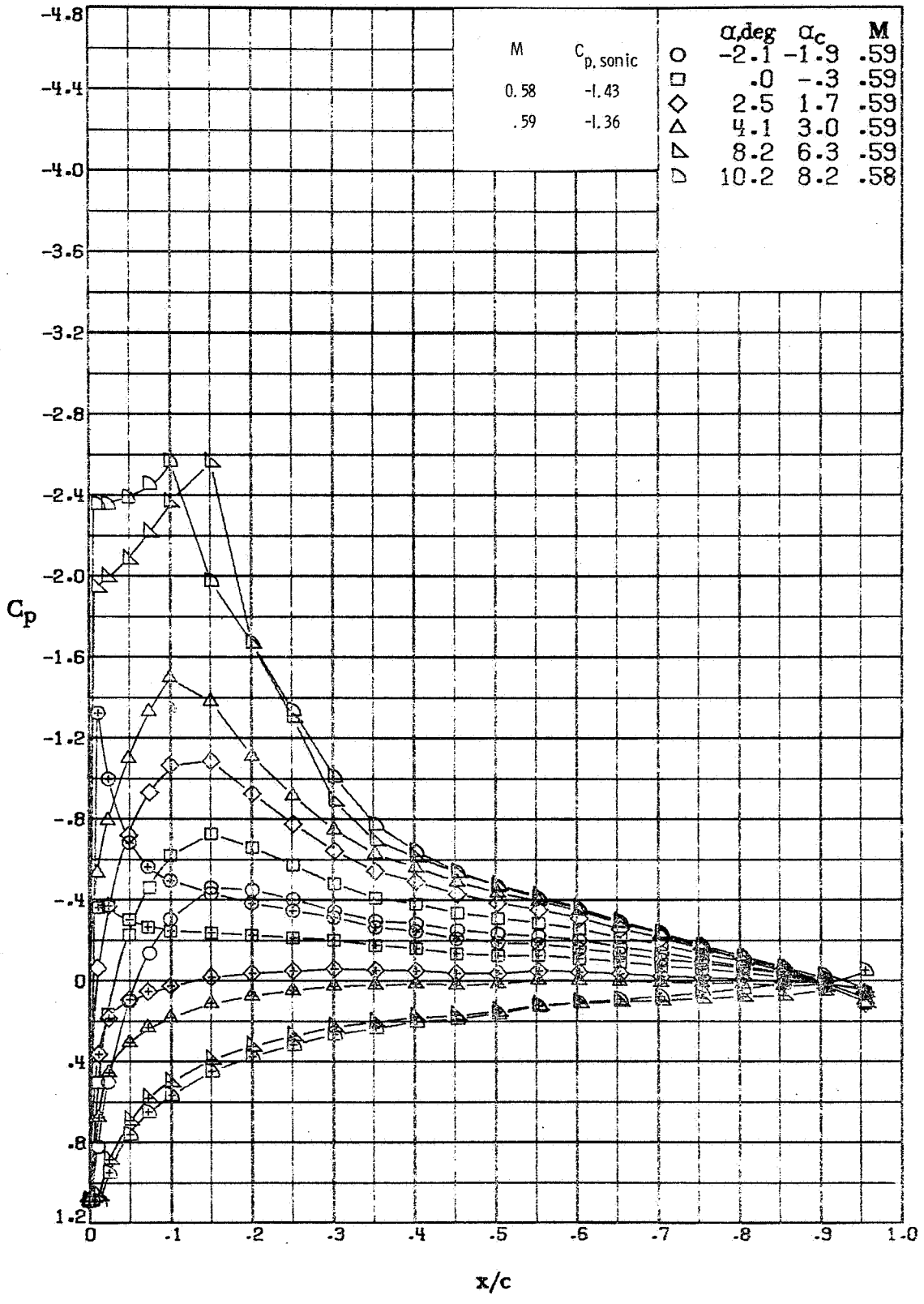

(f) M ≈ 0.59 ; R = 7.3 x 10^6.

Figure A1. - Continued.

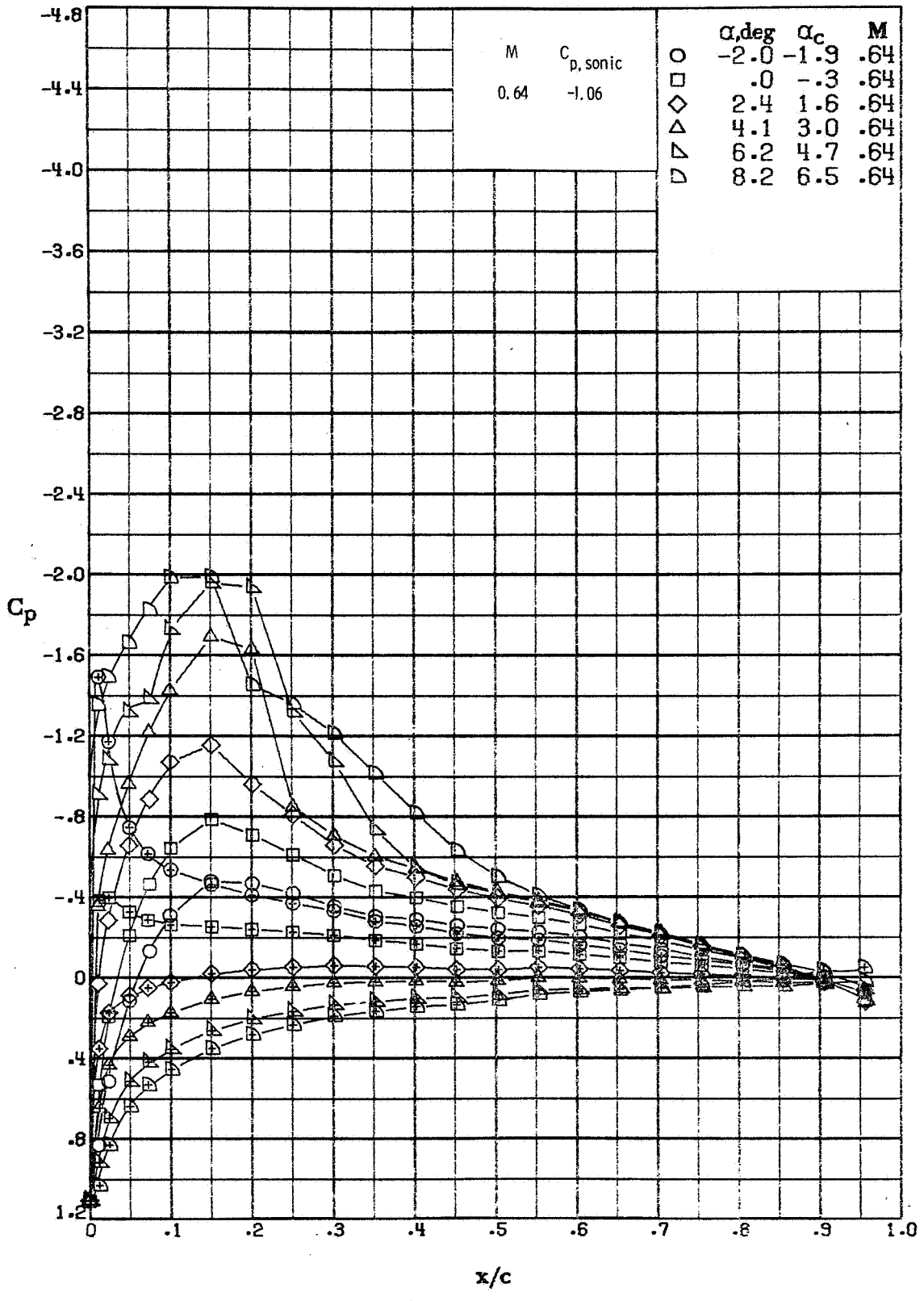

(g) $M \approx 0.64$: $R = 7.8 \times 10^6$.

Figure A1. - Continued.

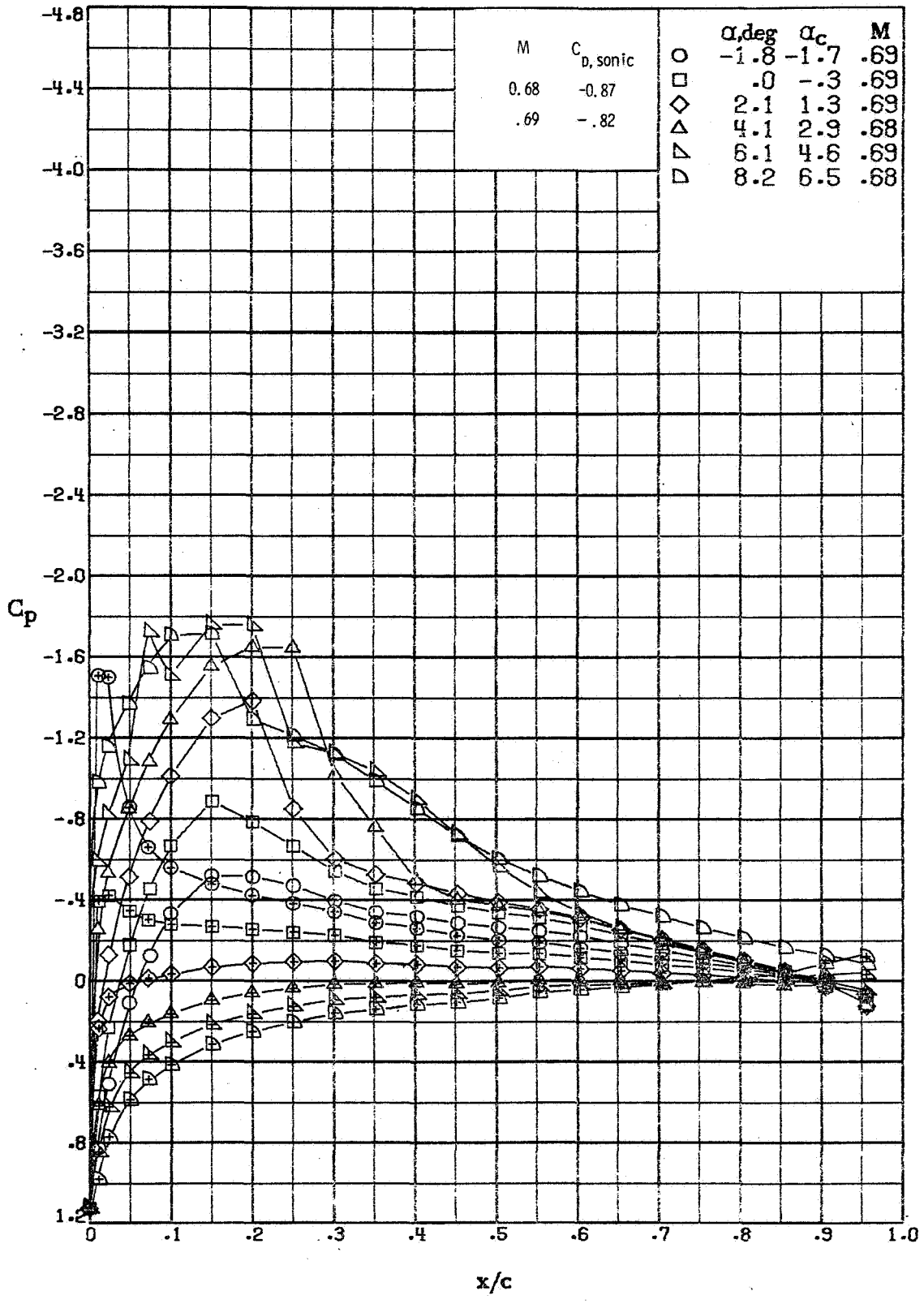

(h) $M \approx 0.69$; $R = 8.2 \times 10^6$.

Figure A1.- Continued.

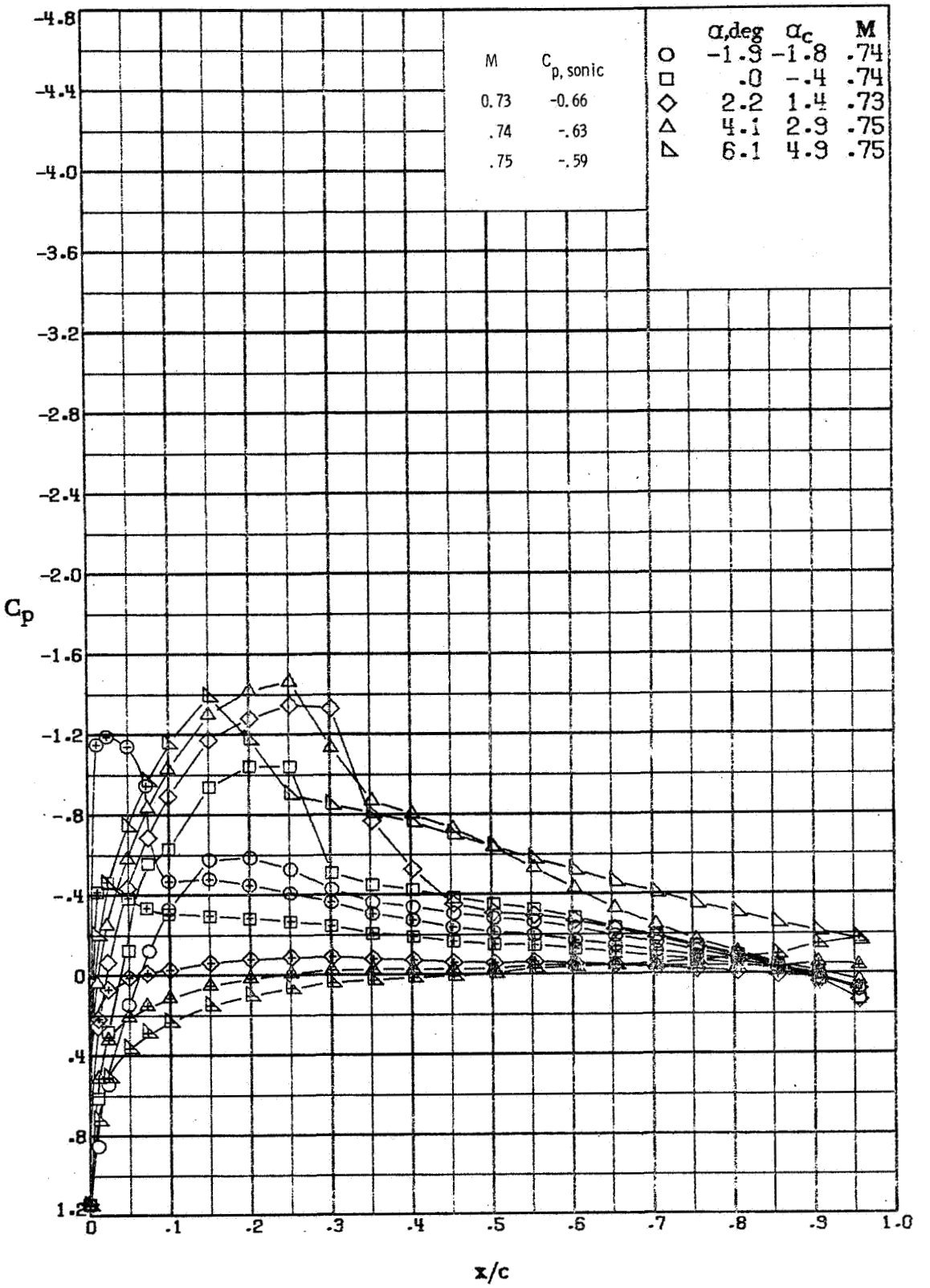

(i) $M \approx 0.75$; $R = 8.6 \times 10^6$.

Figure A1.- Continued.

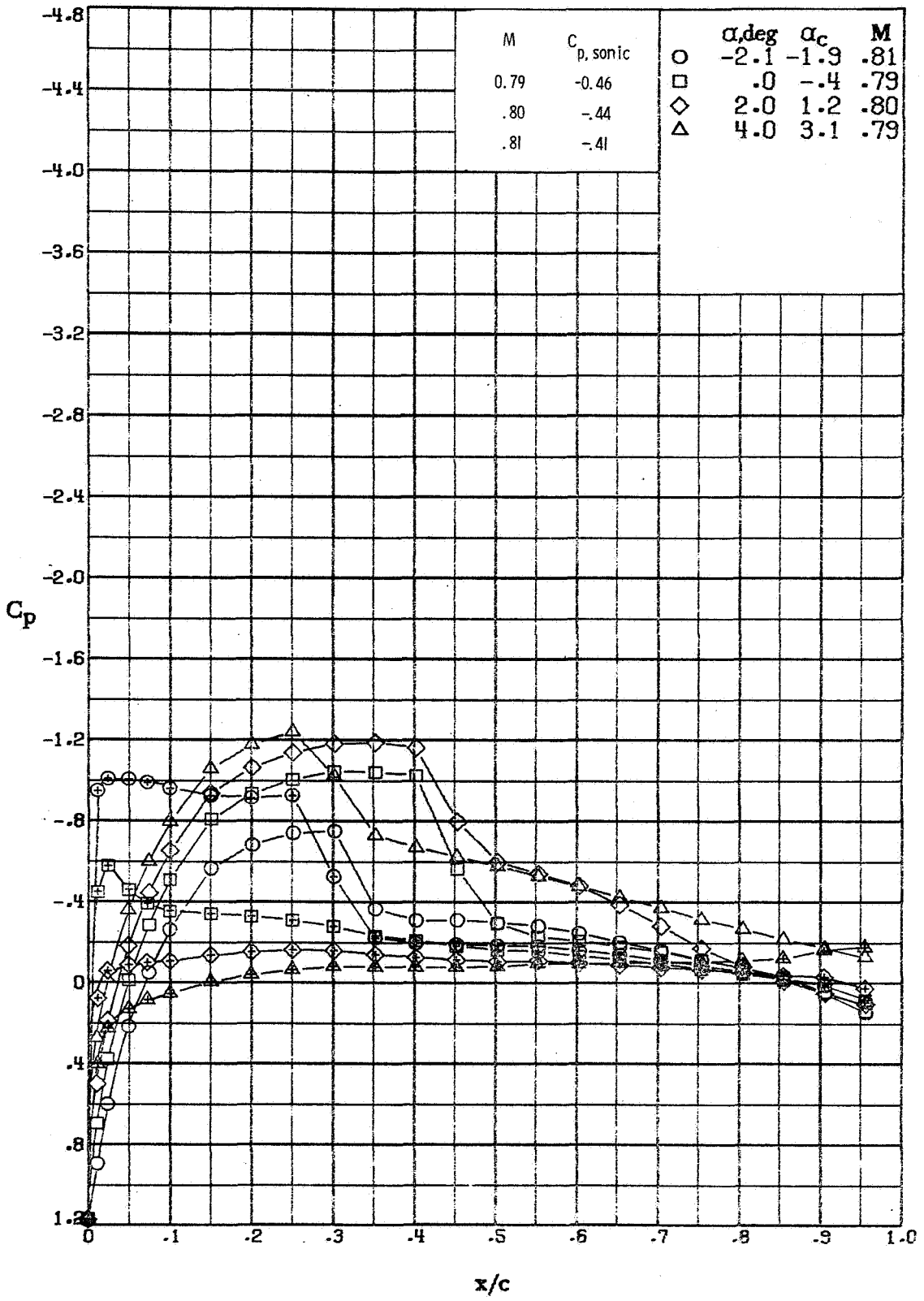

(j) M ≈ 0.80 ; R = 8.9 x 10^6.

Figure A1.- Continued.

REPRODUCIBILITY OF THE
ORIGINAL PAGE

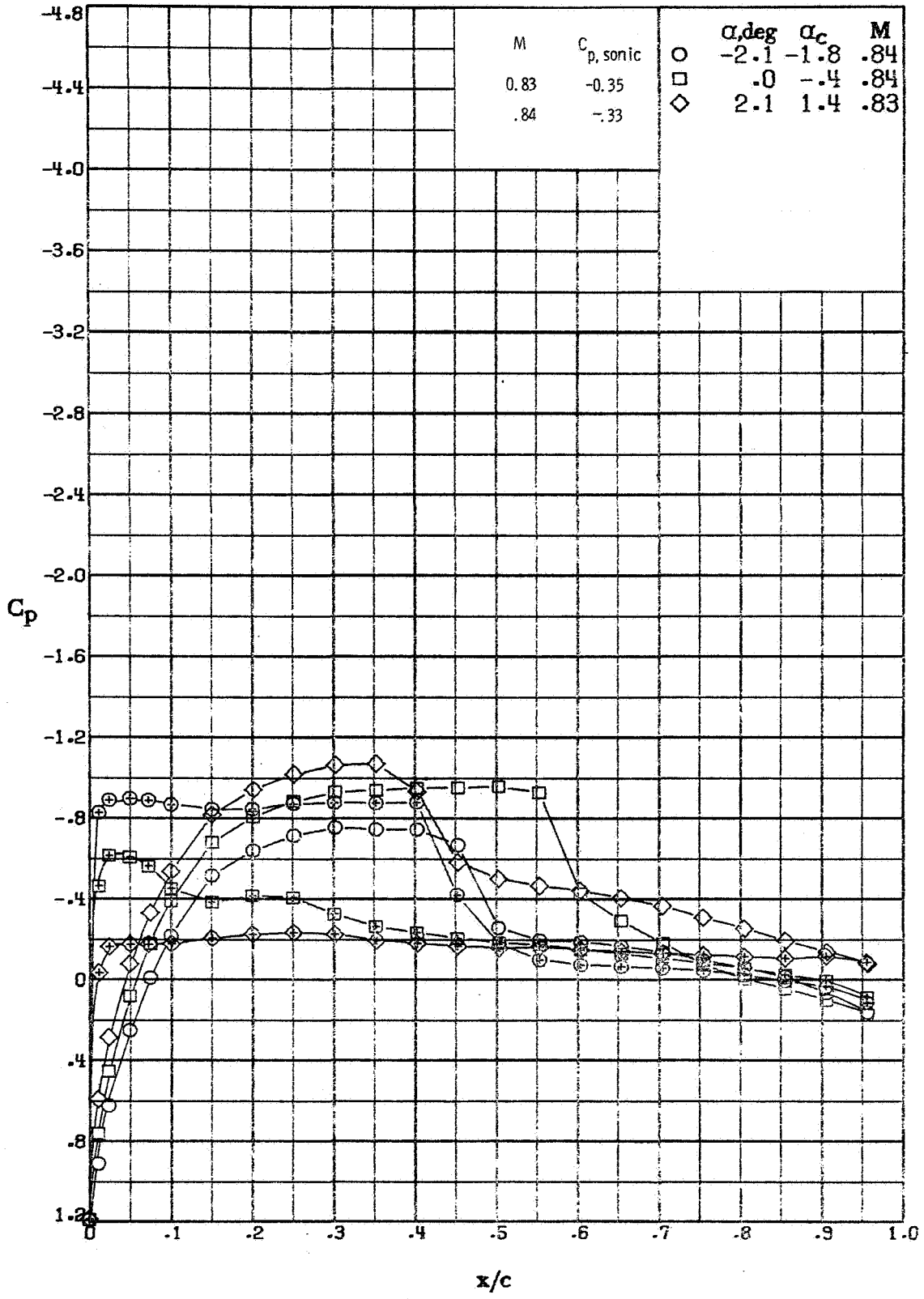

(k) M ≈ 0.84 ; R = 9.2 x 10^6.

Figure A1.- Continued.

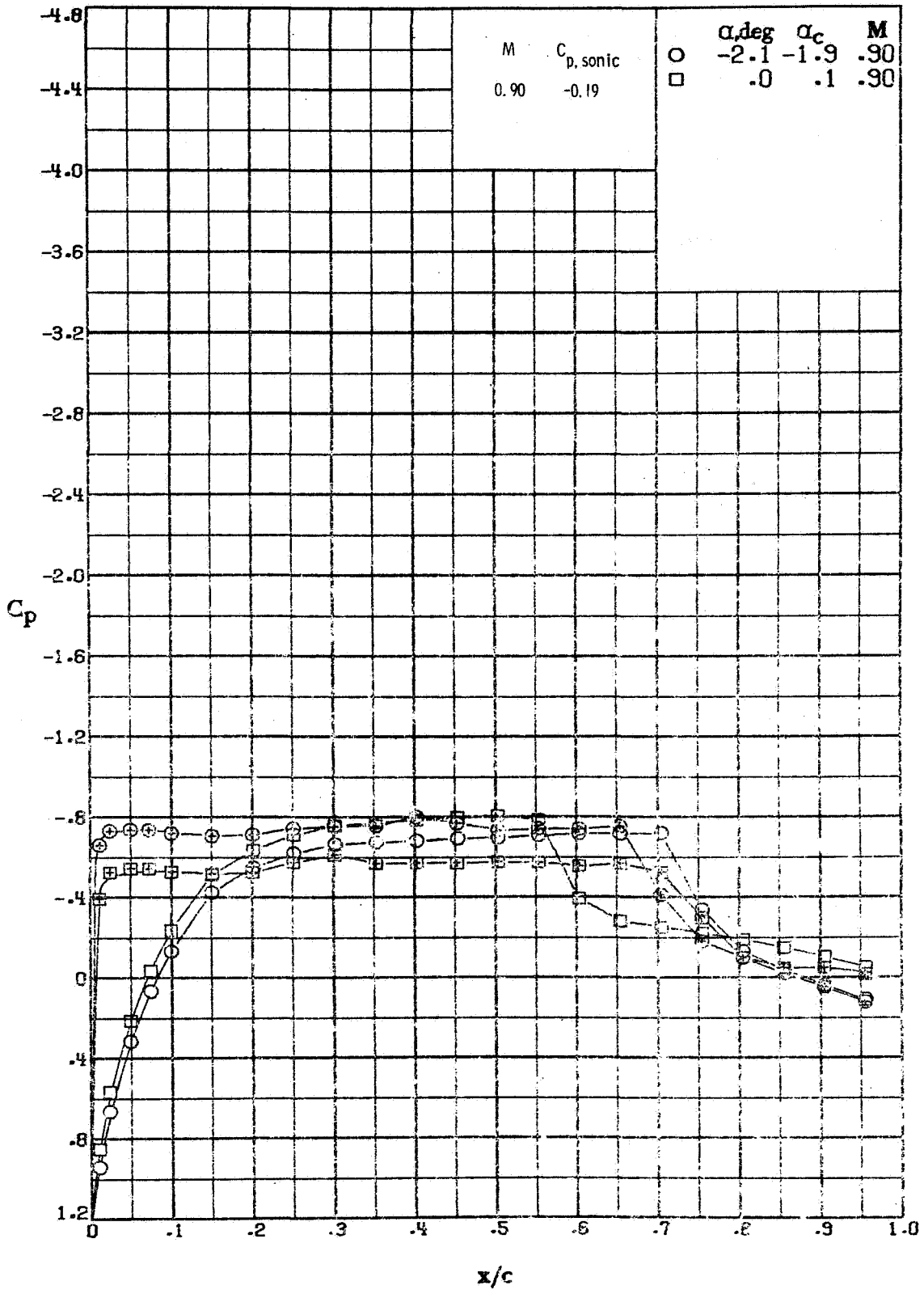

(l) $M \approx 0.90$; $R = 9.8 \times 10^6$.

Figure A1.- Concluded.

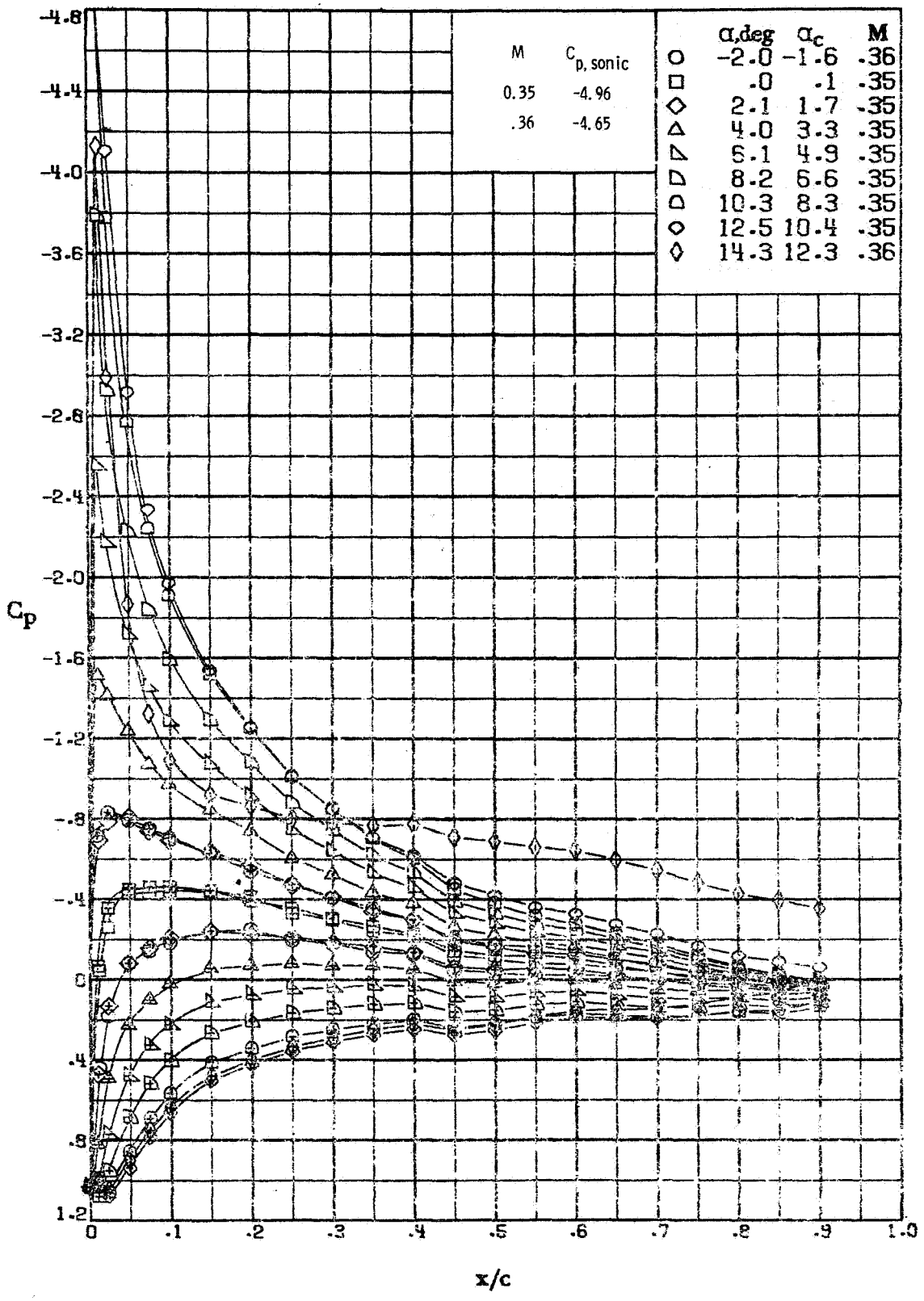

(a) $M \approx 0.35$; $R = 4.7 \times 10^6$.

Figure A2.-Effect of angle of attack on the chordwise pressure distribution of the BHC-540 airfoil measured in the Langley 6x28-inch transonic tunnel.

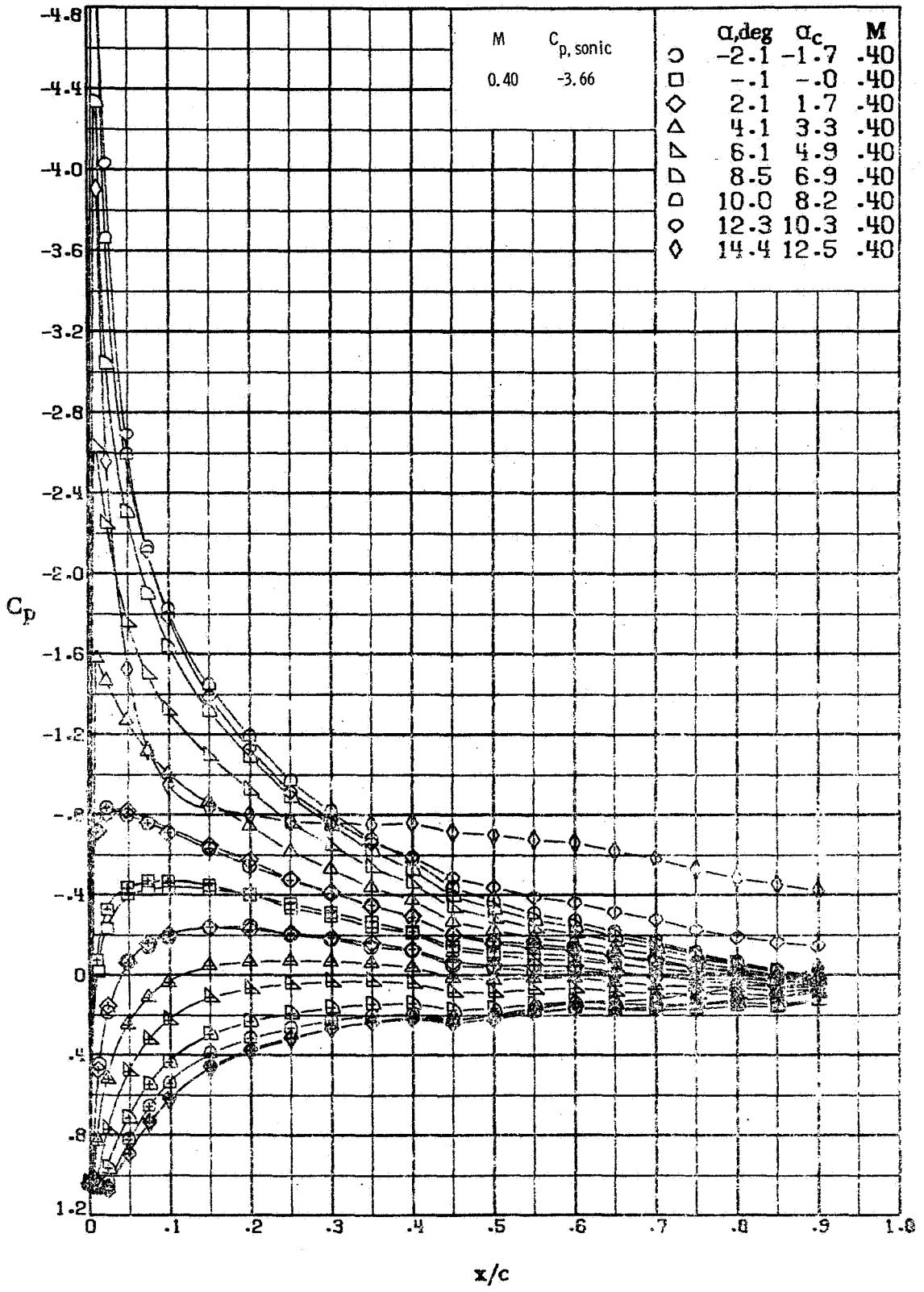

(b) $M \approx 0.40$; $R = 5.5 \times 10^6$.

Figure A2. - Continued.

REPRODUCIBILITY OF THE
ORIGINAL PAGE IS POOR

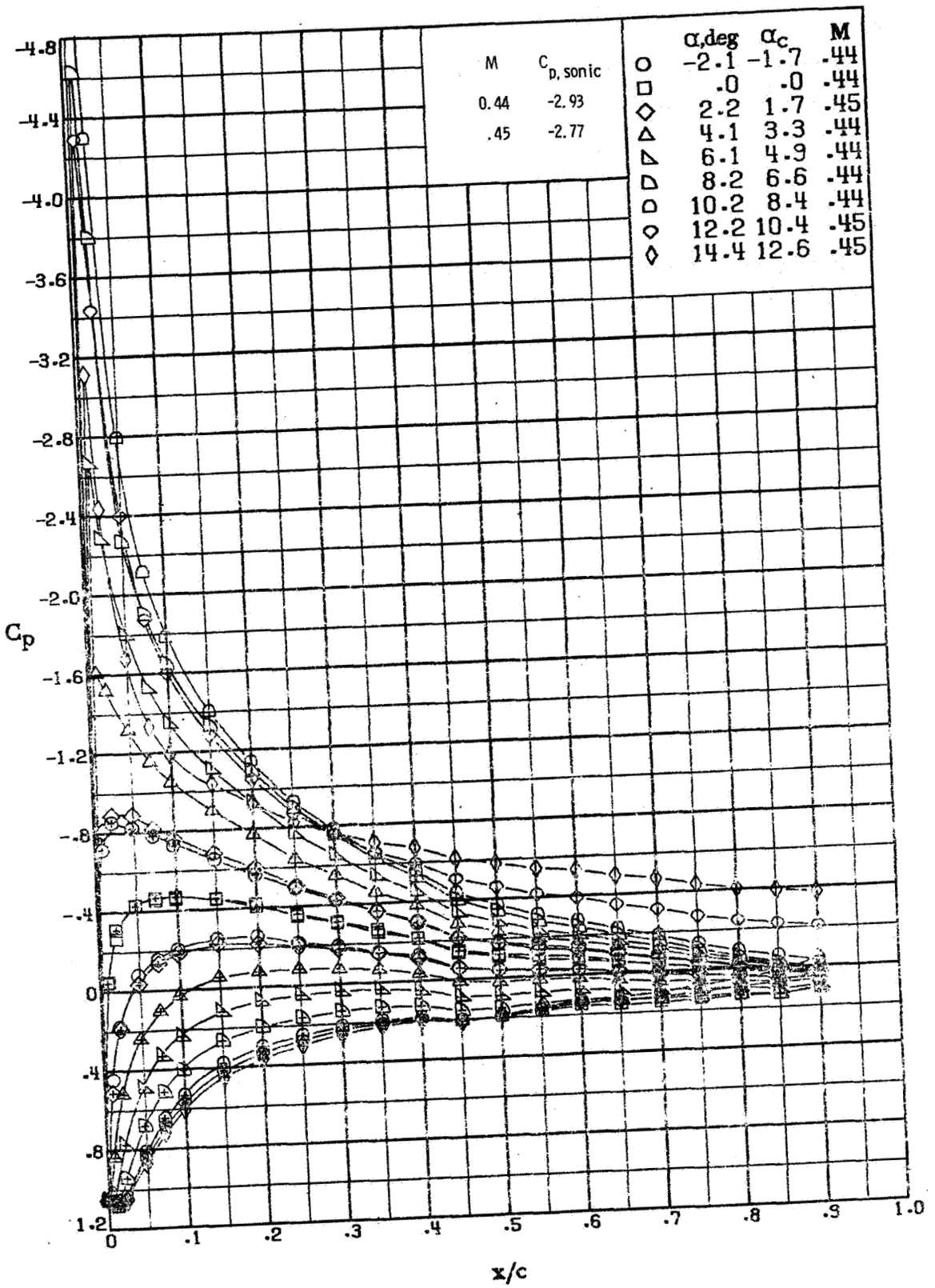

(c) $M \approx 0.44$: $R = 6.1 \times 10^6$.

Figure A2.- Continued.

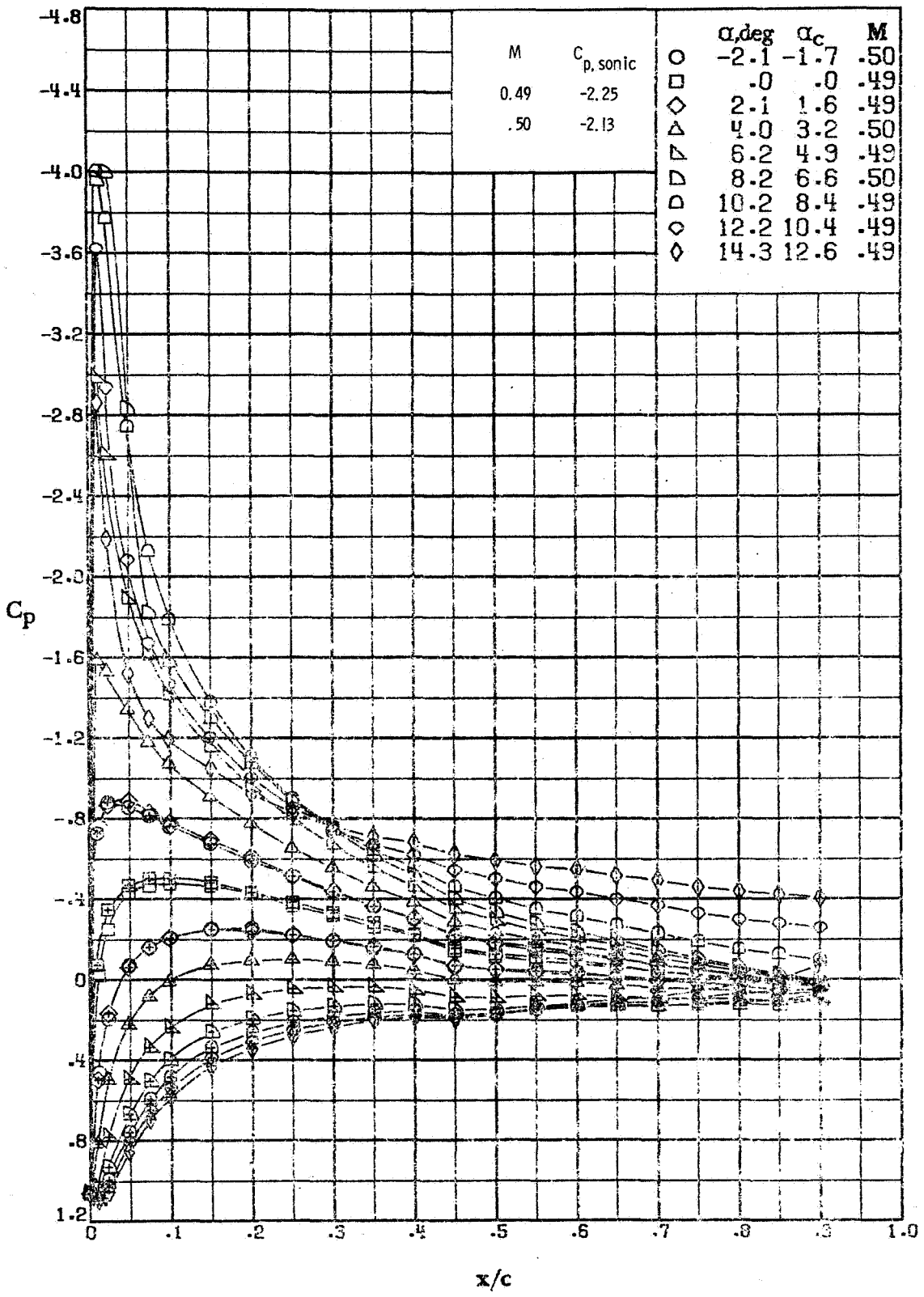

(d) M ≈ 0.49 : R =6.5 x 10^6.

Figure A2. - Continued.

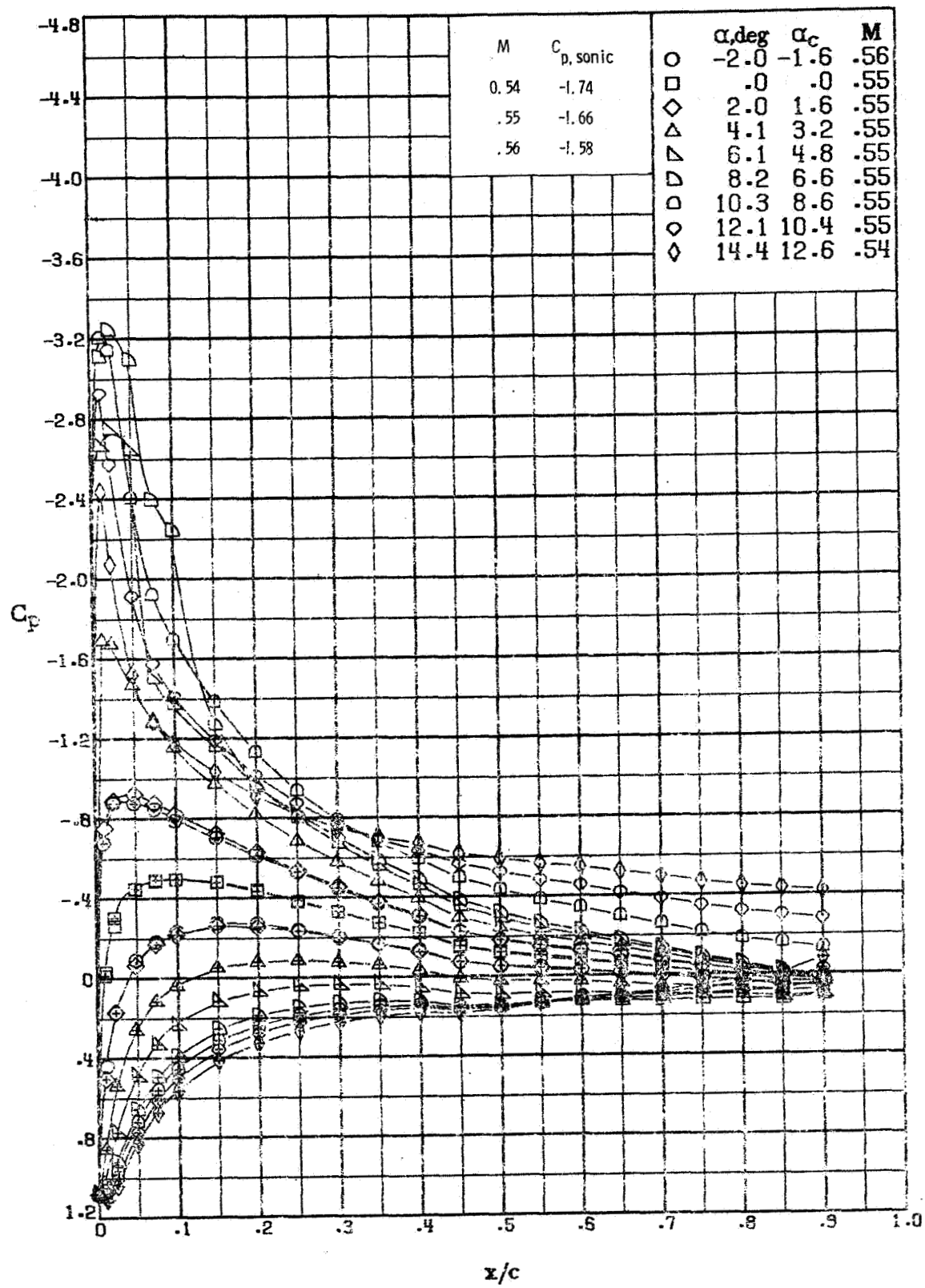

(e) $M \approx 0.55$; $R = 7.1 \times 10^6$.

Figure A2. - Continued.

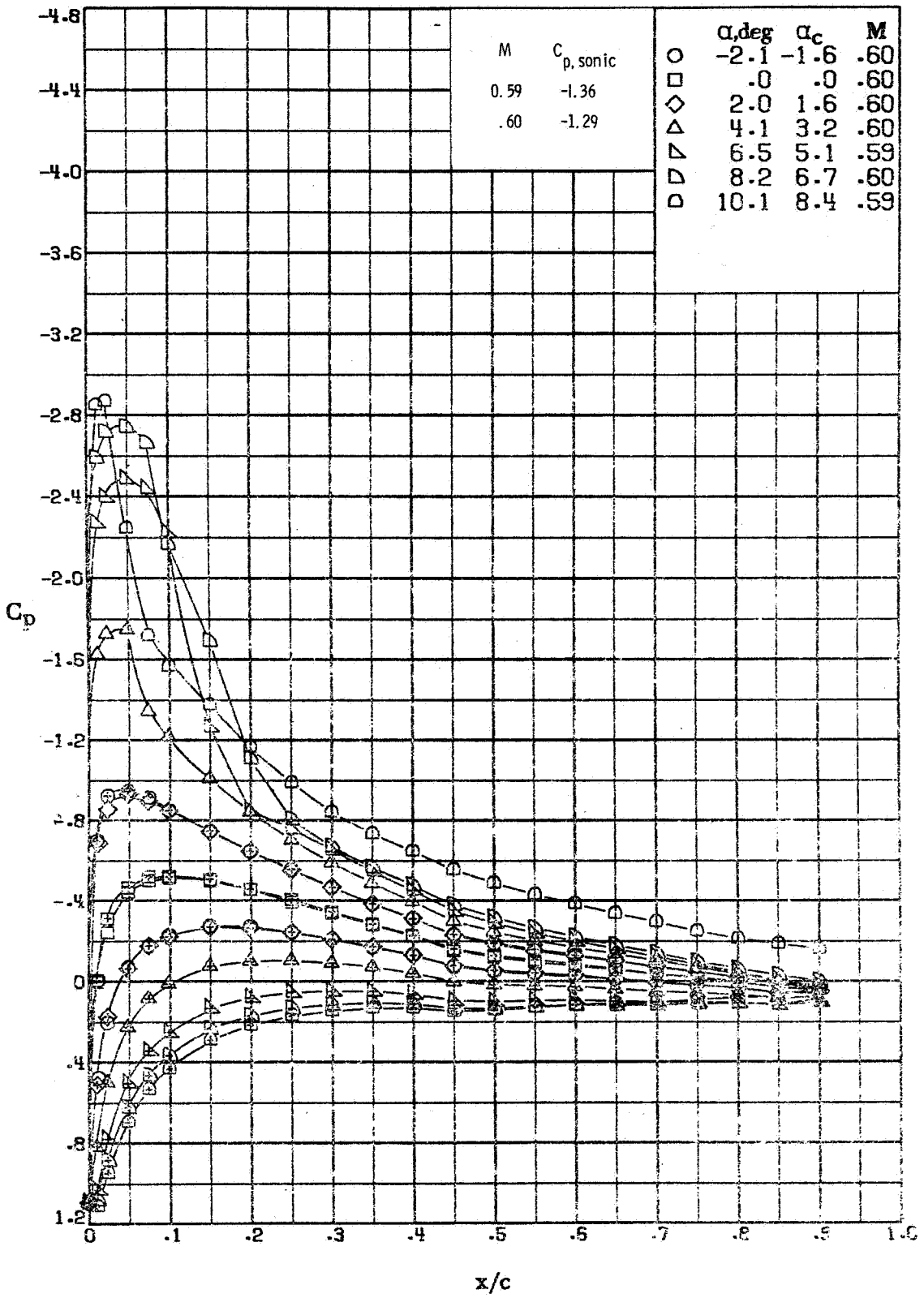

(f) $M \approx 0.60$; $R = 7.5 \times 10^6$.

Figure A2.- Continued.

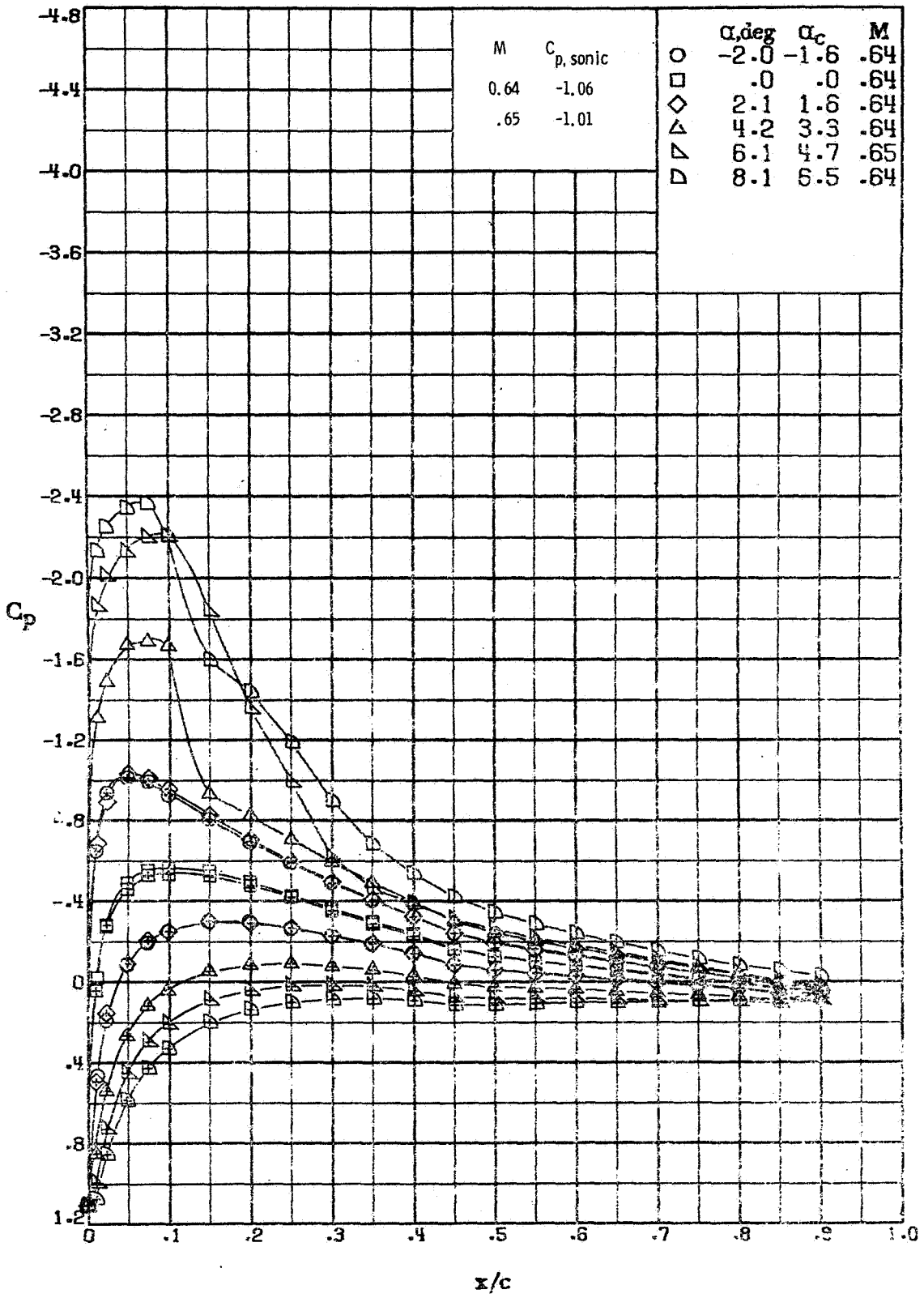

(g) M ≈ 0.64 ; R = 8.0 x 10^6.

Figure A2. - Continued.

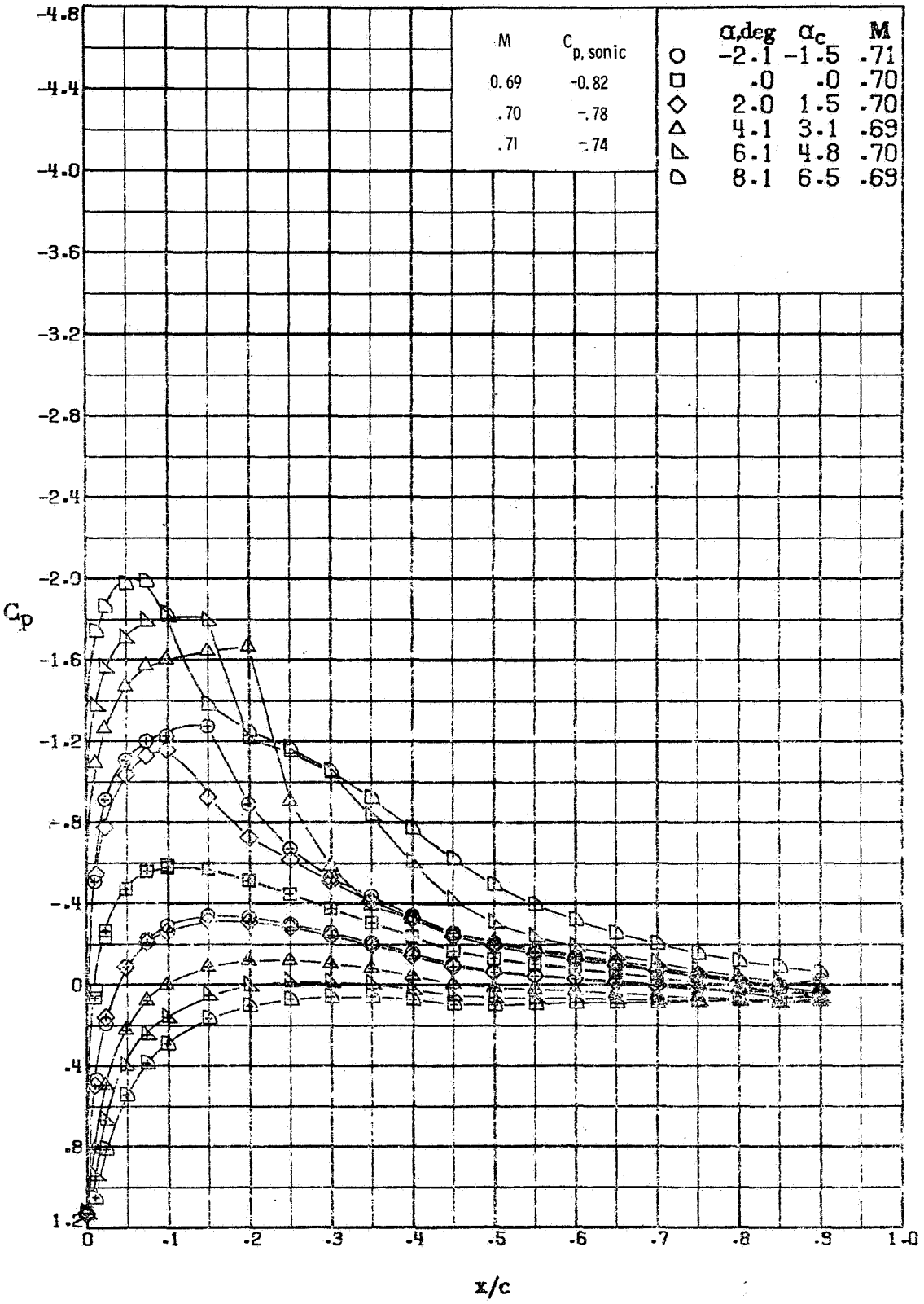

(h) $M \approx 0.70$; $R = 8.4 \times 10^6$.

Figure A2. - Continued.

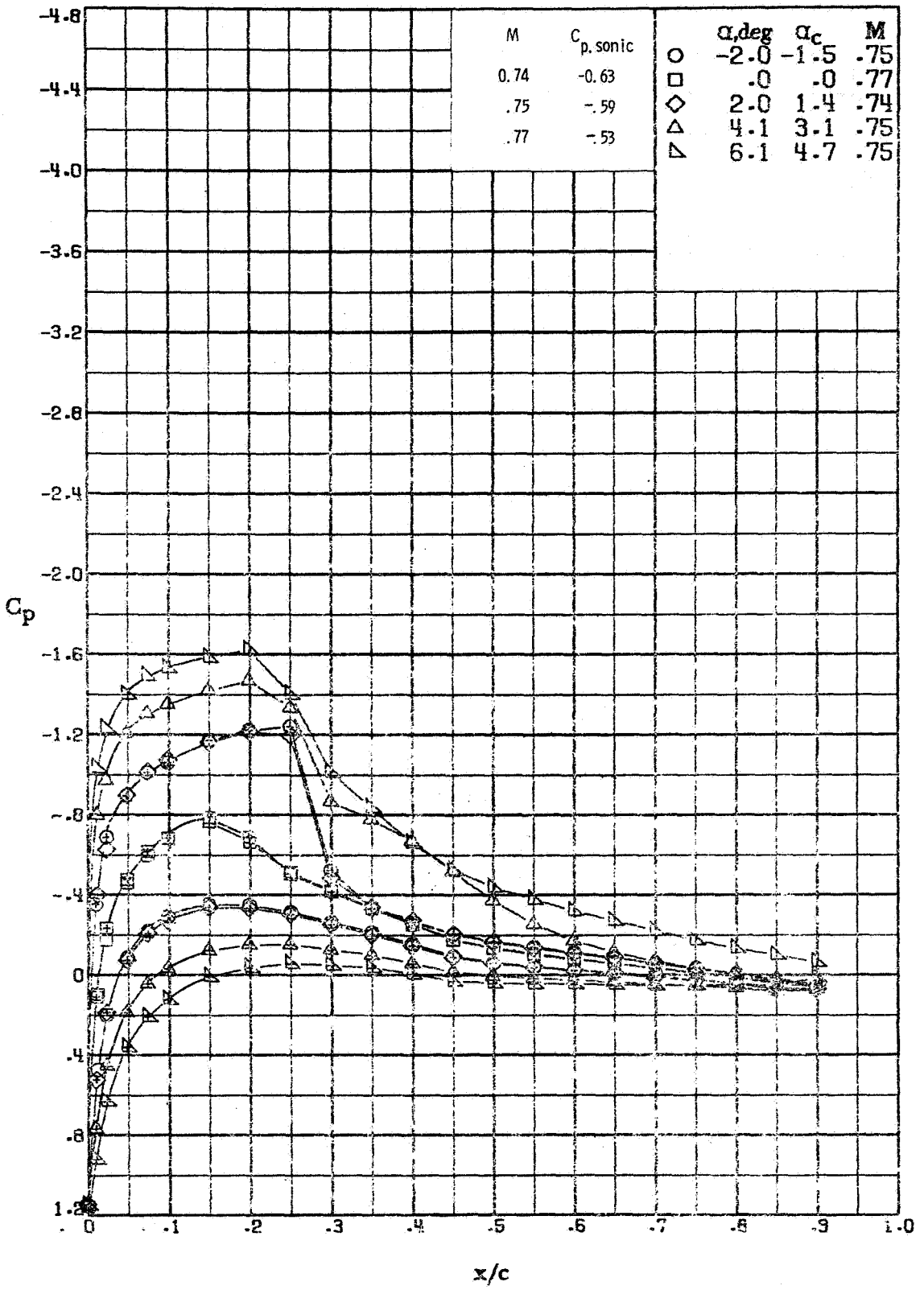

(i) $M \approx 0.75$; $R = 8.8 \times 10^6$.

Figure A2. - Continued.

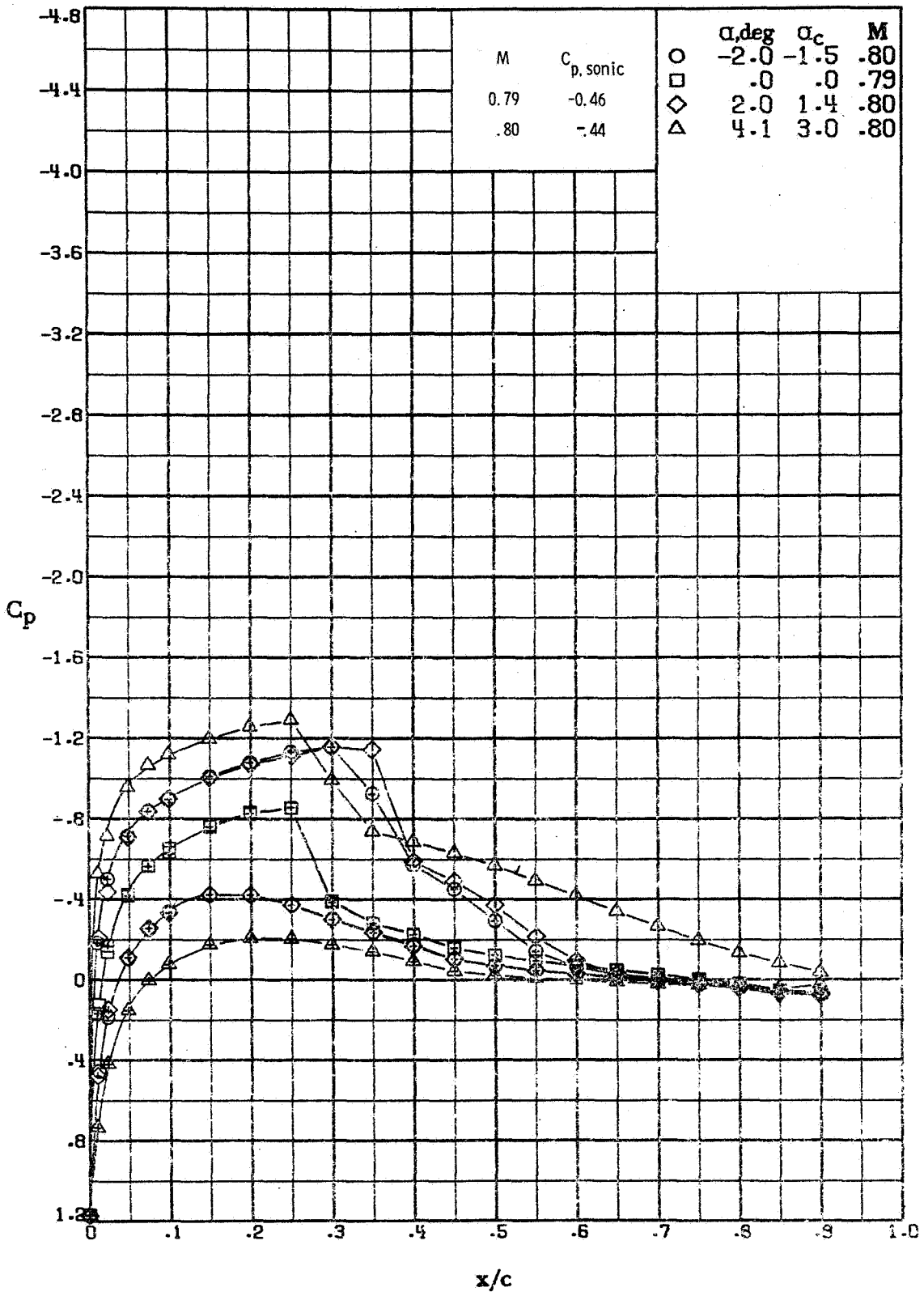

(j) $M \approx 0.80$; $R = 9.0 \times 10^6$.

Figure A2. - Continued.

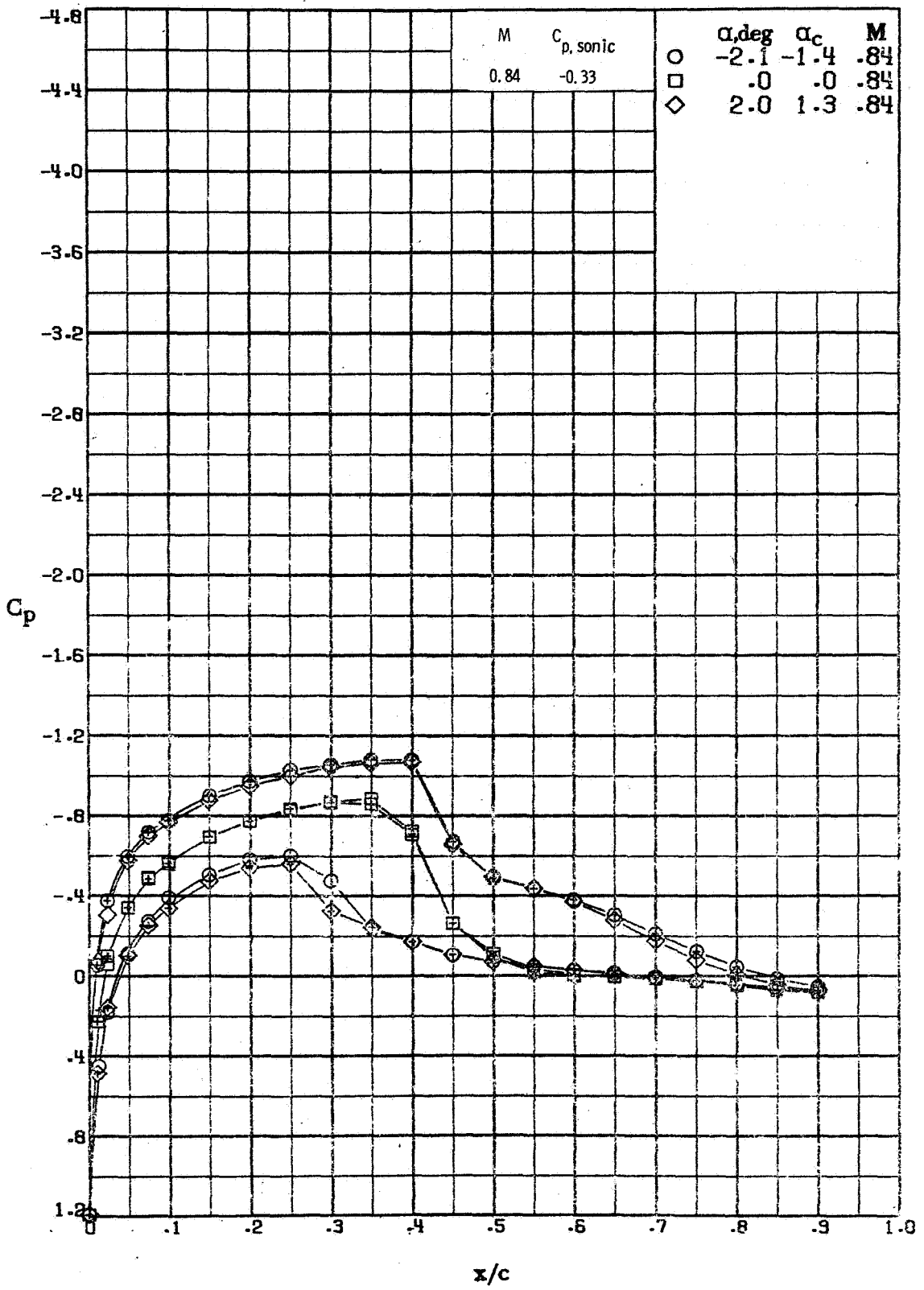

(k) $M \approx 0.84$; $R = 9.2 \times 10^6$.

Figure A2. - Continued.

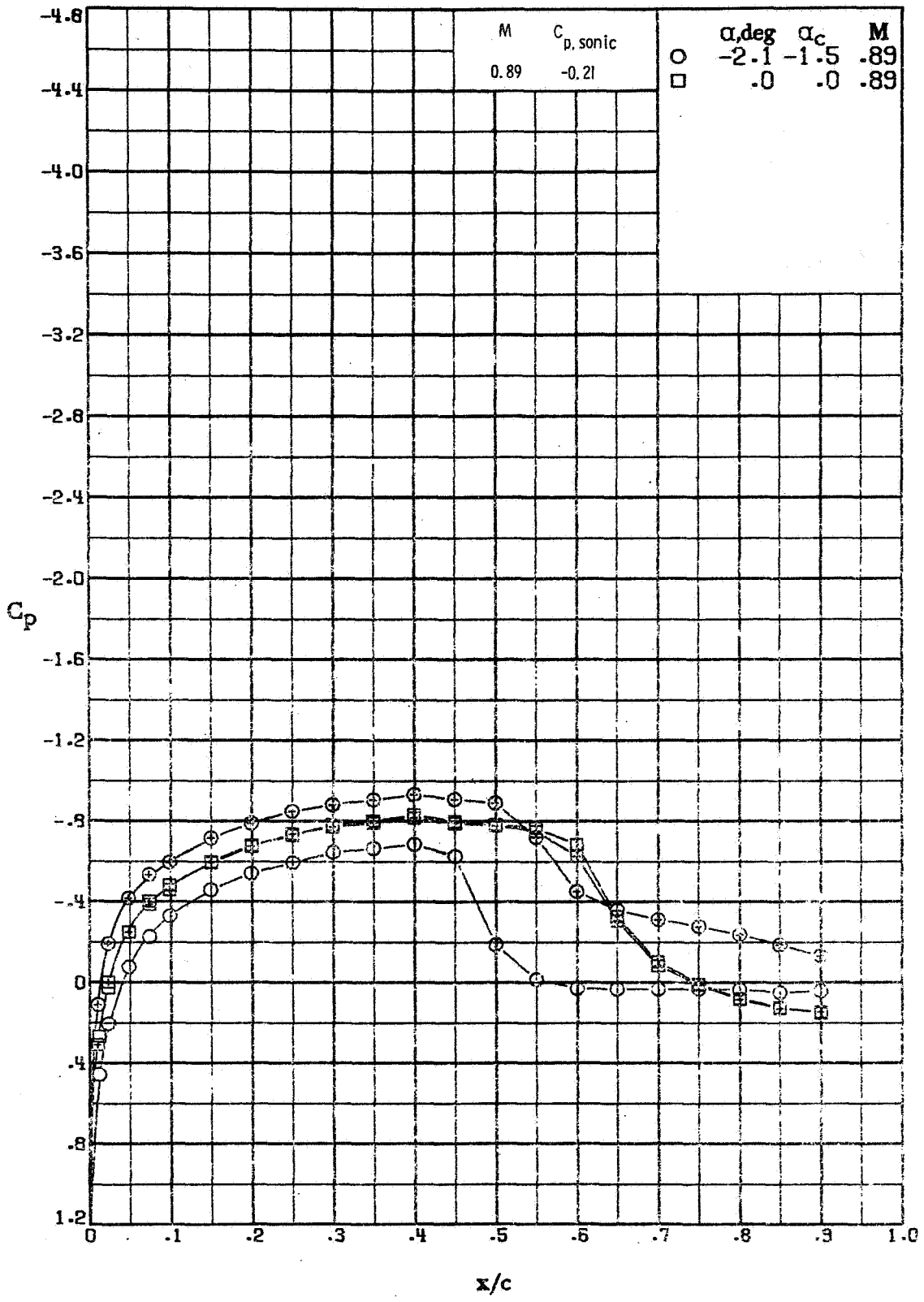

(l) M ≈ 0.89 ; R = 9.4 x 10^6.

Figure A2.- Concluded.

REPRODUCIBILITY OF THE
ORIGINAL PAGE IS POOR

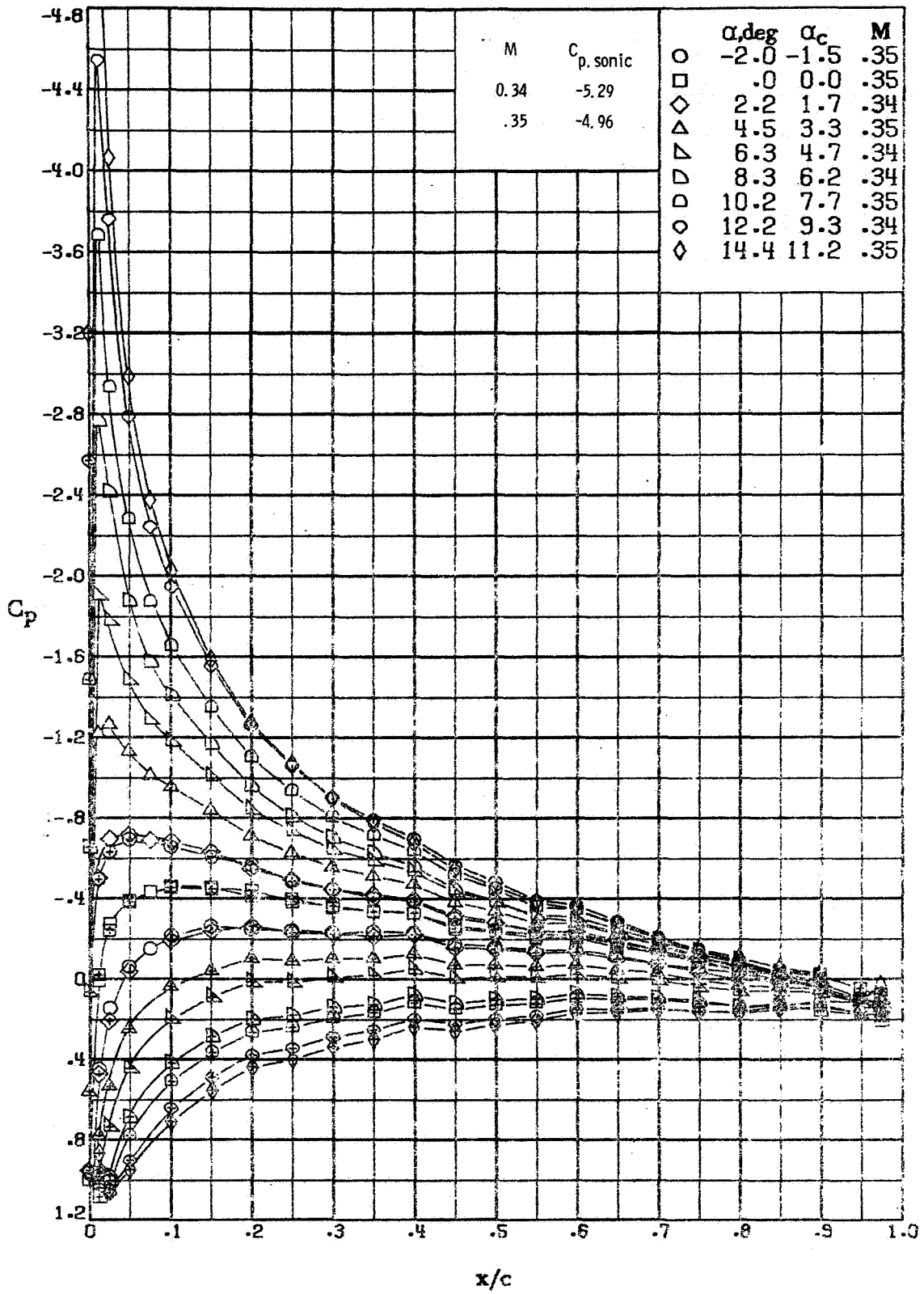

(a) $M \approx 0.35$; $R = 4.9 \times 10^6$.

Figure A3.-Effect of angle of attack on the chordwise pressure distribution of the NACA 0012 airfoil measured in the Langley 6x28-inch transonic tunnel.

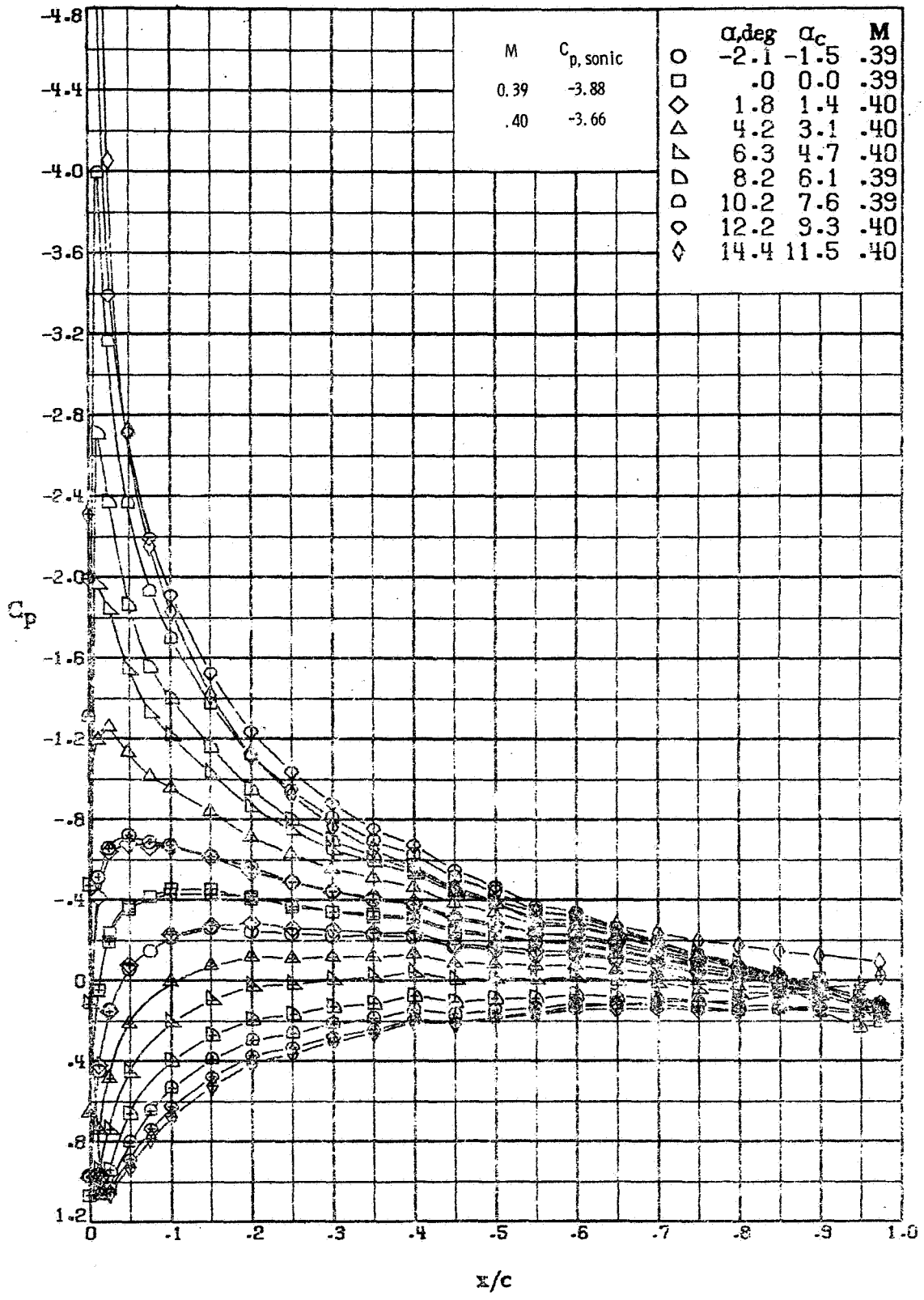

(b) $M \approx 0.40$; $R = 5.5 \times 10^6$.

Figure A3. - Continued.

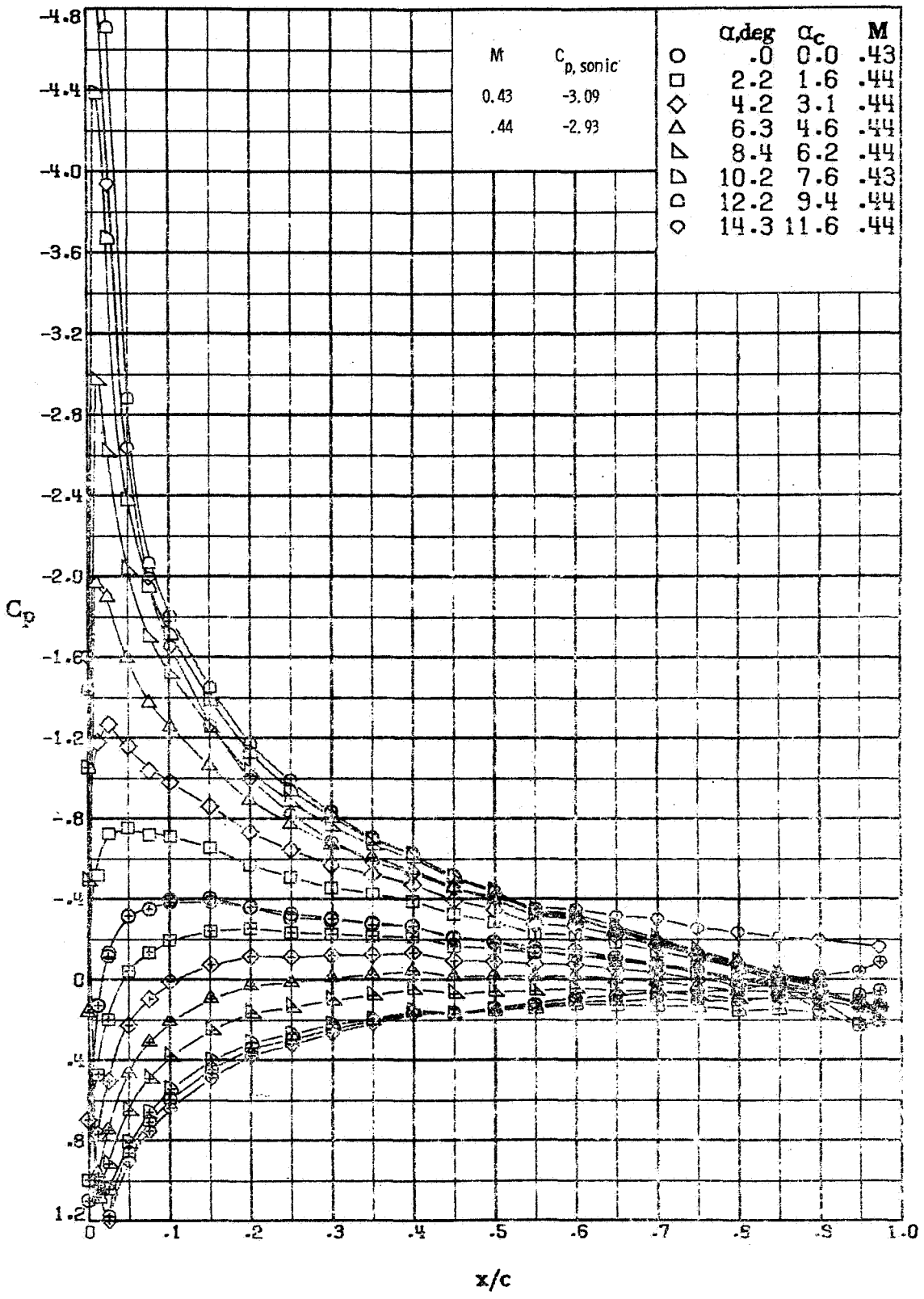

(c) $M \approx 0.44$; $R = 6.0 \times 10^6$.

Figure A3. - Continued.

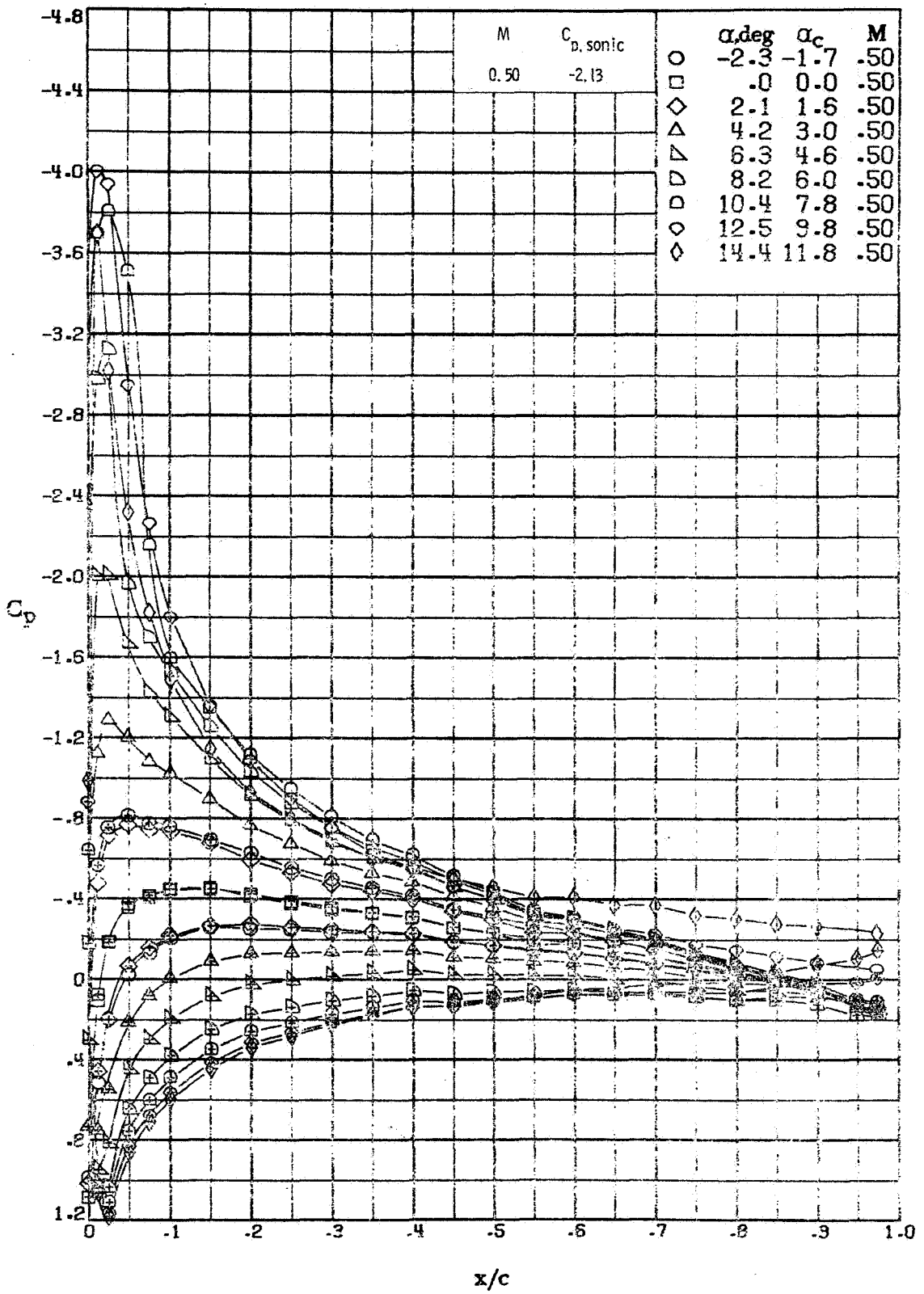

(d) M ≈ 0.50 ; R = 6.7 x 10^6.

Figure A3. - Continued.

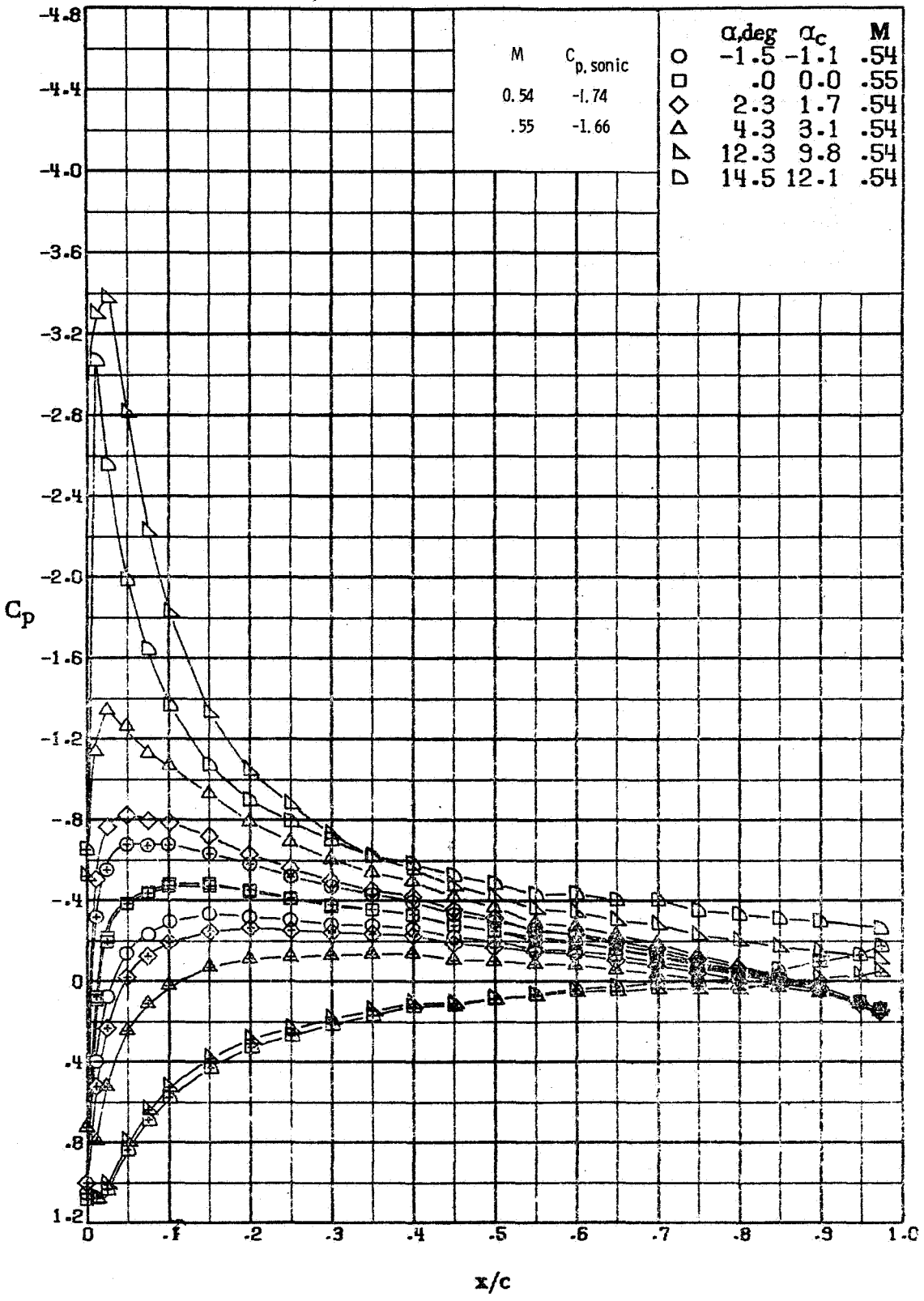

(e) $M \approx 0.54$; $R = 7.1 \times 10^6$.

Figure A3. - Continued.

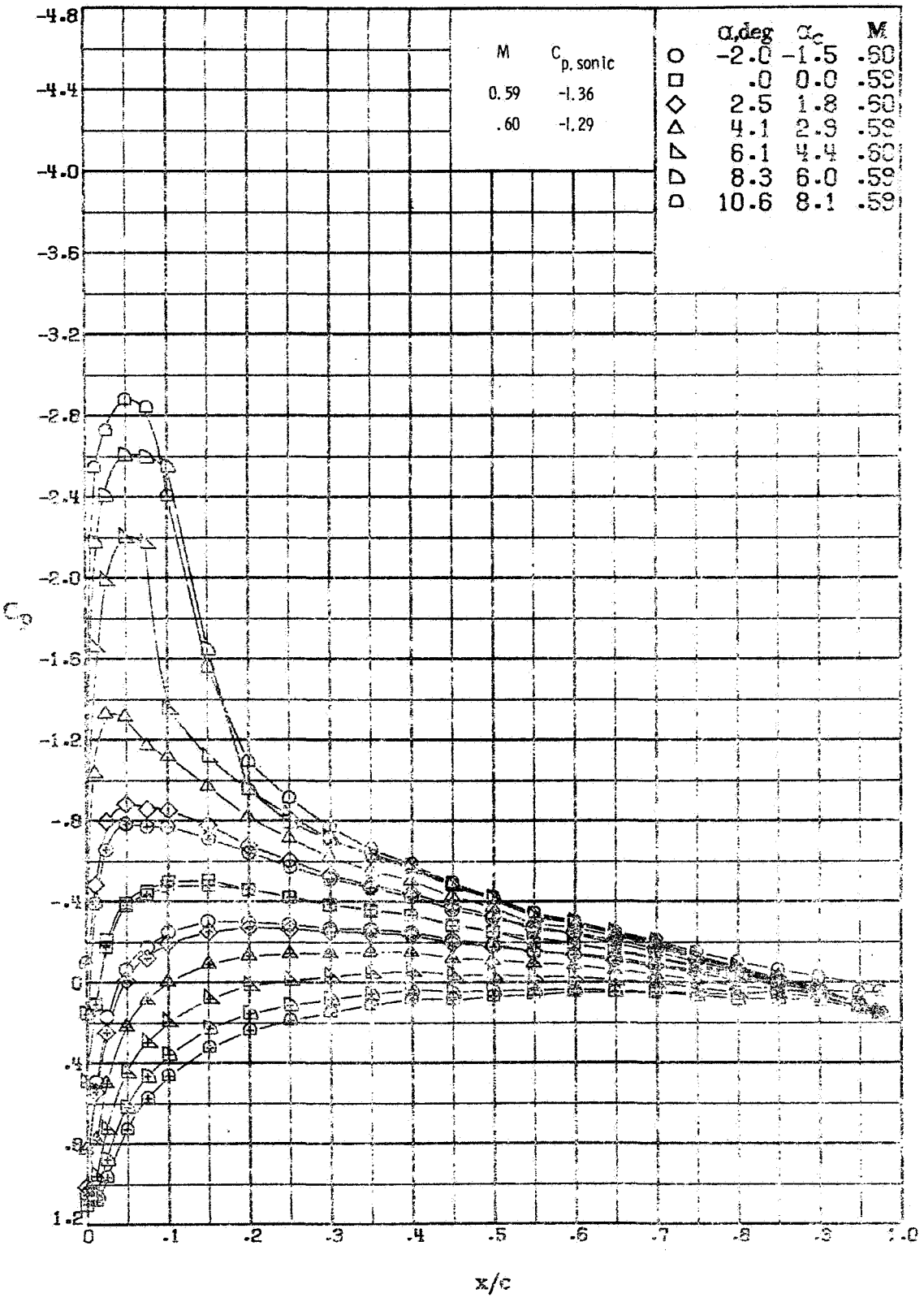

(f) $M \approx 0.59$; $R = 7.4 \times 10^6$.

Figure A3. - Continued.

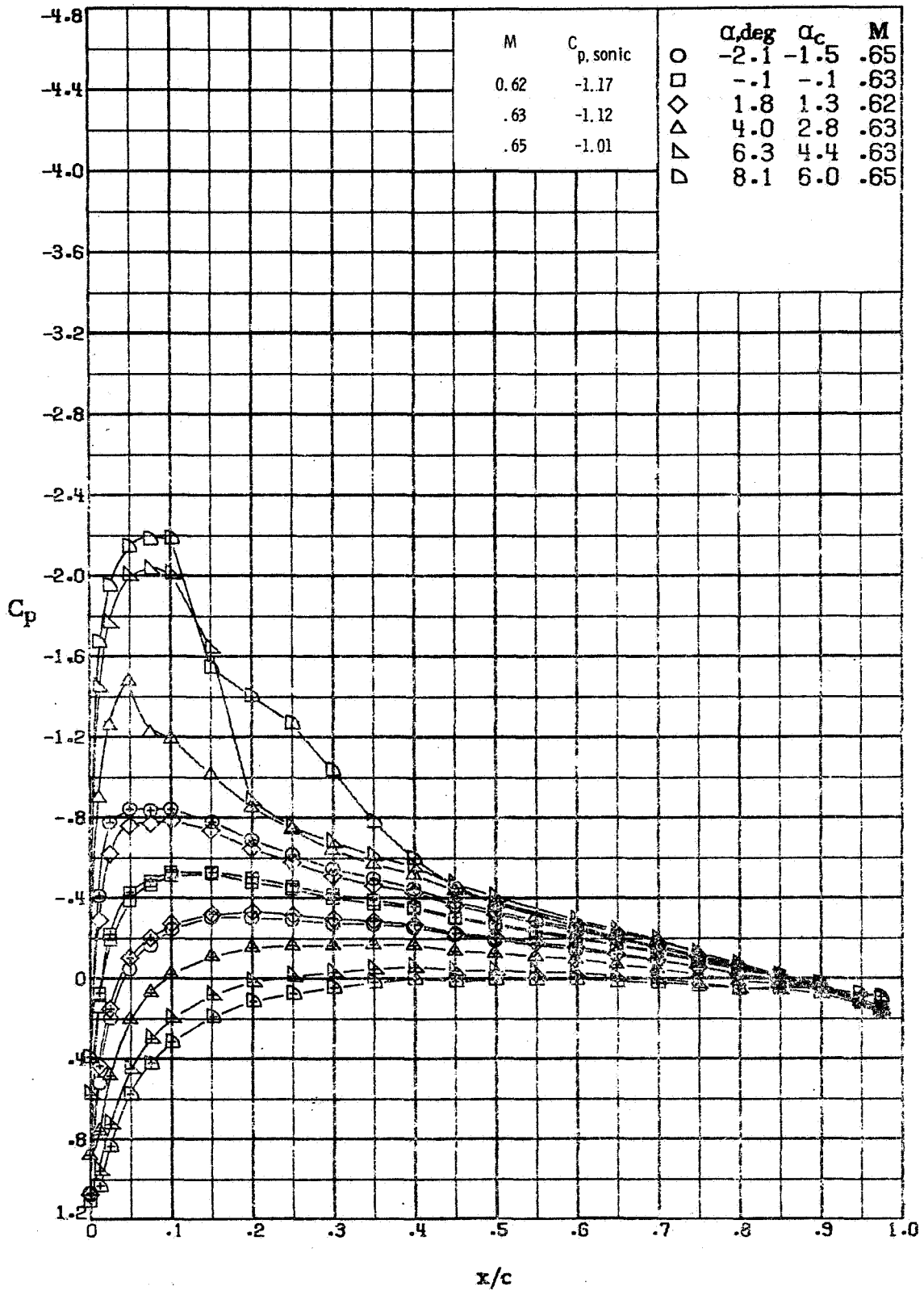

(g) $M \approx 0.63$; $R = 8.1 \times 10^6$.

Figure A3. - Continued.

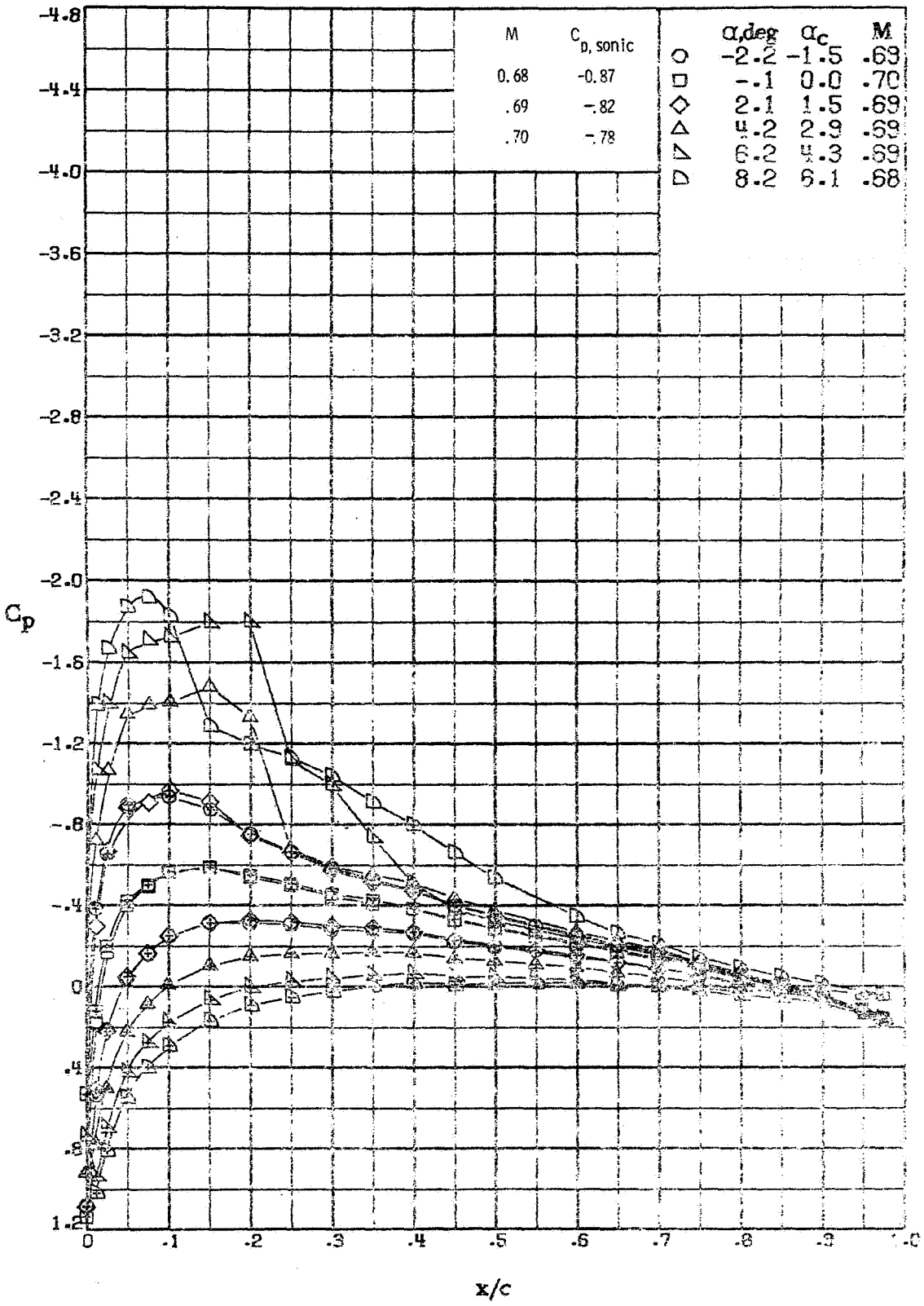

(h) M ≈ 0.69 ; R = 8.5 x 10^6.

Figure A3. - Continued.

REPRODUCIBILITY OF THE
ORIGINAL PAGE IS POOR

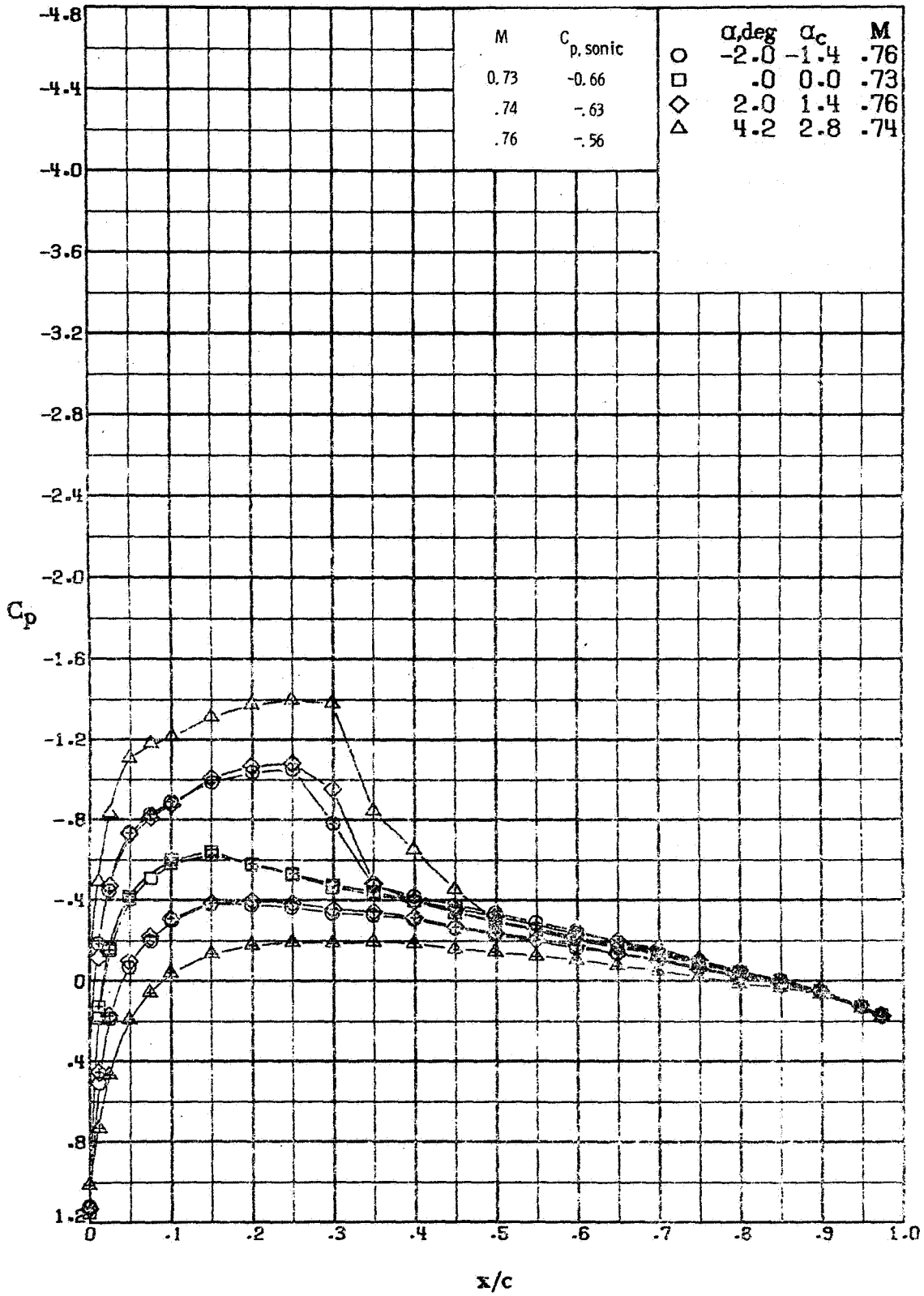

(i) $M \approx 0.76$; $R = 8.8 \times 10^6$.

Figure A3. - Continued.

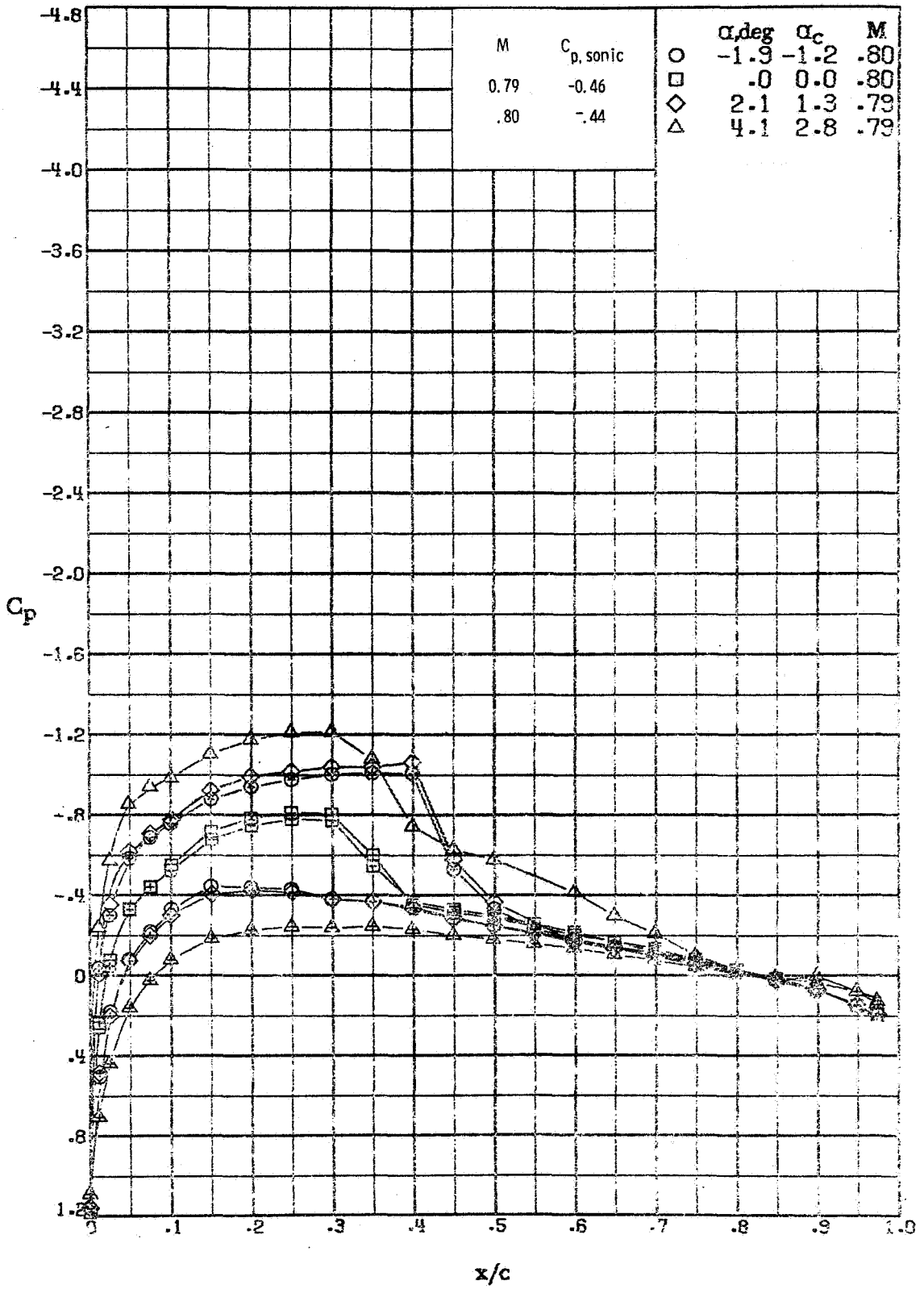

(j) $M \approx 0.79$: $R = 9.2 \times 10^6$.

Figure A3. - Continued.

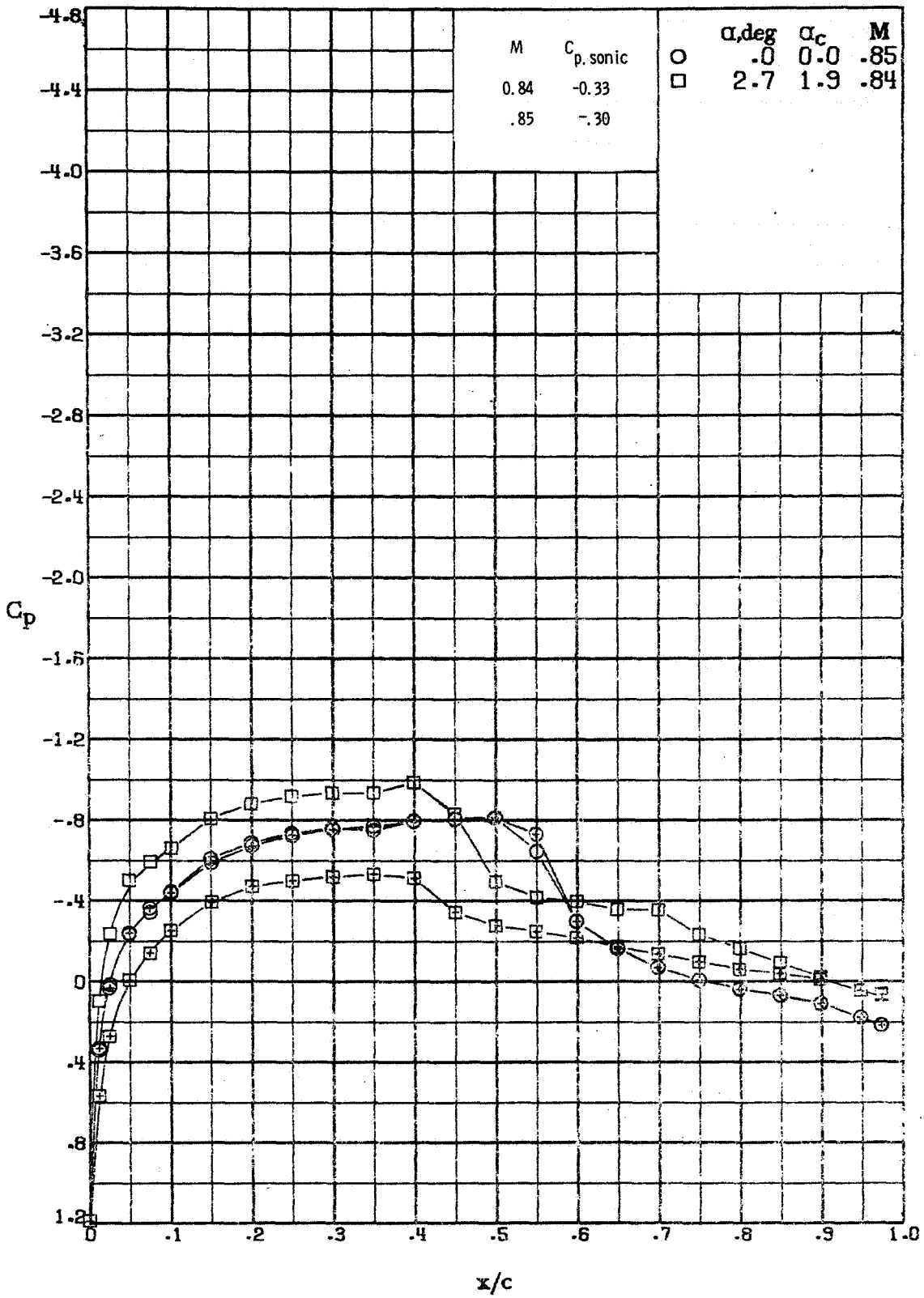

(k) $M \approx 0.85$; $R = 9.6 \times 10^6$.

Figure A3. - Continued.

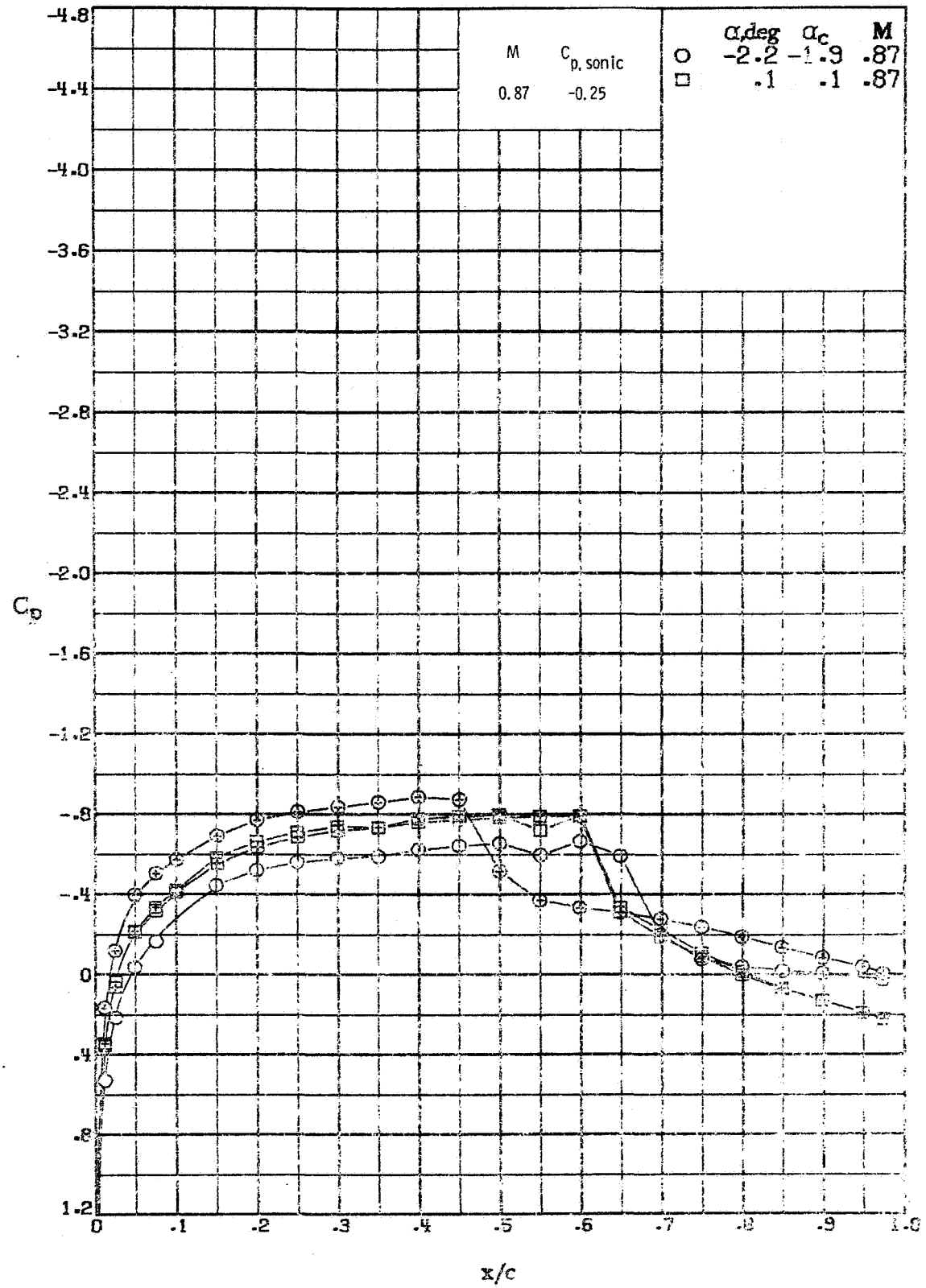

(l) $M \approx 0.87$: $R = 9.8 \times 10^6$.

Figure A3. - Concluded.

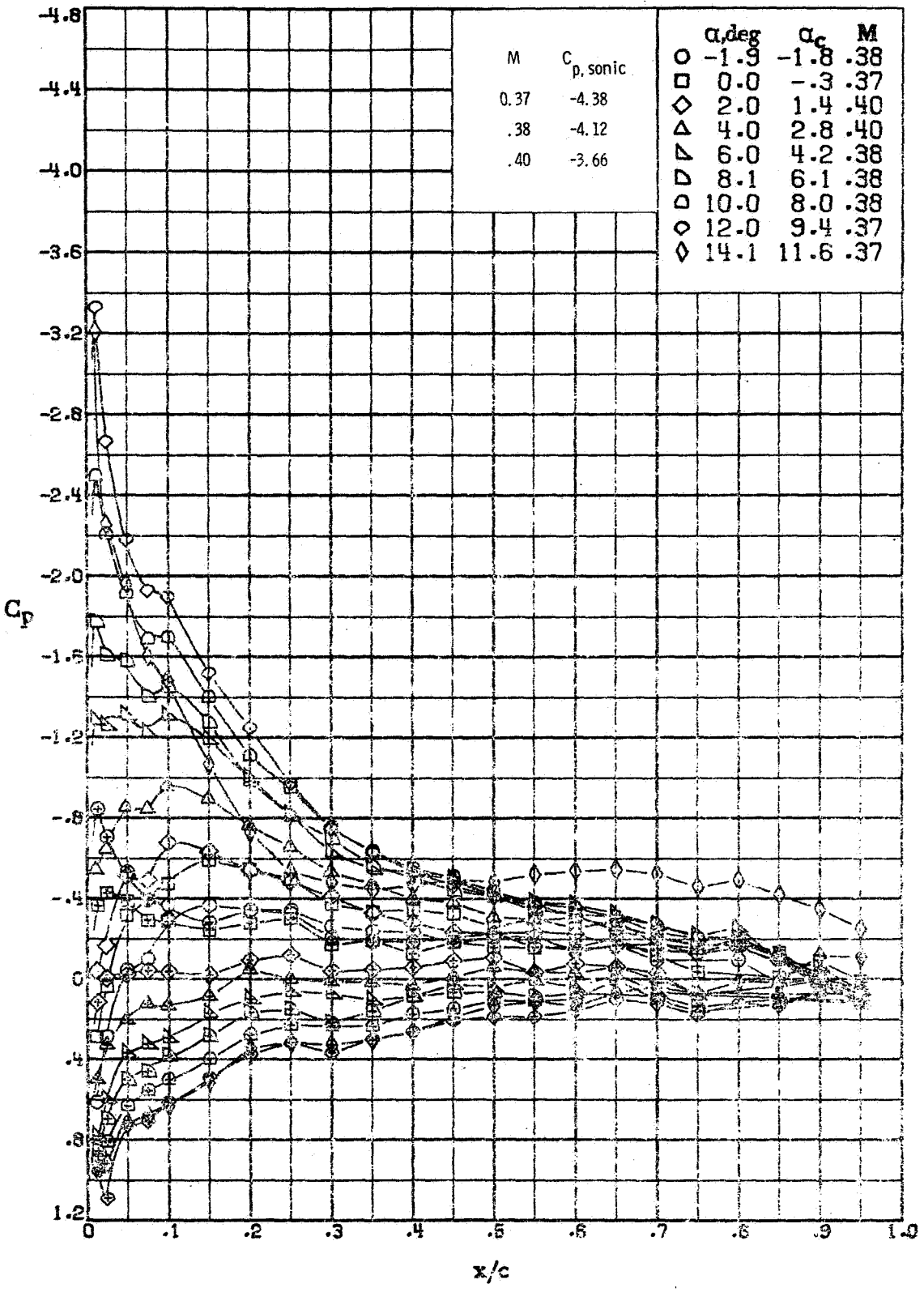

(a) $M \approx 0.38$; $R \approx 0.9 \times 10^6$.

Figure A4.- Effect of angle of attack on the chordwise pressure distribution of the FX69-H-098 airfoil measured in the Langley 6 x 19 inch transonic tunnel.

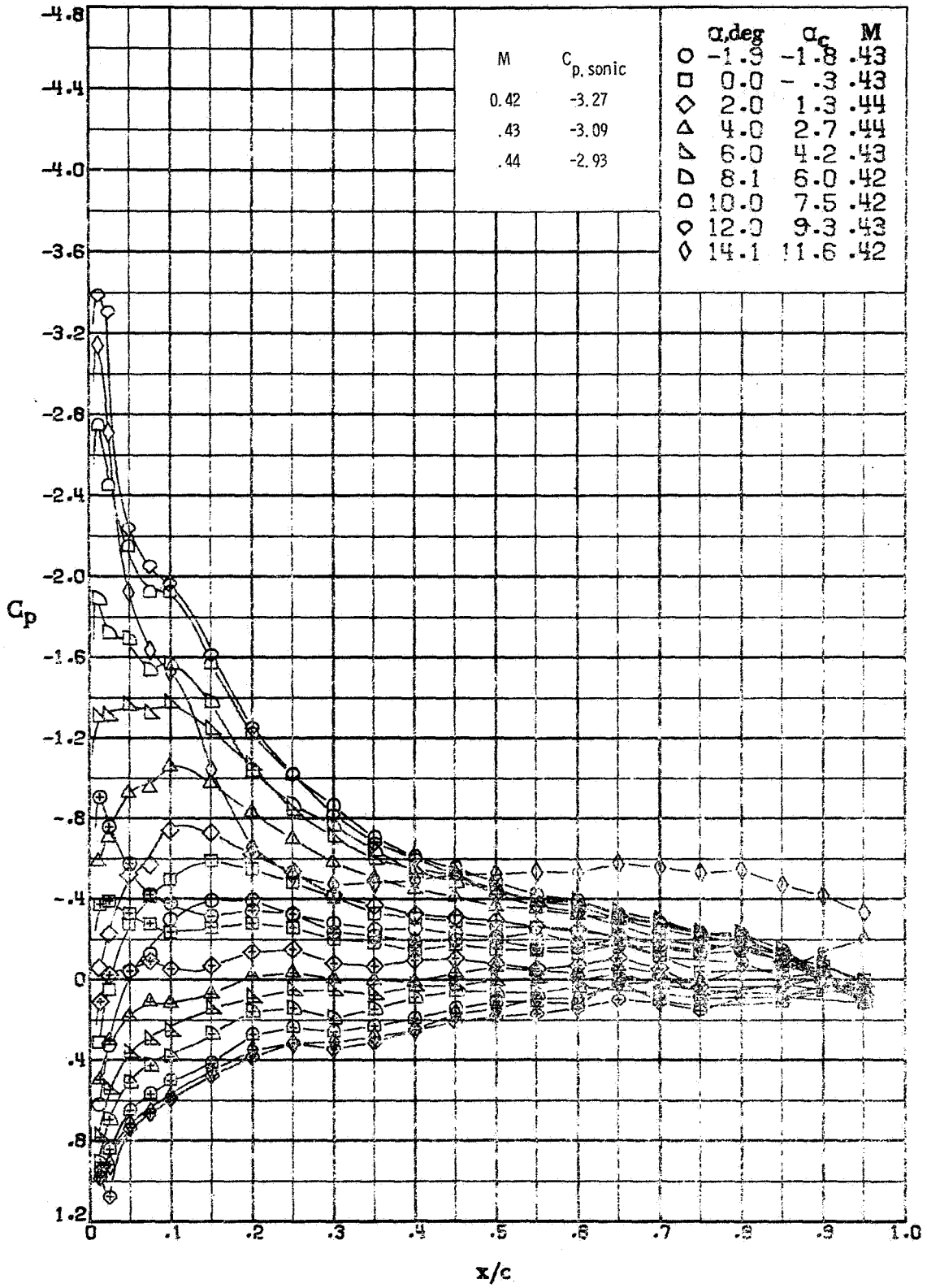

(b) $M \approx 0.48$; $R \approx 1.1 \times 10^6$.

Figure A4.- - Continued.

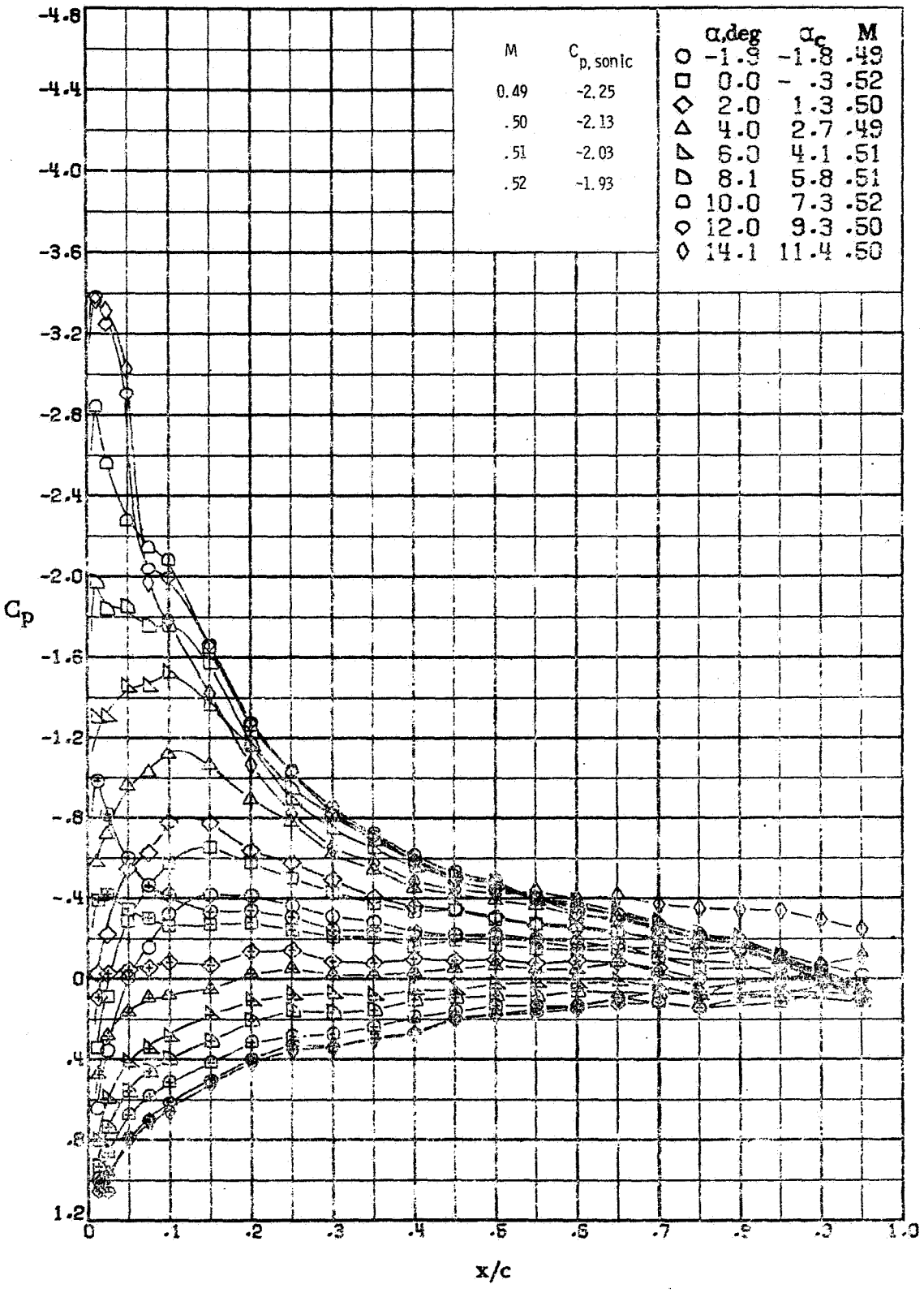

(c) $M \approx 0.50$; $R \approx 1.8 \times 10^6$.

Figure A4. - - Continued.

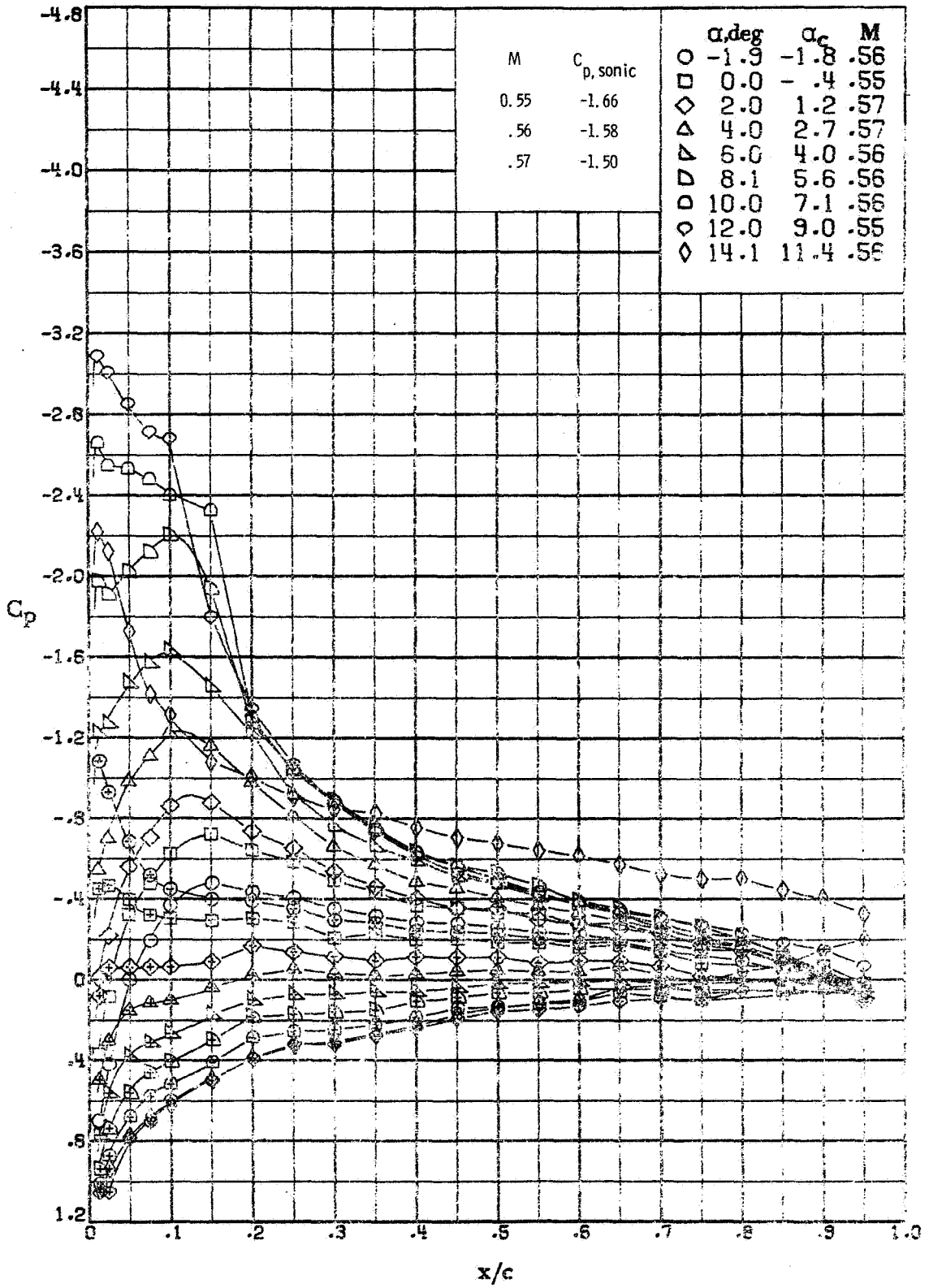

(d) $M \approx 0.56$; $R \approx 1.4 \times 10^6$.

Figure A4.- - Continued.

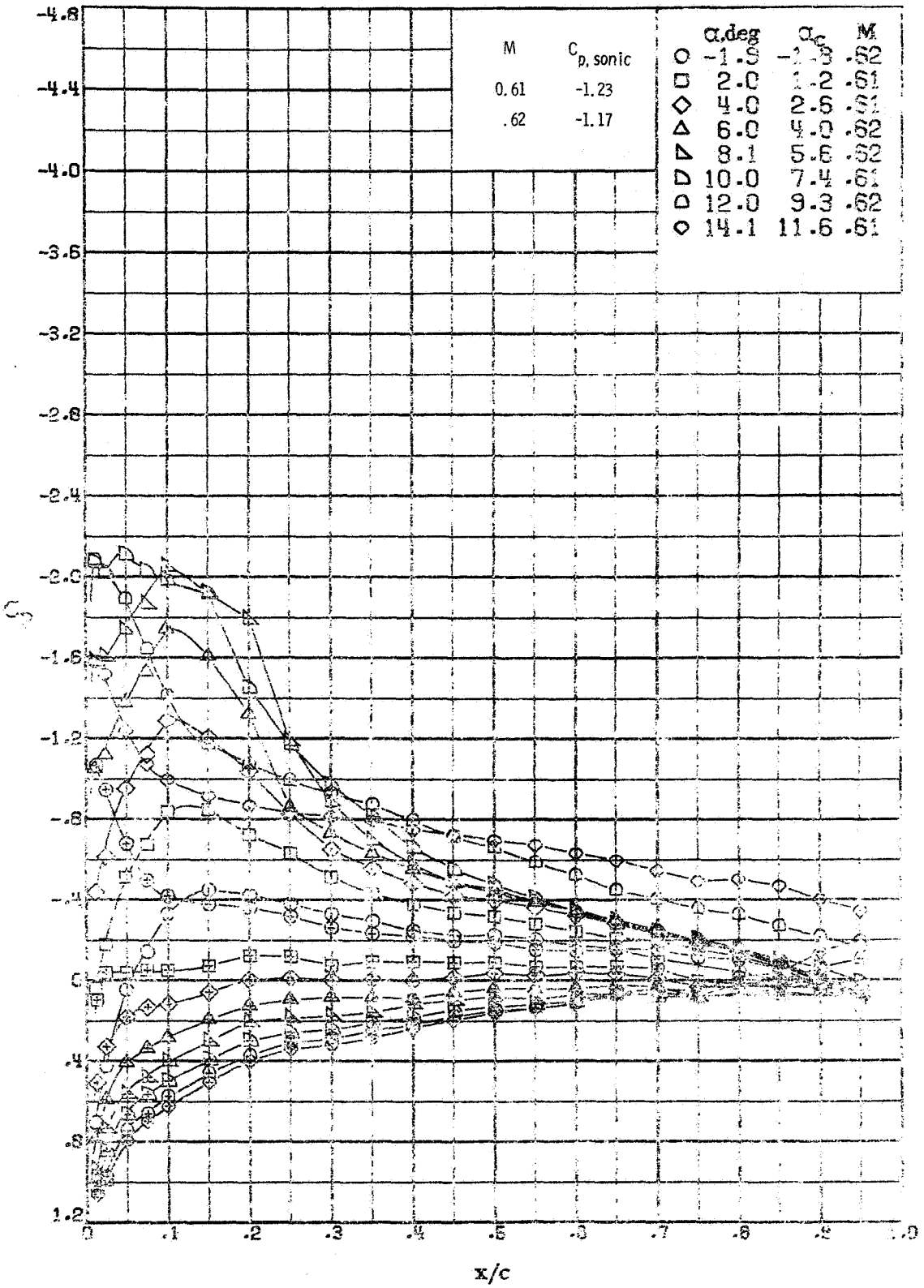

(e) $M \approx 0.62$; $R \approx 1.6 \times 10^6$.

Figure A4. - Continued.

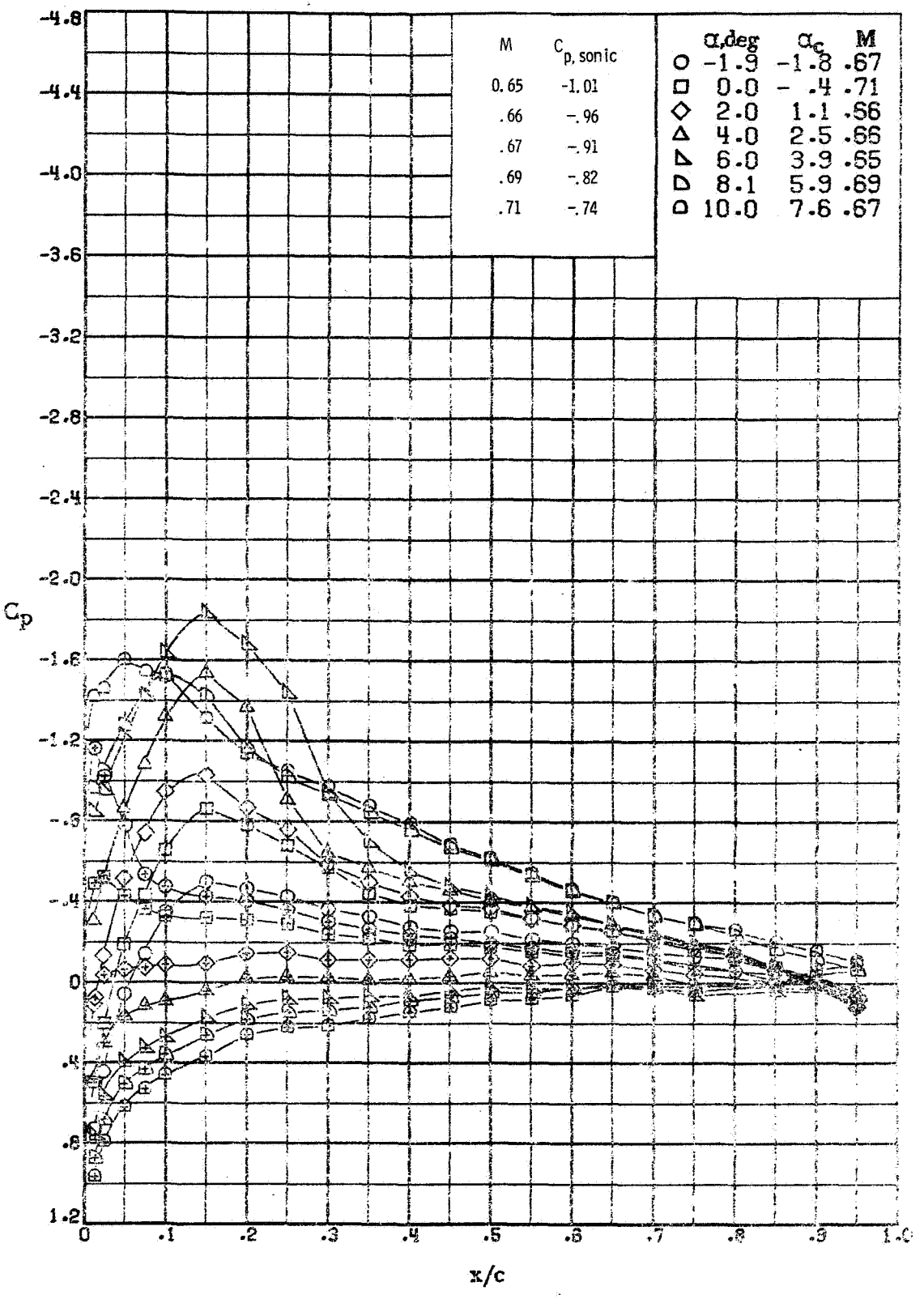

(f) $M \approx 0.67$; $R \approx 1.7 \times 10^6$.

Figure A4. - Continued.

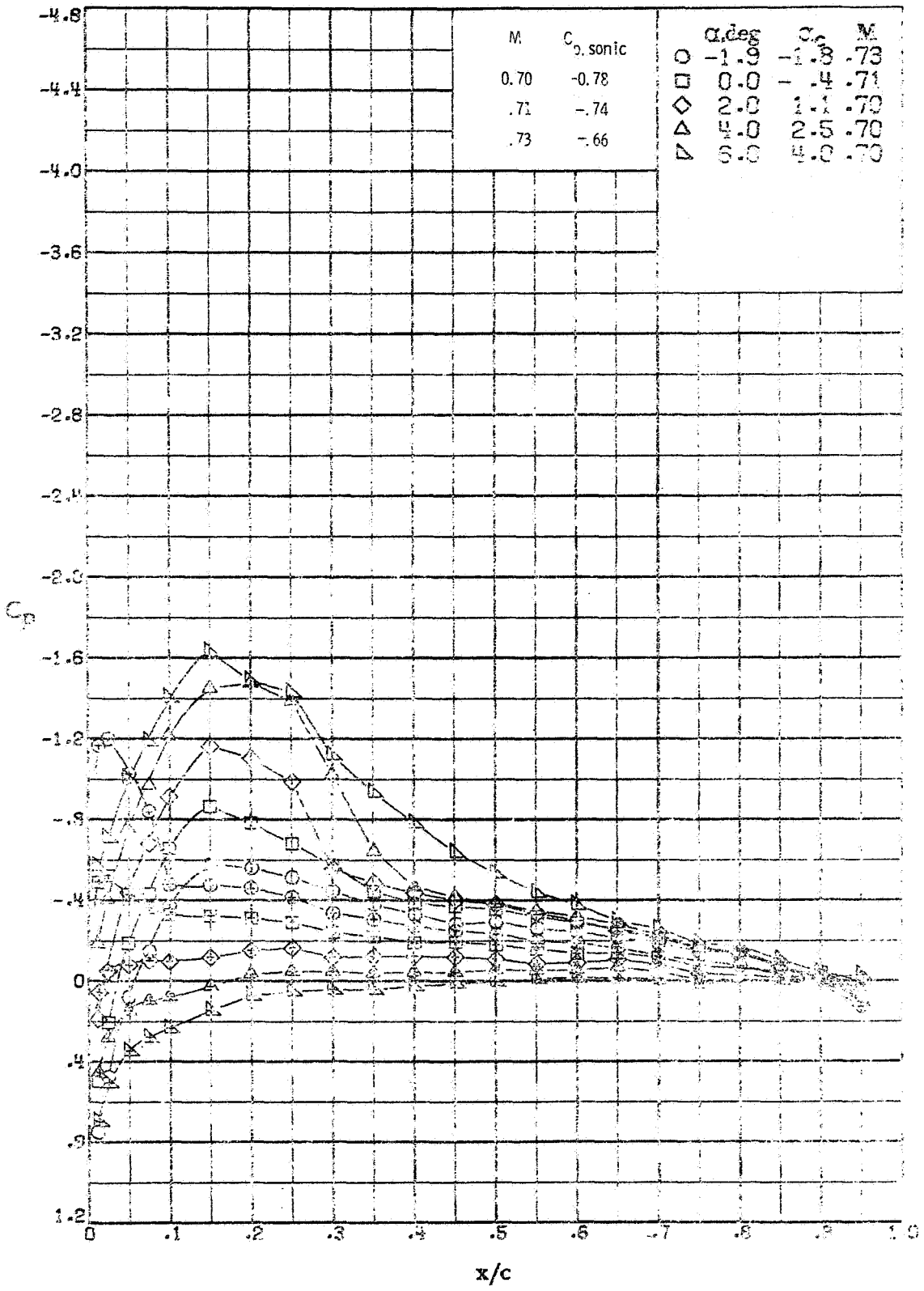

(g) $M \approx 0.70$; $R \approx 1.8 \times 10^6$.

Figure A4.-- Continued.

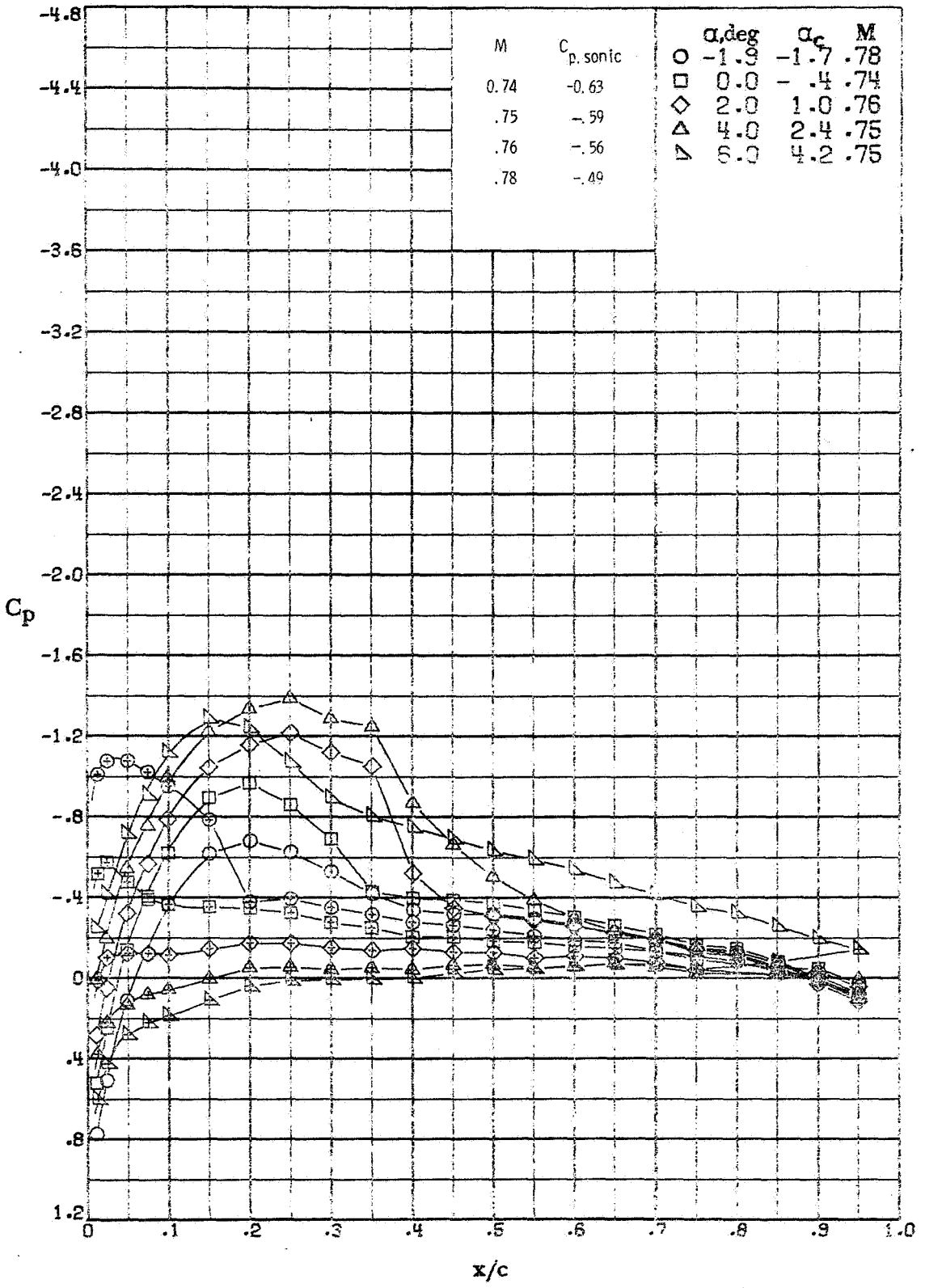

(h) $M \approx 0.75$; $R \approx 1.9 \times 10^6$.

Figure A4.- - Continued.

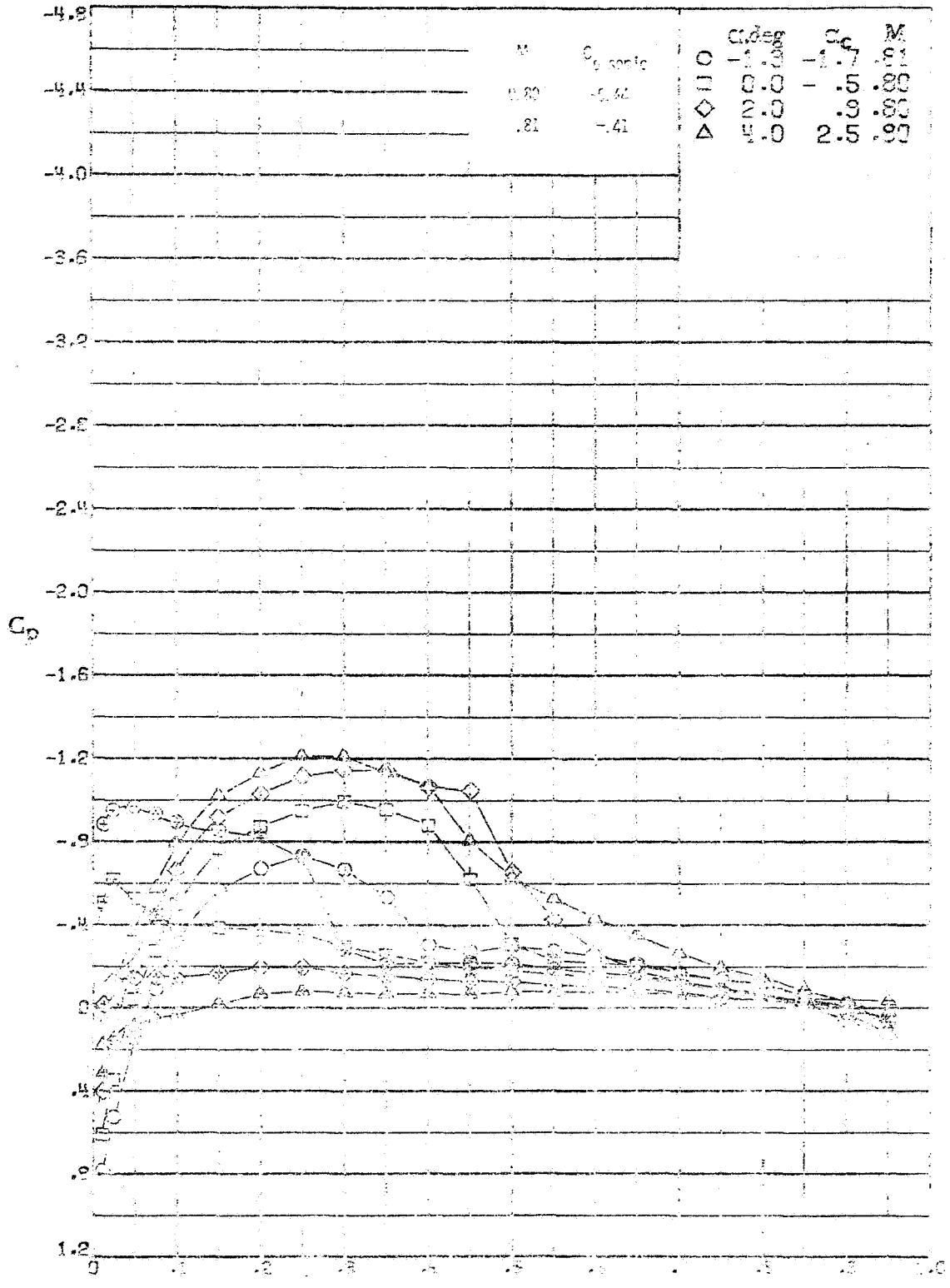

(p) $M \approx 0.80$; $R \approx 2.0 \times 10^6$.

Figure 4.- Continued.

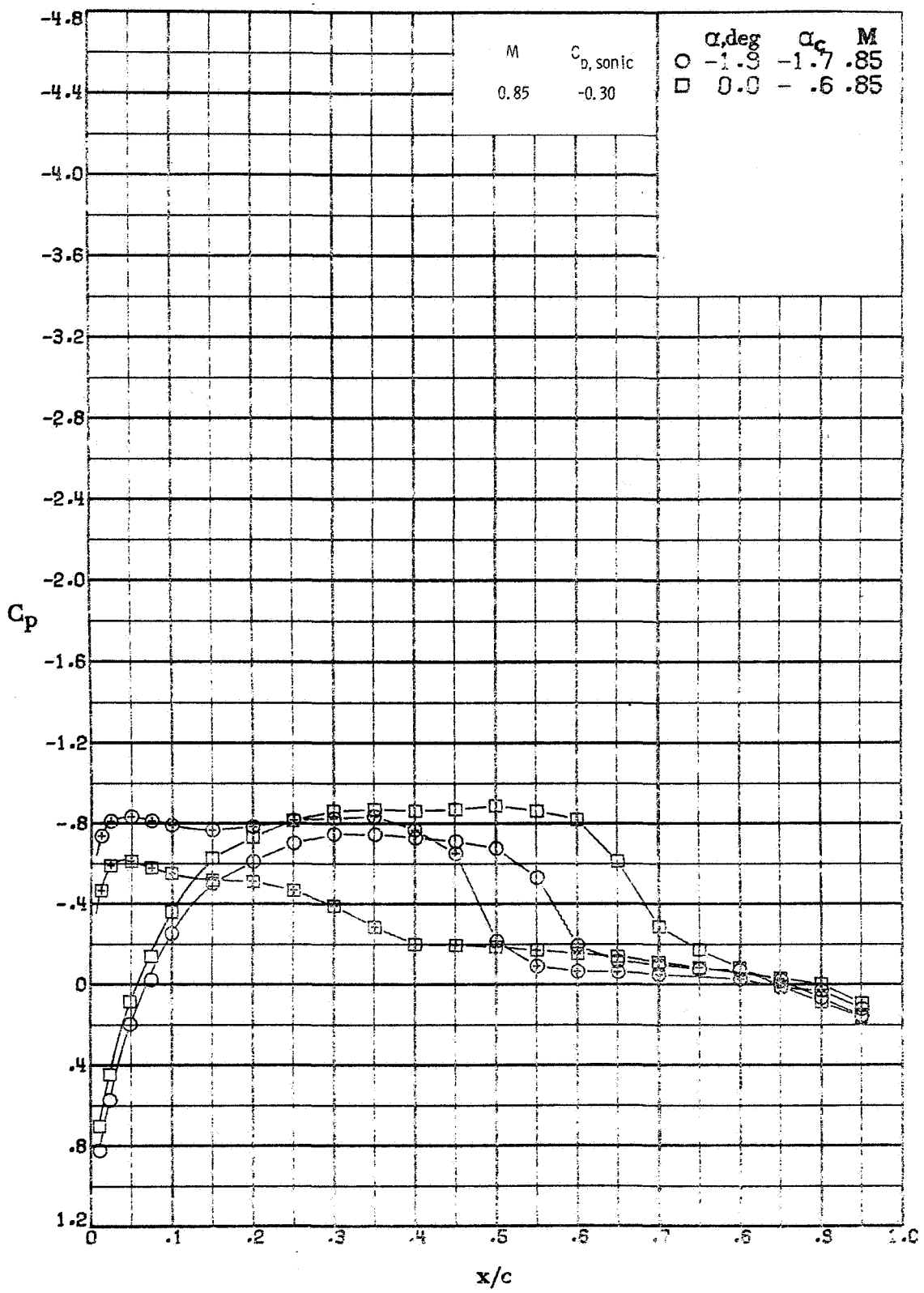

(j) $M \approx 0.85$; $R \approx 2.1 \times 10^6$.

Figure A4. - - Continued.

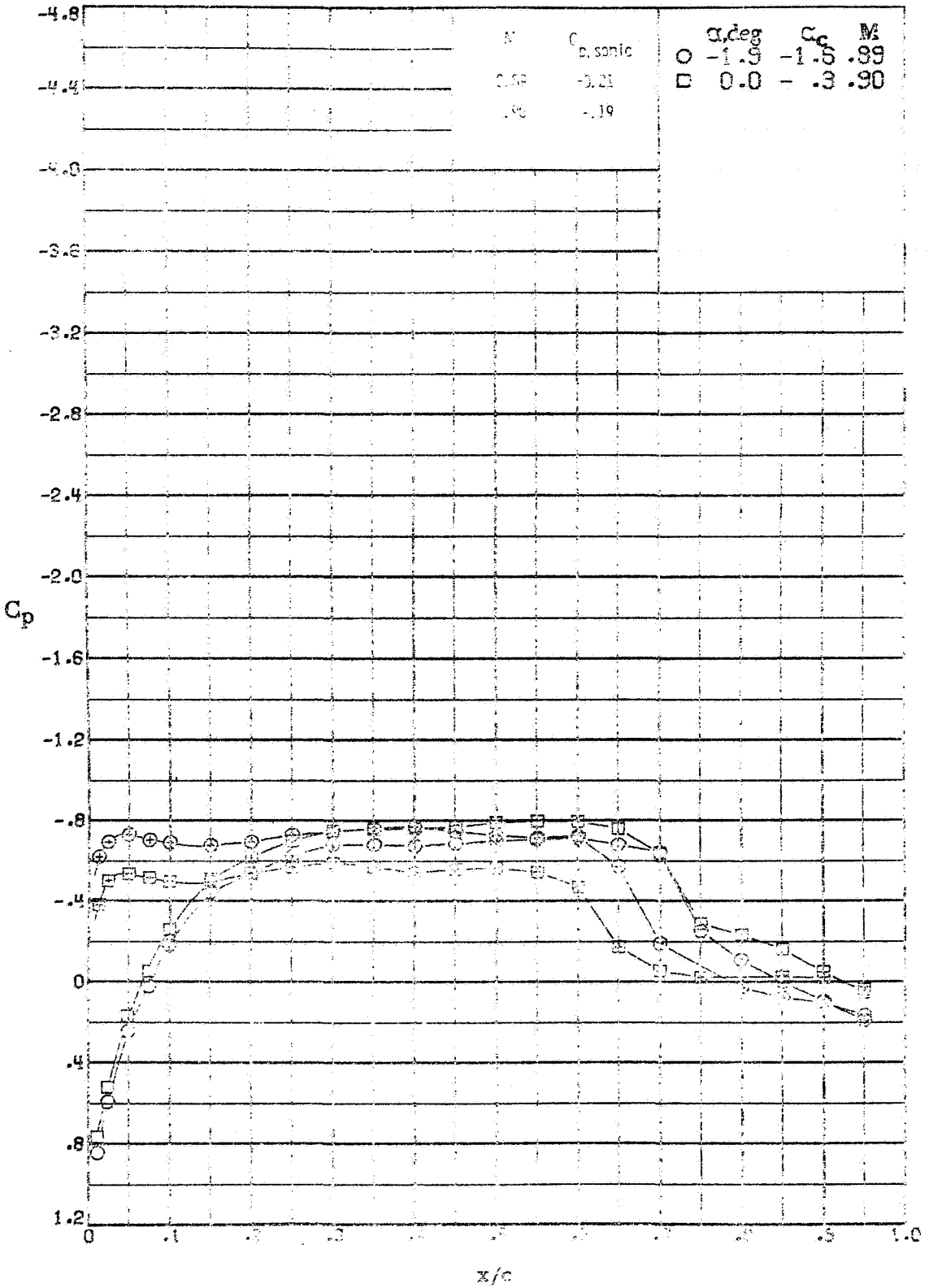

R_c M 0.99; R 2.2×10^6.

Figure A4.- Concluded.

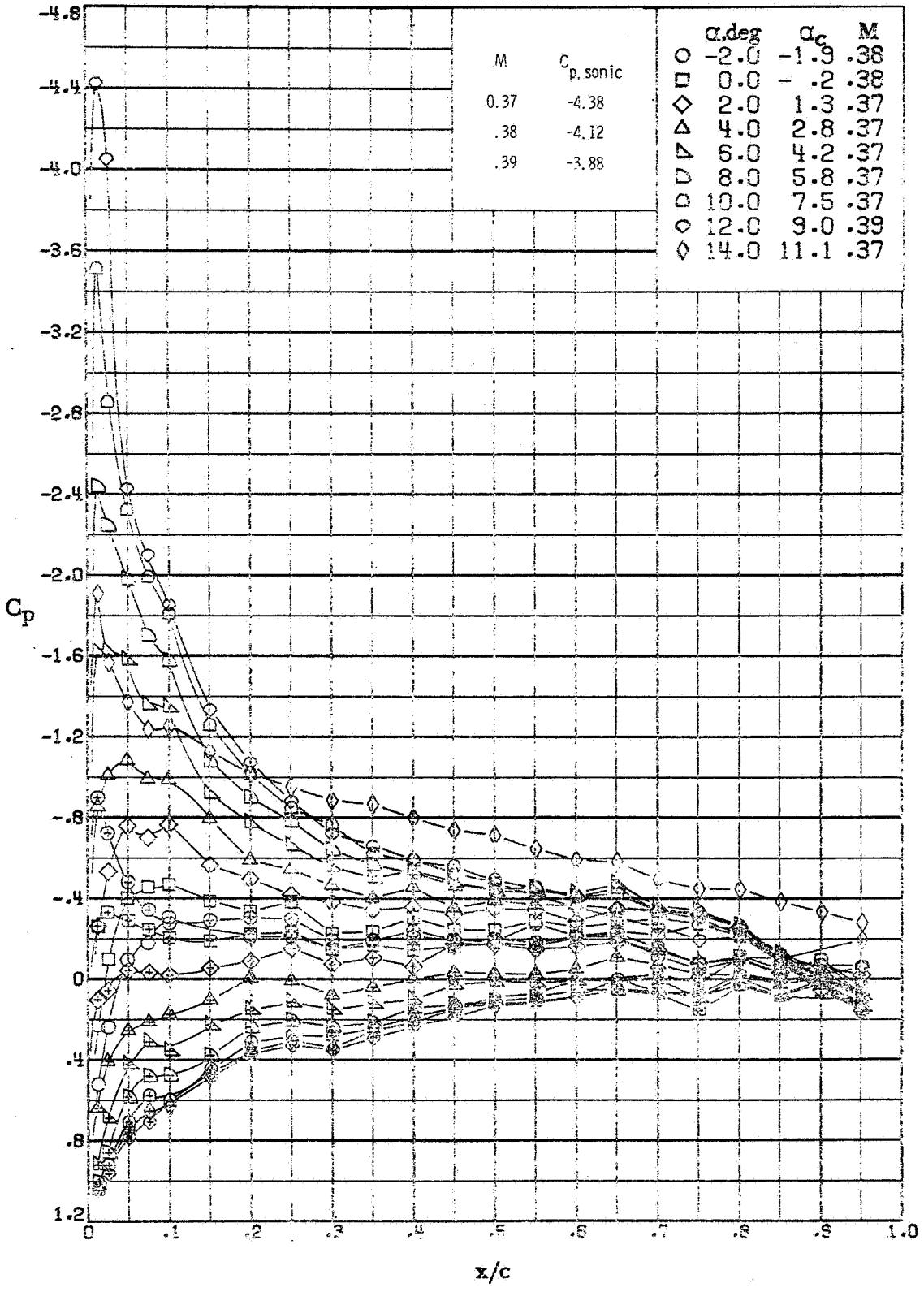

(a) $M \approx 0.37$; $R \approx 0.9 \times 10^6$.

Figure A5.- Effect of angle of attack on the chordwise pressure distribution of the NLR-1 airfoil measured in the Langley 6 x 19 inch transonic tunnel.

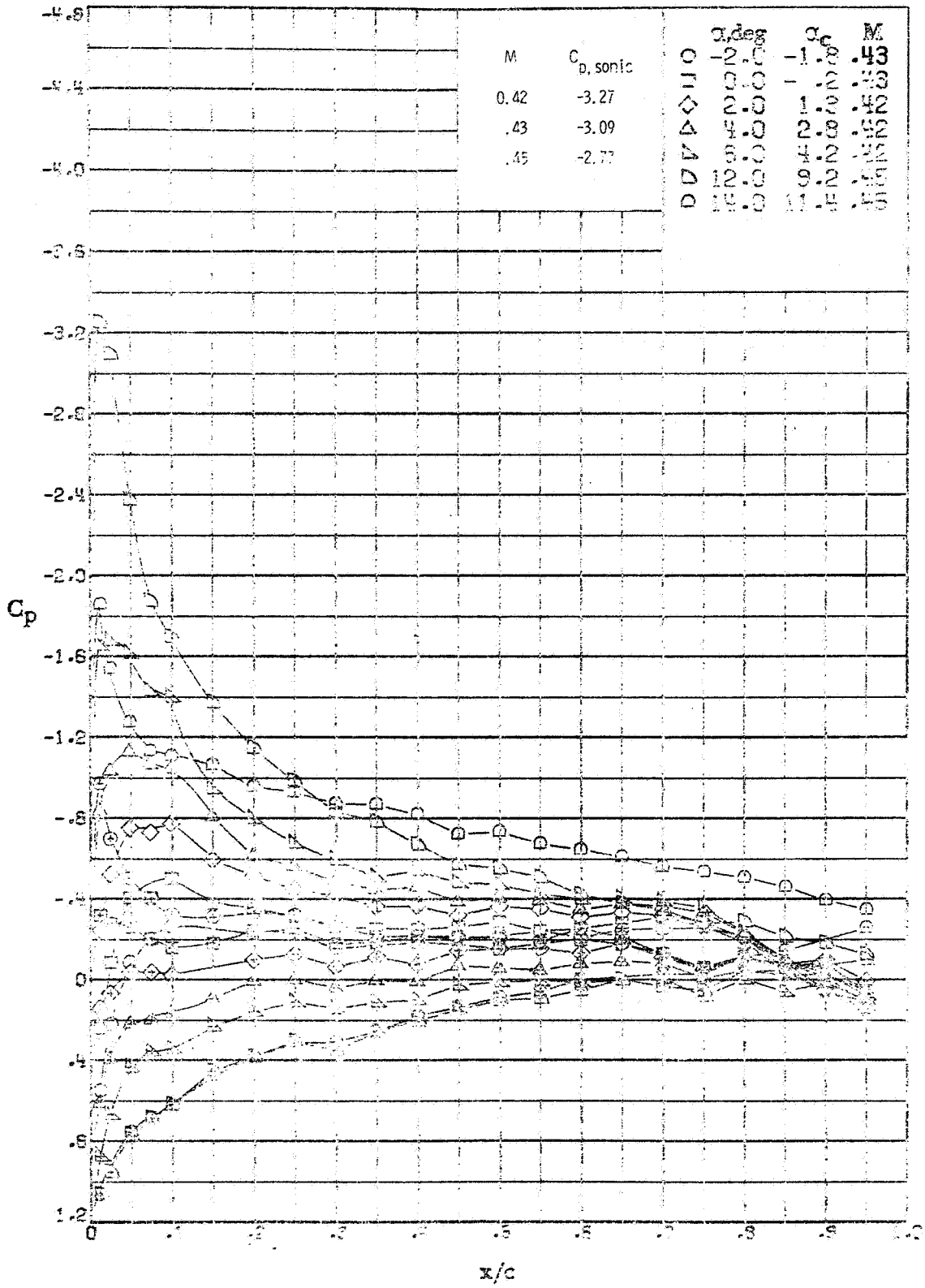

(b) $M \approx 0.42$; $R \approx 1.1 \times 10^6$.

Figure A5. - - Continued.

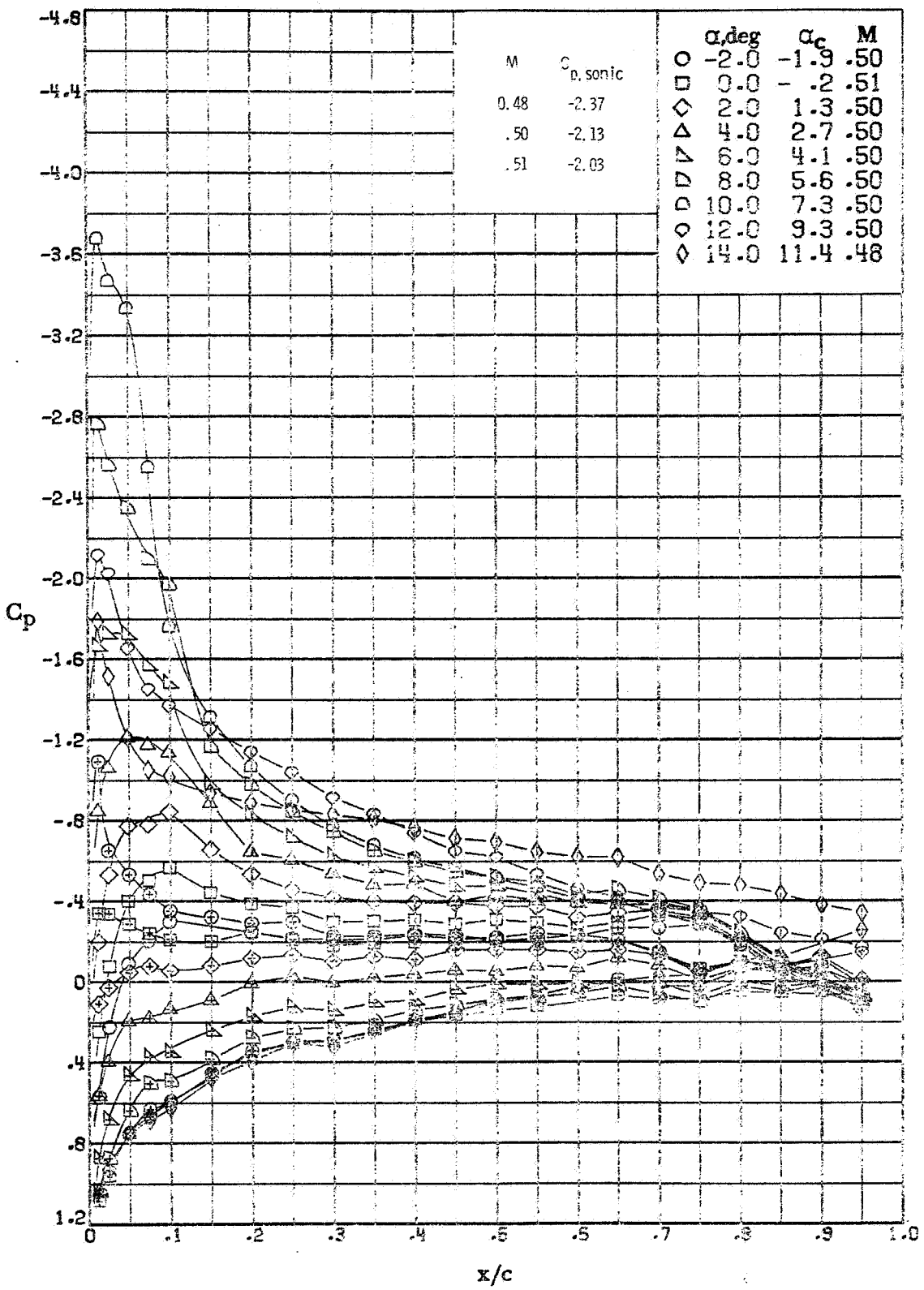

(c) $M \approx 0.50$; $R \approx 1.8 \times 10^6$.

Figure A5. - - Continued.

REPRODUCIBILITY OF THE
ORIGINAL PAGE IS POOR

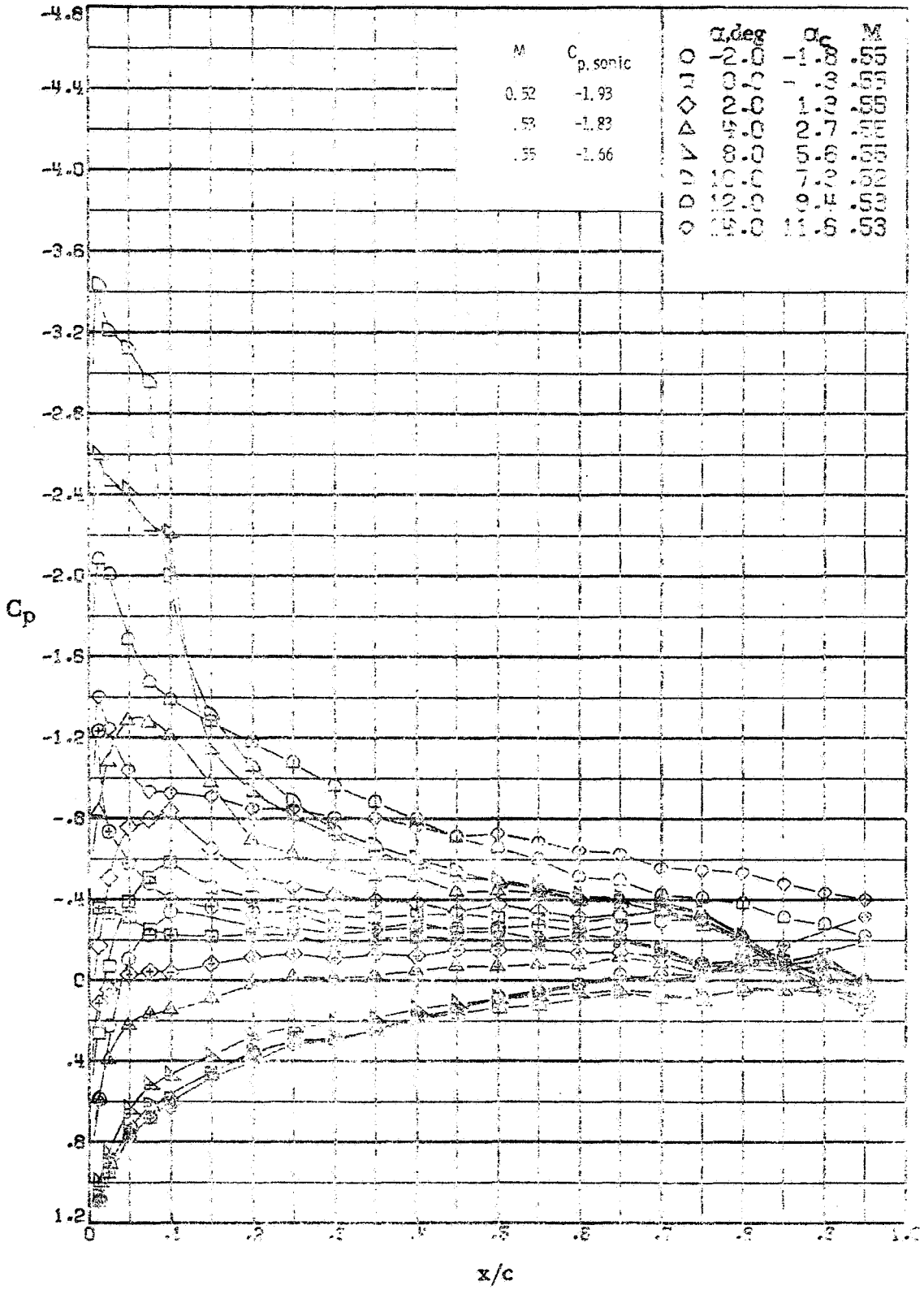

(c) $M \approx 0.55$; $R_c \approx 1.4 \times 10^6$.

Figure A5. -- Continued.

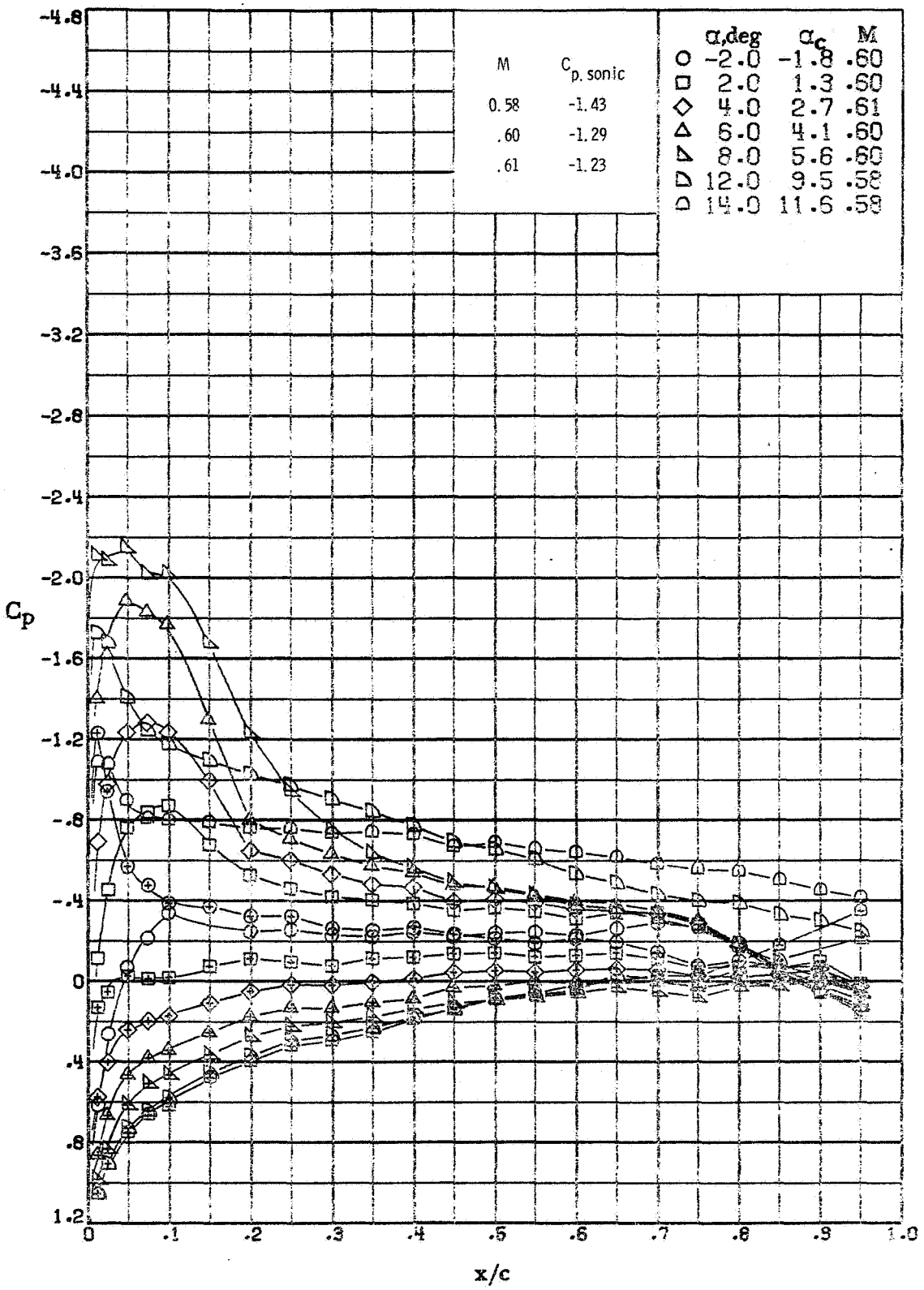

(e) $M \approx 0.60$; $R \approx 1.5 \times 10^6$.

Figure A5. - - Continued.

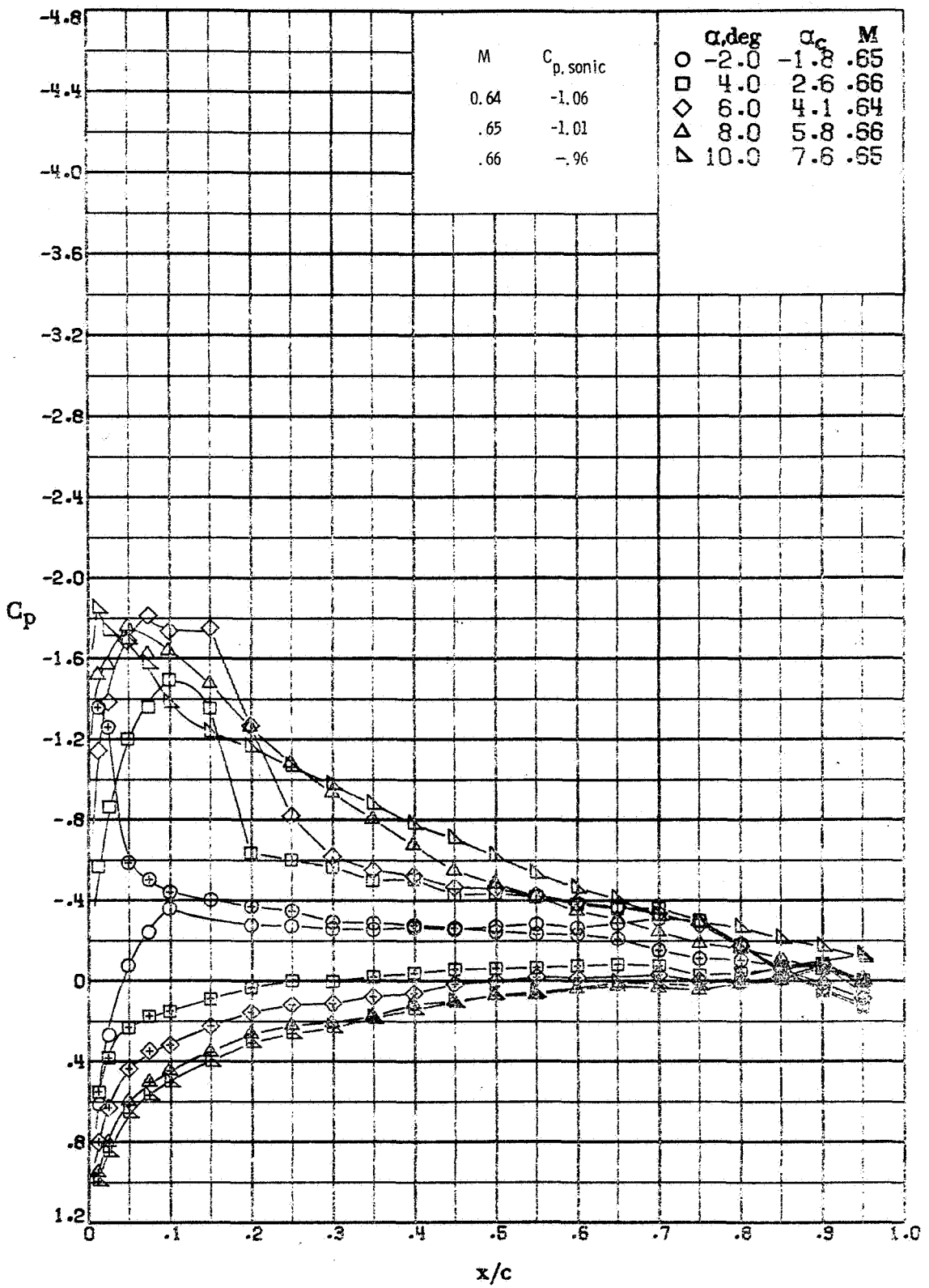

(f) $M \approx 0.65$; $R \approx 1.7 \times 10^6$.

Figure A5.- - Continued.

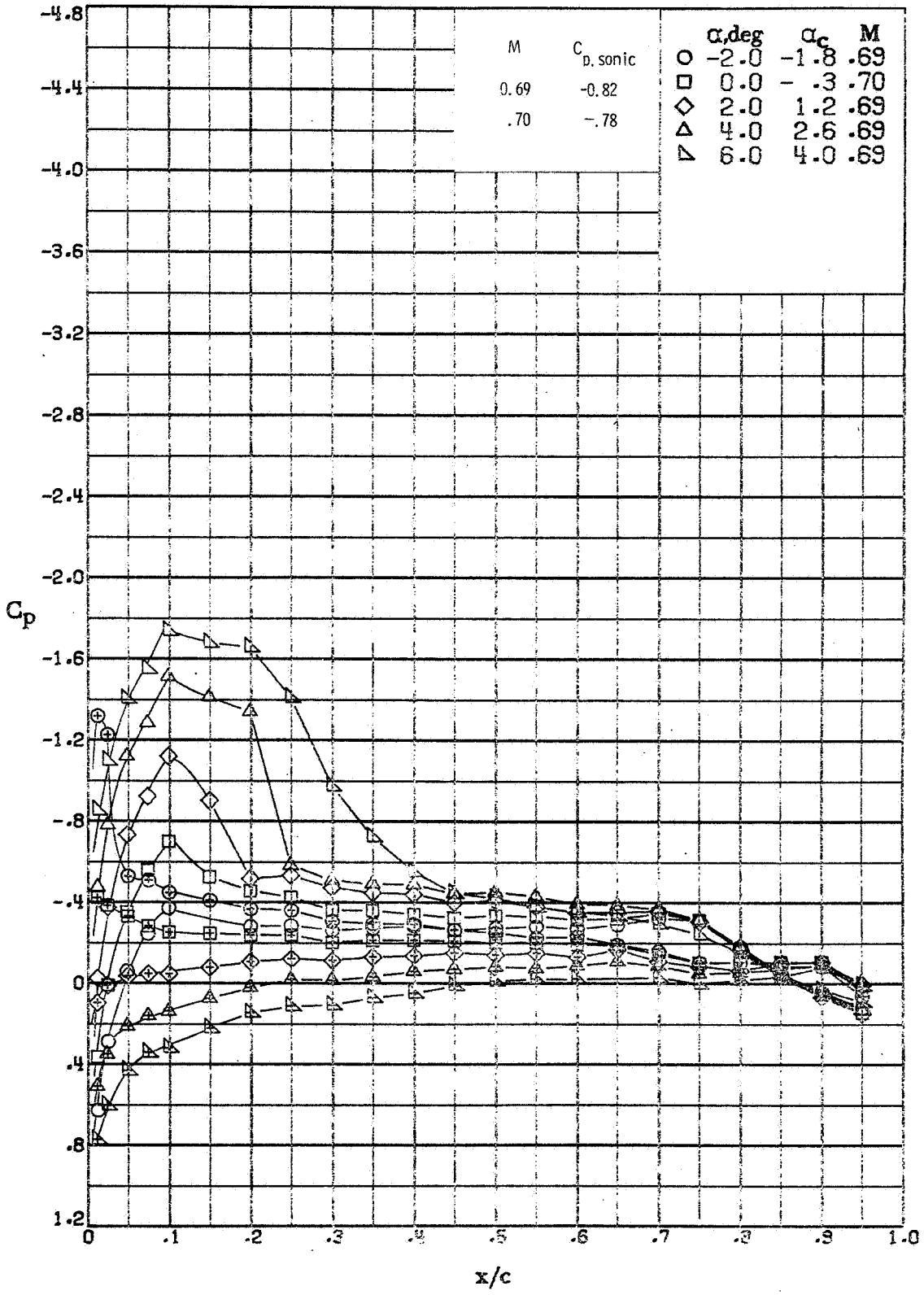

(g) $M \approx 0.69$; $R \approx 1.8 \times 10^6$.

Figure A5.-- Continued.

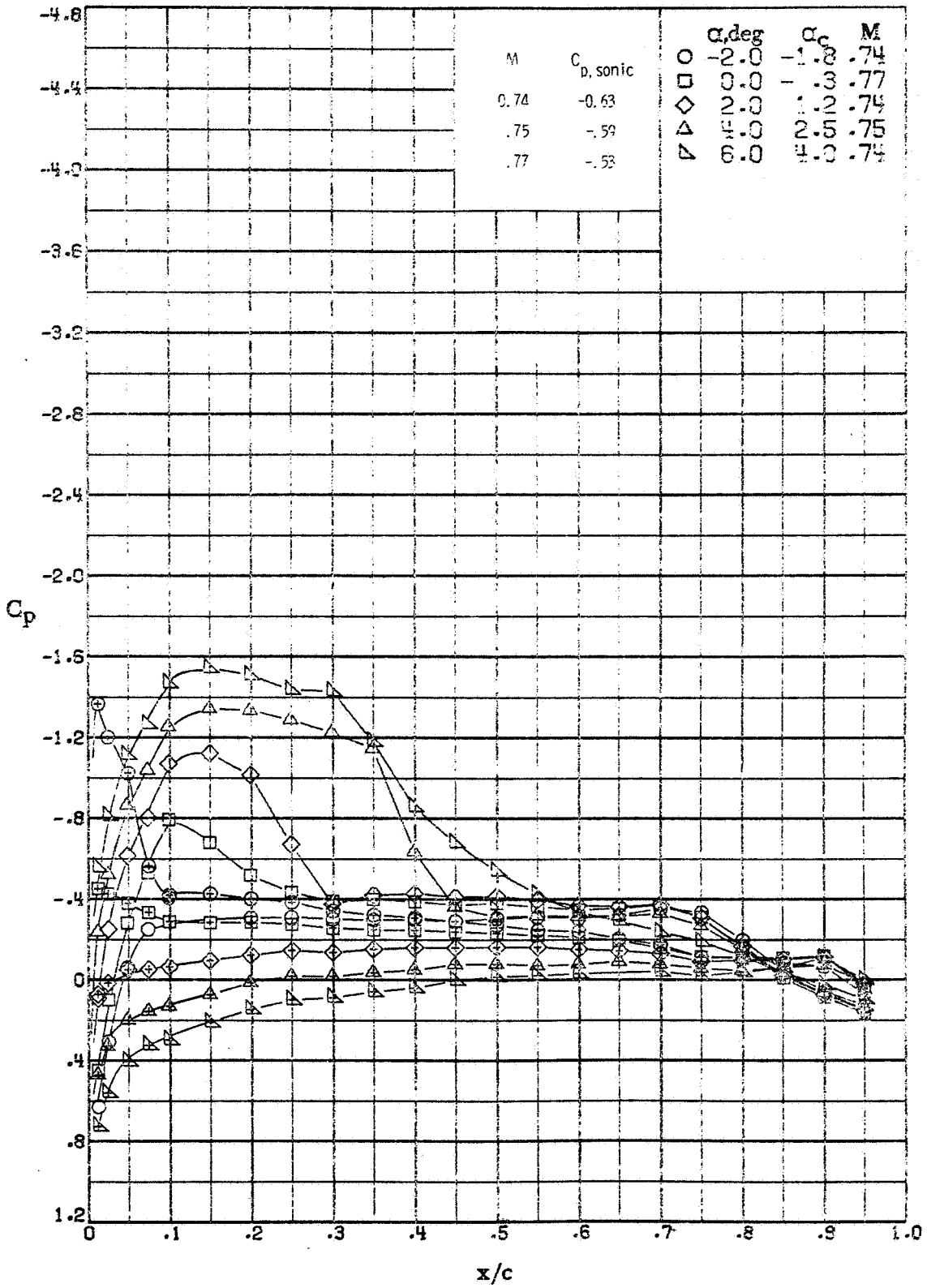

(h) $M \approx 0.74$; $R \approx 1.9 \times 10^6$.

Figure A5. -- Continued.

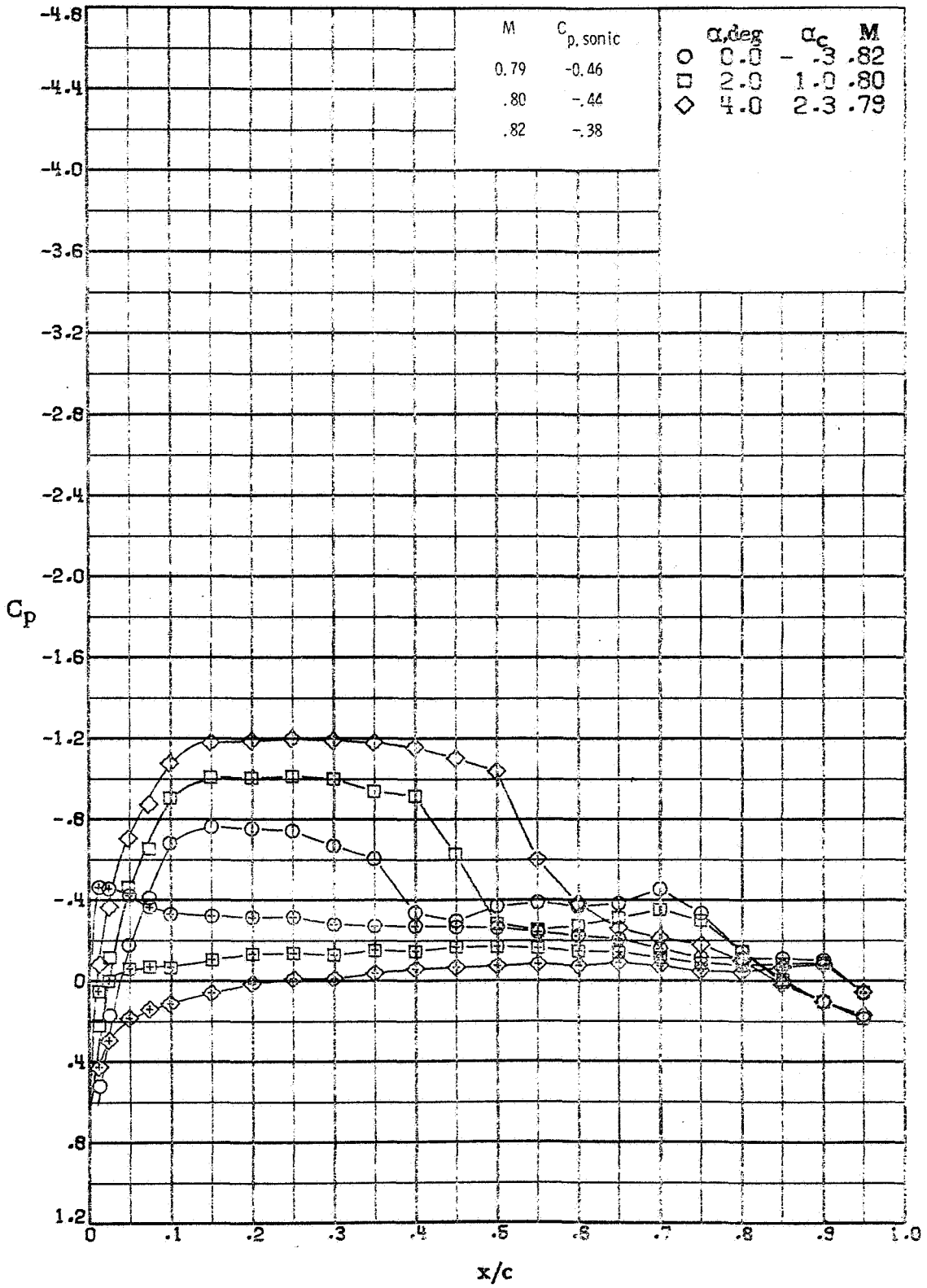

(i) $M \approx 0.82$; $R \approx 2.0 \times 10^6$.

Figure A5.- Concluded.

BILITY OF THE
AL PAGE IS POOR

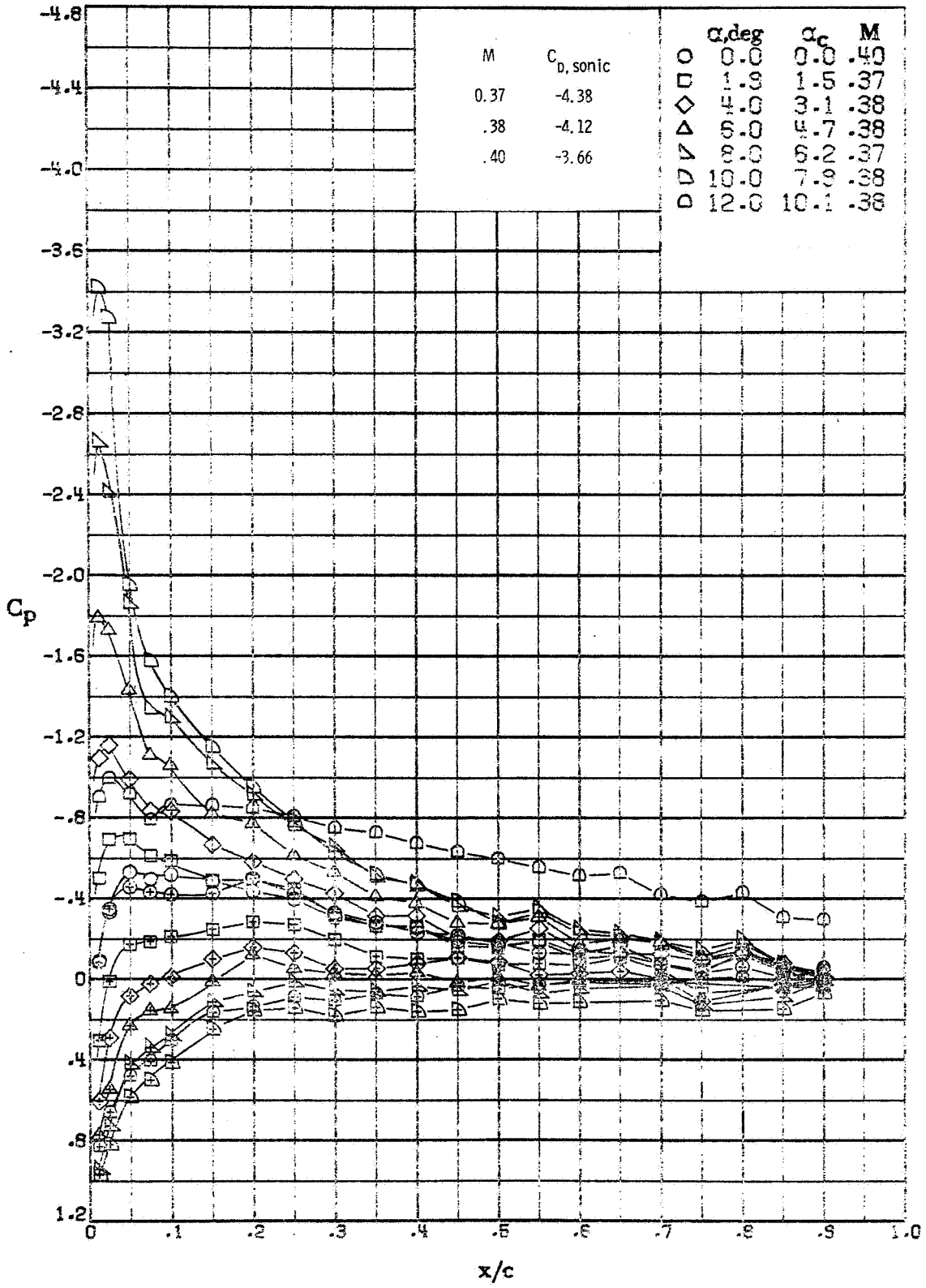

(a) $M \approx 0.38$; $R \approx 0.9 \times 10^6$.

Figure A6.- Effect of angle of attack on the chordwise pressure distribution of the BHC-540 airfoil measured in the Langley 6 x 19 inch transonic tunnel.

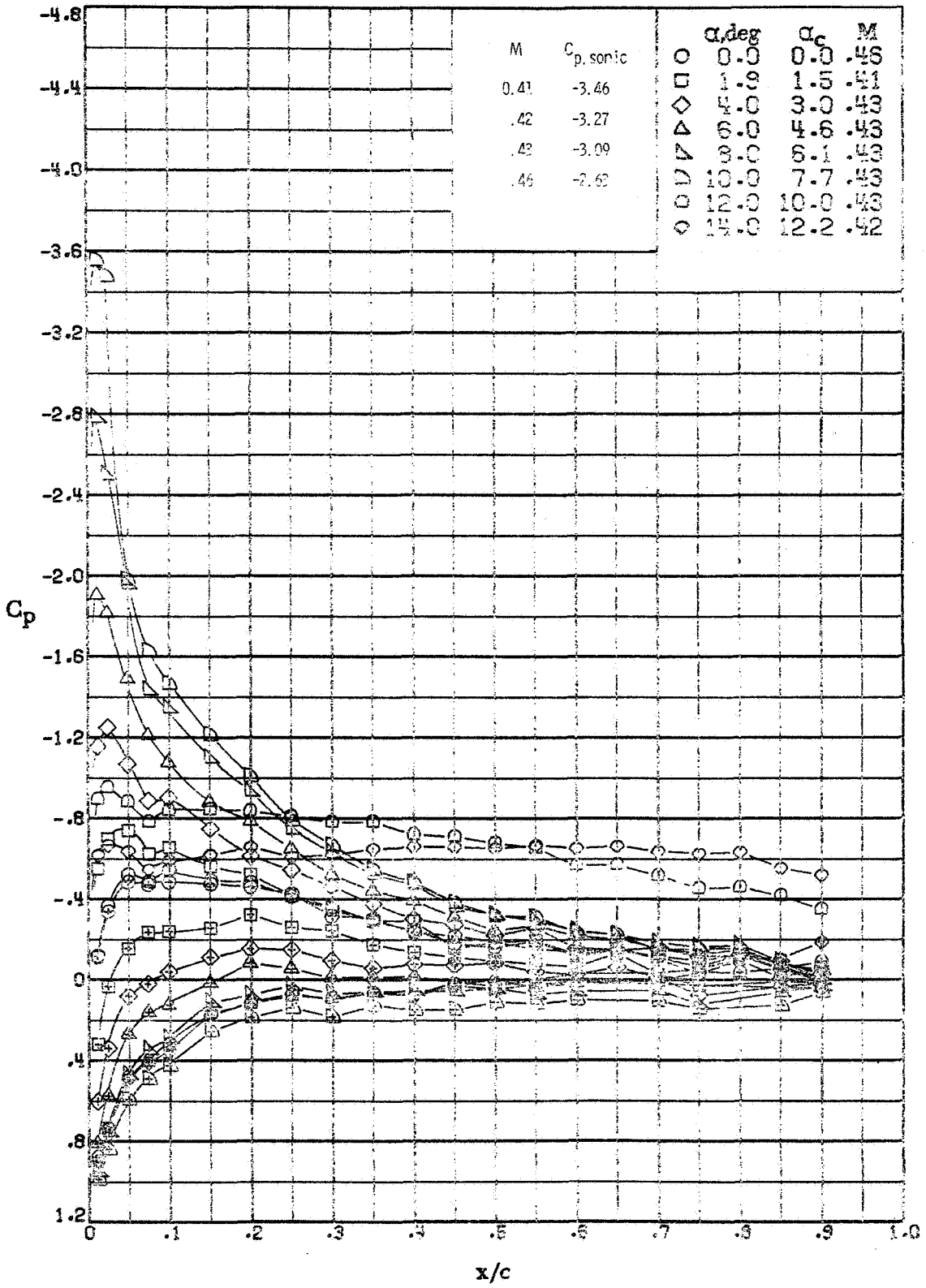

(b) $M \approx 0.48$; $R \approx 1.1 \times 10^6$.

Figure A6.- - Continued.

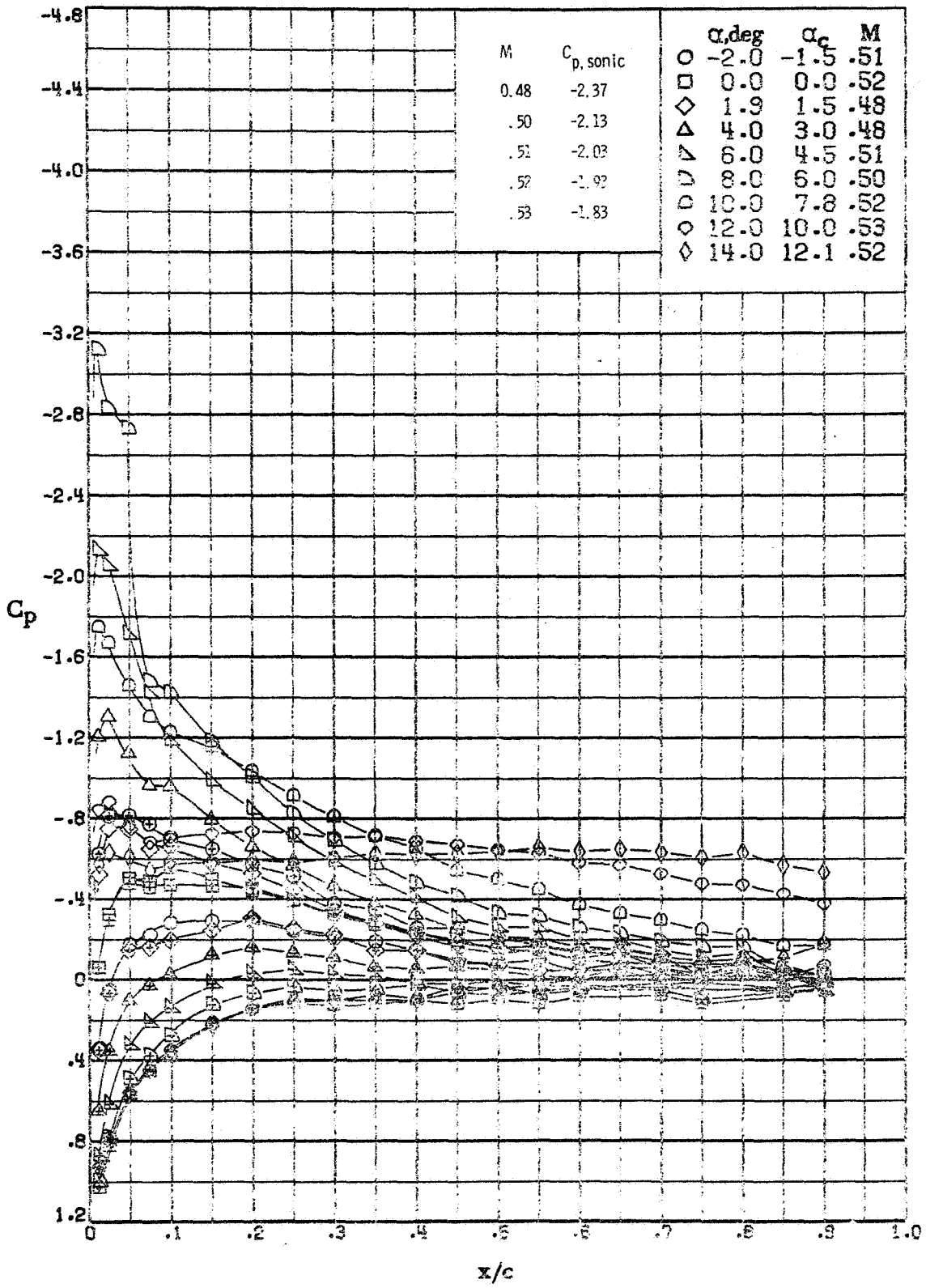

(c) $M \approx 0.52$; $R \approx 1.8 \times 10^6$.

Figure A6. - - Continued.

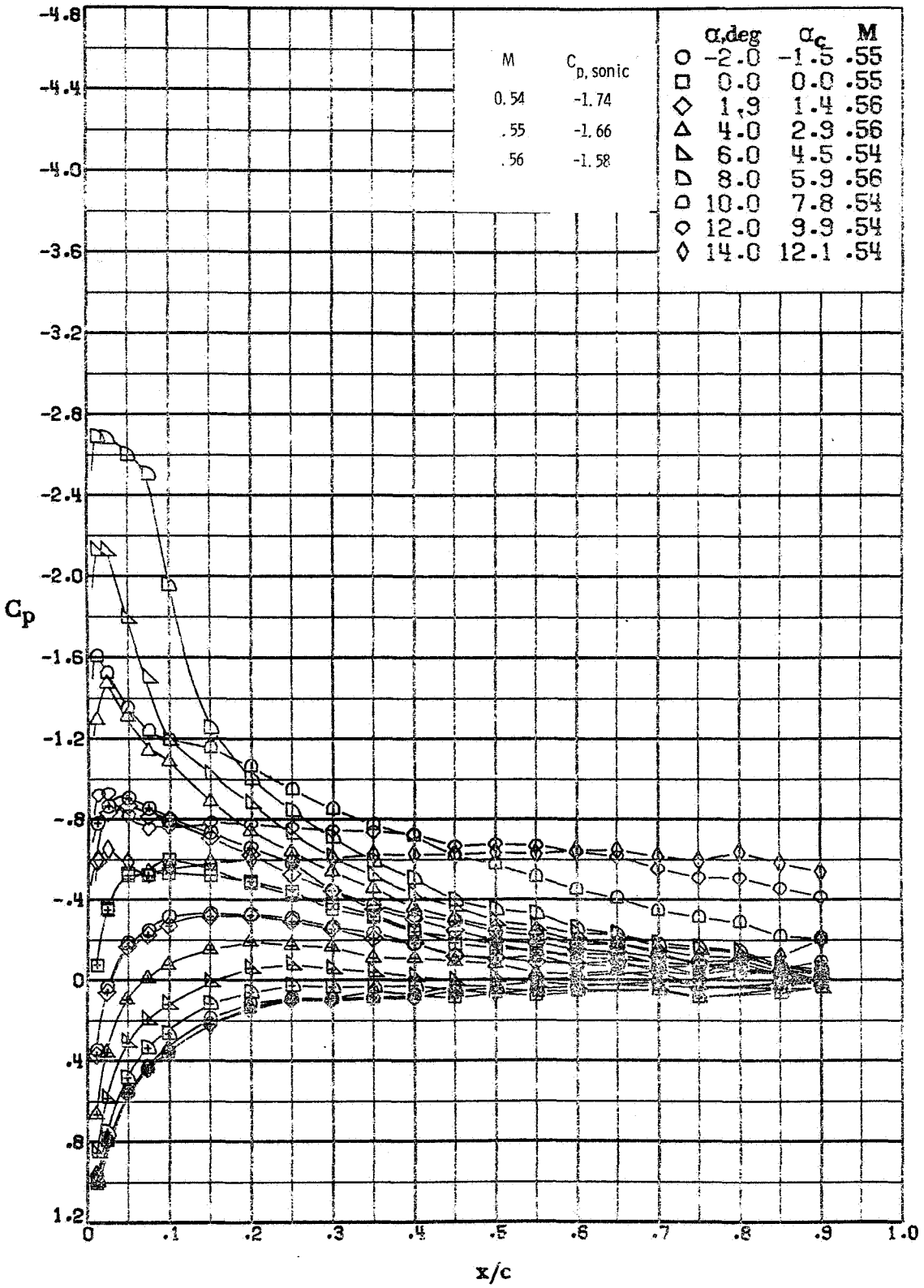

(d) $M \approx 0.54$; $R \approx 1.4 \times 10^6$.

Figure A6. - - Continued.

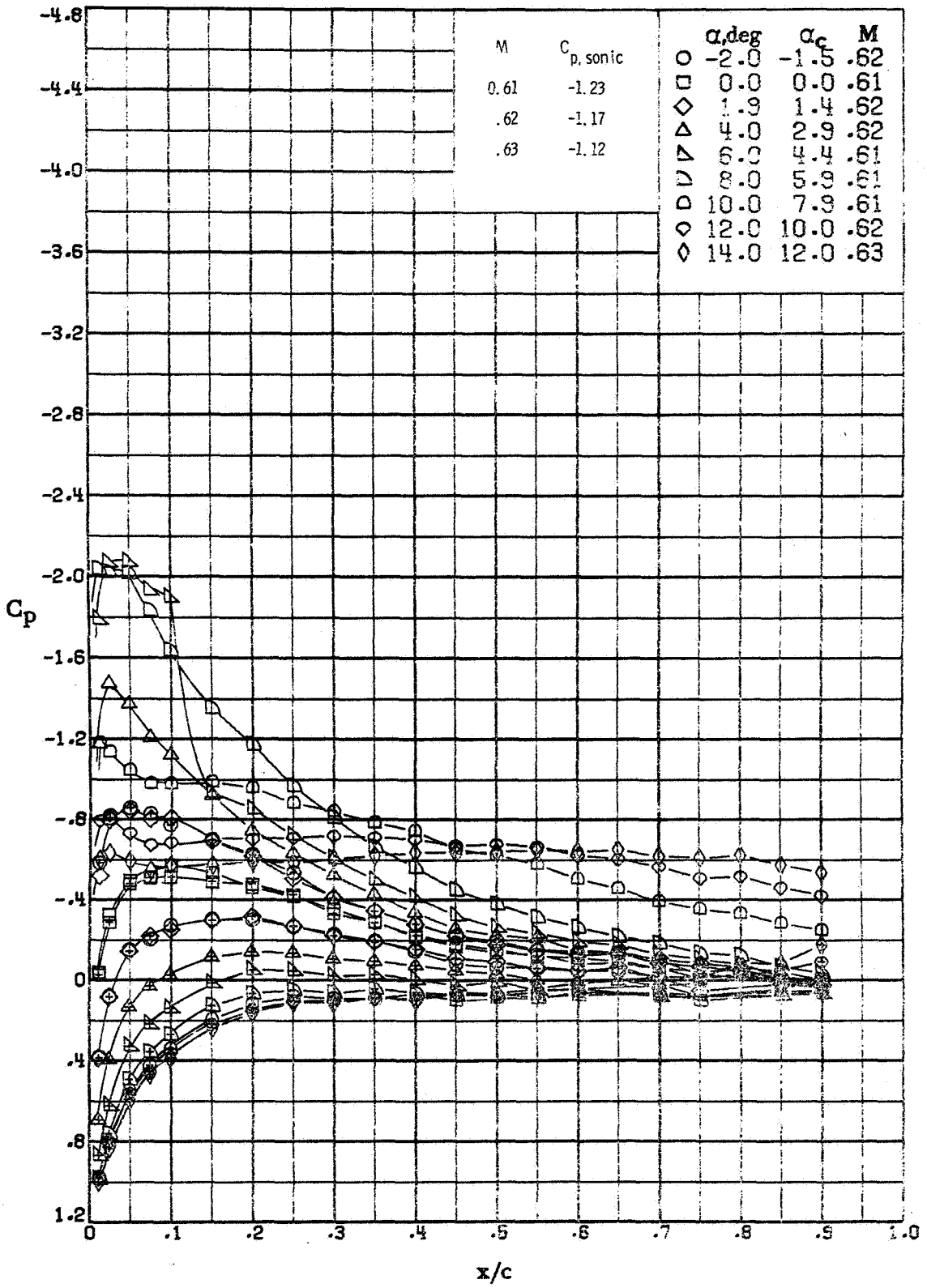

(e) $M \approx 0.62$; $R \approx 1.6 \times 10^6$.

Figure A6. - - Continued.

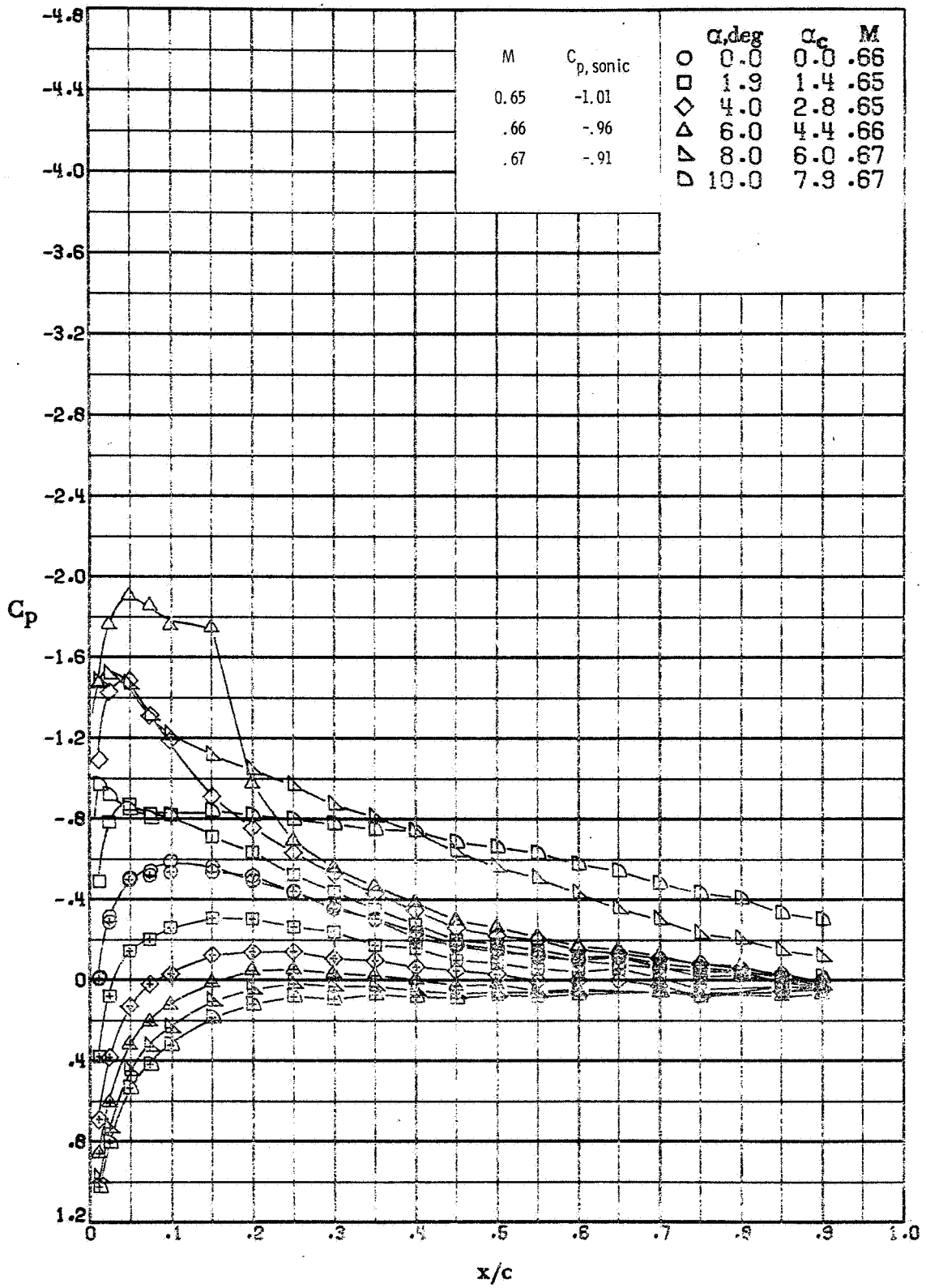

(f) $M \approx 0.66$; $R \approx 1.7 \times 10^6$.

Figure A6. - - Continued.

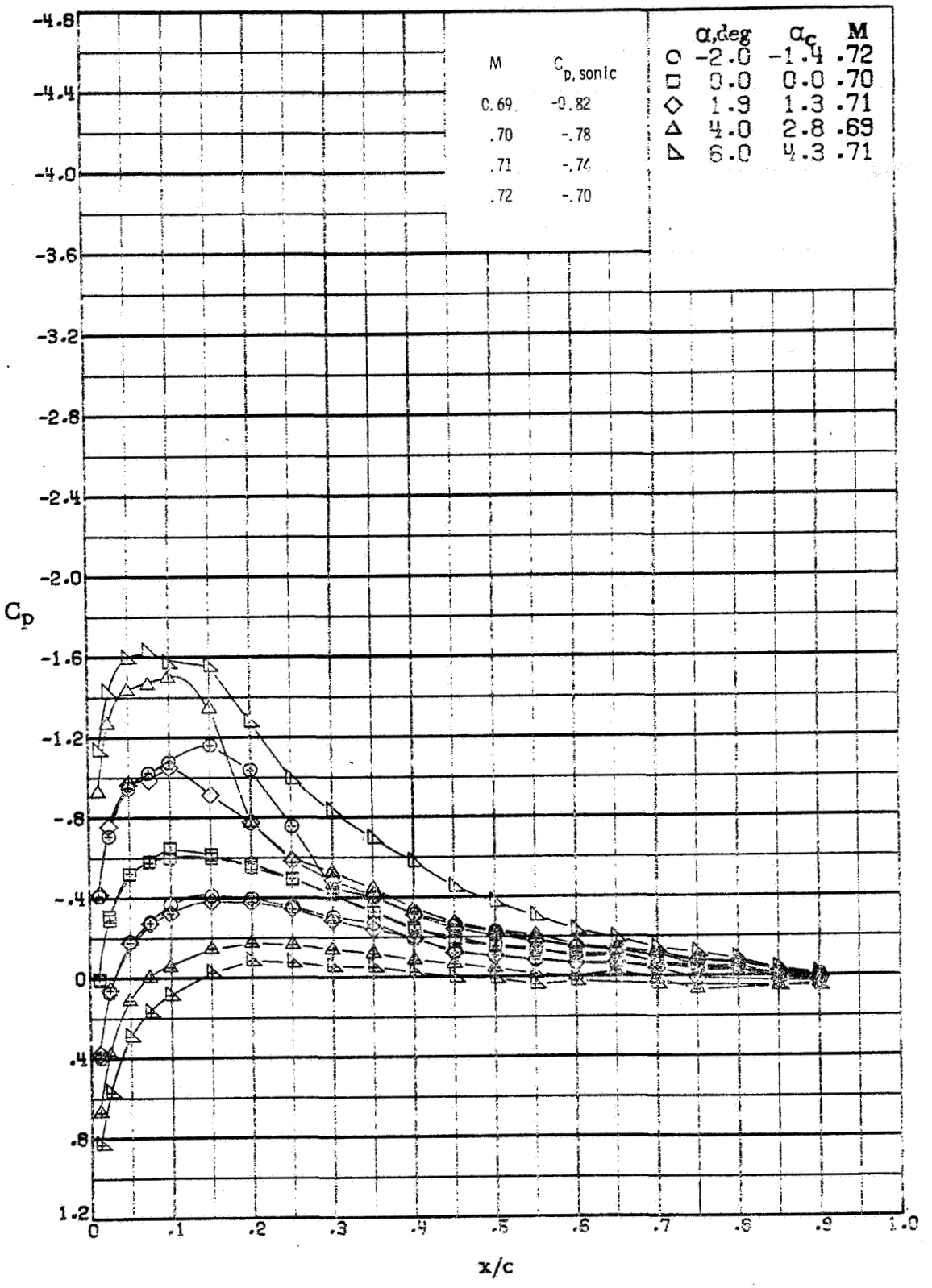

(g) $M \approx 0.71$; $R \approx 1.8 \times 10^6$.

Figure A6. - - Continued.

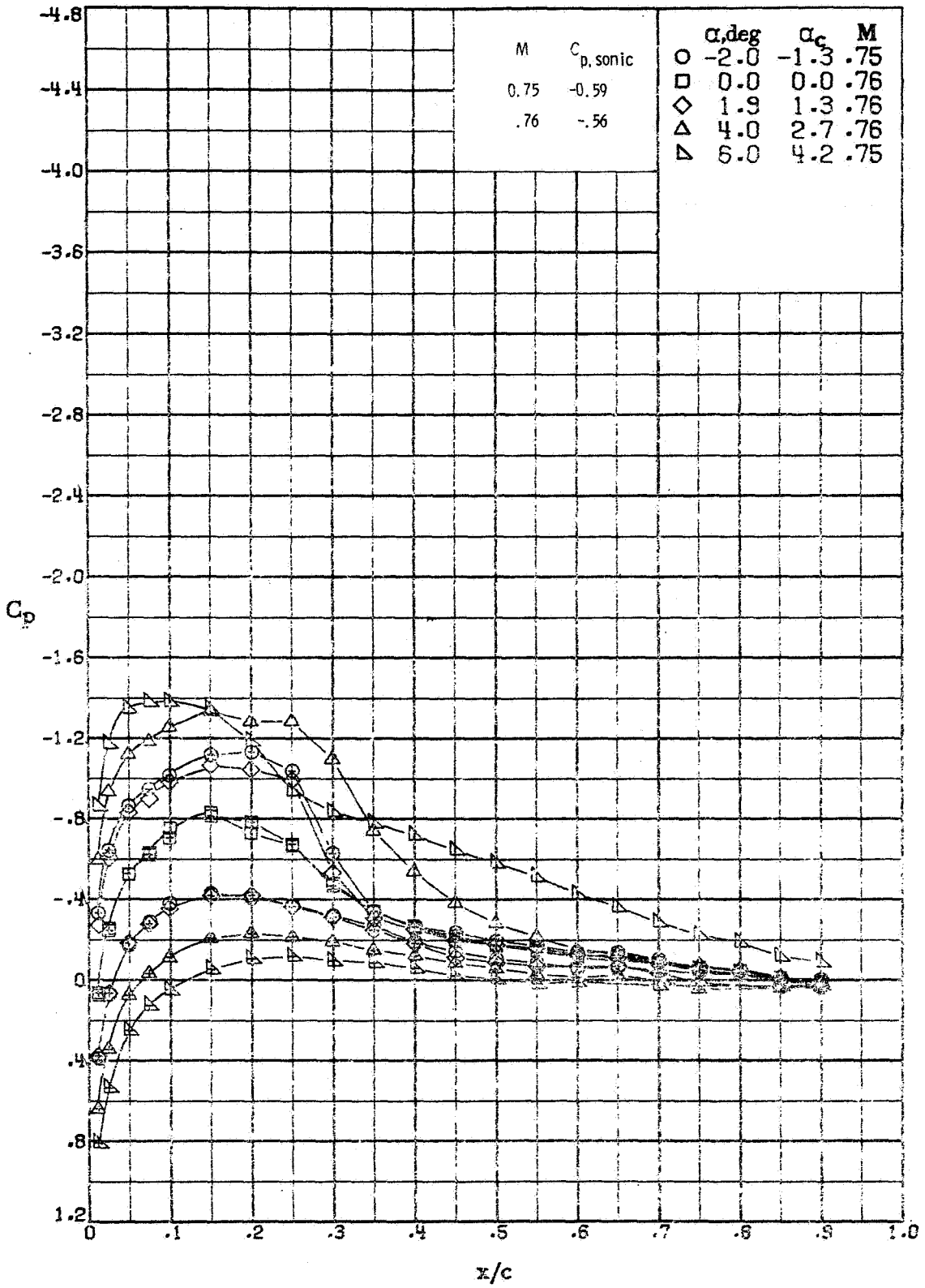

(h) $M \approx 0.76$; $R \approx 1.9 \times 10^6$.

Figure A6.- - Continued.

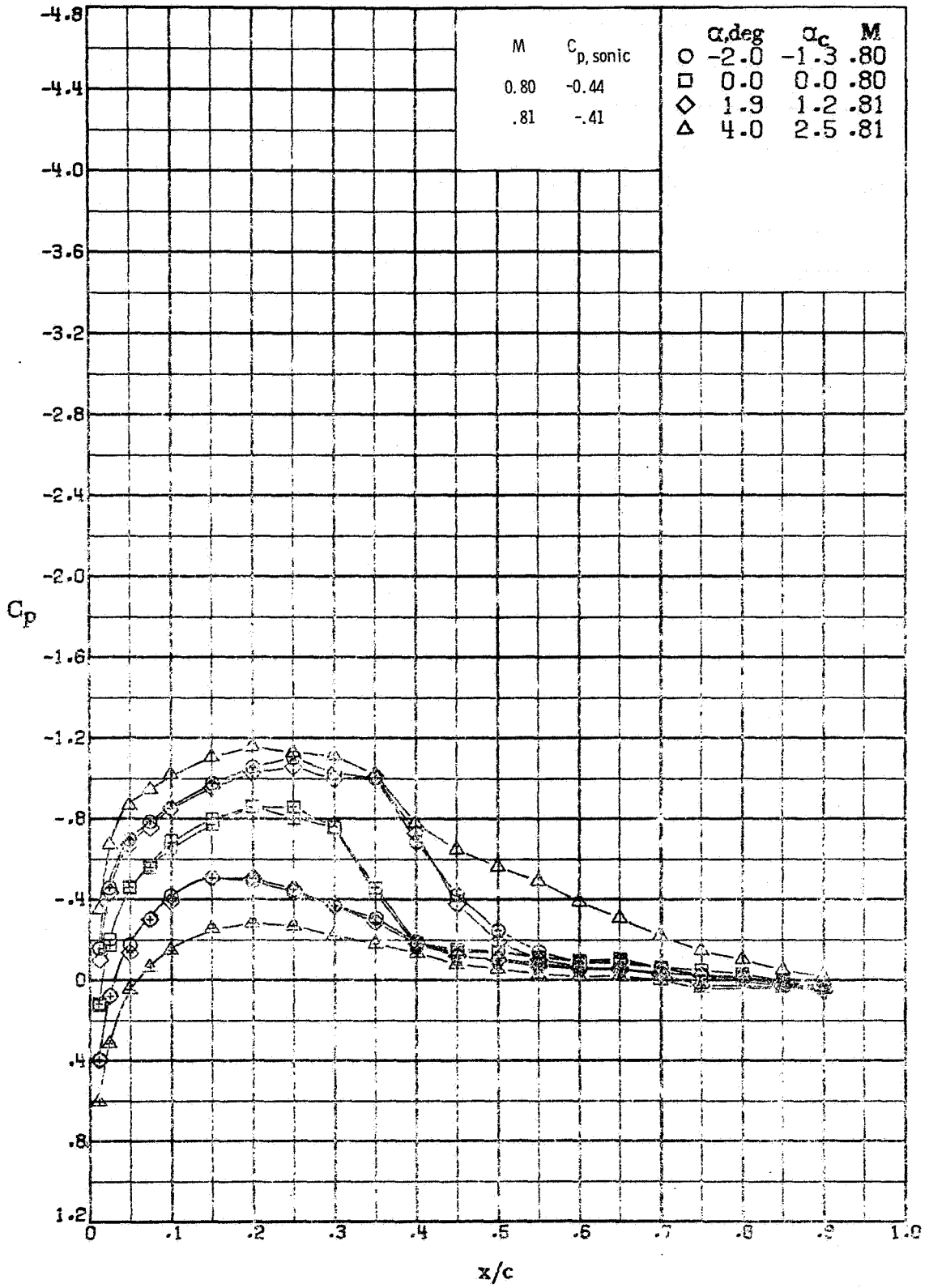

(i) $M \approx 0.80$; $R \approx 2.0 \times 10^6$.

Figure A6. - - Continued.

ODUCIBILITY OF THE
INAL PAGE IS POOR

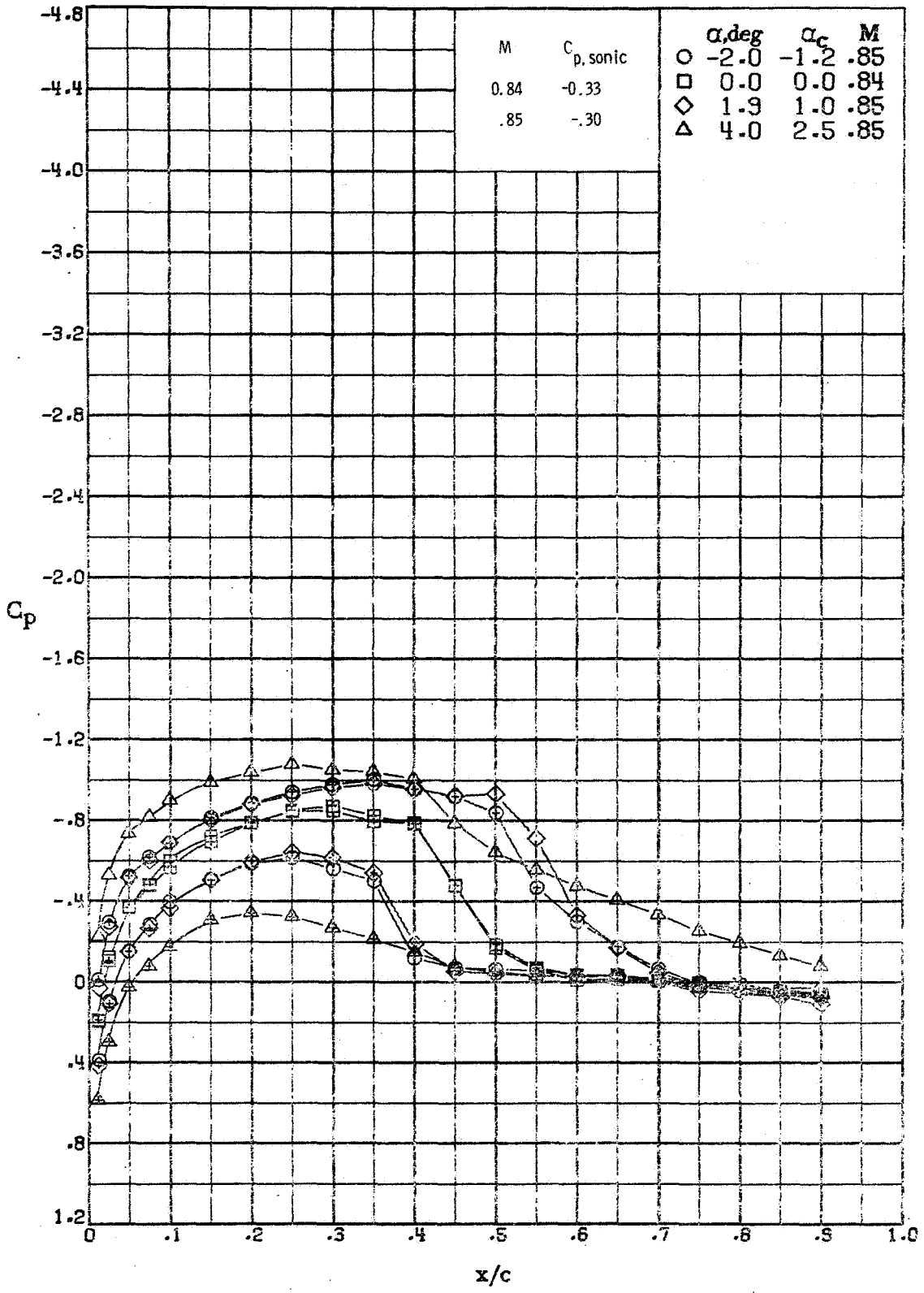

(j) $M \approx 0.85$; $R \approx 2.1 \times 10^6$.

Figure A6.- - Continued.

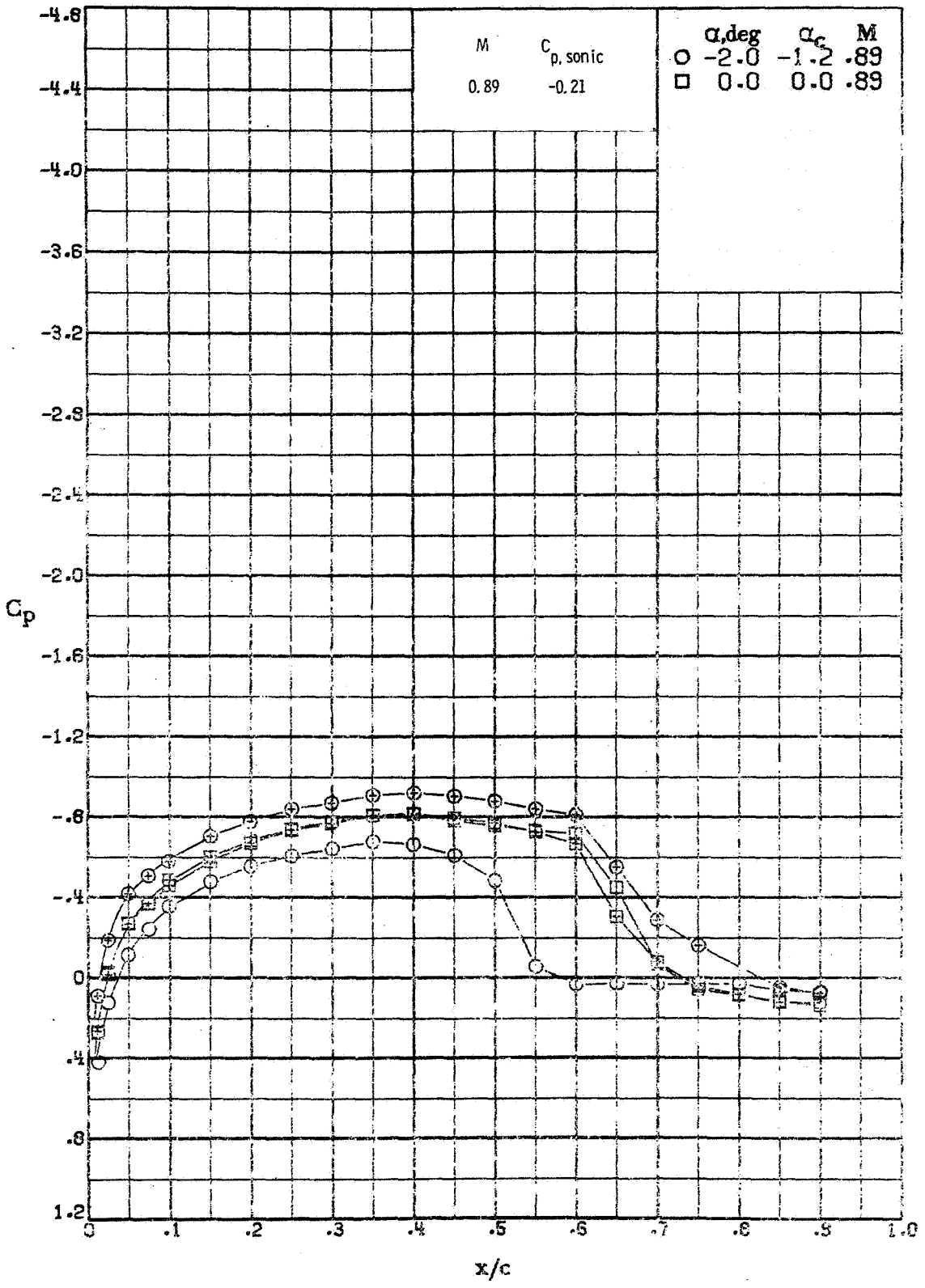

(k) $M \approx 0.89$; $R \approx 2.2 \times 10^6$.

Figure A6.- Concluded.

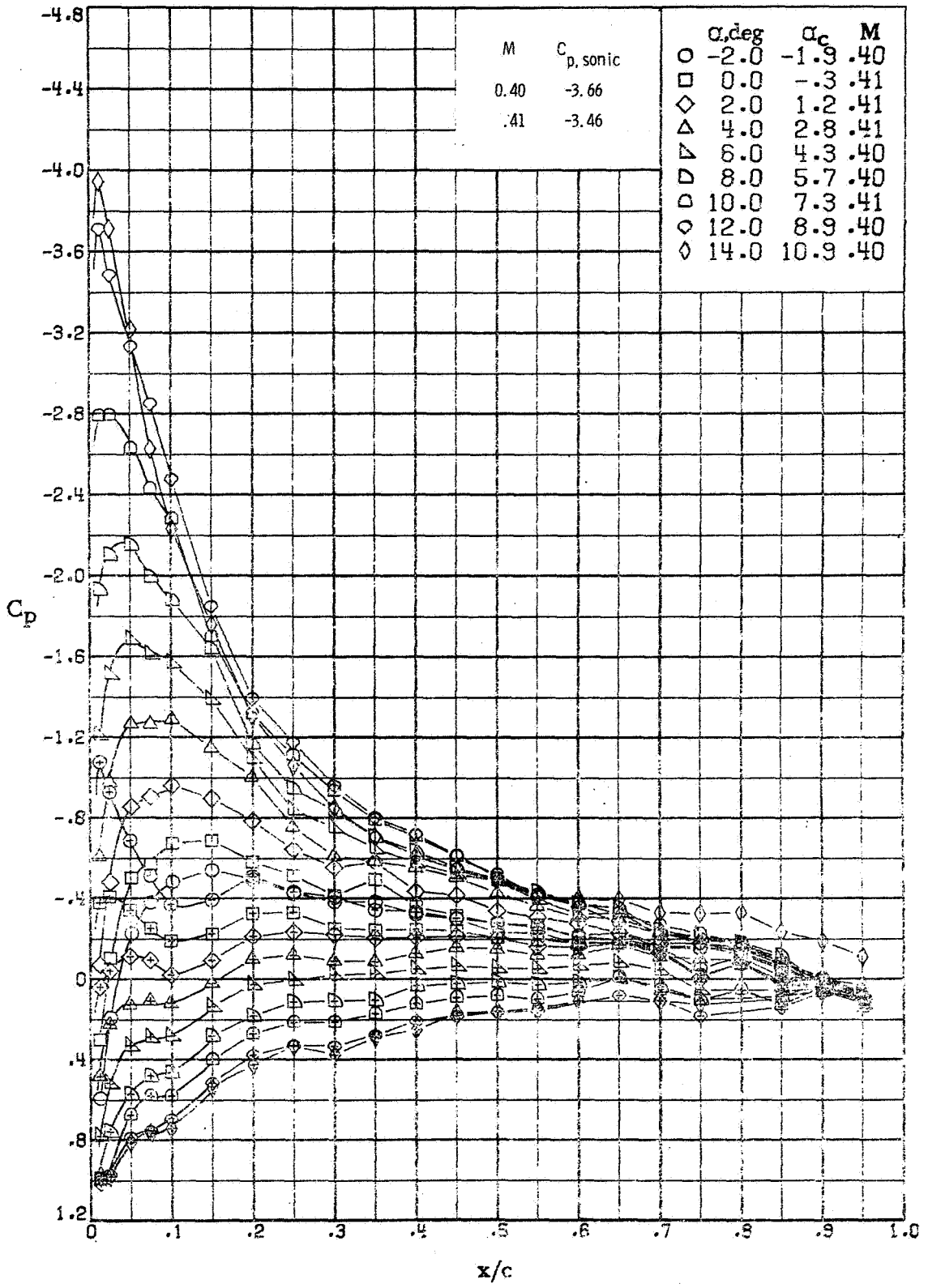

(a) $M \approx 0.40$; $R \approx 1.0 \times 10^6$.

Figure A7.- Effect of angle of attack on the chordwise pressure distribution of the NACA 23012 airfoil measured in the Langley 6 x 19 inch transonic tunnel.

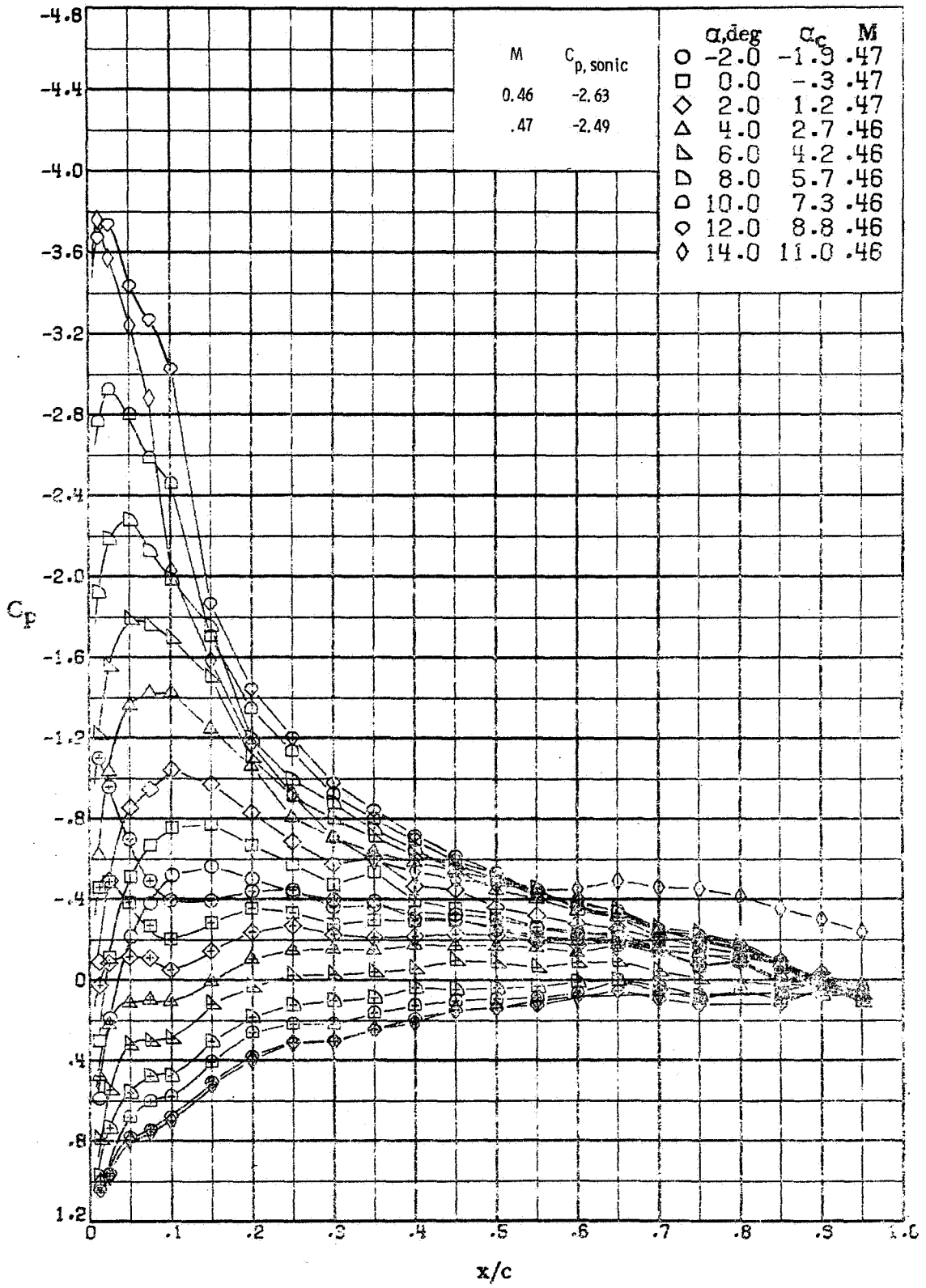

(b) $M \approx 0.46$; $R \approx 1.2 \times 10^6$.

Figure A7.- - Continued.

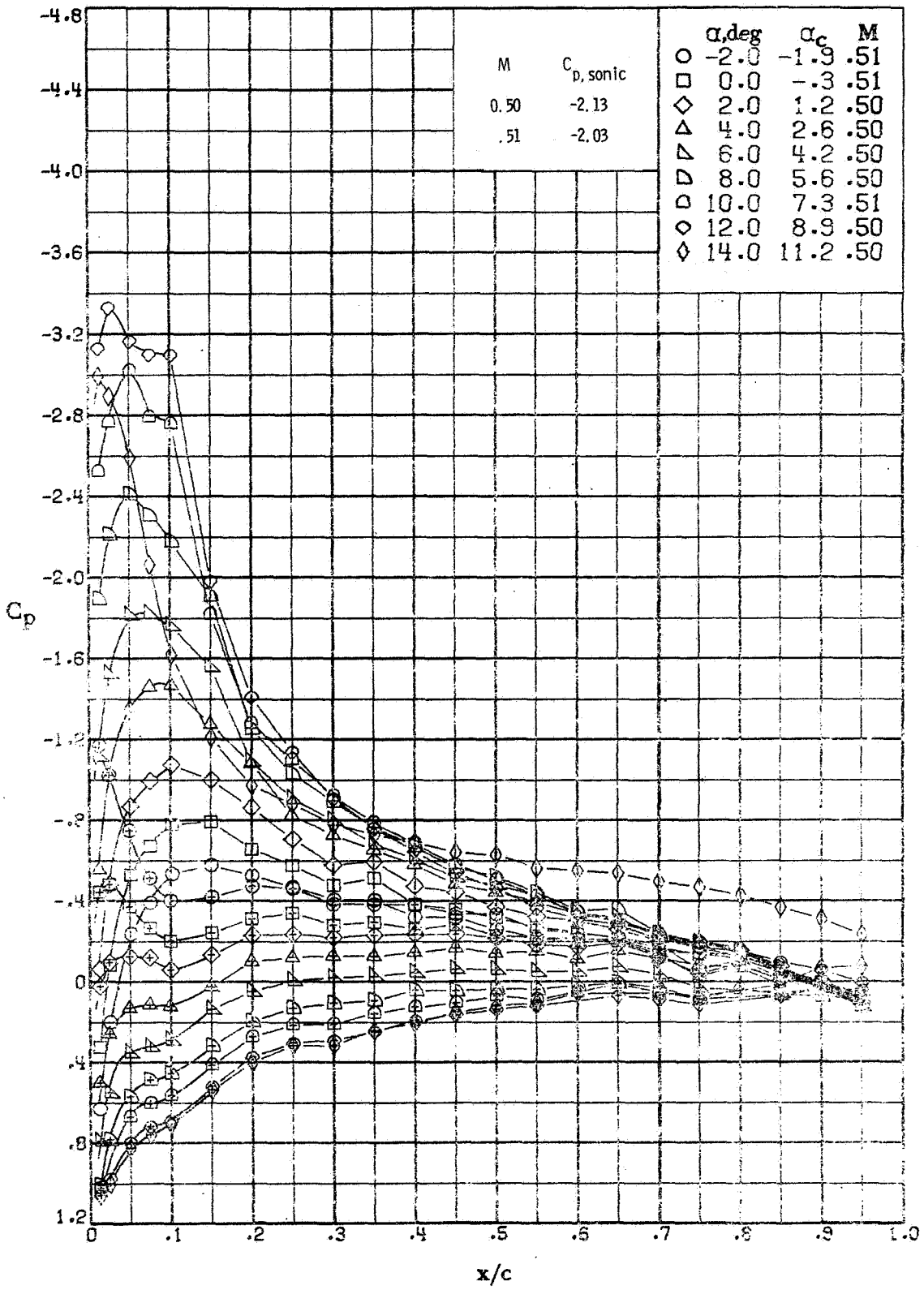

(c) $M \approx 0.50$; $R \approx 1.3 \times 10^6$.

Figure A7.- - Continued.

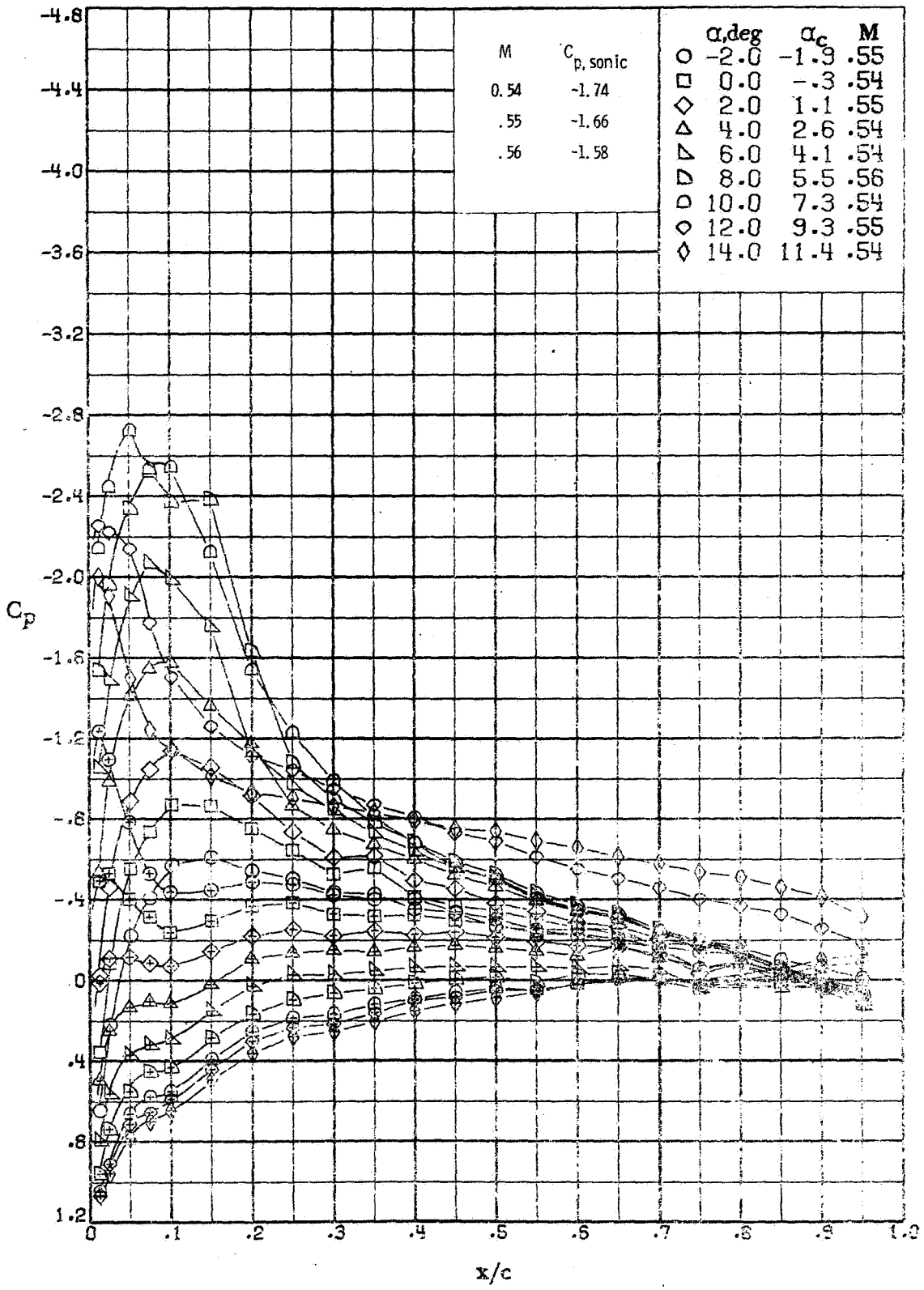

(d) $M \approx 0.55$; $R \approx 1.4 \times 10^6$.

Figure A7.- - Continued.

ODUCIBILITY OF THE
GINAL PAGE IS POOR

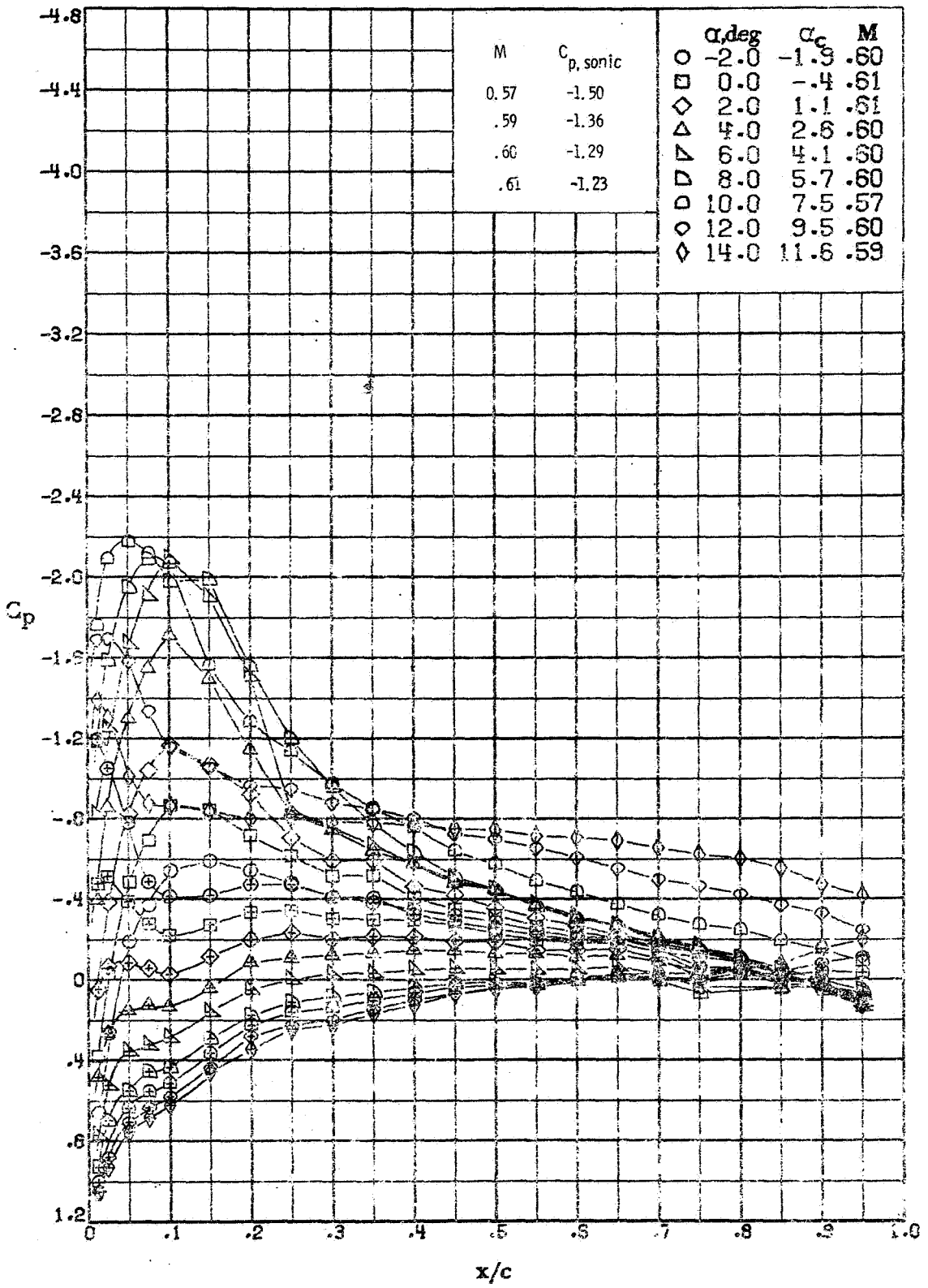

(e) $M \approx 0.60$; $R \approx 1.5 \times 10^6$.

Figure A7. - Continued.

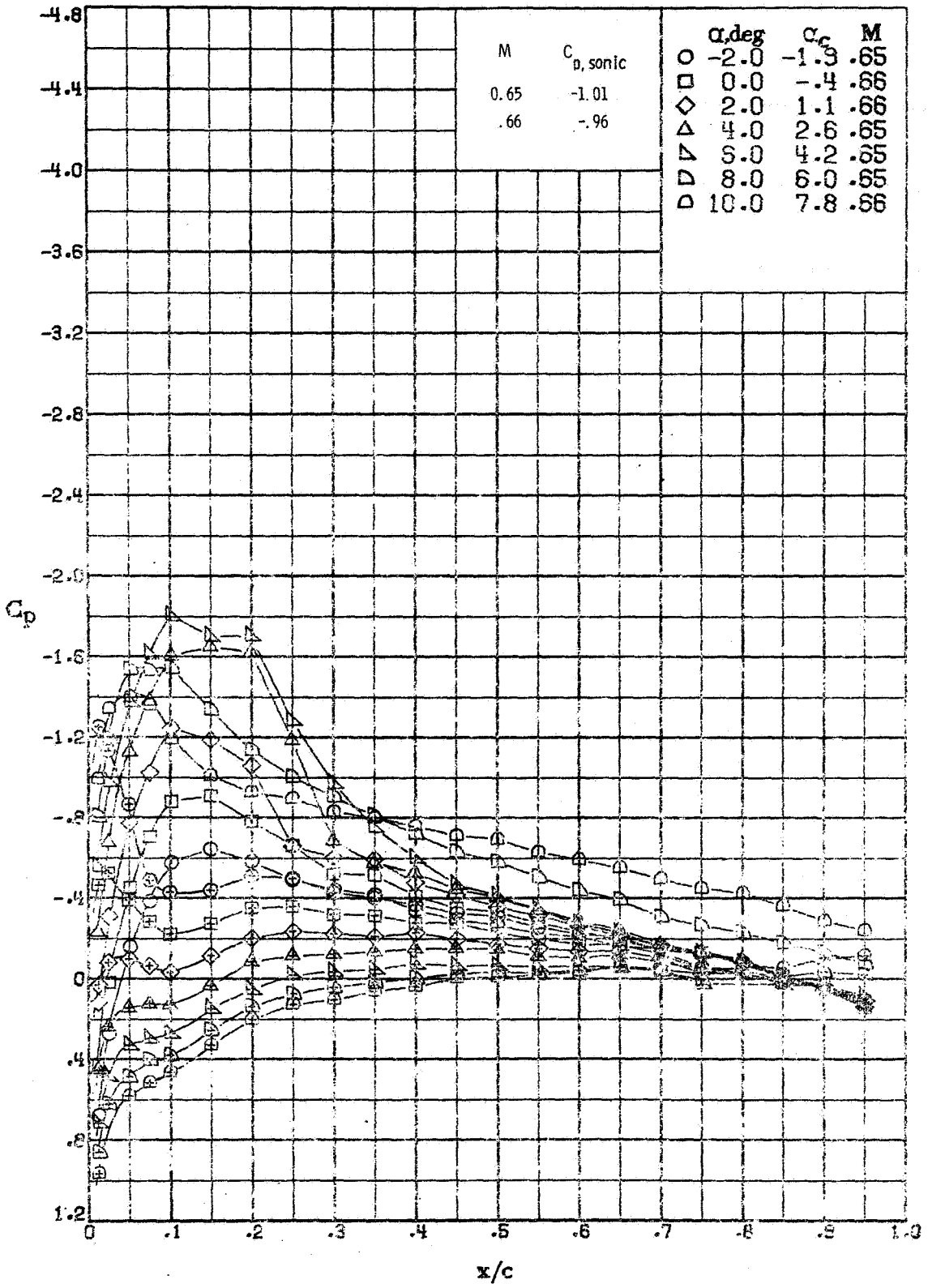

(f) $M \approx 0.65$; $R \approx 1.7 \times 10^6$.

Figure A7. - Continued.

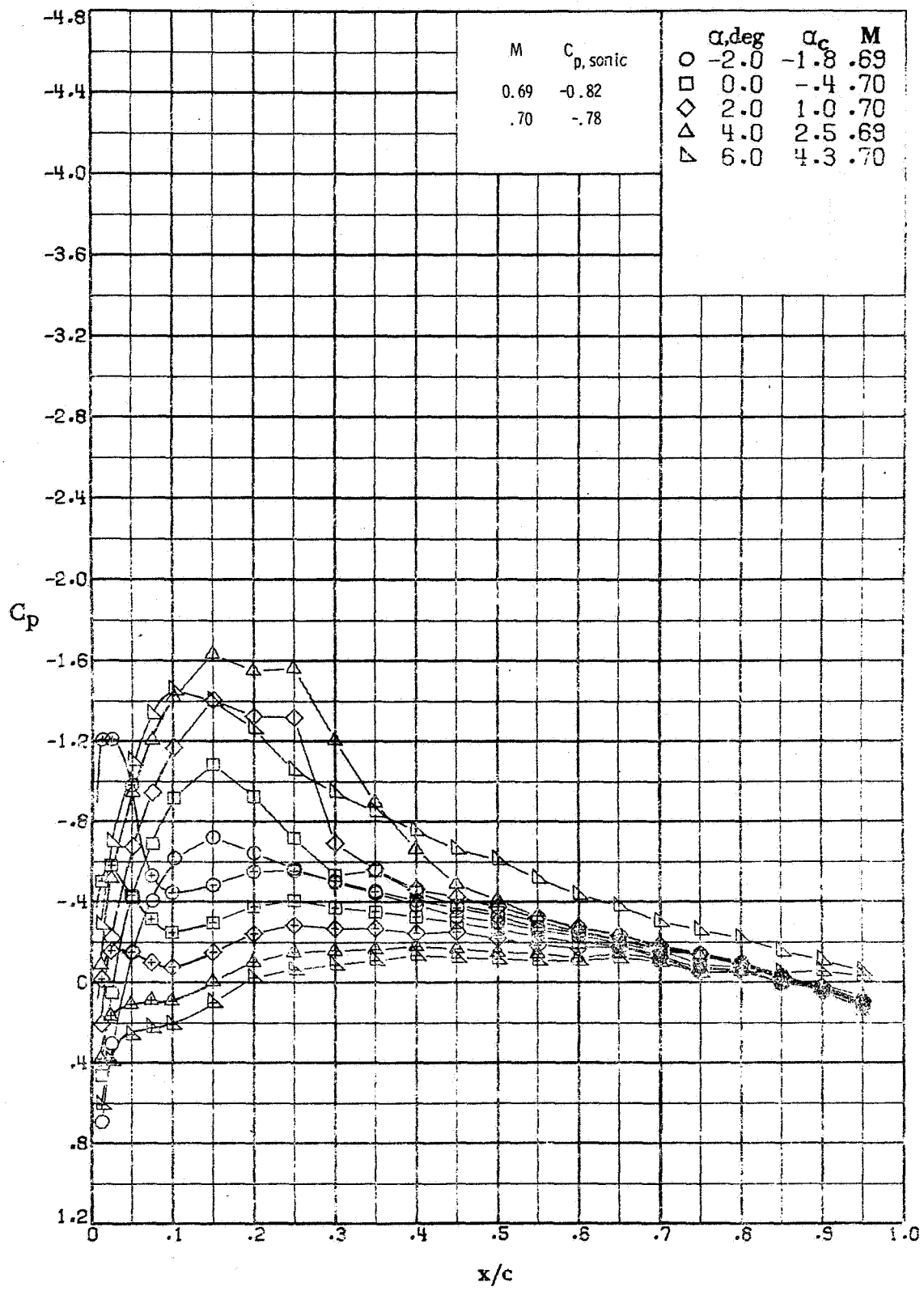

(g) $M \approx 0.70$; $R \approx 1.8 \times 10^6$.

Figure A7.- - Continued.

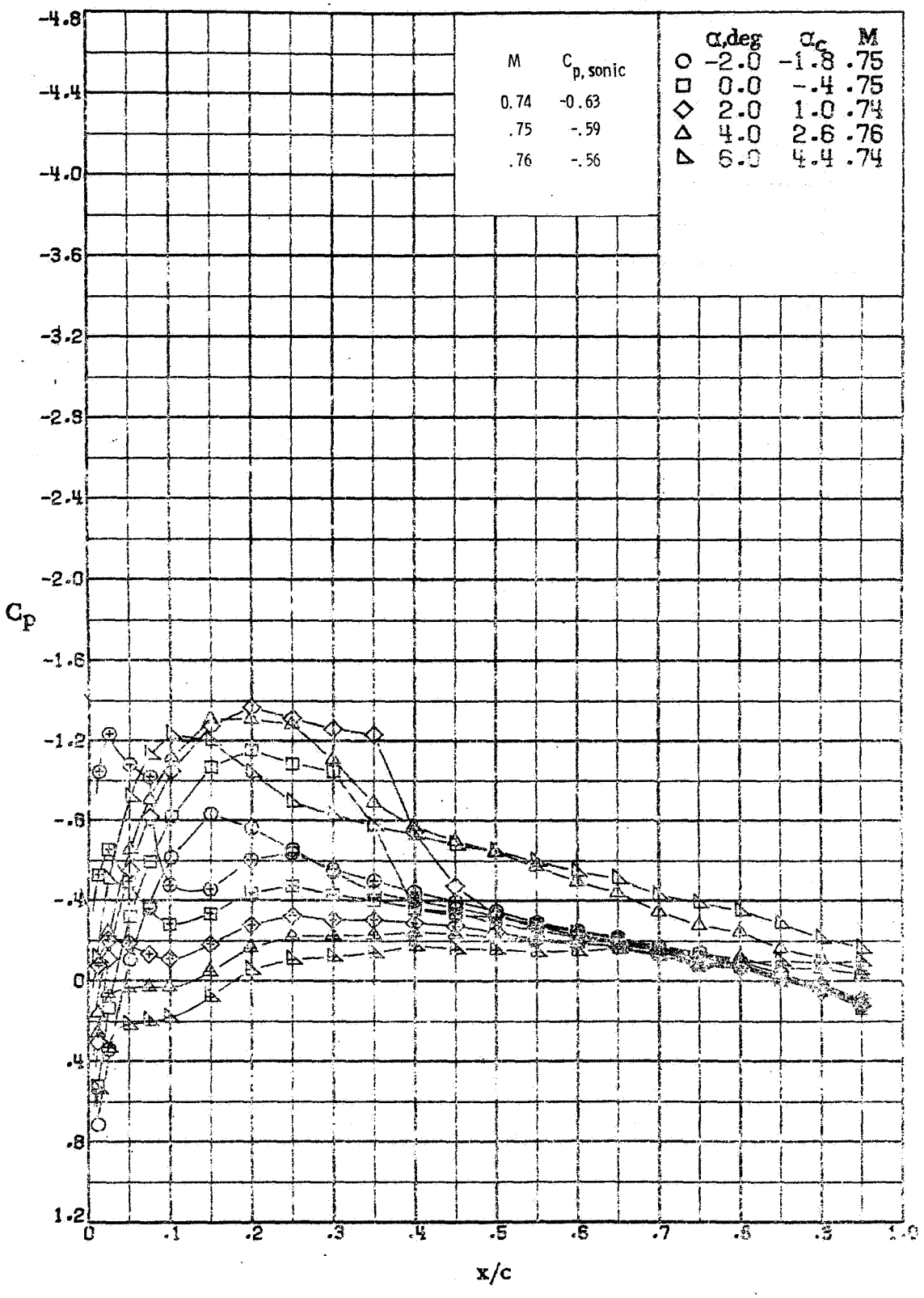

(h) $M \approx 0.75$; $R \approx 1.9 \times 10^6$.

Figure A7.- - Continued.

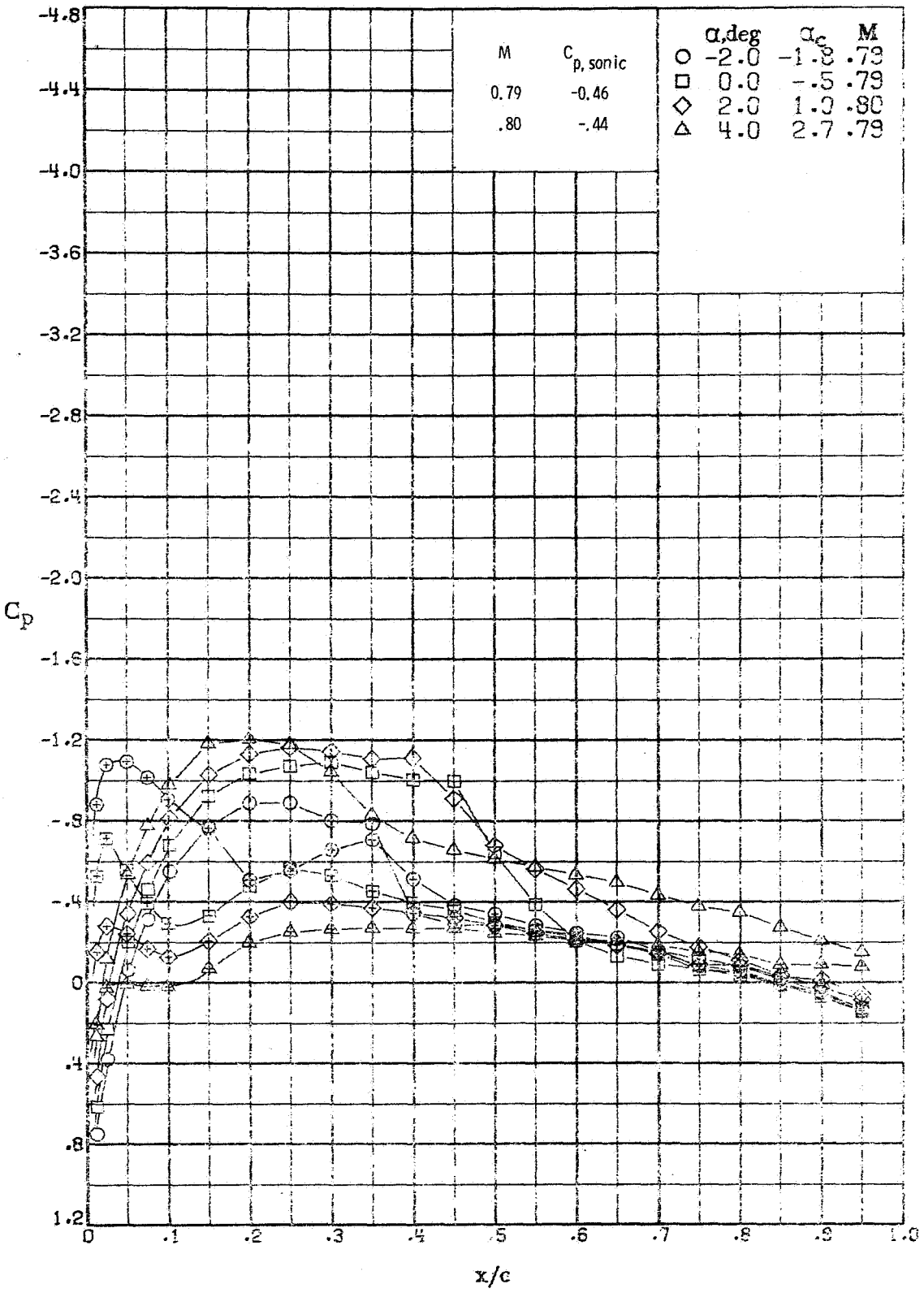

(f) $M \approx 0.79$; $R \approx 2.0 \times 10^6$.

Figure A7.-- Continued.

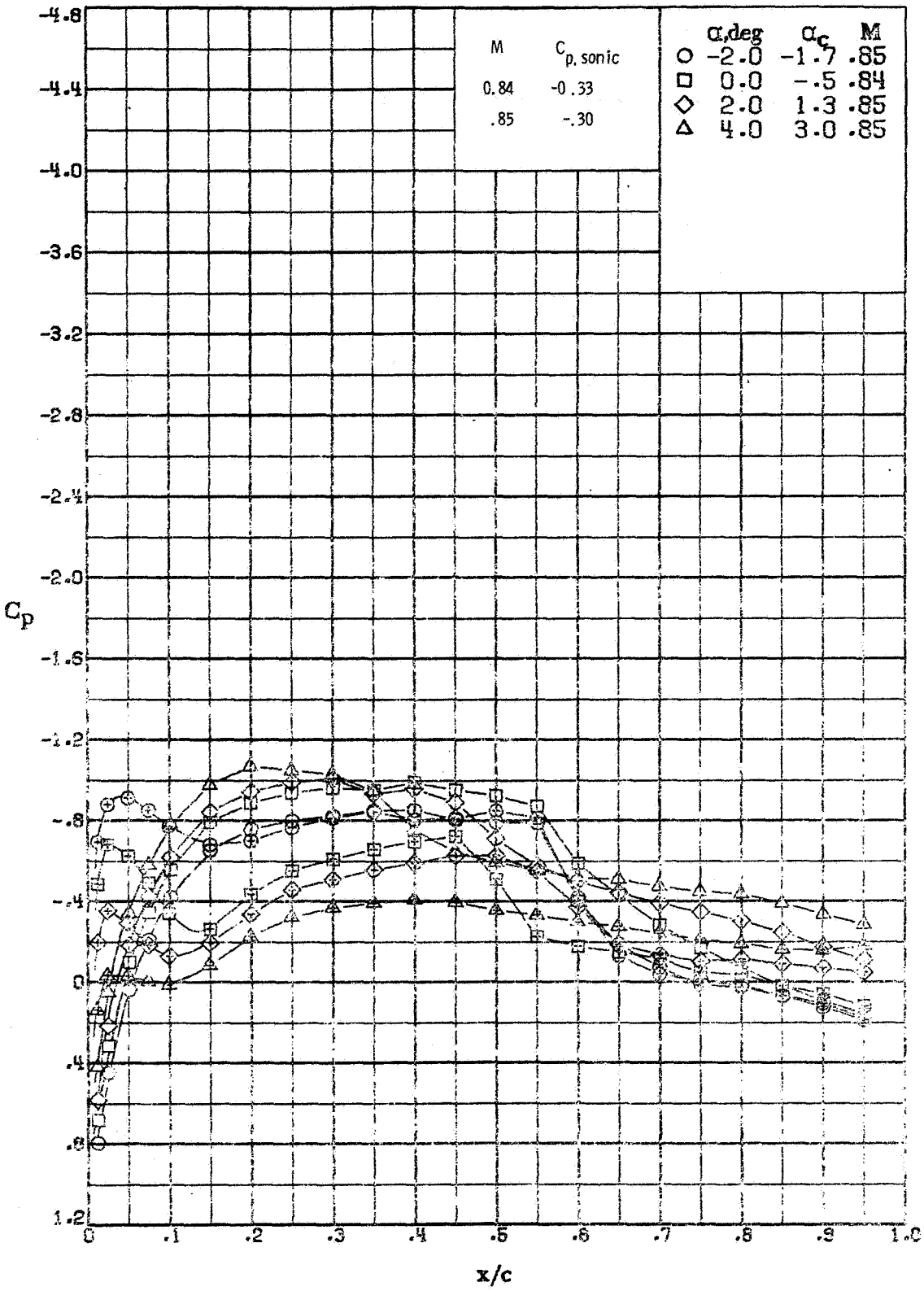

(j) $M \approx 0.85$; $R \approx 2.1 \times 10^6$.

Figure A7. - - Continued.

ODUCIBILITY OF THE
ORIGINAL PAGE IS POOR

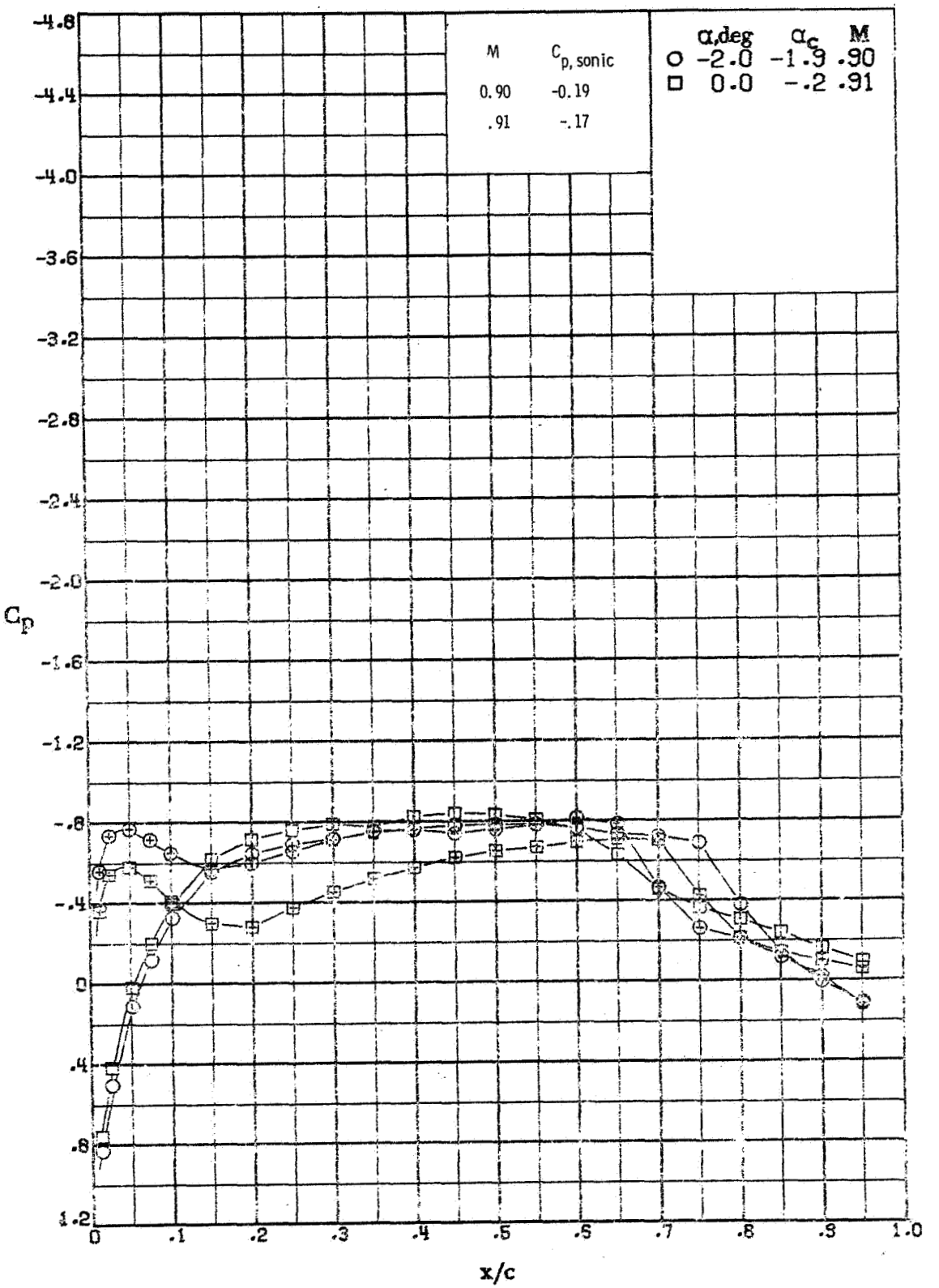

(k) $M \approx 0.90$; $R \approx 2.2 \times 10^6$.

Figure A7.- Concluded.